

2013 RSNA (Filtered Schedule)

Saturday, November 30, 2013

12:00-02:00 PM • [SPPH01](#) • Room: E351 • AAPM/RSNA Physics Tutorial for Residents: Control of Dose in Computed Tomography
02:15-04:15 PM • [SPPH02](#) • Room: E351 • AAPM/RSNA Tutorial on Equipment Selection: Imaging Systems Designed to Reduce CT Dose and Maintain Image Quali...

Sunday, December 01, 2013

10:45-12:15 PM • [SSA19](#) • Room: S403B • Physics (CAD I)
10:45-12:15 PM • [SSA20](#) • Room: S404AB • Physics (Low-dose CT Imaging)
10:45-12:15 PM • [SSA21](#) • Room: S405AB • Physics (Ultrasound)
12:30-01:00 PM • [LL-PHE3075-SUA](#) • • A Comparison of Radiation Dose to the Colon between Single-energy and Dual-energy CT Colonography
12:30-01:00 PM • [LL-PHS-SUA](#) • Room: Lakeside Learning Center • Physics - Sunday Posters and Exhibits (12:30pm - 1:00pm)
02:00-03:30 PM • [RC121](#) • Room: N228 • Medical Physics 2.0: Computed Tomography
02:00-03:30 PM • [RC122](#) • Room: S504AB • Uncertainties in Imaging for Radiation Oncology: Sources and Mitigation Techniques-Image Guidance in the Treat...
02:00-03:30 PM • [RC123](#) • Room: N229 • Minicourse: Current Topics in Medical Physics-Clinically Focused Physics Education: Principles to Practice
02:00-03:30 PM • [RC125](#) • Room: S104A • Quantitative Imaging: Current and Future Practice in Radiology and Clinical Trials

Monday, December 02, 2013

08:30-10:00 AM • [RC221](#) • Room: S404AB • Medical Physics 2.0: Mammography
08:30-10:00 AM • [RC222](#) • Room: S102C • Uncertainties in Imaging for Radiation Oncology: Sources and Mitigation Techniques-Margins and Margin Design
08:30-10:00 AM • [RC223](#) • Room: S403B • Minicourse: Current Topics in Medical Physics-Practice Quality Improvement: Basics and Issues for Medical Phys...
08:30-10:00 AM • [RC225](#) • Room: N229 • Quantitative Imaging: Diffuse Lung Disease Assessment Using CT
10:30-12:00 PM • [SSC13](#) • Room: S403A • Physics (CT-Dose Modulation)
10:30-12:00 PM • [SSC14](#) • Room: S403B • Physics (MRI Techniques I)
12:15-12:45 PM • [LL-PHS-MOA](#) • Room: Lakeside Learning Center • Physics - Monday Posters and Exhibits (12:15pm - 12:45pm)
12:45-01:15 PM • [LL-PHS-MOB](#) • Room: Lakeside Learning Center • Physics - Monday Posters and Exhibits (12:45pm - 1:15pm)
12:45-01:15 PM • [LL-PHS-SUB](#) • Room: Lakeside Learning Center • Physics - Sunday Posters and Exhibits (1:00pm - 1:30pm)
01:30-02:45 PM • [SPPH21](#) • Room: S102D • AAPM/RSNA Basic Physics Lecture for the Radiologic Technologist: Digital Imaging Exposure Indicators-Implicati...
01:30-05:45 PM • [SPPH22](#) • Room: S102C • Physics Symposium: Uncertainties in Radiation Therapy 2
03:00-04:00 PM • [SSE22](#) • Room: S403A • Physics (CAD II)
03:00-04:00 PM • [SSE23](#) • Room: S403B • Physics (Image Reconstruction)
03:00-04:00 PM • [SSE24](#) • Room: S404AB • Physics (Image-guided Radiation Therapy I)

Tuesday, December 03, 2013

08:30-10:00 AM • [RC321](#) • Room: S102D • Medical Physics 2.0: Nuclear Imaging
08:30-10:00 AM • [RC322](#) • Room: E261 • Uncertainties in Imaging for Radiation Oncology: Sources and Mitigation Techniques-Incorporation of Imaging as...
08:30-10:00 AM • [RC323](#) • Room: S404AB • Minicourse: Current Topics in Medical Physics-Radiation Dose Reduction in Medical Imaging
08:30-10:00 AM • [RC325](#) • Room: E353A • Quantitative Imaging: Functional MRI (fMRI)
10:30-12:00 PM • [SSG13](#) • Room: S403A • Physics (Quantitative Imaging I)
10:30-12:00 PM • [SSG14](#) • Room: S403B • Physics (Multi-energy CT)
10:30-12:00 PM • [SSG15](#) • Room: S404AB • Physics (X-ray Imaging)
12:15-12:45 PM • [LL-PHS-TUA](#) • Room: Lakeside Learning Center • Physics - Tuesday Posters and Exhibits (12:15pm - 12:45pm)
12:45-01:15 PM • [LL-PHS-TUB](#) • Room: Lakeside Learning Center • Physics - Tuesday Posters and Exhibits (12:45pm - 1:15pm)
03:00-04:00 PM • [SSJ22](#) • Room: S403A • Physics (Population-Dose Survey)
03:00-04:00 PM • [SSJ23](#) • Room: S403B • Physics (Non-Conventional CT Imaging)
03:00-04:00 PM • [SSJ24](#) • Room: S404AB • Physics (MRI Techniques II)
04:30-06:00 PM • [RC421](#) • Room: E351 • Medical Physics 2.0: Radiography
04:30-06:00 PM • [RC422](#) • Room: S102D • Uncertainties in Imaging for Radiation Oncology: Sources and Mitigation Techniques-Imaging for Target Definiti...
04:30-06:00 PM • [RC423](#) • Room: S403B • Minicourse: Current Topics in Medical Physics-Nuclear Cardiac Imaging for Physicists
04:30-06:00 PM • [RC425](#) • Room: S404AB • Quantitative Imaging: Dynamic Contrast Enhanced MRI (DCE-MRI)

Wednesday, December 04, 2013

08:30-10:00 AM • [RC521](#) • Room: E451A • Medical Physics 2.0: Fluoroscopy
08:30-10:00 AM • [RC522](#) • Room: N229 • Uncertainties in Imaging for Radiation Oncology: Sources and Mitigation Techniques-Site-specific IGRT Applicat...
08:30-10:00 AM • [RC523](#) • Room: N226 • Minicourse: Recording and Reporting Radiation Dose: National and International Perspectives and Activities
08:30-10:00 AM • [RC525](#) • Room: S102AB • Quantitative Imaging: Quantitative Imaging in FDG-PET
10:30-12:00 PM • [SSK19](#) • Room: S403A • Physics (CT-Imaging Phantoms)
10:30-12:00 PM • [SSK20](#) • Room: S403B • Physics (Quantitative Imaging II)
10:30-12:00 PM • [SSK21](#) • Room: S404AB • Physics (Molecular Imaging)
12:15-12:45 PM • [LL-PHS-WEA](#) • Room: Lakeside Learning Center • Physics - Wednesday Posters and Exhibits (12:15pm - 12:45pm)
12:45-01:15 PM • [LL-PHS-WEB](#) • Room: Lakeside Learning Center • Physics - Wednesday Posters and Exhibits (12:45pm - 1:15PM)
03:00-04:00 PM • [SSM19](#) • Room: N228 • Physics (Quantitative Imaging III)
03:00-04:00 PM • [SSM20](#) • Room: S404AB • Physics (CT-Imaging Evaluation)
03:00-04:00 PM • [SSM21](#) • Room: S406B • Physics (X-ray Imaging Techniques)

Thursday, December 05, 2013

08:30-10:00 AM • [RC621](#) • Room: S102C • Medical Physics 2.0: Ultrasonography
08:30-10:00 AM • [RC622](#) • Room: S102D • Uncertainties in Imaging for Radiation Oncology: Sources and Mitigation Techniques-Imaging Moving Targets
08:30-10:00 AM • [RC623](#) • Room: N229 • Minicourse: Recording and Reporting Radiation Dose: Interventional/Angiography/Fluoroscopy
08:30-10:00 AM • [RC625](#) • Room: N226 • Quantitative Imaging: Volumetric CT as a Biomarker for Disease
09:20-10:20 AM • [MSRT52](#) • Room: N230 • ASRT@RSNA 2013: Mastering Digital Radiography: CR and DR Exposures, Techniques and Doses
10:30-12:00 PM • [SSQ19](#) • Room: S403B • Physics (MRI Techniques III)
10:30-12:00 PM • [SSQ20](#) • Room: S404AB • Physics (CT Reconstruction)
12:15-12:45 PM • [LL-PHS-THA](#) • Room: Lakeside Learning Center • Physics - Thursday Posters and Exhibits (12:15pm - 12:45pm)
12:45-01:15 PM • [LL-PHS-THB](#) • Room: Lakeside Learning Center • Physics - Thursday Posters and Exhibits (12:45pm - 1:15pm)

01:30-02:45 PM • [PS50](#) • Arie Crown Theater • Thursday Plenary Session
04:30-06:00 PM • [RC721](#) • Room: N229 • Medical Physics 2.0: Information Management and Display
04:30-06:00 PM • [RC722](#) • Room: S502AB • Uncertainties in Imaging for Radiation Oncology: Sources and Mitigation Techniques-Image Registration
04:30-06:00 PM • [RC723](#) • Room: E351 • Minicourse: Recording and Reporting Radiation Dose: CT
04:30-06:00 PM • [RC725](#) • Room: E352 • Quantitative Imaging: Informatics

Friday, December 06, 2013

08:30-10:00 AM • [RC821](#) • Room: S405AB • Medical Physics 2.0: Magnetic Resonance Imaging
08:30-10:00 AM • [RC823](#) • Room: S403B • Minicourse: Recording and Reporting Radiation Dose: Nuclear Medicine
08:30-10:00 AM • [RC825](#) • Room: E263 • Quantitative Imaging: Quantitative Imaging in Ultrasound
10:30-12:00 PM • [SST14](#) • Room: S403B • Physics (CT-Dose Optimization)
10:30-12:00 PM • [SST15](#) • Room: S403A • Physics (Image-guided Radiation Therapy II)

Physics Case of the Day

[Back to Top](#)

LL-EDE3013

Moderator

Charles E Willis , PhD
William D Erwin , PhD
William R Geiser , MS
Ryan F Fisher , PhD
Robert L Dixon , PhD *
Dustin K Ragan , PhD

Physics Case of the Day

[Back to Top](#)

LL-EDE3013

Moderator

Charles E Willis , PhD
William D Erwin , PhD
William R Geiser , MS
Ryan F Fisher , PhD
Robert L Dixon , PhD *
Dustin K Ragan , PhD

Physics Case of the Day

[Back to Top](#)

LL-EDE3013

Moderator

Charles E Willis , PhD
William D Erwin , PhD
William R Geiser , MS
Ryan F Fisher , PhD
Robert L Dixon , PhD *
Dustin K Ragan , PhD

Physics Case of the Day

[Back to Top](#)

LL-EDE3013

Moderator

Charles E Willis , PhD
William D Erwin , PhD
William R Geiser , MS
Ryan F Fisher , PhD
Robert L Dixon , PhD *
Dustin K Ragan , PhD

Physics Case of the Day

[Back to Top](#)

LL-EDE3013

Moderator

Charles E Willis , PhD
William D Erwin , PhD
William R Geiser , MS
Ryan F Fisher , PhD
Robert L Dixon , PhD *
Dustin K Ragan , PhD

Physics Case of the Day

[Back to Top](#)

LL-EDE3013

Moderator

Charles E Willis , PhD
William D Erwin , PhD
William R Geiser , MS
Ryan F Fisher , PhD
Robert L Dixon , PhD *
Dustin K Ragan , PhD

A Practical Approach to Routine Ultrasound Quality Control Testing

[Back to Top](#)

LL-PHE3071

Donald J Tradup

Scott Stekel
Nicholas J Hangiandreou , PhD
Jeanie Owens , ARRT
Ryan Karshen , ARRT
Stephine Heers , ARRT
Catherine Fuhs , ARRT
Lesley McCoy , ARRT

PURPOSE/AIM

Considering all of the imaging modalities in radiology, ultrasound (US) is the least regulated and routine quality control (QC) for ultrasound has received relatively little emphasis. Requirements for routine QC will likely become more common in US practice accreditation programs. Common perceptions exist that routine US QC is expensive, difficult, time consuming, and beyond the capabilities of clinical staff. We present an efficient and effective US QC program that that has improved quality and safety in our clinical US practice.

CONTENT ORGANIZATION

We discuss our routine US QC program, which includes periodic assessment of (1) physical and mechanical integrity of the US system; (2) image uniformity and artifacts; (3) geometric accuracy for 3D probes; and (4) performance of the electronic displays on the US scanner and on the workstation used for primary image interpretation. For each of these assessments, we describe specific test tools, methods, and guidelines for interpreting results. We will also discuss the program results for our practice, which includes a variety of vendors, scanner models and transducer types. We also discuss the cost of the program in terms of equipment and personnel time.

SUMMARY

Routine US QC can be performed in an efficient and effective manner, and can improve quality and safety in the clinical US practice.

Shielding Design for Mammography Digital Tomosynthesis Rooms: Making Sure You Measure Up

[Back to Top](#)

LL-PHE3072

Timothy J Blackburn , PhD
Jacqueline Gallet , PhD
Gary Arbique , PhD *
Jeffrey B Guild , PhD
Jon A Anderson , PhD

PURPOSE/AIM

The purpose of this exhibit is:

1. To review the NCRP Report No. 147 approach to mammography shielding.
2. To examine the impact of the addition of digital tomosynthesis acquisitions on the validity of assumptions made in NCRP 147 shielding calculations.
3. To discuss modifications in shielding calculations necessary for the design of mammography rooms utilizing digital tomosynthesis.

CONTENT ORGANIZATION

The mammographic exam technique

- Conventional mammography
- Mammography digital tomosynthesis

NCRP 147 shielding design for mammography

- Workload assumptions
- Common shielding materials
- Example of a conventional room shielding design

Additional considerations for mammographic tomosynthesis

- Changes in workload and energy spectra
- Modifications in barrier transmission calculations
- Example of a mammography digital tomosynthesis room shielding design

SUMMARY

The major teaching points for this exhibit are:

1. Mammography tomosynthesis techniques require the use of higher kVp's and HVL's than conventional mammography.
2. Shielding design for conventional mammography based on NCRP 147 makes assumptions that are no longer valid when tomosynthesis is added.
3. Barrier transmissions given in NCRP 147 are not appropriate for mammography shielding design with the addition of tomosynthesis.

A Primer on Physical Principles of Differential Harmonic Tissue Imaging and Its Clinical Applications

[Back to Top](#)

LL-PHE3073

Arash Anvari , MD
Anthony E Samir , MD
Flemming Forsberg , PhD *

PURPOSE/AIM

Differential harmonic tissue imaging (dHTI) is a modern nonlinear sonographic imaging technology designed to combine the advantages of gray scale ultrasonography and conventional harmonic tissue imaging. The exhibition will explain the physical principles of dHTI to radiologists in simple language with figures, schematic diagrams and the clinical applications of dHTI.

CONTENT ORGANIZATION

- Background of harmonic tissue imaging.
- Describing the concepts of fundamental frequency, harmonic frequency, differential frequencies, pulse inversion and cancellation of fundamental signals by pulse subtraction.
- Explaining image generation process.
- Discuss different harmonic tissue imaging methods:
 - a. Conventional tissue harmonic imaging.
 - b. Pulse inversion harmonic imaging.
 - c. Differential tissue harmonic imaging.
- Discuss the advantages of disadvantages of tissue harmonic imaging compared with grey scale imaging.
- Discuss the advantages and limitations of the various harmonic tissue imaging techniques (better border and structure within tissue definition, increased penetration while maintaining spatial resolution)
- Illustrate the dHTI technique with reference to some clinical scenarios (renal and liver imaging).

SUMMARY

Exhibit will help radiologists to bring dHTI into their clinical work by facilitating an understanding of their physics principles.

Diagnostic Value of Grating-based X-ray Phase-contrast Imaging

LL-PHE3074

Marian Willner
Julia Herzen
Michael Chabior
Alexander A Fingerle , MD
Peter B Noel , PhD
Holger Hetterich , MD
Sigrid Auweter
Franz Pfeiffer

PURPOSE/AIM

Grating-based X-ray phase-contrast imaging is an emerging modality that is based on a fundamentally different image formation process compared to conventional attenuation-based imaging and might improve diagnostics in the future by providing additional information and enhanced soft-tissue contrast. The poster intends to give an overview of the potential clinical applications of this new multimodal imaging technique.

CONTENT ORGANIZATION

Selected results from breast, lung, cartilage, vascular and abdominal imaging are presented to illustrate the three contrast mechanisms that can be accessed by grating-based X-ray phase-contrast imaging: conventional attenuation contrast, phase contrast (refraction) and dark-field contrast (scattering). Furthermore, the examples are used to discuss the possibilities of combined data analysis as well as the respective limitations.

SUMMARY

The education exhibit is meant to provide insight into the diagnostic capabilities of grating-based X-ray phase-contrast imaging and its potential clinical benefits.

The Apparent Diffusion Coefficient Value Does Not Depend on the Field Strength and the System Units of Different Vendors for Certain Ranges of Scanning Parameters

[Back to Top](#)**LL-PHE4163**

Akio Ogura
Masanori Ozaki
Takayuki Tamura
Tsukasa Doi
Koji Fujimoto , MD, PhD
Mitsuyuki Takahashi
Tosiaki Miyati , PhD
Yukiko Itoh
Fumie Maeda
Hiroyuki Tarewaki

PURPOSE/AIM

purpose of Aim of the exhibit

1. To review precision of the apparent diffusion coefficient (ADC) value in magnetic resonance imaging.
2. To identify whether the same ADC value can be obtained in certain scanning parameter ranges for different system units and different field strengths.
3. To develop a method for obtaining highly precise ADC values.

CONTENT ORGANIZATION

1. A phantom study of different scanning parameters (e.g., TR, TE, b-value, FOV, slice thickness) considering different field strengths and system units of different vendors.
2. Study of the human brain using different scanning parameters for different field strengths and system units of different vendors.
3. Comparison of the coefficient of variation in ADCs under various scanning conditions.

SUMMARY**The major teaching points of this exhibit are:**

The ADC values are affected by a low signal-to-noise ratio in the diffusion weighted images. In addition, the averaging time was not effective in improving the precision of the ADC values. Therefore, for obtaining high precision ADC value, FOV and slice thickness must be increased instead of increasing the averaging time.

The certain ranges included TR > 2000ms, shortest TE, same b-values, and sufficient SNR.

When Good Lead Aprons Go Bad

[Back to Top](#)**LL-PHE4164**

Franklin Nwoke , MD *
Rydhwana Hossain , MD
James E Silberzweig , MD

PURPOSE/AIM

1. To review current standards for evaluation and disposal of radiation protection garmets.
2. To discuss the criteria for acceptance or rejection of aprons after inspection.
3. To graphically illustrate the steps involved in the quality control, visual, fluoroscopic, and CT inspection of the aprons.
4. To discuss the importance of proper disposal of damaged lead aprons according to federal hazardous waste regulations.
5. To review the advantages and disadvantages of non- lead aprons.

CONTENT ORGANIZATION

-Joint Commission standards regarding evaluation and inspection of Lead Aprons

- Apron tracking
- Visual Inspection
- Fluoroscopic Inspection
- CT Inspection
- Visual illustration of Inspection Protocol
- Disposal of aprons
- Non-Lead aprons

SUMMARY

1. Apron inspection is a requirement of radiation control programs.
2. Aprons should be evaluated at least annually with visual, fluoroscopic or CT inspection and acceptance or rejection should be on the basis of evidence based criteria.
3. Lead Aprons contain hazardous material, necessitating specialized and environmentally sound disposal procedures.
4. Non-lead aprons offer several advantages including ease of disposal but are limited by durability and adequacy of protection against radiation at higher energy levels.

Intravoxel Incoherent Motion MR Imaging: Basic Principles and Clinical Applications

[Back to Top](#)

LL-PHE4165

Chong Hyun Suh, MD
Ho Sung Kim
Hee Mang Yoon, MD
Seung Soo Lee, MD
Namkug Kim, PhD
Choong Gon Choi, MD
Sang Joon Kim, MD

PURPOSE/AIM

The purpose of this exhibit is:

1. To define basic principles of intravoxel incoherent motion (IVIM) MR imaging
2. To discuss the advantages, drawbacks of IVIM MR imaging
3. To present a systematic review of literature on clinical applications of IVIM MR imaging

CONTENT ORGANIZATION

1. IVIM MR basic principles.
 - IVIM model: perfusion fraction (f), diffusion coefficient (D), pseudodiffusion (D*)
 - Sequence: selection of b values, diffusion gradient polarity, breathing acquisition
 - Simplified biexponential models: Le Bihan's simplified method, Lucaiani method, Sigmund method
2. Advantages and drawbacks of IVIM MR imaging
3. Clinical Applications of IVIM MR imaging.
 - Liver: liver cirrhosis, NAFLD, Sorafenib treatment in advanced HCC, metastasis
 - Brain: brain perfusion measurement, malignant brain tumor
 - Head and Neck: salivary gland tumor
 - Genitourinary: prostate cancer, renal tissue under hydration and furosemide flow challenges
 - Pancreas: pancreas cancer

SUMMARY

1. IVIM MR imaging can simultaneously measure the diffusion and perfusion characteristics of lesions without administration of contrast material.
2. IVIM MR imaging can be a non-contrast, noninvasive imaging method for assessing the diffusion and perfusion characteristics of lesions especially in patients with compromised renal function.

Digital Breast Tomosynthesis: Selection of Appropriate Reconstruction Algorithm and Radiation Dose

[Back to Top](#)

LL-PHE4166

Tsutomu Gomi, PhD
Katsuya Fujita, BSc
Tokuo Umeda, PhD
Tohoru Takeda, MD, PhD
Akiko Okawa, MD, RN

PURPOSE/AIM

1) To use filtered back projection (FBP) and iterative reconstruction (IR) to identify indications of digital tomosynthesis (DT) for various radiation doses, 2) to compare DT and radiography, and 3) to select an appropriate reconstruction algorithm and radiation dose for breast lesion detection.

CONTENT ORGANIZATION

1. Overview of FBP and IR algorithms (simultaneous iterative reconstruction techniques; SIRT) for DT and radiography
2. Diagnostic imaging properties
 - Efficacy in normal structure and lesion detection
 - Effects of artifact images
3. Parameter review
 - Contrast-to-noise ratio
 - Root mean square error
 - Artifact spread function [Wu et al. Med. Phys. 31, 2636 (2004)]
 - Average glandular dose
 - Blur
 - Clinical relevance
4. Summary

SUMMARY

DT reveals improved visibility of superimposed structures and can suppress streak artifacts after appropriate IR algorithm selection, which suggests that DT with IR rather than FBP should be further evaluated. The IR algorithm might be the best imaging technique for identification of high-frequency features. Understanding the potential of DT with IR for selecting radiation doses might improve its diagnostic accuracy in clinical applications.

I'm Picking Up Good Vibrations: Optimizing Your Doppler Studies

[Back to Top](#)

LL-PHE4167

Jill A Jones, MD
Eva Diehls, BA, BS
Stanton J Rosenthal, MD

PURPOSE/AIM

In order to ensure high-quality exams, the interpreting provider should have a general understanding of the technical parameters that go into a Doppler Ultrasound study. The purpose of this exhibit is to strengthen this knowledge by: 1) Reviewing practical ramifications of the Doppler Shift equation; 2) Illustrating key Doppler variables and how changes in each parameter can impact image quality; 3) Providing case-based reviews of common Doppler errors

CONTENT ORGANIZATION

This educational exhibit will begin with a review of the Doppler equation. Commonly used Doppler variables will be discussed, including transducer selection, color box size, color gain, color velocity, Pulse Repetition Frequency (PRF) scale, spectral gate size, spectral gain, spectral baseline, and angle correction. Examples will demonstrate the effect modifications of these variables have on the final image. The exhibit will conclude with case reviews of common Doppler mistakes, including corrections that improve image quality.

SUMMARY

Properly performed Doppler ultrasound can answer a wide variety of clinical questions, improving efficiency by eliminating the need for more expensive or invasive studies. The exhibit clarifies important technical aspects which radiologists need to know in order to tailor Doppler studies and avoid diagnostic errors.

CT Model-Based Iterative Reconstruction Technique: Pearls, Pitfalls, and Practical Solutions

LL-PHE4168

Nicolaus A Wagner-Bartak , MD
Corey T Jensen , MD
Xiujiang J Rong , PhD
Erik K Paulson , MD
Dianna D Cody , PhD *
Eric P Tamm , MD

PURPOSE/AIM

To provide an overview of model-based iterative reconstruction (MBIR, GE Healthcare), its unique requirements and its significant impact on reducing noise and facilitating dose reduction.

To review the various CT image artifacts, limitations, and potential solutions for working with MBIR.

CONTENT ORGANIZATION

- A. Overview of exhibit
- B. Background of MBIR
- C. Advantages of MBIR - Impact on noise and dose reduction
- D. Unique requirements of MBIR - networking, server cooling requirements, increased processing time.
- E. Pitfalls of MBIR

Imaging limitations and artifacts with potential solutions:

Concentric ring artifact from motion

Breast shield artifact

Challenges of lean patients/paucity of intraabdominal fat

Truncation artifact associated with large patients

Impact of pitch on MBIR image quality at same dose

Transient ghosting artifact

F. Challenges of working with automatic tube current modulation to maximize dose savings with MBIR

G. Summary

H. References

SUMMARY

MBIR has tremendous promise for reducing CT radiation dose, however, there are challenges that one must be aware of but that can be overcome with a variety of creative solutions, detailed in this exhibit.

Advanced Techniques in Non-contrast-enhanced Hepatic MR Angiography[Back to Top](#)**LL-PHE4169**

Hiroyoshi Isoda , MD
Hironori Shimizu
Seiya Kawahara , MD
Tsuyoshi Ohno
Rikiya Yamashita
Akihiro Furuta
Kaori Togashi , MD, PhD *

PURPOSE/AIM

To learn the technical principles and features of the new techniques for non-contrast-enhanced (NCE) hepatic MR angiography (MRA), including multi-channel radiofrequency (RF) transmission technique at 3T, short tau inversion recovery (STIR) method, spin labelling method using flow-out method, and localized shimming technique. To show the advantages of the new techniques in image quality and the clinical usefulness.

CONTENT ORGANIZATION

- A. Improved image quality using multi-channel RF transmission technique
- B. Comparison of image quality of NCE hepatic MRA acquired with two different fat suppression methods, the chemical shift selective method and STIR method
- C. Theory of two spin labelling methods; flow-in method and flow-out method
- D. Comparison of image quality and clinical usefulness between flow-in method and flow-out method
- E. Reduced artifact using localized shimming technique

SUMMARY

1. Multi-channel RF transmission technique improves image quality by minimized B1-inhomogeneity and increased signal-noise ratio.
2. The STIR method contributes to further suppression of the background signal and improves visualization of vasculatures.
3. NCE hepaticMRA with the flow-out method improves the visualization of vasculatures in comparison with the flow-in method.
4. Localized shimming technique improves image quality by reduced artifact.

Radiofrequency Coils for Musculoskeletal MR Imaging: Explanation and Tips for Radiologists[Back to Top](#)**LL-PHE4170**

Filippo Del Grande , MD, MBA
Francesco Santini , PhD
William A Edelstein , PhD *
John A Carrino , MD, MPH *

PURPOSE/AIM

- 1) Describe the physics and technology behind MR Radiofrequency (RF) coils.
- 2) Illustrate the optimal use and artifacts of RF coils.
- 3) Summarize implementation strategies for musculoskeletal MR imaging.

CONTENT ORGANIZATION

This educational exhibit will provide an overview of design, clinical use, and pitfalls of different types of RF coils. Presentation of classification of coils based on categories such as transmit and/or receive coil, volume or surface coil, and configuration such as simple (linear coil) or complex (Helmholtz, quadrature and multichannel coil). Review of the most important RF coil parameters such quality factor, sensitivity, homogeneity, filling factor and effective range will be provided. Illustration of parallel imaging enabled by multi-channel RF coils, including the features of different reconstruction techniques (k-space based and image based), acceleration factor misuse, and how to properly manipulate the numbers of directions. Demonstration of reconstruction algorithms such as sum of squares (SOS) and adaptive combine (AC) with implementation tips for use with different vendors.

SUMMARY

Understanding the theoretical and practical aspects of radiofrequency coils for Musculoskeletal MR imaging allows radiologists to improve image quality, reduce scan time, and avoid artifacts.

MRI Artifacts Sometimes Are Useful as Diagnostic Tools: Clinical Applications in Abdominal and Musculoskeletal MR Imaging[Back to Top](#)**LL-PHE4171**

Adriana C Montealegre Angarita
Xavier Merino , MD

Juan Pablo Salazar Gutierrez
Victor S Pineda , MD
Sarai Roche Valles , PhD
Rosa Dominguez-Oronoz , MD

PURPOSE/AIM

• Describe briefly the physical principles of the artifacts seen on Magnetic Resonance imaging (MRI). • Show examples of common pathologic conditions for which the use of the some artifacts can be advantageous for diagnosis. • Describe shortly methods for reducing MRI artifacts when they are not advantageous.

CONTENT ORGANIZATION

SUMMARY

Artifacts in MRI affects the diagnostic quality, and usually we try to minimize them, but sometimes they can be applied to help in the detection and characterization of lesions.

Thirty Years of Synthetic MRI: Current Advances with a Historical Perspective

[Back to Top](#)

LL-PHE4172

Hei Shun Yu , MD
Stephan W Anderson , MD
Osamu Sakai , MD, PhD *
Hernan Jara , PhD *

PURPOSE/AIM

Synthetic MRI is a maturing application of quantitative MRI (qMRI) whereby images of arbitrary and continuously adjustable contrast-weighting can be generated post-acquisition by means of a computer program that models the MRI scanning processes using qMRI maps as virtual patients. Synthetic MRI was first described almost thirty years ago when MRI technologies were embryonic and much less capable than today, particularly in terms of image quality and scan speed. The purpose of this exhibit is to review the physical principles and the advances of synthetic MRI over the past thirty years.

CONTENT ORGANIZATION

Synthetic MRI is based on multispectral qMRI (a.k.a. multi-parameter qMRI: PD, T1, T2, T2*, ADC, etc.). The three fundamental technologies of multispectral qMRI are:

- 1) Specialized qMRI pulse sequence(s), which are becoming increasingly efficient, multispectral, and powerful.
- 2) Parameter-mapping algorithms, which are becoming increasingly sophisticated and accurate.
- 3) Image synthesis algorithms for contrast navigation, which are becoming increasing versatile and friendly.

In this work, we will review the current status of the technologies listed above, as reported in the scientific literature.

SUMMARY

Scientific developments of synthetic MRI spanning the past thirty years will be reviewed and illustrated with an evolutionary perspective.

Model Based Iterative Reconstruction: Application in the Emergency Department for Abdominal Imaging in Young Patients

[Back to Top](#)

LL-PHE4173

Dinesh Kumar , MBBS
Lee M Mitsumori , MD, MS *
William P Shuman , MD *
Cryselia Smith , MD
Jared Strote , MD

PURPOSE/AIM

Review the use of Model Based Iterative Reconstruction (MBIR) technique in low dose CT imaging for abdominal emergencies in young patients.

CONTENT ORGANIZATION

1. Summarize MBIR and compare the technique with other available image reconstruction algorithms such as Adaptive Statistical Iteration Algorithm and Conventional Filtered Back Projection.
2. Outline the potential technical advantages of MBIR in terms of image noise reduction and how a radiologist can apply MBIR to perform low dose CT exams.
3. Describe our clinical experience with low-dose and ultra-low dose abdominal CT exams performed with the use of MBIR.
 - a. Advantages in reduction of the effective dose.
 - b. Disadvantages in terms image reconstruction time: Discuss the appropriateness of MBIR in emergent conditions and the resultant time delay.
 - c. Review exam protocols and parameter selection.
 - d. Clinical implementation and involvement of emergency department physicians.
 - e. Discuss special patient scenarios.
 - f. Effect of MBIR on artifacts when compared with other reconstruction techniques.

SUMMARY

MBIR is a new CT reconstruction algorithm that has the potential of achieving further dose reduction and improvements in image quality over other currently available CT image reconstruction techniques used in the ED.

Incorporating Estimates and Calculations of Absorbed Organ Dose from Radiopharmaceuticals into a Nuclear Medicine Protocol Management Intranet

[Back to Top](#)

LL-PHE4174

Nicholas B Bevins , PhD
Beth A Harkness , MS
Thomas Fletcher

PURPOSE/AIM

The purpose of this exhibit is:

1. To demonstrate how a central protocol database for nuclear medicine with absorbed dose information can assist in the clinical workflow,
2. To provide common sources of absorbed dose information for radiopharmaceuticals,
3. To explain how to combine all of this information in a useful and meaningful way.

CONTENT ORGANIZATION

1. Construction of a nuclear medicine protocol information website
2. Sources for absorbed dose information
3. Assembly of dose information into a user-friendly calculator
- Screenshots and examples
4. Incorporation of the calculator into the website and protocol descriptions

SUMMARY

The teaching points of this exhibit are:

1. Making absorbed dose information available to radiologists is beneficial to clinical workflow.
2. Common and free software can be used to improve the usability of dose references.

3. Absorbed dose information can be useful to radiologists, but education regarding the applicability of absorbed dose, and more importantly effective dose, to individual patients is still necessary.

Intravenous Contrast-enhanced CT: An Easy Overview from the Basis to the Phases

[Back to Top](#)

LL-PHE4175

Luis Azpeitia , MD
Jesus H Burboa Noriega , MD

PURPOSE/AIM

CONTENT ORGANIZATION

A) Contrast material pharmacokinetics. B) Vascular and parenchymal phases of contrast enhancement and their synonyms. C) Mono and multi-phasic injection protocols. D) Injection rate, volume and duration of intravenous contrast material. E) Scanning parameters. F) Important factors affecting contrast enhancement and scan timing. G) Common clinical applications.- Sample cases.

SUMMARY

1.- The most important application of dynamic scanning is diagnosis of focal organ disease. 2.- Understanding the basic concepts of contrast material pharmacokinetics and the pathophysiology involved in lesion detection plays an important role in determining an adequate scanning protocol. 3.- Optimizing and standardizing CT contrast-enhanced techniques can improve diagnostic precision.

Understanding the Principle, Image Characteristics, and Radiation Dose of Full- and Hybrid Iterative Reconstruction (IR) at CT

[Back to Top](#)

LL-PHE4176

Wataru Fukumoto
Toru Higaki , PhD
Fuminari Tatsugami
Yuko Nakamura , MD
Akira Taniguchi , RT *
Kazuo Awai , MD *
Takuji Yamagami
Yukiko Honda , MD
Yoko Kaichi

PURPOSE/AIM

1. Understand intuitively the principle of full iterative reconstruction (IR) and hybrid IR at CT
2. Compare the image characteristics of full- and hybrid IR, and of conventional filtered back projection (FBP) algorithms.
3. Describe the radiation dose reduction achieved by full- and hybrid IR.
4. Discuss full utilization of IR in clinical practice.

CONTENT ORGANIZATION

1. Intuitive understanding of the basic principles of image reconstruction
 - Filtered back projection (FBP) algorithm
 - Full iterative reconstruction (IR)
 - Hybrid iterative reconstruction
2. Comparison of the image characteristics of FBP, full IR, and hybrid IR
3. Dose reduction effect of full- and hybrid IR
4. Evaluation of the image characteristics of full- and hybrid IR from the standpoint of diagnostic capability

SUMMARY

Currently there are two type of IR: one is "full IR" from its primary meaning and the other is hybrid IR that is almost same as FBP in essentials, however, it includes various noise reduction techniques which were originally developed for full IR. Both of the techniques can reduce radiation dose in 50-80% as compared with FBP. Although physical image characteristics of full or hybrid IR images is different from that of FBP images, we should objectively validate image characteristics of them from the stand point of diagnostic capability.

Expanding the use of Flow-labeling MRI: Clinical Applications of the Time-spatial Labeling Inversion Pulse (Time-SLIP) Technique

[Back to Top](#)

LL-PHE4177

Wataru Fukumoto
Yuji Akiyama
Fuminari Tatsugami
Yukiko Honda , MD
Yoshimori Kassai , MS *
Kazuo Awai , MD *
Yuko Nakamura , MD
Shuji Date
Yoko Kaichi
Minoru Ishifuro

PURPOSE/AIM

1. Understand intuitively the principle of flow-labeling MRI using the time-spatial labeling inversion pulse (time-SLIP) technique
2. Demonstrate clinical applications of the time-SLIP technique
3. Discuss future aspects of flow-labeling MRI using the time-SLIP technique

CONTENT ORGANIZATION

1. Principle of the time-SLIP technique
2. Clinical applications of flow-labeling MRI
 - (a) Selective demonstration of visceral vessels evaluated preoperatively
 - (b) Demonstration of the peripheral arteries of the lower legs in diabetes mellitus patients
 - (c) Analysis of the cerebrospinal fluid flow
 - (d) Analysis of saliva secretion
 - (e) Analysis of pancreatic secretion
 - (f) Analysis of the urinary flow in patients with vesicoureteral reflux
3. Pitfalls at interpreting flow-labeling images

SUMMARY

Time-SLIP, a flow-labeling MRI technique based on arterial spin labeling does not require contrast media. It uses spatially non-selective IR- and spatially selective tag pulses to show regions and it can be used with FASE or true SSFP sequences. Time-SLIP can be applied not only for the visualization of vascular structures but also for analysis of the CSF flow, saliva and pancreatic secretion, and urine flow. We demonstrate various clinical applications of time-SLIP.

Benefit of 2D MR Spectroscopy with ProFit Quantitation: Applications to Hepatitis C, HIV and Hepatic Encephalopathy

[Back to Top](#)

LL-PHE4178

Rajakumar Nagarajan , PhD
Manoj K Sarma , PhD
Neil Wilson , BS
Michael A Thomas , PhD

PURPOSE/AIM

1. To explain the concept of two-dimensional (2D) localized correlated spectroscopy (L-COSY).
2. To demonstrate the advantage of using 2D Prior Knowledge Fitting (ProFit) algorithm compared to 1D MR Spectroscopy.
3. To demonstrate the cerebral metabolite changes in Hepatitis C, HIV and Hepatic Encephalopathy using 2D MRS with ProFit algorithm.

CONTENT ORGANIZATION

1. Introduction of 1D MRS and 2D MRS in the brain.
2. Concept of 2D L-COSY/ data interpretation.
3. Concept of ProFit algorithm.
4. Detection of more cerebral metabolites with better quantitation.
5. To demonstrate the advantage of 2D MRS with ProFit in Hepatitis C, HIV and Hepatic Encephalopathy.

SUMMARY

- The major teaching points of this exhibit are: 1. Teach the concept of 2D MRS and ProFit algorithm.
2. Illustrate the importance of metabolites quantitation using 2D MRS.
3. Show clinical applications that benefit from 2D MRS Quantitation.

Molecular Imaging through Near Infrared Methods: Review of Diffuse Optical Imaging in Breast Cancer

[Back to Top](#)

LL-PHE4179

Shwayta Kukreti , MD, PhD
Albert Cerussi , PhD
Bruce Tromberg , MD
Enrico Gratton , PhD

PURPOSE/AIM

Near-infrared (NIR) optical methods provide functional imaging based on changes in molecular composition. NIR techniques are sensitive to changes in breast physiology from disease by quantifying total hemoglobin, oxygen saturation, water, and fat content. Breast tumors demonstrate changes in these parameters, as well as other spectral shape changes, thereby providing molecular signatures of cancer. Here we review the principles tissue optics, diffuse optical spectroscopy, and diffuse optical tomography.

CONTENT ORGANIZATION

1. Principles of tissue optics, including the theory of light propagation into tissue, separation of absorption from scattering, and recovery of physiological parameters.
2. Diffuse optical spectroscopy provides focus on spectral resolution. We review techniques to obtain broadband data, including Steady State and Frequency Domain Photon Migration to obtain optical properties in the wavelength continuum of 650-1000nm.
3. Diffuse optical tomography specializes on spatial resolution. We review some of the instruments, including combined structural imaging modalities involving x-ray, ultrasound and MRI for improved resolution.

SUMMARY

Near infrared utilizes intrinsic molecular biomarkers. Diffuse optical imaging opens the possibilities for complementary imaging strategies which are non-invasive, and do not use radiation.

Sub-milli-Sievert CT with Multi-Vendor Iterative Reconstruction Techniques: Success and Failures

[Back to Top](#)

LL-PHE4180

Ranish D Khawaja , MBBS, MD
Sarabjeet Singh , MD
Subba R Digumarthy , MD
Michael A Blake , MBBS *
Mannudeep K Kalra , MD *
Jo-Anne O Shepard , MD *
Garry Choy , MD, MS
Atul Padole , MD
Sarvenaz Pourjabbar , MD
Diego A Lira , MD

PURPOSE/AIM

Increased CT use in modern practice has increased concerns over rising radiation dose. Still, for most CT examinations, radiation doses continue to remain between 2-20 mSv or higher. CT images acquired with less than 1 sub-milli-Sievert (SubmSv) can provide similar diagnostic information obtained with current standard of care CT. In this exhibit we aim to present if currently used and upcoming novel full and hybrid iterative reconstruction (IR) techniques can provide diagnostically acceptable CT images at such low dose.

CONTENT ORGANIZATION

1. Overview of multi-vendor IR techniques (**ASIR, VEO, SafeCT, iDose, IMR, iDOSE, SAFIRE, AIDR 3D**).
2. Protocols for SubmSv CT with above mentioned IR techniques.
3. Effect of these IR techniques on image quality and lesion appearance at SubmSv and standard of care CT doses.
4. Examples illustrating effect of IR techniques on SubmSv CT in (a) *adult abdominal CT*, (b) *adult chest CT*, and (c) *pediatric body CT*.

SUMMARY

Although dose reduction to less than 1 mSv is important and exciting, it must be assessed thoroughly to make it clinically useful. Simultaneously, the effect of IR techniques across different vendors must be taken into account to maintain a balance between image quality and diagnostic accuracy at such a low-dose. Our exhibit will highlight this concept with various examples from multi-vendor IR techniques.

Relationship between Patient Positioning, CT Number Variation, Image Noise and Dose and Possible Effect on Diagnosis

[Back to Top](#)

LL-PHE4181

Jie Zhang , PhD
Nathan Hill
Flavius D Raslau , MD
Edward J Escott , MD *

PURPOSE/AIM

To provide an overview of the effects of patient positioning on mean CT number, image noise and radiation dose during CT examinations and the possible effects on diagnosis.

CONTENT ORGANIZATION

1. To review correlation between patient positioning and the effect of the beam shaping bowtie fil-ter.
2. To review the effects of mismatch between positioning off of iso-center and bowtie filter on mean CT number, noise and radiation dose.
3. To describe the above effects with various acquisition techniques (e.g., tube current modulation on/off)

4. To present a clinical case demonstrating potential misdiagnosis due to patient malpositioning.

SUMMARY

The beam shaping bowtie filter is a very important element provided on modern CT scanners to reduce radiation dose while maintaining diagnostic image quality. However, the efficiency of this filter can be significantly influenced by patient positioning, and in some scenarios, may lead to misdiagnosis due to changes in mean CT numbers, artifact and/or image noise. This overview will help the radiologist understand the relationship between patient positioning, CT number variation, and dose, and the possibility of misdiagnosis by demonstrating these effects with phantom experiments and presenting a clinical case.

Current Techniques and Clinical Usefulness of Non-mammographic Digital Tomosynthesis: What the Radiologist Needs to Know

[Back to Top](#)

LL-PHE4182

Haruhiko Machida, MD
Toshiyuki Yuhara
Masayasu Asanuma
Isao Tanaka
Eiko Ueno, MD
John M Sabol, PhD *
Takuya Nishino
Etsuko Tate

PURPOSE/AIM

1. To describe the basic principles and current techniques of non-mammographic digital tomosynthesis (DT)
2. To demonstrate various non-mammographic DT applications by presenting clinical images
3. To illustrate both the clinical advantages, limitations and optimal strategies of the DT

CONTENT ORGANIZATION

1. Basic principles and current techniques

- DT radiography/fluoroscopy
- image filter/acquisition parameters
- FBP/iterative reconstruction

2. Clinical applications

- pulmonary nodule/TB
- fracture/postoperative follow-up (metallic implant)
- sinonasal/dental disease
- urography/upper GI/Ba enema/ERCP

3. Clinical advantages, limitations and optimal strategies

- improved anatomical visualization/diagnostic accuracy (vs. non-DT radiography/fluoroscopy)
- less dose/metallic artifact/dependency on patients' posture (vs. CT)

SUMMARY

DT easily and swiftly provides tomographic images of selected regions of the body with arbitrary posture in radiography and fluoroscopy. A wide variety of non-mammographic DT applications are clinically useful. DT can improve anatomical visualization and diagnostic accuracy compared to non-DT radiography or fluoroscopy; reduce radiation dose and metallic artifacts with dedicated image filters and iterative reconstruction, and improve workflow and cost-effectiveness compared to CT.

The Combined Application of New Techniques: Spectral CT Imaging and Adaptive Statistical Iterative Reconstruction (ASiR)

[Back to Top](#)

LL-PHE4183

Ying Yu
Na Gao
Hong-Yan Cheng

PURPOSE/AIM

- To describe the basic principles and illustrate with clinical data and images the utility of spectral CT Imaging and ASiR
- To illustrate advantages and limitations of Spectral CT imaging
- To demonstrate with clinical data and images the clinical impact in the combination of spectral CT Imaging with ASiR

CONTENT ORGANIZATION

SUMMARY

Spectral CT imaging, which is different from conventional CT imaging, provides more clinical applications. The combination of spectral CT imaging with ASiR makes it possible to get better image quality and more radiation dose reduction than spectral CT imaging with FBP.

Integrated Circuit Detector in Clinical CT Examinations

[Back to Top](#)

LL-PHE4184

Naoki Nagasawa, RT, PhD
Kakuya Kitagawa, MD, PhD
Akio Yamazaki, RT
Naoya Kubooka, RT
Hajime Sakuma, MD *

PURPOSE/AIM

To describe the principle of integrated circuit detector

To learn advantages and current limitations of integrated circuit detector in comparison with other conventional detector

To explain the utility of integrated circuit detector in chest, coronary, myocardium and abdominal CT examinations

CONTENT ORGANIZATION

Principle of specific integrated circuit detector

Comparison of integrated circuit detector with conventional detector in phantoms and clinical cases

- (a) Signal-to-noise (SNR, MTF, NPS)
- (b) Effective Slice thickness (SSPz)
- (c) Artifacts reduction
- (d) Spatial resolution

Low dose CT using integrated circuit detector? How much reduction can we achieve?

Benefits of integrated circuit detector in chest, coronary, myocardium and abdominal CT examinations

SUMMARY

A recently introduced detector combining the photodiode and the ADC to an integrated circuit can potentially improve image quality, spatial resolution and artifacts by means of reduced cross talk between detector channels. Substantial dose reduction can be achieved without compromising the image quality especially in low-dose and large patient scans. Moreover, higher spatial resolution (0.3x0.3x0.3mm) allows for improved evaluation of coronary artery stenosis and stents.

Photoacoustic Imaging: A Laser-based Technology for Real-time, Simultaneous Structural and Functional Imaging

[Back to Top](#)

LL-PHE4185

Daniela Berritto , MD
Francesca Iacobellis , MD
Maria Paola Belfiore
Giuliano Gagliardi
Luca Saba , MD
Andrea Laghi , MD *
Maria A Mazzei , MD
Dieter Fichs *
Roberto Grassi , MD

PURPOSE/AIM

Photoacoustic imaging imparts the sensitivity and specificity of optical imaging in distinguish materials according to their differences in optical absorption (ie, their colors), with the high spatial and temporal resolution of ultrasonography (US). This technology has been specifically designed for non-invasive real-time in vivo research in small animals.

The aim of this study is to present the photoacoustic imaging system, an emerging laser-based technology, and its application in preclinical real-time imaging.

CONTENT ORGANIZATION

A. Physics principles of photoacoustic imaging B. The Technology: photoacoustic imaging equipment C. The Applications: our preliminary experience on animal models

SUMMARY

This new technology represents an innovative tool in the preclinical research. This exhibit reviews

- a. the physics principles of a laser-based technology
- b. the photoacoustic imaging equipment and some applications
- c. the advantages and disadvantages of photoacoustic imaging

Beam-hardening and Metallic Artifacts Correction Using Single-source Dual-Energy Spectral CT Imaging

[Back to Top](#)

LL-PHE4186

Chuang Yi
Zhiren Chen , MD
Yan Liang , MMed
Chao Cheng
Yongfang Yin
Haiying Mao
Huizhi Cao

PURPOSE/AIM

1) To understand typical beam-hardening artifact in clinical images and why virtual monochromatic images are naturally free of beam-hardening artifact.

2) To demonstrate the advantage of virtual monochromatic images with extra metallic artifact reduction technique (MARs) in a significant reduction metal artifact.

3) To summarize the experience of phantom and clinical study on selecting optimal keV to reduce artifact while remaining the best CNR .

CONTENT ORGANIZATION

1) Various beam-hardening and metal artifacts artifacts in traditional CT examination.

2) Principle of virtual monochromatic imaging using rapidly switching the dual kVp and what is MARs.

3) Monochromatic image demonstrating a significant reduction in artifact from phantom experiment and clinical study

1. Optimal keV and Scan parameters to remove artifacts near contrast agents or bones .

2. Optimal keV with MARs to remove artifacts near metal .

3. Experimental data and various clinical images

SUMMARY

1) This exhibit will be useful to understand the reason and drawback of beam-hardening and metallic artifact.

2) The virtual monochromatic images provide few beam-hardening artifact and lower metallic artifact with MARs.

3) This exhibit is useful to give guide line for optimal keV and when to use MARs in clinical diagnosis.

Recent Improvements and Challenges in Low Contrast and Low Radiation Dose CT: How Low Can We Go?

[Back to Top](#)

LL-PHE4187

Takeshi Nakaura , MD
Masafumi Kidoh
Ryo Itatani
Shinichi Nakamura , MD
Kazunori Harada
Yasuyuki Yamashita , MD *

PURPOSE/AIM

Low kilo-voltage (kVp) CT is well suited for low contrast and low radiation dose CT; however, increased image noise is a problem. To solve this problem, the knowledge about the iterative reconstruction and the adjustment of the tube current setting might be important. We aim to demonstrate the strategies to perform the low contrast and low radiation dose CT without deterioration of image quality.

CONTENT ORGANIZATION

1) Principles of the low kVp CT.

2) How to adjust the tube current setting for low kVp CT.

3) Advantages of iterative reconstruction technique for low kVp scan as compared with filtered back projection.

4) Clinical images from patients with various diseases (liver tumors, ischemic heart disease etc.) scanned with low contrast and low radiation dose CT.

SUMMARY

The major teaching points of this exhibit are:

1. The low kVp and suitable tube current setting offers up to 50% lower contrast and radiation dose reduction without deterioration of image quality.

2. Iterative reconstruction techniques reduce image noise and various artifacts without deterioration of special resolution, and are well suited for low contrast and low radiation dose CT with low kVp setting.

AAPM/RSNA Physics Tutorial for Residents: Control of Dose in Computed Tomography

Saturday, 12:00 PM - 02:00 PM • E351

[Back to Top](#)

QA PH CT

SPPH01 • AMA PRA Category 1 Credit™:2 • ARRT Category A+ Credit:2

Moderator

Richard J Massoth, PhD

LEARNING OBJECTIVES

1) To describe the underlying physics of CT Dose and the technical factors which affect patient dose. 2) To understand different approaches to image reconstruction and their contribution to patient dose reduction. 3) How to develop and review low dose protocols for CT.

SPPH01A • Factors that Affect CT Dose and Dosimetry Methods

Jerry A Thomas MS (Presenter) *

SPPH01B • Image Reconstruction Techniques which Contribute to Patient Dose Reduction

Richard J Massoth PhD (Presenter)

SPPH01C • Low Dose Protocols - Source and Review Methodology

Jerry A Thomas MS (Presenter) *

AAPM/RSNA Tutorial on Equipment Selection: Imaging Systems Designed to Reduce CT Dose and Maintain Image Quality

Saturday, 02:15 PM - 04:15 PM • E351

[Back to Top](#)

QA PH CT

SPPH02 • AMA PRA Category 1 Credit™:2 • ARRT Category A+ Credit:2

Moderator

Jerry A Thomas, MS *

LEARNING OBJECTIVES

1) To understand the differences in design and imaging reconstruction in commercial systems designed for CT imaging and aftermarket image post processing systems. 2) To appreciate the impact dose reduction techniques have on image quality and the clinical management of disease. 3) To develop a business model for incorporating dose reduction into CT imaging.

SPPH02A • Image Equipment Overview - CT Dose Reduction Techniques

Jerry A Thomas MS (Presenter) *

SPPH02B • Impact of Dose Reduction on Image Quality and Medical Diagnosis

Richard J Massoth PhD (Presenter)

SPPH02C • Building a Business Case for Dose Reduction Technologies in CT

Jerry A Thomas MS (Presenter) *

Physics (CAD I)

Sunday, 10:45 AM - 12:15 PM • S403B

[Back to Top](#)

PH IN CT

SSA19 • AMA PRA Category 1 Credit™:1.5 • ARRT Category A+ Credit:1.5

Moderator

Heang-Ping Chan, PhD

Moderator

Kyongtae T Bae, MD, PhD *

SSA19-01 • Virtual Colon Tagging Based Dual-energy Electronic Cleansing for Fecal-tagging CT Colonography

Wenli Cai PhD (Presenter) ; **Se Hyung Kim** ; **Da Zhang** PhD ; **June-Goo Lee** PhD ; **Yasuji Ryu** MD ; **Hiroyuki Yoshida** PhD *

PURPOSE

Material decomposition ability in dual-energy CT (DE-CT) provides a promising solution to identify tagged fecal materials in electronic cleansing (EC) for fecal-tagging CT colonography (CTC). The purpose of this study was to develop and evaluate a novel dual-energy electronic cleansing (DE-EC) scheme based on 'virtual colon tagging' (VCT) for minimizing EC artifacts in the cleansed CTC images.

METHOD AND MATERIALS

Based on our localized three-material decomposition model for DE-CT, we developed a DE-EC scheme denoted as VCT-EC, with the following steps: 1) DE-CTC images were decomposed into three material mixture fields of luminal air, soft tissue, and iodine-tagged fecal material; 2) a Poisson-based derivative smoothing algorithm smoothed the gradients and implicitly smoothes each material mixture field; 3) VCT images were calculated by virtually elevating the CT value of luminal air to be as high as that of tagged fecal materials and thus virtually tagging the entire colonic lumen, and 4) the entire colonic lumen was segmented and thus cleansed by its high values in VCT images. Twenty-one patients underwent a bowel preparation with a low-fiber, low-residue diet, and oral administration of iodine contrast agents. Dual-energy CT scanning (SOMATOM Definition Flash) was performed at two photon voltages of 140 kVp and 80 kVp with the automatic dose exposure control module (CARE Dose 4D) in both supine and prone positions. Resulting DE-CTC data were subjected to VCT-EC scheme. For comparison purpose, we applied a conventional single-energy EC (SA-EC) to the standard fused DE-CTC images.

RESULTS

A visual assessment was performed by two radiologists for evaluating the cleansing quality by counting of the regions with distractive cleansing artifacts observed in the fly-through of the colon. Compared to SA-EC, the total number of EC artifacts in VCT-EC was reduced significantly by 72%. In specific, the numbers of three types of EC artifacts were reduced by 63% (type1 - caused by pseudo-enhancement), 75% (type 2 - caused by partial volume effect), and 70% (type 3 - caused by inhomogeneous tagging), respectively.

CONCLUSION

Our VCT-based DE-EC scheme provides an effective solution for significantly reducing EC artifacts by use of the material decomposition ability in dual-energy CT.

CLINICAL RELEVANCE/APPLICATION

New dual-energy EC method can substantially reduce EC artifacts and it may lead to artifact-free visualization of the colon.

SSA19-02 • Computer Aided Detection of Ureter Abnormalities on Multi-detector Row CT Urography

PURPOSE

To develop a CAD system for automated detection of ureter abnormalities in multi-detector row CT urography, which potentially can assist radiologists in detecting ureter cancer.

METHOD AND MATERIALS

Our CAD system consists of two stages. In the first stage, an automatic tracking of the ureter is performed by previously proposed COMbined Model-guided Path-finding Analysis and Segmentation System (COMPASS). Given an initial starting point, the ureter is tracked by COMPASS based on the CT values of the contrast filled lumen. In the second stage, lesion candidates are identified using histogram analysis within the ureter to differentiate the abnormality from the background, which is the ureter filled with contrast material. A uniformity measure is designed to detect non-uniformity of the CT values within the ureter volume. If an abnormality is present in the ureter, the uniformity of the CT values will be distorted and reduce the uniformity measure. The size and shape of the detected region further differentiate lesions from noise. In this pilot study, a limited data set of 15 patients (13 malignant and 2 benign) with biopsy-proven ureter lesions was used. Experienced radiologists identified 30 biopsy-proven ureter lesions (25 cancers and 5 benign) on the multi-detector row CT images. The average lesions size was 3.4 mm (range: 2.1 mm – 7.6 mm). The average conspicuity was 3.5 (range: 2 to 5) on a scale of 1 to 5 (5 very subtle).

RESULTS

The COMPASS successfully tracked the ureters in all patients. 90% (27/30) of the ureter lesions including 88% (22/25) of the ureter cancers were detected with 2.5 (37/15) false positives per patient. The three missed cancers were small lesions with average size of 2.2 mm.

CONCLUSION

The preliminary results show that our COMPASS and CAD system can track the ureter and detect ureter cancer of medium conspicuity and relatively small size. Further study is underway to improve the detection performance with a larger data set. This pilot study is a first step towards the development of a CAD system for detection of ureter cancer in multi-detector row CT urography.

CLINICAL RELEVANCE/APPLICATION

An accurate CAD system has the potential to assist radiologists in detection of ureter cancers at an early stage which usually are small in size with subtle appearance.

SSA19-03 • Detecting Vertebral Degenerative Disease on 18F-NaF PET/CT Using a Novel Cortical Shell Map

Jianhua Yao PhD * ; **Hector Munoz** ; **Joseph E Burns** MD, PhD ; **Karen A Kurdziel** MD * ; **Peter L Choyke** MD * ; **Le Lu** PhD ; **Ronald M Summers** MD, PhD (Presenter) *

PURPOSE

Vertebral degenerative disease can mimic metastatic disease on 18F-NaF PET/CT. The purpose of this study is to develop a computer system to automatically detect vertebral degenerative disease on 18F-NaF PET/CT.

METHOD AND MATERIALS

The dataset consisted of 46 18F-NaF PET/CT scans (36 men, 10 women, mean age 65±9 yrs). All patients were scanned on a Philips GEMINI TF scanner. The PET resolution was 4*4*4mm. The CT portion of the studies was performed with 5mm slice thickness and without intravenous contrast. The PET data was first resampled to have the same resolution as the CT data. The spine was segmented on the CT images. The cortical shell of each vertebral body was then extracted and unwrapped to a 2D map using a cylindrical coordinate system. The maps were stacked to form a panoramic map of the spinal column (figure). The novel panoramic cortical shell map converted the complex 3D detection problem to a 2D problem. Morphological and physiological features derived from both CT and PET were projected onto the map. A three-tier classification scheme was then applied to detect spinal degenerative osteophytes. The annotated location markers for the osteophytes were used as the reference standard to train the classifiers at each stage. The system was trained on 20 cases and tested on 26 cases. The performance was evaluated using FROC analysis.

RESULTS

The numbers of osteophytes larger than 5mm were 163 and 179 in the training and testing sets, respectively. The sensitivities and false positives per case were 82.2% and 4.7, and 77.1% and 4.6 for the training and test sets respectively. The performance with CT and PET data alone were 69% (4.7) and 59% (4.4) respectively. Missed osteophytes were most commonly due to image artifact. Common false positives include the costovertebral junction and partial volume averaging.

CONCLUSION

This is the first CAD system to detect spinal osteophytes on 18F-NaF PET/CT. The novel unwrapped cortical shell map facilitates the detection and visualization of degenerative disease. The combination of PET and CT features improved the performance of CAD.

CLINICAL RELEVANCE/APPLICATION

By enabling the detection of degenerative change on PET/CT, it may in future be possible to exclude such areas from the images to improve the ability of physicians to perceive metastatic lesions.

SSA19-04 • Automated Axial Right Ventricle to Left Ventricle Diameter Ratio Computation in Computed Tomography Pulmonary Angiography (CTPA)

German Gonzalez PhD (Presenter) ; **Kanako K Kumamaru** MD, PhD ; **Daniel Jimenez-Carretero** MSc ; **Elizabeth George** MBBS ; **Maria J. Ledesma-Carbayo** PhD ; **Frank J Rybicki** MD, PhD * ; **Sara Rodriguez-Lopez** ; **Raul San Jose Estepar** PhD ; **Dimitris Mitsouras** PhD ; **Arash Bedayat** MD

PURPOSE

The RV/LV diameter ratio is a proven metric of prognosis in patients with CT pulmonary angiography (CTPA) findings of acute pulmonary embolism (PE). The purpose of this report is to introduce and test, using radiologist and clinical outcomes reference standards, a completely automated algorithm to output the right ventricular to left ventricular (RV/LV) diameter ratio from CTPA images.

METHOD AND MATERIALS

A completely automated algorithm with the following six steps was designed to compute the RV/LV diameter ratio. Step 1: image pre-processing. Step 2: right and left heart detection based on machine-learning techniques. Step 3: detection on clustering and seed positioning. Step 4: septum detection. Step 5: right and left heart segmentation based on level-sets with curvature constraints and edge priors. Step 6: caliper positioning and ratio computation. Implemented in Matlab, the algorithm analyzes 600 CTPA reconstructed slices in 10 minutes (Intel i7 computer). Automated reports with snapshots of the slices where the RV and LV diameters are found are sent to the physician for reporting. The algorithm was tested in 198 consecutive patients with acute PE diagnosed with CTPA using (a) reference standard RV/LV radiologist measurements and (b) 30-day PE-specific mortality plus the need for intensive therapies.

RESULTS

Using radiologist reference standard, the algorithm correctly detected and segmented 96% (190/198) of CTPA studies. Even including failure cases, the correlation between the RV/LV diameter ratio obtained by the algorithm and that obtained by the radiologist was high ($r=0.72$). Compared to the radiologist, the algorithm equally achieved high accuracy in predicting 30-day PE-specific mortality plus the need for intensive therapies, with area under the curve of 0.74 for the automated method and 0.77 for the radiologist measurements. Failure cases were readily identified by the output snapshots available to the radiologist.

CONCLUSION

An automated algorithm for determining the CT derived RV/LV diameter ratio in patients with acute PE has high accuracy when compared to measurements made by a radiologist and prognostic significance when tested against reference standard outcomes.

CLINICAL RELEVANCE/APPLICATION

An automated RV/LV diameter ratio algorithm has promise to generate data for prognosis in patients with acute PE that can be readily implemented into clinical reporting.

SSA19-05 • Computer-aided Diagnosis (CADx) as a Surrogate Measure of Image Quality: Dependence of CADx Performance on Reconstruction Parameters in Dedicated Breast CT

Ingrid Reiser PhD (Presenter) ; **Robert M Nishikawa** PhD * ; **John M Boone** PhD * ; **Karen K Lindfors** MD * ; **Kai Yang** PhD

PURPOSE

The purpose of this work was to investigate whether the performance of computer-aided diagnosis (CADx) of breast masses in CT images with different reconstructions parameters can serve as surrogate measure for image quality. The first step towards this goal is an investigation into the relationship between reconstruction parameters and CADx performance, which is presented here.

METHOD AND MATERIALS

The data set consisted of cone-beam breast CT data from 69 patients containing 78 masses (24 benign, 54 malignant). 3cm³ regions-of-interest centered on each mass were reconstructed with the FDK reconstruction algorithm. Volumes were generated for two apodization filter cut-off values (L=1.0 and L=0.5) and three reconstructed image voxel sizes (150 μm, 300 μm and 450 μm isotropic). All parameters produced images that were visually judged to be of diagnostic quality. From each set of ROIs, lesions were segmented and feature analysis was performed using algorithms that were developed previously. Three features were manually selected to ensure that variation in CADx performance was due to different image parameters rather than different feature sets. ROC analysis was used to estimate CADx performance in the task of distinguishing benign from malignant lesions using a leave-one-out resampling scheme.

RESULTS

Visually, reconstruction parameters affected the sharpness and apparent noise of the images. As expected, L=0.5 produced smoother images than L=1.0, and images with smaller voxel size had a noisier appearance. CADx performance, measured as area under the ROC curve (AUC), ranged between 0.78 and 0.86, with larger reconstructed voxels, and smoother images (L=0.5) producing higher AUC values. This trend was also observed for individual features.

CONCLUSION

Our study indicates that CADx performance depends on reconstruction parameters and therefore it has the potential to measure the quality of the reconstructed images. The next step of this research is to measure the correlation between CADx and radiologists' performance as reconstruction parameters are changed.

CLINICAL RELEVANCE/APPLICATION

This CADx methodology has potential for assessing clinical performance of reconstruction algorithms, and ultimately to improve diagnostic accuracy by optimizing CT reconstruction.

SSA19-06 • Computerized Risk Assessment Imaging System for Predicting the Likelihood of Breast Cancer

David Izhaky PhD (Presenter) * ; **Tamar Sella** MD ; **Maya Cohen** MD ; **Arnaldo Mayer** PhD * ; **Tanir Allweis** MD ; **Miriam Sklair-Levy** MD *

PURPOSE

Early detection and prevention strategies for breast cancer depend on the ability to accurately identify individuals with significantly increased breast cancer risk. Currently, such risk assessment models are statistical in nature and rely mainly on clinical features such as genetic susceptibility, family history or mammography breast density. The purpose of this study is to develop a computerized imaging system and method for assessing the likelihood of a malignant tumor based on breast vascular maps.

METHOD AND MATERIALS

3D breast vascular maps of 334 women were included in the study. IRB approval was obtained. Vascular maps were acquired using a prototype 3D functional infrared imaging device (Real Imaging). Of these 334 women, 209 were healthy (mammography BIRADS 1), 36 had benign lesions (mammography BIRADS 2) and 94 had biopsy proven breast cancer. A linear discriminant classifier with feature selection which was previously trained to compute the cancer likelihood on image dataset was applied. Analysis was blinded to clinical and pathological diagnosis. The diagnostic accuracy of the breast cancer likelihood was evaluated using receiver-operating characteristic (ROC) analysis and bootstrapping.

RESULTS

An area under the ROC curve of 0.84 (95% CI 0.77-0.89) was obtained for determining the cancer likelihood.

CONCLUSION

A risk assessment model for predicting the likelihood of malignant tumor based on vascular maps was developed. The results warrants further evaluation in a larger population-based clinical trial.

CLINICAL RELEVANCE/APPLICATION

A novel imaging system and method for assessing the likelihood of breast cancer was developed with accurate performance. This technology could be implemented as an adjunct to mammography.

SSA19-07 • Effect of Adaptive Iterative Dose Reduction (AIDR 3D) on a Computer-aided Detection System for Lung Nodules: Performance Evaluation Using CT Scans in Standard to Ultra-low-Dose Range

Sumiaki Matsumoto MD, PhD (Presenter) * ; **Yoshiharu Ohno** MD, PhD * ; **Takatoshi Aoki** MD, PhD ; **Tae Iwasawa** MD, PhD ; **Fumito Okada** MD ; **Kota Aoyagi** * ; **Hiroyasu Inokawa** * ; **Hitoshi Yamagata** PhD * ; **Kazuro Sugimura** MD, PhD *

PURPOSE

To assess the effect of adaptive iterative dose reduction (AIDR 3D) on the stand-alone performance of a prototype computer-aided detection (CAD) system for lung nodules using CT data acquired at standard-, low-, and ultra-low-dose levels.

METHOD AND MATERIALS

This study used CT data of 60 patients who prospectively underwent a chest CT examination using a multidetector-row scanner with a protocol including standard-dose (125 mAs), low-dose (25 mAs), and ultra-low-dose (5 mAs) unenhanced scans. Each scanned data were reconstructed into 1-mm-thick images without and with AIDR 3D. The following groups of CT images, each consisting of 60 datasets, were thus obtained: (S-wo) at 125 mAs, without AIDR 3D; (S-w) at 125 mAs, with AIDR 3D; (L-wo) at 25 mAs, without AIDR 3D; (L-w) at 25 mAs, with AIDR 3D; (U-wo) at 5 mAs, without AIDR 3D; (U-w) at 5 mAs, with AIDR 3D. Two experienced chest radiologists carefully reviewed the group S-wo and determined a gold standard of nodules ranging 5-30 mm in diameter by consensus. Based on the gold standard, the sensitivity and false positive rate of the CAD system on all groups were determined. Regarding sensitivities, the group S-wo and each of the other groups were compared using McNemar's test; similar comparisons regarding false positive rates were made using signed rank test.

RESULTS

The reference standard consisted of 198 (104 solid and 94 subsolid) nodules. The sensitivity and false positive rate (per patient) on the group S-wo were 58.6% and 0.97. The sensitivities (corresponding p values of the comparisons with the group S-wo) on the other groups

(S-w, L-w, L-w, U-w, and U-w) were 67.7% (CONCLUSION

Regarding sensitivities, 25-mAs and 5-mAs groups with AIDR 3D were comparable to the 125-mAs group without AIDR, whereas 25-mAs and 5-mAs groups without AIDR 3D were inferior to the latter group; furthermore, the 125-mAs group with AIDR 3D was superior to that without AIDR 3D. Regarding false positive rate, corresponding comparisons showed no highly significant difference.

CLINICAL RELEVANCE/APPLICATION

In terms of the performance of a CAD system for lung nodules, standard-dose CT with AIDR 3D and low- or ultra-low-dose CT with AIDR 3D can respectively surpass and parallel usual standard-dose CT.

SSA19-08 • Computer-aided Detection of Colitis in Computed Tomography Examinations

Evrin B Turkbey MD (Presenter) ; Le Lu PhD ; Jianhua Yao PhD * ; Zhuoshi Wei PhD ; Ronald M Summers MD, PhD *

PURPOSE

To develop a computer aided detection (CAD) tool for automated detection of regions with colitis in CT examinations.

METHOD AND MATERIALS

One representative axial CT image per patient passing through the cecum or ascending colon was selected from 17 colitis patients (mean age= 38±13 yrs, 8 women, 9 men) and 25 healthy subjects (mean age=44±13yrs, 18 women, 7 men). Colitis was defined as presence of colonic wall thickening (>3mm) accompanied by pericolonic fat stranding and was manually segmented by a radiologist. The CAD method is three-tiered. An image intensity and gradient checker, trained from annotated colitis regions, is used to quickly discard non-informative image areas. A discriminative scanning window detector using covariance descriptor, selective data resampling and extended Gaussian kernel support vector machine follows for image patch classification as colitis or not. Finally, the local patch detections with confidences are spatially aggregated to form statistical features per image that label the whole dataset as with or without colitis. A k-nearest neighbor classifier is used. Three-fold cross validation is employed for classification performance assessment.

RESULTS

The mean wall thickness at colitis segments was 9.3 mm (range: 4.2-20.2 mm) whereas it was 2.3 mm (range: 1.2-3.2 mm) at normal colon segments (P=0.0001). The overall per patient classification accuracy is 83.3%. For colitis patients, the sensitivity is 88.2% (15 out of 17). 19 out of 25 healthy subjects are classified correctly with the specificity of 76% .

CONCLUSION

The CAD tool introduced in the current study can detect colitis affecting the cecum/ascending colon region with high sensitivity and good specificity. The challenge of colitis image pattern being visually ambiguous is solved by the high description power of covariance descriptor, hard negative bootstrapping and the tiered classification at local and global image levels.

CLINICAL RELEVANCE/APPLICATION

Early diagnosis of colitis is critical to prevent bowel necrosis and perforation in immunosuppressive patients. A computer-aided detection tool may help to increase detection rates of colitis in CT.

SSA19-09 • A Computer-aided Diagnosis System for Detecting Renal Extracolonic Findings on CT Colonography

Jian Fei L Liu MD ; Shijun Wang ; Marius G Linguraru DPhil, MS ; Ronald M Summers MD, PhD (Presenter) *

PURPOSE

To accurately detect renal calculi and lesions on CT colonography (CTC) by computer-aided diagnosis.

METHOD AND MATERIALS

We studied 66 patients (age range, 43-72 years; mean 57±7 years) undergoing CT colonography. The slice thickness was 1 mm. There were 52 renal calculi (size range, 1-7mm; mean size, 2±1 mm) and 58 renal lesions (size range, 3-51mm; mean size, 16±10 mm). 36 lesions and 25 calculi were located in the left kidney, and 22 lesions and 27 calculi in the right kidney. We first segmented both kidneys on the supine CTC images. Total variational (TV) flow was used to remove image noise in the kidney regions for a maximally stable extremal region (MSER) detector to extract calculi candidates. We detected lesions by performing manifold diffusion on the kidney surface and searching for points with local maximum diffusion response. Both calculus and lesion candidates were finally classified by a support vector machine to determine the final detected calculi and lesions. There were 30 patients in the training dataset and 36 patients in the test set for renal calculi and lesion detection. The training set contained 20 calculi and 24 lesions, and the test set had 32 calculi and 34 lesions. We performed a free-response receiver operating characteristic analysis on the test set to validate the results.

RESULTS

There were 41 true detections on calculi (from 29 unique calculi) and 417 false positives. The sensitivity of renal calculi detection was 80% at 1 false positive per patient. There were 33 true detections on renal lesions (from 31 unique lesions) and 277 false positives. The sensitivity of lesion detection was 87% at 7 false positives per patient.

CONCLUSION

Detection of renal calculi and lesions is challenging on CTC images because the primary purpose of CTC is to screen for colon cancer and the studies are typically done with lower dose and without intravenous contrast. TV-flow and MSER detector are efficient means to detect renal calculi by reducing image noise and extracting image regions with high intensity values. The manifold diffusion efficiently detects kidney lesions based on their geometric properties. Our method can detect renal calculi larger than 1 mm with few false positives and renal lesions with moderate false positive rates.

CLINICAL RELEVANCE/APPLICATION

Our CAD system accurately detects renal calculi and lesions on CTC images and, with future clinical validation, may lead to improved diagnosis.

Physics (Low-dose CT Imaging)

Sunday, 10:45 AM - 12:15 PM • S404AB

QA PH CT

[Back to Top](#)

SSA20 • AMA PRA Category 1 Credit™:1.5 • ARRT Category A+ Credit:1.5

Moderator

Willi A Kalender , PhD *

Moderator

John M Boone , PhD *

SSA20-01 • Is Low-dose CT with Model-based Iterative Image Reconstruction an Advantageous Strategy for Reducing Radiation Dose in Follow Up of Patients with Testicular Cancer? Preliminary Results of a Prospective Study

Kevin Murphy MBBCh, MRCS (Presenter) ; Lee Crush MBBCh, FFRRCSI ; Siobhan O' Neill MBBCh ; Micheal A Breen MD ; Adrian P Brady FFRRCSI, FRCR ; Paul Kelly MBBCh ; Derek Power ; Jackie Bye BA * ; Michael M Maher MD, FRCR ; Kevin N O'Regan MD

CONCLUSION

MBIR facilitated a 66% reduction in ED while producing images that were comparable or superior to CD with standard reconstruction in terms of noise, signal to noise ratio and diagnostic acceptability

Background

National Comprehensive Cancer Network (NCCN) and other guidelines recommend CT surveillance usually up to 5 years for patients with early stage testicular cancer. This is generally a young patient cohort and therefore considered an at-risk group for high cumulative lifetime dose of ionizing radiation. We report the early results of a prospective trial to examine the effectiveness of model-based iterative reconstruction (MBIR) to reduce effective dose (ED) due to CT in follow up of these patients.

Evaluation

Following ethical approval, 23 patients referred for follow up of testicular cancer [mean age 34 years, range 18-60] consented to undergo an additional simultaneous low-dose (LD) CT of chest, abdomen and pelvis at the time of routine surveillance CT. The conventional dose (CD) and LD images both at standard reconstruction (SR) with 40% adaptive-statistical iterative reconstruction (ASIR) and reconstruction with MBIR of the initial 5 patients of the cohort were independently reviewed by two radiologists who assessed for diagnostic acceptability and graded images using published image quality indices. The ED and size specific dose estimates (SSDE) for each study was calculated.

Discussion

The mean ED (and SSDE) for LD and CD CT were 3.5 ± 1.6 mSv (6.1 ± 2.9 mGy SSDE) and 10.3 ± 3.7 mSv (17.7 ± 4.5 mGy SSDE), a mean dose reduction of 66% (p

SSA20-02 • Comparison of Hybrid (iDose) and Model-based (IMR) Reconstruction Techniques in Sub Milli-Sievert Chest and Abdominal CT: An Ongoing Prospective Blinded Study

Ranish D Khawaja MBBS, MD (Presenter) ; **Michael A Blake** MBBS * ; **Garry Choy** MD, MS ; **Matthew D Gilman** MD ; **Mannudeep K Kalra** MD * ; **Subba R Digumarthy** MD ; **Amita Sharma** MBBS ; **Avinash R Kambadakone** MD, FRCR ; **Sarabjeet Singh** MD ; **Atul Padole** MD ; **Sarvenaz Pourjabbar** MD ; **Diego A Lira** MD ; **Kevin M Brown** MS * ; **Mukta Joshi** *

PURPOSE

To assess diagnostic quality of sub milli-Sievert (submSv) chest and abdominal CT reconstructed with iterative model reconstruction (IMR) and iDose⁴.

METHOD AND MATERIALS

In a prospective clinical study, 20 patients (BMI2, **chest**, n=10 *age range*:26-90; **abdomen**, n=10 *age range*:30-84) gave written informed consent for the acquisitions of submSv additional images (0.9mSv) on a 256-slice CT (iCT, Philips). In addition to their clinical standard-dose (SD) CT (chest: 2.9mSv; abdomen: 5.6mSv), submSv images were reconstructed with low-dose (LD) FBP, iDose⁴ (idose levels ID₂, ID₄) and IMR (i1-5) techniques resulting in 9 stacks. Two thoracic and 3 abdominal radiologists independently evaluated in a blinded manner for *lesion detection*, *lesion margins*, *diagnostic acceptability* and *visibility of small structures*. Objective noise was measured in the descending thoracic aorta and abdominal aorta and noise spectral density (NSD) was obtained. Data were analyzed using Wilcoxon Signed Rank test and analysis of variance (ANOVA).

RESULTS

Lesion detection in abdominal CT (11 lymph nodes, 9 liver/renal lesions, and 8 kidney stones) and chest CT (31 lung nodules, and 10 ground glass opacities), and *lesion margin* evaluation was identical for SD-FBP, LD-FBP, iDose⁴ and IMR. Lesion margins were better seen for 30% of detected chest lesions (mostly emphysematous air-pockets and nodules) with IMR compared to SD-FBP, LD-FBP and iDose⁴. Visibility of abdominal structures (adrenal glands and pancreatic contour), and overall diagnostic acceptability of submSv iDose and IMR were similar to SD-FBP (*kappa value* 0.72-0.88; p_{2,iD₄} and 51%-85% noise reduction with IMR (i1-5; p

CONCLUSION

Although lesion detectability is not compromised in chest and abdominal CT examinations acquired at sub-mSv radiation doses, IMR image reconstruction of sub-mSv CT data helps improve delineation of lesion margins when compared to low-dose and standard-dose FBP, and iDose⁴ techniques.

CLINICAL RELEVANCE/APPLICATION

Preliminary results from this ongoing prospective clinical trial show the potential of IMR for lesion evaluation in chest and abdomen CT examinations acquired at sub milli-Sievert radiation doses.

SSA20-03 • Sub-mSv Cerebral CT Perfusion Using PICCS

Jie Tang PhD (Presenter) ; **Guang-Hong Chen** PhD * ; **Patrick A Turski** MD * ; **Vivek Prabhakaran** MD, PhD ; **Kari A Pulfer** ; **Howard A Rowley** MD *

PURPOSE

With increasing concern regarding ionizing radiation from CT examinations, the radiation dose should be kept as low as possible while maintaining sufficient diagnostic information. The purpose of this study is to evaluate whether the radiation dose from a cerebral CT perfusion (CTP) scan can be kept under 1 mSv while maintaining diagnostic perfusion maps.

METHOD AND MATERIALS

An IRB approved protocol was used to perform a reduced-dose (RD) CTP scan immediately following standard-dose (SD) clinical CTP scan for the same subject. The SD CTP protocol used a 16 slice axial Shuttle mode on a GE CT750HD scanner, with 80 kV, 500 mA, 0.4 s gantry speed (200 mAs) and 17 time frames which lasts 45 s, with effective dose = 3.74 mSv. RD CTP used 100 mA (40 mAs) with other parameters the same as SD, with effective dose = 0.75 mSv. 20 subjects were enrolled in this study. The SD scans were reconstructed using FBP (filtered back projection) and the RD scans were reconstructed using FBP, ASiR(with 100% setting) and an iterative reconstruction algorithm, PICCS (prior image constrained compressed sensing with iterative reconstruction). Perfusion maps (CBF, CBV and MTT) were then generated by GE Perfusion 4 software using the Perfusion 3 algorithms. All image series were randomized and each series was scored by 2 neuroradiologists using a 5-point scale (1: non-diagnostic; 2: poor; 3: fair; 4: good; 5: excellent). Clinical findings were recorded for each series.

RESULTS

The mean scores for the SD FBP series are $3.9(\pm 0.5)$, $3.9(\pm 0.5)$ and $3.9(\pm 0.5)$ for CBF, CBV and MTT maps respectively; corresponding scores are $2.2(\pm 0.4)$, $2.1(\pm 0.4)$ and $2.3(\pm 0.5)$ for the RD FBP series; $2.7(\pm 0.5)$, $2.6(\pm 0.5)$ and $2.7(\pm 0.5)$ for RD ASiR series, and $3.4(\pm 0.6)$, $3.4(\pm 0.5)$ and $3.5(\pm 0.5)$ for RD PICCS series. Subjective scores of the RD PICCS image series are higher than RD FBP series (p

CONCLUSION

Prior image constrained compressed sensing with iterative reconstruction (PICCS) provides diagnostic quality perfusion maps with 20% of the radiation dose compared to current clinical protocols.

CLINICAL RELEVANCE/APPLICATION

Diagnostic quality sub-mSv cerebral CT perfusion imaging can be achieved using PICCS reconstruction.

SSA20-04 • Adaptive Statistical Iterative Reconstruction for Low Dose Quantitative Myocardial CT Perfusion: A Microspheres Validation Study

Aaron So PhD (Presenter) ; **Jiang Hsieh** PhD * ; **Jean-Baptiste Thibault** * ; **Kelley Branch** MD * ; **Ting-Yim Lee** MSc, PhD *

PURPOSE

We validated the effectiveness of adaptive statistical iterative reconstruction (ASIR, GE Healthcare (GE)) for minimizing image noise in low dose quantitative myocardial perfusion (MP) imaging against microspheres MP measurement.

METHOD AND MATERIALS

Iodinated contrast (Isovue 370, 0.7 mgI/kg) was injected at 3 to 4 ml/s into 68±25 kg normal pigs via an ear vein and the heart was scanned using a GE Discovery 750HD scanner with a prospectively ECG triggered dynamic protocol (Snapshot Pulse (SSP), GE): axial scan every 1-2 heart beats for 22 scans using 140 kV, 0.35 s gantry period and 80 mA (normal dose). MP measurement was repeated with the x-ray tube current reduced to 20 mA (low dose). The normal- and low-dose SSP images were reconstructed using filtered backprojection (FBP) (SSP80) and both FBP (SSP20_{FBP}) and ASIR (SSP20_{ASIR}) respectively. All images were corrected for beam hardening from which MP maps were generated using CT Perfusion (GE). After the CT perfusion studies, fluorescent microspheres were injected into the left atrial appendage of the heart to measure MP. Mean MP measured with microspheres and the three CT image sets in 45 segments from the lateral, apical and septal wall in 15 slices from three pigs were compared using linear regression and Bland-Altman analysis. Effective dose (ED) of each SSP protocol was estimated from the dose-length product provided by the scanner.

RESULTS

SP80 images exhibited the highest correlation with microspheres (R=0.69) compared to SSP20_{ASIR} (R=0.60) and SSP20_{FBP} (R=0.57). SSP80 images also showed the smallest difference in mean MP from microspheres and narrowest limits of agreement with microspheres (7.0 and -32.9 to 46.8 ml/min/100g (80)) compared to SSP20_{ASIR} (11.3 and -35.3 to 57.8 (93)) and SSP20_{FBP} (15.7 and -32.8 to 64.1 (97)). ED of the SSP80 and SSP20 protocols were 4.5 and 1.1 mSv respectively.

CONCLUSION

Noise in low dose SSP images reconstructed with FBP was excessive which led to less accurate and reproducible MP estimation with CT Perfusion but such errors could be reduced with ASIR.

CLINICAL RELEVANCE/APPLICATION

With the proposed image acquisition and reconstruction approaches, MP measurement with low dose CT Perfusion is a feasible alternative to MRI and SPECT for studying ischemic heart disease.

SSA20-05 • Low-dose Pelvic CT Using Adaptive Iterative Dose Reduction 3D: A Phantom Study

Remko Kockelkoren (Presenter) ; **Hiromitsu Onishi** MD ; **Tonsok Kim** MD ; **Masatoshi Hori** MD ; **Atsushi Nakamoto** MD ; **Noriyuki Tomiyama** MD, PhD ; **Makoto Sakane** MD ; **Mitsuaki Tatsumi** MD, PhD

PURPOSE

To evaluate the image quality and radiation dose reduction in pelvic CT reconstructed using an adaptive iterative dose reduction 3D (AIDR 3D) technique with a phantom model.

METHOD AND MATERIALS

An anthropomorphic phantom (CTU-41; Kyoto Kagaku, Kyoto, Japan) and a Catphan phantom containing low-contrast objects (Catphan 500; Phantom Laboratory, Salem, NY) were scanned with a 320 detector row CT scanner (Aquilion ONE; Toshiba Medical Systems, Otawara, Japan) in eight tube current levels (ranged from 25 mA to 500 mA) at 80 kV and 120 kV, respectively. The rotation period was 0.5 second and the helical pitch was 0.828 (53/64). Standard filtered back projection (FBP) images and AIDR 3D images were reconstructed for each setting and were compared. For the quantitative evaluation, image noise (standard deviation of CT number) and contrast to noise ratio (CNR) between the model bladder and the surrounding area of the anthropomorphic phantom were calculated. For the qualitative evaluation, image noise, image artifacts, delineation of the organs and overall image quality in the anthropomorphic phantom were assessed by three radiologists. The detectability of the low-contrast objects of the Catphan phantom were also evaluated using a receiver operator characteristic analysis. Sensitivities and specificities were compared by using McNemar's chi-square test.

RESULTS

In the quantitative evaluation, AIDR 3D resulted in a substantial noise reduction compared to FBP and revealed higher CNRs than FBP. In the subjective evaluation, the image noise, image artifact such as photon starvation, and overall image quality improved with AIDR 3D. In the detectability evaluation, at 120 kVp, the sensitivities, the specificities, and the Az values were 16.7%, 100%, 0.78 for image at 100 mA (50 mAs) with AIDR 3D, 33.3%, 100%, 0.75 for images at 150 mA (75 mAs) with AIDR 3D, and 33.3%, 100%, 0.81 for those at 200 mA (100 mAs) with FBP. There were no statistically significant differences.

CONCLUSION

Our results in a phantom study shows that AIDR 3D technique may allow approximately 25-50% radiation dose reduction compared to FBP technique in pelvic CT examinations maintaining the image quality and the diagnostic performance.

CLINICAL RELEVANCE/APPLICATION

Radiation at the pelvic region is of special importance particularly for the young patients because of the genetic risk and AIDR 3D technique may allow the radiation dose reduction in pelvic CT.

SSA20-06 • Synergistic Radiation Dose Reduction by Combining Automatic Tube Voltage Selection and Iterative Reconstruction

Jeremy R Wortman MD (Presenter) ; **Alexander J Adduci** MD, PhD ; **Tim O'Connell** MD, MEng * ; **Aaron D Sodickson** MD, PhD

PURPOSE

To evaluate radiation dose and image quality in CT pulmonary angiography (CTPA) exams with automated tube voltage selection (CarekV) before and after implementation of sinogram affirmed iterative reconstruction (Safire).

METHOD AND MATERIALS

The cohort included: 1) 61 consecutive CTPAs performed on a Siemens AS+ scanner from 5/7/12 to 5/31/12 using CarekV (vascular image quality selection, reference kVp 120, reference mAs 180), and 2) 59 consecutive CTPAs performed from 7/1/12 to 7/18/12 using CarekV with reference mAs reduced to 120 and images reconstructed using Safire at strength of 3. All scans were performed with longitudinal and in-plane tube current modulation (CareDose 4D). CarekV on a vascular setting uses the topogram x-ray attenuation to select the scan kVp expected to produce the lowest achievable CTDIvol while maintaining the desired iodine contrast to noise ratio and respecting the maximum x-ray tube current limits. We measured patient size (effective diameter = $\sqrt{\text{AP} \times \text{Lat}}$), signal (mean CT density) and noise (standard deviation), and recorded local CTDIvol at the level of the main pulmonary artery. Linear regression models were created for the dependent variables $\ln(\text{CTDIvol})$, signal, noise, and signal to noise ratio (SNR) as a function of independent variables size, age, gender, and reconstruction technique.

RESULTS

The 33% reduction in reference mAs in the Safire group allowed CarekV to select reduced kVp in larger patients than in the FBP group, with an overall reduction in 120 kVp scans from 42.9% to 0% and an associated increase in 100 kVp scans from 53.6% to 62.0% and 80 kVp scans from 3.5% to 38.0%. When controlling for size and demographics, the combination of Safire and CarekV yielded an overall CTDIvol reduction of 44.5% ($p < .0001$), a signal increase of 96 HU ($p = .002$), and an increase in image noise ($p = .004$) with no significant change in SNR ($p = .70$).

CONCLUSION

The combination of CarekV and Safire resulted in a 44.5% dose reduction, substantially greater than the 33% reduction that would be achieved by reducing the reference mAs alone. This is accomplished with preserved image quality as the reduced reference mAs allows CarekV to scan larger patients at reduced kVp.

CLINICAL RELEVANCE/APPLICATION

Synergistic dose reduction can be achieved by combining automatic kVp selection with global mAs reduction (as used in concert with iterative reconstruction) with no negative impact on image quality.

SSA20-07 • Systematic Dose Evaluation of Iterative Reconstructed Computed Tomography in a Contrast Enhanced Cadaveric Model

PURPOSE

To systematically test the potential for dose savings in computed tomography (CT) through iterative reconstruction in a contrast enhanced human cadaveric model.

METHOD AND MATERIALS

Fifteen human cadavers scheduled for contrast enhanced virtual autopsy were injected with hyperdense contrast agent through the iliac arteries. A series of thoracic and abdominal tube current scaled CT scans (11 scans, 20mAs_{eff} - 200 mAs_{eff} in steps of 20mAs) were performed and reconstructed using standard filtered back projection (FBP) and iterative reconstruction algorithms (IR) in soft and sharp reconstruction kernels. The imaging datasets were evaluated in randomizedly and blinded to the reconstruction method by defining minimally necessary doses for CT quality criteria as defined in EU16262 (36 items, 17 thoracic, 6 mediastinal, 13 abdominal) independently by three radiologists (36x15x3x4=6480 data points). Minimal doses for every of the two reconstruction methods and kernel types in their respective applications were compared statistically.

RESULTS

In all subjects a sufficient contrast filling for further analysis was achieved. Average minimal doses for soft tissue applications (soft kernels) were 132.3±44.6 mAs (FBP) vs. 115.6±46.7 mAs (IR, p=0.0001), for bone and lung applications (sharp kernels) 140.9±47.1 mAs (FBP) vs. 130.9±49.1 mAs (IR, p=0.0001). The achieved amount of tube current saving were 12.6% (soft kernels) and 7.1% (sharp kernels).

CONCLUSION

In a blinded, randomized study, iterative reconstruction yielded a statistically significant dose saving in soft tissue and sharp kernel applications. While many publications claim dose savings of up to 50% throughout the spectrum of CT vendors, the savings yield was considerably lower in this study. Most probably, the reason for this result is the comparison to lowest achievable doses also in standard algorithms (and not the usual 160-180mAs). Hence the dose savings numbers of iterative reconstruction of earlier studies might be partially explained by unused dose saving potential in standard FBP.

CLINICAL RELEVANCE/APPLICATION

The results give an insight in to how high the dose saving potential of iterative reconstruction but also filtered back projection is, potentially translating in to clinical CT parameter choices.

SSA20-08 • Massive Dose Reduction and Image Quality Improvement Using a Commercial Iterative Reconstruction Algorithm in CT

Artur Latorre-Musoll MSc (Presenter) ; Agustin Ruiz Martinez MSc ; Rosa M Pallerol Pinzano ARRT ; Pablo Carrasco De Fez PhD ; Teresa Eudaldo Puell PhD ; Nuria Jornet Sala PhD ; Montserrat Ribas Morales PhD

CONCLUSION

Dose reductions up to 66% with no significant loss of image quality can be achieved using iDose compared to FBP algorithm. In the light of these promising results, iDose is increasingly used in our hospital. As dose and image quality should be balanced according to patient needs, we are presently studying the adequate choice of iDose level using clinical data.

Background

Radiation exposure from medical imaging has become a public health concern due to the increasing use of CT. Attempts to lower the radiation dose associated with CT studies are limited by image noise on FBP-based reconstructions. We assessed the dose reduction capabilities and in-phantom image quality metrics of a commercial iterative reconstruction algorithm.

Evaluation

We compared the performance of the iterative reconstruction algorithm iDose to the standard FBP algorithm supplied with the 256-slice MDCT Brilliance iCT (Philips Healthcare). We used a Catphan 504 (The Phantom Laboratory) to assess image quality in terms of CT number calibration, image noise, low contrast detectability and spatial resolution. We reconstructed 35 helical acquisitions (varying kV and mAs/slice) using FBP and 6 noise reduction levels provided by iDose. We measured the dosimetric index CTDI_{vol} of all acquisitions using the solid state detector/multimeter CT Dose Profiler/Barracuda (RTI Electronics) and a phantom assembled with 3 standard PMMA body phantoms of 32 cm diameter and 3x15 cm length.

Discussion

CT number calibration obtained using iDose levels and FBP was compatible within 1%. iDose reduced image noise from 10% (iDose1) to 41% (iDose6) compared to FBP, regardless of the CTDI_{vol} of the study. Conversely, the dose reduction capability of iDose ranged from 19% (iDose1) to 66% (iDose6) maintaining the same image noise as FBP. These results are compatible with the manufacturer's specifications. Low contrast detectability improved compared to FBP, as contrast-to-noise ratio increased because of the noise reduction: from 11% (iDose1) to 71% (iDose6). Spatial resolution improved slightly compared to FBP. However, we are now devising new measurements to fully quantify the iDose spatial resolution capabilities.

SSA20-09 • Evaluation of TV-minimization-based Reconstruction for Low-dose Dedicated Breast CT

Junguo Bian PhD (Presenter) ; Kai Yang PhD ; Xiao Han MSc ; Karen K Lindfors MD * ; Erik A Pearson BS, BEng ; Emil Y Sidky PhD ; John M Boone PhD * ; Xiaochuan Pan PhD *

PURPOSE

Current dedicated breast CT is of low SNR in projection data and high noise in reconstruction images because a small imaging dose is distributed into large number of projections. The small contrast and fine structure of breast tissues, together with low-SNR data has made reconstruction improvement from low-dose breast-CT data very challenging. We have developed and tailored a TV-minimization based reconstruction algorithm for breast CT and performed reconstruction for more than 10 patient cases. In the work, we evaluated the image quality of TV-minimization-based reconstructions against images currently reconstructed by use of FBP algorithm. We demonstrate that image quality can be improved over the currently used FBP-based algorithms for low-dose breast CT.

METHOD AND MATERIALS

The reconstruction is formulated into a constrained-TV-minimization problem. We developed and tailored an ASD-POCS algorithm for solving the problem. Patient data were collected during an ongoing clinical trial performed at UC-Davis. We performed reconstruction of the whole volume for more than 10 patient cases from the low-SNR data. Special attention was paid to minimize the blocky appearances that are typically observed in images reconstructed by use of TV-minimization-based algorithms from low-dose data sets. We use the difference between adjacent slices to quantify quantum noise and use the power-law exponent, Beta, fitted from log-log plot of the image power spectra to quantify anatomical noise. A smaller Beta value for the reconstruction images indicates a better observer performance on lesion detection. We also performed a 2AFC experiment in which the observers were asked their preference between images currently reconstructed by use of FBP and the proposed algorithms.

RESULTS

Visual inspection shows images reconstructed with proposed algorithm have improved contrast and details. The noise variances and beta values are consistently smaller for image reconstructed with the proposed algorithm. The results of 2AFC study also show observers' preference of images reconstructed by use of the proposed algorithm over those currently reconstructed by use of FBP algorithms.

CONCLUSION

The results demonstrated that the proposed algorithm can improve image quality for current dedicated breast CT.

Physics (Ultrasound)**Sunday, 10:45 AM - 12:15 PM • S405AB**[Back to Top](#)**SSA21 • AMA PRA Category 1 Credit™:1.5 • ARRT Category A+ Credit:1.5****Moderator****Paul L Carson**, PhD ***Moderator****Emad S Ebbini**, PhD ***SSA21-01 • Simulator-based Comparison of 2D, 3D and Fusion 3D Transrectal Ultrasound (TRUS) Needle Guidance Accuracies for Biopsy (Bx) of Prostate MRI Lesions****Derek W Cool** MD, PhD (Presenter) * ; **Xuli Zhang** BSc ; **Cesare Romagnoli** MD ; **Walter M Romano** MD ; **Jonathan Izawa** ; **Aaron Fenster** PhD ***PURPOSE**

Prostate MRI's high sensitivity to early stage prostate cancer (PCa) permits targeted biopsy as an alternative to the current non-targeted systematic TRUS biopsy. Biopsy needle guidance under TRUS is the most economical option, but spatial correspondence of MRI findings with TRUS is non-trivial. The accuracy of sampling MRI lesions under 2D and 3D TRUS and 3D TRUS fusion is quantified.

METHOD AND MATERIALS

Three experts performed simulated biopsies on 12 patients (Pros. Vol=37±11g, PSA=9.0±5.1ng/ml) with a total of 15 Bx-confirmed PCa MRI lesions (0.8±0.8g) who were selected from 90 patients undergoing MRI-3D TRUS fusion biopsy. Two core-biopsies were targeted at each MR lesion using 2D TRUS, 3D TRUS and MRI-3D TRUS fusion for needle guidance, using a validated Bx simulator. Additional single core-biopsies were directed toward common regional targets defined for all patients. Regions included: left-anterior transition zone (TZ), left mid-gland, right apex and right base. The simulated Bx core locations were compared to the original MRI to evaluate the sampling accuracy.

RESULTS

The 15 PCa tumors were distributed as follows: Base=4, Mid-gland=5, Apex=6, with 7 lesions along the anterior prostate. Only 44±4% and 51±14% of tumors were sampled with 2D and 3D TRUS, respectively, compared to 98±4% with fusion biopsy. Bx sampling rates were not significantly different between anterior and posterior tumors for any modality. The Bx sampling errors for the regional targets were significantly higher (p<0.001).

CONCLUSION

Biopsy of prostate MRI lesions under 2D or 3D TRUS without MR-fusion may be inaccurate and lead to a falsely negative biopsy.

CLINICAL RELEVANCE/APPLICATION

Targeting biopsies at suspicious lesions seen on prostate MRI using 2D or 3D TRUS without image fusion is likely not accurate enough to adequately detect many significant prostate cancers.

SSA21-02 • Quantifying Tendon Damage with Ultrasound (US) Shear Wave Elastography Using a Porcine Flexor Tendon Tear Model**Ryan J DeWall** PhD (Presenter) ; **Jingfeng Jiang** ; **John Wilson** MD, MS ; **Kenneth S Lee** MD ***PURPOSE**

Shear wave imaging (SWI) is an US elastography technique that measures tissue elasticity, a tissue property that often correlates with pathology. The purpose of this study was to evaluate the ability of SWI to visualize partial tears and quantify damage in porcine flexor tendons.

METHOD AND MATERIALS

Thirty porcine flexor tendons were pre-loaded to 1.25 N and stretched from 0%-2% strain using a Mark-10 (Mark-10 Corp; Copiague, NY) testing system while being imaged using SWI (Aixplorer; Supersonic Imagine; Aix-en-Provence, France). After imaging the normal tendon, the deep portion was cut to 25% (n = 10), 50% (n = 10), and 75% (n = 10) of the tendon thickness and reassessed with SWI. The deep-to-superficial wave speed ratio of the deep third (cut) and superficial third (uncut) of the tendon were compared in regions-of-interest (ROIs) centered on (C), proximal to (P), and distal to (D) to the tear, excluding the area within the tear. Tukey multiple comparisons were used to assess differences between normal and torn tendons.

RESULTS

Shear wave speed (i.e. elasticity) increased significantly with increasing tissue strain in normal and cut tendons, except in the deep third of the 75% tear (0%, 6.7 ± 1.2 m/s; 2%, 7.7 ± 1.4 m/s). The deep-to-superficial wave speed ratio decreased significantly between normal and cut tendons in the 50% tear in ROIs centered on (0%, 0.98 ± 0.06 to 0.91 ± 0.09; 1%, 0.97 ± 0.06 to 0.81 ± 0.09; 2%, 0.99 ± 0.07 to 0.84 ± 0.10) and distal to (1%, 0.95 ± 0.08 to 0.85 ± 0.08) the tear and in the 75% tear proximal to (1%, 1.00 ± 0.07 to 0.82 ± 0.12; 2%, 1.00 ± 0.07 to 0.81 ± 0.16), centered on (0%, 1.03 ± 0.09 to 0.70 ± 0.10; 1%, 0.99 ± 0.06 to 0.60 ± 0.11; 2%, 0.95 ± 0.10 to 0.61 ± 0.13), and distal to (1%, 0.96 ± 0.15 to 0.79 ± 0.14) the tear.

CONCLUSION

The decrease in deep-to-superficial wave speed ratio in cut tendon relative to normal tendon suggests loading changes in the damaged fibers. SWI demonstrates the potential for assessing tendon damage in partially torn tendons.

CLINICAL RELEVANCE/APPLICATION

SWI has the potential to add quantitative information to validated US outcome measures, providing a powerful tool for future outcomes analysis using US to monitor and assess tendon injuries.

SSA21-03 • Optimizing Microbubble Formulation for Indirect Lymphosonography: Quantitative Comparison of Nanobubbles vs. Standard Microbubbles**Chan Kyo Kim** MD, PhD (Presenter) ; **Boem Ha Yi** MD, PhD ; **Omid Yeganeh** MD ; **Wenjin Cui** ; **Christopher Barback** ; **Robert F Mattrey** MD ***PURPOSE**

Indirect lymphosonography where microbubbles (MB) are injected subcutaneously within the sentinel lymph nodes (SLN) drainage field was developed to non-invasively detect, mark and possibly stage the SLN pre-operatively. Early clinical data suggest accurate localization but limited characterization. Since entry into the lymph duct (LD) is limited to particles

METHOD AND MATERIALS10⁸ MBs of Definity (1-3 μm) (Lantheus Medical Imaging) or a new formulation of DSPC/DSPE-PEG and perfluorohexane (0.2-1 μm) in 0.2ml were injected in either footpad of 6 normal rabbits. The Siemens Sequoia 15L8 probe was fixed over the popliteal node that was

imaged with CPS. Immediately after injection, a few MBs entered the LD to place an ROI over the SLN and its afferent LD. The US field was cleared and the footpad massaged for 20 sec. A time-intensity curve (TIC) was constructed in real-time using a prototype Siemens software that analyzes the linearized CPS data but also uses the B-mode data to correct for motion while scanning at low MI and 15 frames/sec. At 20 minutes or when the TIC returned to baseline, the US field was cleared and the 20-sec massage repeated until peak enhancement and the process repeated until no enhancement occurred. The TIC following the 1st massage and the number of massages that refilled the SLN following each injection were recorded.

RESULTS

Both agents enhanced the SLN and LD after massage. NBs caused greater SLN ($p=0.003$) and LD ($p=0.001$) enhancement that lasted for 20min vs. 8 min. The SLN refilled >20 times following a NB dose but only 8 times following a MB dose ($p= 0.001$).

CONCLUSION

NBs not only improve the filling of the duct and SLN, but also provided more functional bubbles at the injection site. We will next compare their ability to characterize nodes.

CLINICAL RELEVANCE/APPLICATION

Nanoscale bubbles increase duct filling and node enhancement and provide more functional bubbles at the injection site to refill the duct and node to improve detection and possibly characterization.

SSA21-04 • Ultrasound Shear Wave Speed Estimation in Elastic Phantoms: Sources and Magnitude of Variability in a QIBA Multicenter Study

Andy Milkowski MS (Presenter) * ; **Timothy J Hall** PhD * ; **Michael P Andre** PhD * ; **Paul L Carson** PhD * ; **Shigao Chen** PhD ; **Claude Cohen-Bacrie** * ; **Stephanie Franchi-Abella** MD ; **Brian S Garra** MD ; **Stephen McAleavey** PhD * ; **Steve Metz** * ; **Kathryn Nightingale** PhD * ; **Mark Palmeri** MD, PhD ; **Anthony E Samir** MD ; **Laurent Sandrin** PhD * ; **Mickael Tanter** PhD *

PURPOSE

To test commercial and research ultrasound SWS systems to identify the sources and magnitude of bias and variability in SWS measurements.

METHOD AND MATERIALS

Eleven phantom pairs were built from stiff and soft batches of Zerdine by CIRS. Larger phantoms were also prepared for correlative testing using magnetic resonance elastography. All phantoms were initially tested by one lab to determine manufacturing variation and were then shipped to 11 different labs for SWS measurements. At each site, 3-5 operators measure each phantom at three times at each of three depths according to a randomized schedule. Each measurement consists of the average of ten valid SWS acquisitions as has been reported in the clinical literature. The data are analyzed using crossed Gage R and R methodology with ANOVA. Bias is estimated by comparing the results with known values of elastic modulus (converted to SWS) from the manufacturer and from mechanical testing performed across a broad range of shear wave frequencies at two sites. Estimates of linearity can also be obtained since stiff and soft phantoms are tested at each site.

RESULTS

Mechanical test results from the two sites performing those measurements were in excellent agreement. Initial analysis of US SWS measurements shows overall variability of 5-7% in SWS mean values for several sites. ANOVA shows that site and measurement depth are the dominant sources of variation with operator variability being a minor component. Variation in SWS for all phantoms was 3-5% on initial testing of all phantoms. A 5-10% depth dependence (lower SWS at deeper depths) was also seen. Also, a small bias in SWS estimates of 5-6% was seen. Similar variability and bias are seen for both stiff and soft phantoms.

CONCLUSION

Initial results show a relatively small amount of variability in SWS estimates and also show that operator variability contributes little to total measurement variation. Phantom variation may be a significant source of the variability in measurements. Given these encouraging results, we will add measurements from additional sites, explore the causes of the depth dependence of SWS, and extend our work to lossy (viscoelastic) phantoms which more closely mimic human liver tissue.

CLINICAL RELEVANCE/APPLICATION

This work by QIBA is the first step in development of a protocol for US SWS measurement that gives accurate and repeatable results across a range of instruments for drug testing, clinical and research use

SSA21-05 • Visualization of Vascularity in Breast Lesions Using US Contrast Enhanced 3D Subharmonic Imaging

Anush Sridharan ; **John R Eisenbrey** PhD ; **Flemming Forsberg** PhD (Presenter) * ; **Priscilla Machado** MD ; **Daniel A Merton** ; **Kirk Wallace** PhD * ; **Carl Chalek** PhD * ; **Kai E Thomenius** PhD *

PURPOSE

To develop a method for improving visualization of vascularity in breast lesions using 3D contrast-enhanced subharmonic imaging (SHI).

METHOD AND MATERIALS

A modified Logiq 9 (GE Healthcare, Milwaukee, WI) scanner with a 4D10L probe was used for 3D harmonic imaging (HI) and SHI of breast lesions in 72 patients after bolus injection of an ultrasound contrast agent (UCA; Definity, Lantheus Medical Imaging, N Billerica, MA; dose: 0.25mL for HI and 20?L/kg for SHI). Fifteen biopsy-proven malignant cases were selected for image processing. A region-of-interest (ROI) corresponding to UCA flow (within the lesion) and tissue in both 3D HI and SHI were selected for each case. A volumetric map of the time-intensity curve for each slice within the volume was generated over time. Slices showing presence of UCA were identified and isolated. To improve visualization of flow a volumetric background template was generated (from baseline) and used to filter out tissue signals. Contrast-to-tissue ratios (CTRs) were calculated for 3D HI and SHI before and after background subtraction for vessel-tissue ROIs and also compared between the isolated slices and the entire volume.

RESULTS

Both 3D HI and SHI showed significant suppression of tissue signal after background filtering (p

CONCLUSION

3D SHI showed better visualization of vasculature in all cases via increased tissue suppression and sensitivity to UCA flow. The improvement in visualization of vasculature based on isolation of slices demonstrates the importance of 3D imaging to visualize breast cancer flow.

CLINICAL RELEVANCE/APPLICATION

Visualizing the vascular structure of breast lesions may help improve characterization.

SSA21-06 • Quantitative Biomarkers for the Assessment of Fibrosis Using M-Mode US and Shear Wave Elastography

Lauren Rosenblum BSc ; **Priscilla Machado** MD ; **Patrick L O'Kane** MD * ; **Andrej Lyshchik** MD ; **Flemming Forsberg** PhD (Presenter) *

PURPOSE

To determine if M-mode or Shear Wave Elasticity (SWE) imaging (independently or combined) provide quantitative markers of liver fibrosis compared to conventional grayscale ultrasound (US) imaging and pathology (the reference standard).

METHOD AND MATERIALS

Twelve subjects scheduled for an US-guided liver biopsy and 5 healthy volunteers were scanned with a broad bandwidth curvi-linear array using an IU22 (Philips Medical Systems, Bothell, WA; for grayscale and M-mode imaging) and an Aixplorer scanner (SuperSonic

Imagine, Aix-en-Provence, France; for SWE imaging). The M-mode images were quantified using the scanners existing calculation software package and by a novel algorithm (implemented in Matlab; Mathworks, Natick, MA) extracting distances between lines of similar intensities (L2LD) as a quantitative biomarker of liver status. Liver stiffness (in kPa) was recorded from the SWE images, while a radiologist (blinded to the other results) scored the grayscale US for degree of fibrosis (on a 0-4 scale). ANOVA and Wilcoxon's sign rank tests were used to compare the classification of liver fibrosis by SWE, M-mode (i.e., L2LD) and radiologists scoring with fibrosis determined by pathology as the reference standard.

RESULTS

In this pilot study, the radiologist was correct in 53% of assessments, which was not different from pathology when using a non-parametric test ($p=0.3$). SWE did not differentiate between degrees of fibrosis ($p > 0.71$), while the new L2LD biomarker was able to perform a correct classification ($p = 0.044$). The best differentiation was achieved between normal subjects (fibrosis score = 0) and the subjects with fibrosis scores greater than or equal to 1 (0.30 ± 0.041 vs. 0.43 ± 0.085 ; $p < 0.005$).

CONCLUSION

A new biomarker for noninvasive US evaluation of liver status, based on extracting distances between lines of similar intensities from M-mode images, have been developed. Initial results indicate this parameter can correctly classify degree of fibrosis; albeit based on a limited sample size.

CLINICAL RELEVANCE/APPLICATION

If these results are reproducible in a larger patient population, it may be possible to replace some liver biopsies with evaluations based on noninvasive, quantitative US biomarkers.

SSA21-07 • Dynamic Contrast-enhanced Ultrasound Parametric Maps for the Evaluation of Intratumoral Vasculature: Preclinical Study

Stephanie Pitre-Champagnat ; Ingrid Leguerney ; Jacques Bosq ; Fabian Kiessling MD ; Benedicte Coiffier (Presenter) ; Nathalie B Lassau MD, PhD *

CONCLUSION

Parametric maps from raw linear data can be performed in short process time with moving average model, and reflect reliably the heterogeneous histological measures within tumor by considering the contribution of the vessel size in the variations of intratumoral blood volume.

Background

Parametric maps from Dynamic Contrast-Enhanced Ultrasonography (DCE-US) appear as a useful tool to describe the intratumoral vasculature and its heterogeneity. This study was designed to identify the best processing of parametric maps from raw data and to compare the results to histologic vascularity measurement.

Evaluation

DCE-US was performed on 17 melanoma-bearing nude mice after a 0.1mL bolus injection of SonoVue (Bracco, Italy). Parametric maps treated time intensity curves (TIC) from raw linear data to extract pixelwise two parameters related to blood volume that were area under the curve (AUC) and peak intensity (PI). Three mathematical models were compared to fit the TIC in each pixel: a polynomial model used in clinical routine, a moving average model and a combination of two linear regressions. Parametric maps performed from the best fit approach were compared with histology for both region of interest (ROI) of whole tumor and several subROIs of 15mm² within each tumor to reflect intratumoral vascular heterogeneity. As ground truth correlate, microvessel densities (MVD) were determined, and vessels size only for subROIs.

Discussion

The moving average approach was the best compromise between values determination and processing pixelwise time (40m (rAUC=0.90 ($p=0.012$); rPI=0.83 ($p=0.041$)).

SSA21-08 • Effects of Ultrasound Parameters on Cavitation-assisted Delivery of PLGA-PEG Nanoparticles into Tumors: Phantom Study and Preliminary In Vivo Results

Tzu-Yin Wang (Presenter) ; Jung Woo Choe ; Steven B Machtaler PhD ; Rammohan Devulapally ; Butrus T Khuri-Yakub PhD ; Ramasamy Paulmurugan PhD ; Juergen K Willmann MD *

PURPOSE

Ultrasound(US)-microbubble(MB)-mediated drug delivery is a promising technique for image-guided, targeted cancer therapy. To optimize this technique for clinical translations, we performed a systematic study on effects of various US and MB parameters on cavitation and the corresponding delivery results of an FDA approved drug carrier, poly(D,L-lactide-co-glycolide)-block-poly(ethylene glycol) (PLGA-b-PEG-COOH) nanoparticles (NPs) into tumors.

METHOD AND MATERIALS

Cavitation was induced by exposing lipid shelled, perfluorocarbon encapsulated MBs to 1.8-MHz US pulses. Cavitation was evaluated with passive detection of the inertial cavitation dose (ICD) and active imaging of MB destruction. Effects of peak negative pressure, pulse length, pulse repetition frequency (PRF), MB concentration, and focal scanning strategies, on cavitation were studied in an agar tissue phantom. Preliminary in vivo studies were performed to study the feasibility of delivering PLGA-PEG NPs into hepatocellular tumors in mice.

RESULTS

Passive cavitation detection showed that the ICD increased with pressures increasing from 0.5 to 5MPa, and with PRFs increasing from 10 to 100 Hz (N=6 each). The ICD also increased with increasing MB concentration from 4×10^6 to 1×10^8 bubbles/mL, but saturated at higher concentration (N=6 each). No significant effect was found for pulse lengths below 15 cycles. Active cavitation imaging confirmed more MB destruction with increasing pressures. When the pressure exceeded 3MPa, more violent cavitation was observed as flickering bright spots at the focus of US. Compared to single focus treatment, electronic focal steering over a large target volume resulted in more homogeneous treatment (N=4 each). Preliminary in vivo experiments showed successful delivery of PLGA-PEG NPs to a hepatocellular tumor.

CONCLUSION

The pressure, PRF, MB concentration, and focal scanning strategies, have distinct effects on cavitation, while no significant influence was found for short pulse lengths. Preliminary in vivo results demonstrated the feasibility of delivering PLGA-PEG NPs into tumors for targeted cancer therapy.

CLINICAL RELEVANCE/APPLICATION

This study presents a clinically translatable systematic approach for spatially localized and optimized delivery of large drugs/carriers to target sites based on quantitative measurement of cavitation

SSA21-09 • Comparing Immunohistochemical Markers of Angiogenesis to Subharmonic Imaging of Vascularity in a Murine Breast Cancer Model

Andrew Marshall ; Jaydev K Dave PhD, MS ; Flemming Forsberg PhD (Presenter) * ; Valgerdur Halldorsdottir MSc ; Anya I Forsberg ; Manasi Dahibawkar BSc ; Traci B Fox MS, RT ; Ji-Bin Liu MD *

PURPOSE

To compare contrast-enhanced subharmonic ultrasound imaging (SHI) of breast tumor neovascularity to three immunohistochemical markers of angiogenesis in nude rats.

METHOD AND MATERIALS

Seventy athymic, nude, female rats were implanted with 5×10^6 breast cancer cells (MDA-MB-231) in the mammary fat pad. The contrast agent Definity (Lantheus Medical Imaging, N Billerica, MA) was injected in a tail vein (dose: 36 μ l) and fundamental ultrasound imaging as well as pulse-inversion SHI was performed in triplicate with a modified Sonix RP scanner (Ultrasonix Imaging, Richmond, BC, Canada) using a L9-4 linear array (transmitting at 8 MHz and receiving at 4 MHz in SHI mode). Studies were performed 21, 24 and 28 days post implantation (based on our prior experience). After the experiments, specimens were stained for endothelial cells (CD31), vascular endothelial growth factor (VEGF), and cyclooxygenase-2 (COX-2). Fractional tumor vascularity (FV) was calculated from digital images as contrast enhanced pixels over tumor area (for SHI; averaged over the 3 injections) and staining over tumor area (for specimens). Results were compared using a linear regression analysis.

RESULTS

Of the 70 rats implanted 45 (64 %) exhibited tumor growth and 32 were successfully imaged. SHI depicted the tortuous morphology of tumor neovessels and delineated areas of necrosis better than fundamental ultrasound imaging, due to the marked suppression of tissue signals. VEGF varied significantly over time (p

CONCLUSION

Quantitative contrast-enhanced SHI measures of tumor neovascularity in a breast cancer xenograft models appear to provide a noninvasive marker for angiogenesis corresponding to the expression of VEGF; albeit based on a limited sample size.

CLINICAL RELEVANCE/APPLICATION

In the future SHI may be used to monitor response for patients treated with anti-VEGF drug therapies.

A Comparison of Radiation Dose to the Colon between Single-energy and Dual-energy CT Colonography

Sunday, 12:30 PM - 01:00 PM

[Back to Top](#)

LL-PHE3075-SUA

Da Zhang , PhD

Wenli Cai , PhD

Xinhua Li , PhD

Tianyu Liu

Bob Liu , PhD

Background

With recent technical advances, dual energy CT (DE-CT) became widely available in clinical practice. However, the radiation dose is one of the major concerns for the application of DE-CT in clinical practice. CT dose index (CTDIvol) is a conventional radiation metric reported by a scanner, and is based on uniform cylindrical phantoms. To optimize the radiation dose of different imaging protocols for low-dose DE-CT colonography, we measured the radiation dose to the colon at different scanning modes under the same level of reported CTDIvol.

Evaluation

A custom-ordered anthropomorphic colon phantom was scanned on a DE-CT scanner (Siemens SOMATON Definition Flash). The phantom was scanned in three modes: 1) a single energy (SE) mode at tube voltage of 120 kVp, 2) a DE mode with Tube A at 80 kVp and tube B at 140 kVp with Sn filter (A80, B140 Sn), and 3) a DE mode with Tube A at 140 kVp and tube B at 80 kVp (A140, B80). Automatic tube current modulation was fully activated at each mode to achieve clinical relevant dose distribution. By manually adjusting the reference tube current at each scanning mode, all the scans were performed with the same reported CTDIvol of 1 mGy. A thimble ionization chamber (Radcal 10x6-0.6) was placed at six different places near the colonic surface within the phantom for dose measurements. The doses at six places were recorded during the scanning at each mode and were compared.

Discussion

With the same reported CTDIvol of 1 mGy, the mean absorbed dose were 1.77 mGy, 1.59 mGy, and 1.44 mGy for the (A80, B140 Sn) DE mode, SE mode, and (A140, B80) DE mode, respectively. The dose distribution in the colon was lower at both ends of the scanned range in the axial direction, and reached the peak at the middle of the scanned range, due to the accumulation of scatter radiation.

CONCLUSION

Scanner reported CTDIvol is a measure of radiation output, which is substantially different from the organ absorbed dose. The actual radiation dose to the colon may vary at different scanning modes under the same level of CTDIvol.

Physics - Sunday Posters and Exhibits (12:30pm - 1:00pm)

Sunday, 12:30 PM - 01:00 PM • Lakeside Learning Center

[Back to Top](#)

PH

LL-PHS-SUA • AMA PRA Category 1 Credit™:0.5

Host

Xiao Han , MSC

LL-PHS-SU1A • A New Concept of CT with Fixed Anodes (Fixed Anodes CT, FA-CT)

Markus Kellermeier (Presenter) ; Reinhold Muller

PURPOSE

We started with studies to thermal loads of X-ray anodes. Based on the best results an optimal CT concept was newly developed and compared with a common clinical system.

METHOD AND MATERIALS

The energy deposition in a X-ray anode was obtained by Monte Carlo simulation (GAMOS/GEANT4). Using acquired initial values the temperature distribution was calculated in space and time by applying of Finite Element Method (COMSOL Multiphysics). Out of common dimensions for anodes we developed a simulation model for fixed and rotary anodes. Geometric dimensions and material uncertainties were considered parametrically.

2500 K were adjusted as maximum temperature for tungsten as target layer. For cooling, a heat bath of 300 K was defined on a copper body base.

Simulations were carried out presuming short-term exposure (1 μ s \leq 1 s).

Long-term loads are examined in terms of the continuous operation of FA-CT.

A virtual model was created using characteristics of sources and detectors.

RESULTS

Simulations to thermal loads of anodes are in good agreement with literature data regarding absolute values and trends. Optima from parametric studies lead to the concept of fixed anodes, FA-CT.

Results from virtual model evidence profits up to 6 times in scan time or performance. Short integration times per projection of about 10 μ s lead to a higher amount of data (>25x). A dense physical information system handled by pre- or post-processing allows a familiar image quality and enhanced resolution in the axial direction.

CONCLUSION

Several promising improvements can be recognised for FA-CT in comparison to a conventional clinical CT. The elimination of mechanical moving components results in an arrangement of a row of 1160 small fixed anodes covering 360°. The distribution around the patient

leads to a source ring in parallel to a detector ring. It is not necessarily restricted to a circular arrangement. The components enable a compact design, making it easier to be combined with other imaging devices (MRI/PET/SPECT) and also to have a close combination of X-ray therapy devices (e.g. LINACs, particle accelerators, and also brachy therapy) with real-time imaging.

CLINICAL RELEVANCE/APPLICATION

The FA-CT technology without mechanical moving components provides by several factors shorter scanning, promises a great leap forward in image-based medicine.

LL-PHS-SU2A • A Simple and Accurate Measurement Method of Temporal Resolution for Cardiac Computed Tomography

Kazuya Ohashi (Presenter) ; **Katsuhiko Ichikawa** PhD ; **Makoto Kawano** ; **Yuta Shibamoto** MD, PhD

PURPOSE

The temporal resolution (TR) has been used for image evaluation of cardiac computed tomography (CT). However, since the practical method for measuring TR for cardiac CT has not been established, most of papers about the cardiac CT have used nominal TR values for TR descriptions, which are generally indicated in technical manuals. The purpose of this study was to propose a simple and accurate TR measurement method for the cardiac CT.

METHOD AND MATERIALS

We employed a dual source CT (DSCT) system (Somatom Definition, Siemens Medical Solutions) equipped with two X-ray tubes with an angular offset of 90°. The DSCT system has three reconstruction modes with nominal TRs of 83, 125, and 165 ms. We measured TR for each mode using an impulse signal method. In this method, the temporal impulse signal was generated by using a metal ball with an 11-mm diameter, which pass through scan planes at a very high speed (>5 m/sec) during cardiac CT scanning. By using this method, we were able to obtain phase sensitivity profiles (PSPs) as correct indices of TR of the cardiac CT. PSP was measured from region of interest (ROI) values in reconstructed impulse response CT images at every phase percentages of the cardiac cycle. We also calculated temporal MTFs by Fourier transform of PSPs for respective TR modes, and compared them.

RESULTS

The shapes of the 83- and 165-ms TR modes were simple trapezoids with full width at half maximum (FWHMs) of exact 83 ms and 165 ms, respectively. However, since the 125-ms mode presented a complicated PSP shape like a convex, its FWHM could not be evaluated. In contrast, the temporal MTF curves provided effective results for the TR comparison. From the temporal MTF results, we found that the three TR modes of DSCT have valid TRs equivalent to their nominal values.

CONCLUSION

PSP of the cardiac CT was able to be measured accurately by using the impulse method we proposed in this study. The temporal MTF calculated from the PSP was also effective to compare the TR in case of PSP with a complicated shape. Although this method can not be applied to the multi segment reconstruction modes, the half reconstruction modes which are becoming the standard can be evaluated by this method.

CLINICAL RELEVANCE/APPLICATION

The correct TRs measured using our proposed method would be effective for clarifying the relationship between TR and cardiac CT image quality.

LL-PHS-SU3A • Metal Artifact Reduction for Orthopedic Implants in Lower Extremity Angiography: Evaluation of Image Quality and Vessel Visualization

Kwang Nam Jin MD (Presenter) ; **Jee Won Chai** MD ; **Hyo Bin Seo** ; **Young Ho Choi** MD ; **Young Ho So** ; **Su Jin Kim** MD ; **Youkyung Lee** MD ; **Jae Yeon Wi** MD ; **Hyun Kyong Lim** MD

PURPOSE

The purpose of this study was to evaluate whether O-MAR (metal artifact reduction algorithm for orthopedic implants) improve the image quality and vessel visualization in lower extremity CT angiography.

METHOD AND MATERIALS

In 15 patients who had orthopedic implants in the hip (n = 6) or knee (n = 19) and underwent lower extremity CT angiography, we reconstructed O-MAR corrected 5 mm-thick axial CT images (OM) and non-corrected images (NC) in each patient. We recorded the type of implants in total 25 limbs. For each limb, 2 reviewers evaluated the subjective image quality, using 3-point scale, in terms of overall beam hardening artifact reduction (0, no; 1, minimal; 2, marked; 3, no residual artifact) and peri-implant artifact in OM (0, no; 1, artifact not invading vessels; 2, artifact invading vessels and diagnosis of thrombus or stenosis is possible; 3, artifact invading vessels and making diagnosis impossible), respectively. For subjective evaluation of vessel visualization, we counted the number of axial images, in which vessel was evaluable, and total number of images covering whole implants. We compared percentage of image with evaluable vessel in OM and NC, respectively.

RESULTS

There were 18 limbs with total knee replacement implants (TKR), 6 with total hip replacement implants (THR), 1 limb with cruciate ligament reconstruction (CLR). Marked reduction of overall beam hardening artifact was achieved in all patients for both reviewers. There was peri-implant artifact invading adjacent vessels on OM in 17 patients (68.0 %) for R1 and 18 (72.0 %) for R2 (100 % in 17 limbs with TKR and 0 % in 6 with THR). Number of images with evaluable vessels was higher in OM than NC (19.0 ± 10.8 vs 17.6 ± 11.0 , $p < 0.001$). Percentage of images with evaluable vessel was 76.5 ± 17.4 in OM and 69.8 ± 19.8 in NC ($p < 0.001$). Although the difference was significant in 17 limbs with TKR (69.0 ± 12.7 in OM and 60.7 ± 12.5 in NC, $p < 0.001$), there was no significant difference in 6 with THR (100.0 ± 0.0 in OM and 98.5 ± 2.8 in NC, $p = 0.25$).

CONCLUSION

With the use of O-MAR algorithm, image quality and vessel visualization of lower extremity angiography can be improved in patient with orthopedic implants.

CLINICAL RELEVANCE/APPLICATION

Postoperative CT imaging in patients with orthopedic implants in hip or knee is challenging. O-MAR will help the diagnosis of deep vein thrombosis or atherosclerosis by reducing artifacts.

LL-PHS-SU4A • Changing from Excision Biopsy to Core Biopsy in the Diagnosis of Neck Lymphoma - An Audit of 4 Years Experience

Kit H Chow MBBCh, FRCR (Presenter) ; **Unnikrishnan Anoop** MBBS, FRCR ; **Rathinavelu Balamurugan** MBBS ; **Chris Stonard** ; **Yuliya Khober**

CONCLUSION

Core biopsy should be the initial biopsy technique for diagnosis of lymphoma.

Background

The process of change from excision biopsy (EB) to core biopsy (CB) for neck lymphoma is often a creeping development of an imaging service. This purpose of this study is to discover changes that had taken place over a period of four years in an UK, NHS district general hospital, when the initial technique for initial tissue evaluation of lymphoma has changed from EB in 2008 to CB in 2011, with incremental implementation from 2009-2010.

Discussion

All clinicians preferred CB as the method of tissue biopsy for the initial pathological diagnosis of lymphoma despite its lower diagnostic

rate compare to EB. The advantage of Ultrasound Guided CB technique is the ease of this cheap relatively non-invasive technique. The number of cases diagnosed from neck biopsy increased in 2011 by 67%. This finding would require further research and may reflect: - 1) Lead-time. 2) Neck preferred body biopsy site. 3) Improved histo-chemistry.

LL-PHS-SU5A • Application of Low-dose Dual-energy Electronic Cleansing to Sub-mSv Fecal-tagging CT Colonography

Wenli Cai PhD (Presenter) ; **Simone Mazzetti** ; **Daniele Regge** MD ; **Hiroyuki Yoshida** PhD *

PURPOSE

Application of dual-energy fecal-tagging CTC (DE-CTC) to electronic cleansing (EC), denoted as DE-EC, provides a promising EC solution for identifying and cleansing iodine-tagged fecal materials in CTC images. With the technical advances in image reconstruction and post-processing, low-dose DE-EC offers the technical feasibility for visualization of the entire colonic surface. The purpose of the study was to develop a low-dose DE-EC scheme that works efficiently for sub-mSv DE-CTC.

METHOD AND MATERIALS

17 patients underwent a 24-hour bowel preparation with a low-fiber, low-residue diet, and oral administration of 150 ml of iodinated contrast agent. Dual-energy CT scanning (SOMATOM Definition Flash) was performed with the following low-dose imaging protocol: Tube A at 80 kVp / 40 mAs and tube B at 140 kVp / 15 mAs with Sn Filter, automatic dose exposure control module (CARE Dose 4D), and SAFIRE iterative reconstruction (I30f). CT dose index (CTDIvol) and effective dose length products (DLP) were recorded in each scan for dose measurement. Resulting DE-CTC images were subjected to the low-dose DE-EC scheme consisting of the following steps: (1) initial segmentation of the colon, (2) noise reduction using our previously developed dual-energy structural diffusion filter, (3) virtual colon tagging (VCT) using material maps calculated with our localized 3-material decomposition model, (4) computation of Hessian response field in VCT images, and (5) segmentation and removal of the fecal materials in the colonic lumen.

RESULTS

The average radiation dose per position was 1.08 mGy / 0.89 mSv, which was less than 70% than that of the recommended radiation dose for conventional single-energy CTC screening (2.5 ~ 2.8 mSv). Visual assessment of the virtual colon fly-through indicated that our low-dose DE-EC achieved the similar quality as that of DE-CTC cases scanned with normal radiation dose. Preliminary evaluation showed that all submerged polyps were clearly visualized with 0-1 minor EC artifacts per case compared to 5-6 significant EC artifacts per case in single-energy EC.

CONCLUSION

Our low-dose DE-EC scheme may provide an effective solution in electronically cleansing sub-mSv DE-CTC images in colon cancer screening.

CLINICAL RELEVANCE/APPLICATION

New low-dose dual-energy EC can substantially reduce the radiation dose and it may lead to sub-mSv CT colonography for colon cancer screening.

LL-PHS-SU6A • Minimizing Radiation Dose in Children Paranasal Sinuses CT with a Model-based Iterative Reconstruction Algorithm

Ji Hang Sun (Presenter) ; **Yun Peng** MD

PURPOSE

To evaluate the clinical value of a model-based iterative reconstruction (MBIR, trade name 'VEO') to minimize radiation dose in children paranasal sinuses CT.

METHOD AND MATERIALS

15 leukemia children (10 months to 11y of age, median age 4 years) for the follow-up CT examination within 2 months of the initial scan (control group) were included in the study group. The children in the study group underwent an extremely low dose helical scan using 80kV and 10mA, and images were reconstructed using VEO technique with 0.625mm slice thickness. The scans in the control group used a standard protocol with 120kV, automatic tube current modulation for noise index (NI) of 14. Images in this group were reconstructed with filtered back projection (FBP) with 0.625mm slice thickness. Two radiologists independently evaluated the multi planar reformat (MPR) images including the subjective image noise, the bones of paranasal sinuses, and the soft tissue on a 5-point scale with 3 being clinically acceptable (5 is the best); Quantitative image noises on the left vitreous body and the thickness of Maxillary sinus wall were measured and statistically compared between the two groups. The CT dose index (CTDIvol) and dose-length product (DLP) were recorded.

RESULTS

CONCLUSION

Compared with routine-dose CT with FBP, the lower-dose CT with VEO provided 95.0% dose reduction in pediatric paranasal sinuses CT examinations, while maintaining diagnostically acceptable images.

CLINICAL RELEVANCE/APPLICATION

The use of a full model-based iterative reconstruction algorithm (VEO) provides significant radiation dose reduction to eyes in pediatric paranasal sinuses CT.

LL-PHS-SU7A • IMRT, Hybrid IMRT, and 3D Conformal Plan for Carcinoma Esophagus-A Dosimetric Comparison from a Prospective Randomized Controlled Study

Pritee Chaudhari (Presenter) ; **Seema Sharma** MS ; **Supriya Mallick** MBBS ; **Subhash Chander** MD, MBBS ; **Sushmita Pathy** MD, MBBS ; **Durai Manigandan** PhD ; **Pk Julka** ; **Ashish A Patil** MBBS

LL-PHE-SU8A • CT Radiation Dose: A Review of the Current Controversies and Dose Reduction Strategies through Clinical Scenarios and Patient/Clinician Questions

Justin E Costello DO (Presenter) ; **Nathan D Cecava** MD ; **Jonathan Tucker** ; **Jennifer L Bau** MD

PURPOSE/AIM

1. Awareness and compilation of radiation doses of typical exams performed on patients entering through the ER and in the hospital setting 2. To discuss BEIR VII strengths and weaknesses in calculating potential cancer risks associated CT 3. To demonstrate increased risk (if any) of future cancers, through theoretical patient scenarios, based on CT dose and application of BEIR VII biologic models 4. To review strategies for CT dose reduction

CONTENT ORGANIZATION

Attention to patient radiation dose, as well as dose reduction strategies are of paramount concern. In this educational exhibit, we will track theoretical patients entering through the ER using an interactive format with the learner to answer questions about radiation doses, specific organ doses, and potential cancer risk. We will report the risk (if any) of future cancer development using BEIR VII biological models. Opportunities and ideas for radiation dose reduction will be presented, as they relate to our clinical scenarios.

SUMMARY

1. Knowledge of effective doses for typical emergency room CT exams 2. Understanding the application of and controversies associated with BEIR VII in the calculation of cancer risk associated with CT scans 3. Implication of current modulation, low-voltage protocols, breast shields, and iterative reconstruction as CT dose reduction strategies

LL-PHE-SU9A • Artifacts a Novice Sonologist May Encounter: How to Recognize, Correct or Utilize Them!

PURPOSE/AIM

During ultrasonography artifacts are commonly encountered by sonologist which may confuse them. In this article, we will review common artifacts in grey scale, spectral and color doppler imaging. For each artifact, emphasis is placed on the physics behind it, imaging appearance, diagnostic importance, and when applicable, scanning technique modifications to improve image quality

CONTENT ORGANIZATION

This work was carried out at our institution in department of Radio-Diagnosis on diseased patients and on healthy volunteers using My LAB 60 ESAOTE ultrasound machine. Causes of artifacts :- those resulting from (i) improper scanning technique and equipment setting (ii) anatomic factors (iii) technical limitations of modality. Based on our study common artefacts encountered during routine grey scale imaging are beam width, side lobe, reverberation, comet tail, ring-down, mirror image, speed displacement, attenuation, shadowing, and increased through transmission. Common artefacts during spectral and Doppler ultrasound are gain setting error, aliasing and velocity scale errors, mirror image artefacts; color in non vascular structures, direction ambiguity and spectral broadening artefact.

SUMMARY

Misdiagnosis can be avoided when the sonologist is aware to these artifacts and thus improve quality of his scans and provide optimal patient care.

Medical Physics 2.0: Computed Tomography

Sunday, 02:00 PM - 03:30 PM • N228



[Back to Top](#)

RC121 • *AMA PRA Category 1 Credit*™:1.5 • *ARRT Category A+* Credit:1.5

Co-Director

Ehsan Samei, PhD *

Co-Director

Douglas E Pfeiffer, MS *

LEARNING OBJECTIVES

1) To understand the current recommendations for computed tomography testing and quality control. 2) To understand impact of accreditation and regulation on CT quality assurance. 3) To understand current dosimetry and dose-reporting considerations.

ABSTRACT

Many organizations have contributed to the methodology for testing computed tomography scanners. These have included state regulatory agencies, the Food and Drug Administration, the American Association of Physicists in Medicine, and the American College of Radiology, among many other groups and individuals. These contributions have included many good ideas, but also much confusion as to what is required. Further, the complexity of modern CT scanners has rendered some tests obsolete or difficult to implement. This presentation focuses mainly on the testing delineated by the 2012 American College of Radiology Computed Tomography Quality Control Manual and that required under the Intersocietal Accreditation Commission. Recommended and required tests will be identified but not described in detail.

RC121A • Computed Tomography Perspective

Mahadevappa Mahesh MS, PhD (Presenter) *

LEARNING OBJECTIVES

1) To reflect on MDCT technology enabling volumetric data acquisition. 2) To evaluate new innovations enabling dose reductions in CT.

ABSTRACT

This talk will provide brief overview on the innovations that has led to the development of CT technology (single slice (SDCT) to multiple slices (MDCT)). Past decade saw the rapid evolution in the capability to obtain multiple slices per gantry rotation (4-320 slices). Having achieved the capability to acquire volumetric data (covering entire cardiac anatomy in half of gantry rotation), the race is currently towards acquiring CT images at very low radiation dose. Volume CT, dual energy CT, Iterative reconstruction, quantitation are some of the new challenges that will be discussed in this talk. 1. CT Technology 1a. MDCT detector configuration 1b. Volume CT ♦ Wide detector and dual source CT 2. New Challenges 2a. Iterative reconstruction 2b. Dual energy 2c. Dose check

RC121B • Computed Tomography 1.0

Douglas E Pfeiffer MS (Presenter) *

LEARNING OBJECTIVES

1) To understand the current recommendations for computed tomography testing and quality control. 2) To understand impact of accreditation and regulation on CT quality assurance. 3) To understand current dosimetry and dose-reporting considerations.

ABSTRACT

Many organizations have contributed to the methodology for testing computed tomography scanners. These have included state regulatory agencies, the Food and Drug Administration, the American Association of Physicists in Medicine, and the American College of Radiology, among many other groups and individuals. These contributions have included many good ideas, but also much confusion as to what is required. Further, the complexity of modern CT scanners has rendered some tests obsolete or difficult to implement. This presentation focuses mainly on the testing delineated by the 2012 American College of Radiology Computed Tomography Quality Control Manual and that required under the Intersocietal Accreditation Commission. Recommended and required tests will be identified but not described in detail.

RC121C • Computed Tomography 2.0

Ehsan Samei PhD (Presenter) *

LEARNING OBJECTIVES

1) To become familiar with the major new developments of physics support for clinical CT operations. 2) To understand the need and the definitions of the new CT performance metrics for dose and quality. 3) To understand the testing implications of new CT technologies. 4) To understand the need for operational optimization of CT systems.

ABSTRACT

Uncertainties in Imaging for Radiation Oncology: Sources and Mitigation Techniques-Image Guidance in the Treatment Room

Sunday, 02:00 PM - 03:30 PM • S504AB



[Back to Top](#)

RC122 • *AMA PRA Category 1 Credit*™:1.5 • *ARRT Category A+* Credit:1.5

LEARNING OBJECTIVES

1) Terminology to describe uncertainties. 2) Methodologies for evaluating uncertainties in IGRT. 3) Uncertainties in IGRT technologies, including mitigation strategies (generic, not site-specific).

RC122A • Terminology to Describe Uncertainties and Methodologies for Evaluating Uncertainties in IGRT

Laurence E Court PhD (Presenter)

LEARNING OBJECTIVES

1) Understand the different sources of uncertainty in radiation therapy. 2) Be able to identify the different terminology used to categorize uncertainties in radiation therapy. 3) Have the rationale to judge published work, and determine whether the reported uncertainties are appropriate and applicable to the local institution.

ABSTRACT

IGRT is now standard-of-care for many treatment sites. The appropriate use of IGRT has the potential to reduce uncertainties in the radiation therapy treatment, and can potentially allow for reducing treatment margins. The first step in reducing margins is to understand the different sources of uncertainty. Institutions may establish their own uncertainties, and may also utilize published data. In order to do this, it is important that the physicist understands the different potential sources of uncertainty in radiation therapy, and also understands different approaches to categorizing uncertainties, systematic and random. There is currently no consensus on how these uncertainties are measured or reported, and this can lead to confusion when interpreting published data. This presentation will describe the different sources of uncertainty, and introduce the learner to different approaches used in the literature to quantify these uncertainties.

RC122B • Uncertainties in IGRT Technologies, Including General Mitigation Strategies

Timothy Craig PhD (Presenter) *

LEARNING OBJECTIVES

1) Appreciate the breadth of IGRT technologies used in the radiation therapy treatment room. 2) Understand the different sources of uncertainty for different IGRT approaches. 3) Understand approaches to mitigating the limitations of different IGRT technologies.

ABSTRACT

There is a large variety of technologies available for image-guided radiation therapy (IGRT), including 2D projection x-ray imaging (kilovoltage (kV) and megavoltage (MV)), computed tomography (conventional, MV, and cone-beam), ultrasound, and radiofrequency emitting markers. There are also different methodologies for using these technologies, or combinations of these technologies. Each technology has its own uncertainties and limitations which should be well described and understood. Similarly, each technology has different approaches available for mitigating these uncertainties that need to be appreciated. In this presentation we will describe and compare the different technologies and IGRT approaches, and give an overview of the uncertainties involved in the use of each.

Minicourse: Current Topics in Medical Physics-Clinically Focused Physics Education: Principles to Practice

Sunday, 02:00 PM - 03:30 PM • N229

PH **ED**

[Back to Top](#)

RC123 • AMA PRA Category 1 Credit™:1.5 • ARRT Category A+ Credit:1.5

Moderator

Perry Sprawls , PhD *

LEARNING OBJECTIVES

ABSTRACT

URL's

<http://www.sprawls.org/clinphys>

RC123A • Clinically Focused Physics Education: Principles to Practice-Part A

Perry Sprawls PhD (Presenter) *

LEARNING OBJECTIVES

1) Describe the general characteristics of mental knowledge structures of physics and technology that are required for effective clinical applications. 2) Describe conditions and activities that contribute to the formation of effective knowledge structures. 3) Identify the different levels of learning that can occur and relate them to specific actions that can be performed and potential outcomes. 4) Analyze learning activities for effectiveness and efficiency in producing desired outcomes with available human effort and resources. 5) Identify the opportunities to use digital technology to enhance human performance for both learners and learning facilitators. 6) Identify resources that can be used to optimize the effective-efficiency relationship of learning activities. 7) Provide effective learning activities.

RC123B • Clinically Focused Physics Education: Principles to Practice-Part B

Debra L Monticciolo MD (Presenter)

LEARNING OBJECTIVES

1) To review the need for updated physics education in the clinical setting. 2) To review the use of computer-based learning in the clinical setting for physics education of radiology residents.

ABSTRACT

Quantitative Imaging: Current and Future Practice in Radiology and Clinical Trials

Sunday, 02:00 PM - 03:30 PM • S104A

RS **PH** **BQ**

[Back to Top](#)

RC125 • AMA PRA Category 1 Credit™:1.5 • ARRT Category A+ Credit:1.5

Director

Michael F McNitt-Gray , PhD *

RC125A • RSNA Perspective and Initiatives

Daniel C Sullivan MD (Presenter)

LEARNING OBJECTIVES

1) Describe the benefits of implementing more quantitative image interpretation in clinical radiology practice. 2) Understand the activities

that RSNA supports to help move the profession of radiology from a primarily qualitative interpretation paradigm to a more quantitative-based interpretation model. 3) Describe the challenges of extracting uniform, standardized quantitative measures from clinical imaging scans.

ABSTRACT

The RSNA Strategic Plan strives to advance the radiological sciences and foster the development of new technologies in part by promoting the quantification of imaging results. The added value of quantification in both research and clinical environments is likely to increase as health care initiatives place increased pressure on radiologists to provide decision support for evidence-based care. There remain substantial barriers to the widespread use of quantitative measures in clinical radiology including inherently large number of variables that impede validation of specific metrics, diversity of proprietary industry platforms, and lack of acceptance by radiologists. A critical barrier to the implementation of QI in radiology is the lack of standardization among vendor platforms. Collaboration in the pre-competitive space is challenging yet crucial to address standardization, and integrating quantitative measurement into workflow will be necessary for wide adoption. The obstacles to overcome with practicing radiologists are a distrust of the reliability of QI and the fear of losing value of radiologists' expertise through automation and commoditization. The Quantitative Imaging Biomarkers Alliance (QIBA) was officially launched in 2007 as a means to unite researchers, healthcare professionals, and industry stakeholders in the advancement of quantitative imaging. QIBA's mission is to: Improve the value and practicality of quantitative biomarkers by reducing variability across devices, patients and time. QIBA's six active technical committees (DCE-MRI, fMRI, FDG-PET, volumetric CT, COPD-Asthma, US shear-wave speed) develop QIBA Profiles (i.e., documents) of standardized specifications for image acquisition, collection, and post-processing.

RC125B • NCI's Quantitative Imaging Network (QIN): Progress and Impact on Clinical Trials

Paula M Jacobs PhD (Presenter)

LEARNING OBJECTIVES

1) Describe various methods for prediction and measurement of therapy response. 2) Understand which imaging modalities and software tools are best suited for this clinical goal. 3) Understand the complexity of quantitative imaging methodology and how to compare the performance of different. 4) Understand how NCI Research Networks function to create a consensus on imaging methodology and public resources to meet these aims. 5) Learn about NCI funding opportunities for this research area.

RC125C • American College of Radiology Imaging Network/Eastern Cooperative Oncology Group (ACRIN/ECOG) Perspective

Mitchell D Schnall MD, PhD (Presenter)

LEARNING OBJECTIVES

1) Identify the importance of quantitative imaging principles in the setting of clinical trials. 2) Identify conditions required for successful application of quantitative imaging principles. 3) Analyze quantitative imaging techniques and apply this knowledge to protocol development in the setting of clinical trials.

Medical Physics 2.0: Mammography

Monday, 08:30 AM - 10:00 AM • S404AB

PH **DM** **BR**

[Back to Top](#)

RC221 • *AMA PRA Category 1 Credit*™:1.5 • *ARRT Category A+* Credit:1.5

Co-Director

Ehsan Samei, PhD *

Co-Director

Douglas E Pfeiffer, MS *

RC221A • Mammography Perspective

Douglas E Pfeiffer MS (Presenter) *

LEARNING OBJECTIVES

1) Understand the history and development of mammographic imaging equipment. 2) Understand the impact of equipment development on testing protocols. 3) Understand the impact of equipment development on regulation.

ABSTRACT

Mammographic imaging has undergone tremendous change since its inception. Rapid development from screen-film imaging to nearly universal acceptance of digital imaging has required a shift in testing methodology. This talk will briefly introduce the developments that have taken place and discuss the impact that this development has had on testing and regulation.

RC221B • Mammography 1.0

Melissa C Martin MS (Presenter)

LEARNING OBJECTIVES

1) Current requirements for Quality Control for Hologic Digital Mammography Units. 2) Current requirements for Quality Control for General Electric Digital Mammography Units. 3) Current requirements for Quality Control for Fuji Computed Radiography for Mammography Units. 4) Current requirements for Quality Control for Printers used with Digital Mammography Units. 5) Current requirements for Quality Control for Monitors used with Digital Mammography Units.

RC221C • Mammography 2.0

Eric A Berns PhD (Presenter)

LEARNING OBJECTIVES

1) To provide an overview of how the Medical Physicist can prepare for the future of clinical mammography physics. 2) To provide a landscape of mammography imaging technologies. 3) To describe methods of image quality metrics, dose reduction, and quality control in relation to mammography technologies. 4) To describe the future roles of the Medical Physicist in clinical mammography physics.

Uncertainties in Imaging for Radiation Oncology: Sources and Mitigation Techniques-Margins and Margin Design

Monday, 08:30 AM - 10:00 AM • S102C

PH **RO**

[Back to Top](#)

RC222 • *AMA PRA Category 1 Credit*™:1.5 • *ARRT Category A+* Credit:1.5

Co-Director, Moderator

Laurence E Court, PhD

LEARNING OBJECTIVES

- 1) Incorporating IGRT uncertainties into treatment margins.
- 2) Approaches to using margins to mitigate uncertainties.

RC222A • Incorporating IGRT Uncertainties into Treatment Margins

Timothy Craig PhD (Presenter) *

LEARNING OBJECTIVES

1) Be able to identify the different terminology used to describe margins in radiation therapy. 2) Understand how different types of uncertainty contribute to the appropriate treatment margin. 3) Demonstrate an understanding of the many factors that can influence the margins required to account for treatment uncertainties. 4) Have the rationale to determine which approaches could/should be applied in their own practice.

ABSTRACT

During treatment planning a safety margin is added to the clinical target volume to ensure that the planned dose is actually delivered to the target. This margin may be calculated by correctly combining the contributions to the overall treatment uncertainty from numerous individual uncertainties. Once the uncertainties have been categorized, there are many ways in which they can be combined to give the actual treatment margin, and this must be done in a considered way. In this presentation we will describe how different uncertainties should be combined. We will describe published margin recipes, including the impact of different assumptions made in each recipe. These concepts will be discussed in the context of guidance documents from the International Commission on Radiation Units and Measurements.

RC222B • Approaches to Using Margins to Mitigate Uncertainties

Laurence E Court PhD (Presenter)

LEARNING OBJECTIVES

1) Understand practical approaches used to determine appropriate treatment margins. 2) Have the knowledge/skills to apply margin formulae in the IGRT era. 3) Appreciate the limitations and risks of applying margin formulae.

ABSTRACT

One advantage of IGRT is the potential for reducing margins. Clinical margins are typically determined in one of 3 ways: (1) Use same margins as before (pre-IGRT), (2) Reduce margins based on supposed improvement in accuracy/precision, perhaps based on published data, or (3) Evaluate institutions own uncertainties, and establish appropriate margins. The first two are probably the most common. However, each of these approaches has its own pitfalls: (1) does not take full advantage of our new technologies, (2) is fraught with potential error, including the fact that many published works do not adequately assess uncertainties, and (3) can be difficult, and not all physicists have the background knowledge to do this. In this presentation we will describe some practical approaches to using margin formulae and other methods used to determine safe clinical margins. The limitations, risks and pitfalls will be described.

Minicourse: Current Topics in Medical Physics-Practice Quality Improvement: Basics and Issues for Medical Physicists

Monday, 08:30 AM - 10:00 AM • S403B

QA PH

[Back to Top](#)

RC223 • AMA PRA Category 1 Credit™:1.5 • ARRT Category A+ Credit:1.5

Moderator

G. Donald Frey, PhD

RC223A • Introduction

Richard L Morin PhD (Presenter)

LEARNING OBJECTIVES

1) The participant will have an overall orientation to the role of medical physics in nuclear cardiology.

RC223B • Practice Quality Control: The ABR Perspective

G. Donald Frey PhD (Presenter)

LEARNING OBJECTIVES

1) The participant will understand the role of PQI in the ABR MOC process.

ABSTRACT

This section is an overall introduction to the course and will place Practice Quality Improvement (PQI) into the perspective of the ABR Maintenance of Certification (MOC) process.

RC223C • Basics and Practical Projects

Paul G Nagy PhD (Presenter)

LEARNING OBJECTIVES

1) Learn why quality methodologies can be useful for physicists. 2) Discuss PQI projects a physicist can do in diagnostic radiology. 3) Learn the basics of quality techniques with a discussion around practical PQI projects. 4) Talk about how the physicist can be a real resource to physicians conducting PQI projects.

ABSTRACT

Quantitative Imaging: Diffuse Lung Disease Assessment Using CT

Monday, 08:30 AM - 10:00 AM • N229

PH CT BQ CH

[Back to Top](#)

RC225 • AMA PRA Category 1 Credit™:1.5 • ARRT Category A+ Credit:1.5

Director

Michael F McNitt-Gray, PhD *

RC225A • The Role of Quantitative CT in the Assessment of Diffuse Lung Disease

Jonathan G Goldin MBChB, PhD (Presenter)

LEARNING OBJECTIVES

1) Identify the application of quantitative imaging principles in the assessment of patients with Diffuse Lung Disease. 2) Identify conditions required for successful application of quantitative imaging principles. 3) Analyze quantitative imaging techniques and apply this knowledge to protocol development and patient management in the setting of both clinical workup and clinical trials involving patients

with Diffuse Lung Disease.

RC225B • Quantitation in the Assessment of COPD

David A Lynch MBBCh (Presenter) *

LEARNING OBJECTIVES

1) Describe the methodology and limitations of non-invasive imaging in quantifying lung structure. 2) Describe the opportunities for non-invasive imaging in understanding the structure of the lung, and how that relates to phenotyping subjects for clinical trials and longitudinal studies. 3) Understand the clinical relevance of quantitative imaging of COPD. 4) Learn how to interpret quantitative CT results in the lung.

ABSTRACT

COPD is characterized on CT by emphysema, bronchial wall thickening, and small airway abnormalities. These morphologic findings may be quantified and grouped into phenotypes, with different clinical presentations and prognosis. Clinicians are increasingly using these quantitative imaging techniques to study COPD. This course will provide information on the results of large-scale clinical trials ongoing in COPD. The limitations and sources of variation of current quantitative imaging methods will be discussed. Relationships between quantitative CT measures, genetic markers, and clinical abnormalities will be stressed.

RC225C • Standardization of Imaging and Measurement Protocols

Matthew S Brown PhD (Presenter) *

LEARNING OBJECTIVES

1) Understand sources of quantitative lung CT measurement variation including technical, physiologic, and algorithmic. 2) Review strategies for standardization across multiple sites and imaging platforms. 3) Assess the impact on sample size in multicenter clinical trials.

Physics (CT-Dose Modulation)

Monday, 10:30 AM - 12:00 PM • S403A



[Back to Top](#)

SSC13 • AMA PRA Category 1 Credit™:1.5 • ARRT Category A+ Credit:1.5

Moderator

Michael F McNitt-Gray, PhD *

Moderator

James T Dobbins, PhD *

SSC13-01 • Experimental Validation of Shaped Filter Design with Variable Source-to-Filter Distance for Breast CT with Respect to Image Quality and Dose

Ferdinand Lueck Dipl Phys * ; **Daniel Kolditz** PhD (Presenter) * ; **Martin Hupfer** PhD * ; **Willi A Kalender** PhD *

PURPOSE

To validate the use of a single shaped filter with variable source-to-filter distance (SFD) for dedicated breast CT (bCT) and arbitrary breast sizes.

METHOD AND MATERIALS

The shaped filter was designed using simulations of a dedicated bCT system with the goal to achieve noise homogeneity and dose reduction for breast diameters of 80 to 180 mm. This was accomplished with a filter design method that aims to achieve a homogeneous detector noise but considering a correction factor for the filtered back projection process. According to the simulations a single shaped filter designed for the largest breast diameter works for all breast diameters if SFD can be adjusted. To validate these results the filter was manufactured of an aluminum alloy. The measurements were performed on a bCT prototype with breast phantoms (80% adipose, 20% glandular tissue) of diameters from 80 to 180 mm. The filter was positioned at SFDs from 54 to 112 mm according to the phantom diameter. Image quality was evaluated for the reconstructed volume by assessing CT value accuracy, noise homogeneity and spatial resolution. Furthermore, scatter distribution was determined with the use of a beam-stop phantom with and without shaped filter. Dose reduction was measured using a calibrated ionization chamber in the center and in the periphery of the phantom.

RESULTS

The results with a single shaped filter at variable SFD resulted in improved noise homogeneity and dose reduction for all breast diameters: noise homogeneity was improved from 15% down to 5% and the overall dose was reduced by about 30 to 40% for all breast diameters. Furthermore, scatter reduction of about 60% was achieved, which reduced cupping artifacts and improved the CT value accuracy. Spatial resolution was not affected by the shaped filter.

CONCLUSION

By means of shaped filters designed for bCT, significant dose reduction can be achieved and image quality can be improved by reducing noise inhomogeneity as well as scatter-induced artifacts. A single shaped filter designed for the largest breast diameter used with variable SFD appears to be a good solution for bCT.

CLINICAL RELEVANCE/APPLICATION

The use of a shaped filter for bCT appears essential to keep patient dose as low as reasonably achievable.

SSC13-02 • An Automated Method to Estimate Organ Dose from Tube Current Modulated (TCM) CT Scans Using Software to Extract Regional Tube Current Values

Maryam Khatonabadi (Presenter) * ; **Tim O'Connell** MD, MEng * ; **Aaron D Sodickson** MD, PhD ; **Michael F McNitt-Gray** PhD *

PURPOSE

Regional CTDI_{vol} has proven to be a valuable metric for estimating dose from TCM CT scans; however, its practicality has not been established. The purpose of this study was to evaluate an automated landmark recognition software which can be used to extract basic landmarks within a CT exam to calculate both regional CTDI_{vol}, and regional water equivalent diameter (WED) metrics to enable automated organ dose estimates.

METHOD AND MATERIALS

Image data and tube current modulation data were collected from 10 patients who underwent either an abdomen/pelvis (N=4) or thorax (N=6) exams. An automated software program was used to analyze each patients' image data and identify the type of exam and to extract image numbers corresponding to important landmarks of regional anatomy: for thorax, locations of the lung apices and the top of the diaphragm were extracted; for A/P, locations of the top of the diaphragms and iliac crests were extracted. The extracted image numbers were used to calculate a regional CTDI_{vol} based on DICOM header-reported mAs values as well as the WED of each image. Regional CTDI_{vol} and WED were used to estimate dose to lungs and breasts from thorax and dose to liver, kidneys, and spleen from abd/pel exams, using a predictive model capable of estimating organ dose using regional information. For these same patients, the image data was used to create voxelized models used in Monte Carlo simulations in which dose to each of the relevant organs was estimated. Estimated organ doses from automated method were compared with those obtained through simulations and a Root Mean Square error

between methods was calculated.

RESULTS

Estimated doses using the automated method resulted in RMS error of 33%, whereas estimates using the manual approach resulted in lower RMS error of 15% across all organs.

CONCLUSION

This work has demonstrated that automated methods to estimate organ dose for CT scans performed with tube current modulation yield reasonable results in a small number of patients having either A/P or thorax exams. Further work is needed to improve automated extraction of regions, especially for extraction of regional data to estimate thoracic organ doses (particularly breast dose), where tighter organ-specific regions would be preferable.

CLINICAL RELEVANCE/APPLICATION

Automated body landmark recognition can facilitate the calculation of multiple regional CTDIvol values from a single TCM exam for use in organ dose estimation.

SSC13-03 • Phase Based Dose Modulation for Improved Dose Efficiency in Cardiac CT

Adam Budde MS (Presenter) * ; **Brian E Nett** PhD *

PURPOSE

In cardiac half-scan reconstruction a smooth weighting function is typically used to weight the sinogram data. We assess if knowledge of this weighting function and the prescribed cardiac phase can be used to improve dose efficiency.

METHOD AND MATERIALS

In prospectively triggered cardiac CT, data is typically acquired such that a prescribed phase and some adjacent phases can be reconstructed (e.g. prescribed phase and nominal phase padding). During the reconstruction process of any given phase a smooth temporal weighting is applied to reduce motion artifacts. In this work a phase based mA modulation is proposed, such that less dose is delivered to the views which will receive a down weighting during the reconstruction process. The base protocol for comparison was a half scan acquisition with a gantry rotation period of 280ms with 50ms of phase padding on each side. A comparison, using numerical simulations of a 20cm water phantom, was performed between the standard and the phase based dose modulation, where the integral of the mA was conserved between the two acquisitions.

RESULTS

The image noise at the center of the phantom was assessed through region of interest measurements of the variance of voxel values, as this metric varies inversely with dose. Modulating the mA while keeping the total dose constant reduced the image variance by 12.2% at the center reconstructed phase, 12.0% at the reconstructed phase 25ms from center, and by 6.2% at the reconstructed phase 50ms away from the prescribed phase.

CONCLUSION

Prospective phase based dose modulation enables improved dose efficiency for cardiac CT scanning.

CLINICAL RELEVANCE/APPLICATION

Radiation dose reduction in cardiac CT can be achieved while maintaining the same level of image noise through phase based modulation.

SSC13-04 • Method to Achieve Specific Image Quality and Dose Targets over a Range of Patient Sizes by Optimizing CT Tube Current Modulation Parameters

David B Larson MD (Presenter) * ; **Daniel J Podberesky** MD *

PURPOSE

Automated tube current modulation (ATCM) can reduce CT radiation dose by adjusting the tube current according to patient size. However, ATCM does not establish image quality or dose targets nor does it ensure that those targets are met. Our purpose was to develop a method for achieving specific image quality targets over a range of patient sizes by adjusting the ATCM parameters of standard deviation of noise (\diamond SD \diamond) and minimum and maximum mA values.

METHOD AND MATERIALS

A mathematical optimization model, based on a 320-detector row scanner (Aquilion ONE, Toshiba, Otawara, Japan), was developed to predict noise and size-specific dose estimates (SSDE) based on scanner settings, including ATCM parameters, which has been presented previously. The model was applied to a quantitative noise target curve as a function of patient size, which has also been presented previously. The three ATCM variables (SD and minimum and maximum mA) were adjusted in the model to enable explicit matching of predicted image noise with target image noise over a range of patient sizes. Mean deviation and mean absolute deviation (MAD) of the predicted from the target noise and SSDE were obtained for water-equivalent diameters corresponding to weight ranges of 0-15 kg, 16-30 kg, 31-45 kg, 46-70 kg, 71-100 kg, and 100+ kg. Values obtained using mA limits were compared to those not using mA limits.

RESULTS

The ATCM noise curve without mA limits resulted in excessive noise (insufficient dose) for smaller patient diameters and lower-than-necessary noise (excessive dose) for larger patient diameters (Fig. 1). MAD for noise and SSDE not using mA limits were 1.88 HU and 1.57 mGy, respectively. Values obtained using mA limits were 0.32 HU and 0.30 mGy, respectively. Use of mA limits decreased MAD for noise and SSDE by 83% and 81%, respectively.

CONCLUSION

Predicted CT image noise and SSDE can be closely matched to target noise and SSDE curves over a specified size range by adjusting the SD and minimum and maximum mA settings using a mathematical optimization model. Without setting minimum and maximum mA limits according to the model, the ATCM algorithm tends to use insufficient dose for smaller patients and excessive dose for larger patients.

CLINICAL RELEVANCE/APPLICATION

Using the model, ATCM parameters can achieve target noise and SSDE over a range of patient sizes, enabling reliable image quality and dose based on imprecise patient size estimates such as weight.

SSC13-05 • Towards Accurate Monte Carlo Simulations of Tube Current Modulation CT Dosimetry: Model Validation and Technical Considerations

Kyle McMillan (Presenter) * ; **Maryam Khatonabadi** * ; **Christopher H Cagnon** PhD ; **John J Demarco** PhD ; **Michael F McNitt-Gray** PhD *

PURPOSE

The purpose of this study is to establish the appropriate level of detail needed within Monte Carlo models to accurately simulate dose from tube current modulation (TCM) CT scans of patients.

METHOD AND MATERIALS

A Monte Carlo model was developed in MCNPX for use in CT dose quantification. In order to validate the suitability of this model to accurately simulate patient dose from a TCM CT scan, a two-part validation scheme was devised. In the first phase, relatively simple geometries requiring varying levels of x-, y- and z-modulation were explored, including a cylindrical CTDI phantom, an elliptical body phantom and a rectangular water equivalent phantom. In the next phase, a more complex anthropomorphic phantom was investigated. Each phantom was scanned in a Siemens Sensation 64 scanner under the conditions of fixed tube current (FTC) and TCM. Dose measurements were made at various surface and depth positions within each phantom. Simulations using each phantom were performed

for FTC, full x-y-z TCM and z-axis (along patient length) only TCM, and dose was tallied at the same locations where measurements were obtained.

RESULTS

For simple geometries, the average absolute difference between the FTC measurements and simulations was 4.6%. The difference between TCM measurements and full TCM and z-axis only TCM simulations was 4.1% and 9.7%, respectively. Dose differences in the water equivalent phantom, whose rectangular shape contains considerably more x-y modulation than the other phantoms, were as high as 37.2% when z-axis only TCM was simulated. For the anthropomorphic phantom, the difference between TCM measurements and full TCM and z-axis only TCM simulations was 1.2% and 8.9%, respectively. For FTC measurements and simulations, the difference was 1.6%.

CONCLUSION

This work exhibited good agreement between measured and simulated values under both simple and complex geometries including an anthropomorphic phantom. This work also showed the increased dose differences for z-axis only TCM simulations, which demonstrates the importance of using full TCM data for Monte Carlo simulations.

CLINICAL RELEVANCE/APPLICATION

Results from this investigation highlight details that need to be included in Monte Carlo simulations of TCM CT scans in order to yield accurate, clinically viable assessments of patient dosimetry.

SSC13-06 • Monte Carlo Patient Dosimetry for Computed Tomography Examinations with Automatic Tube Current Modulation Using Precalculated Organ Dose Databases

Daniel J Long PhD (Presenter) ; **Elliott J Stepusin** BS ; **Lindsay Sinclair** PhD ; **Wesley E Bolch** PhD

PURPOSE

The demand for accurate, easily-accessible patient dosimetry for computed tomography examinations has been on the rise in recent years. Programs utilizing precalculated organ dose databases such as CTDosimetry and CT-Expo have seen widespread use for their ease-of-use; however, they fail to inherently account for modern examinations which use automatic tube current modulation (ATCM). This work seeks to develop a methodology by which to account for ATCM in patient dosimetry within the framework of a precalculated organ dose database program.

METHOD AND MATERIALS

Organ dose measurements using OSL detectors were made at Shands Hospital at the University of Florida on three female cadavers of varying BMI (17.4, 35.2, and 43.9) for four standardized CT protocols (CAP, chest, abdomen, and pelvis) utilizing ATCM. Voxel phantoms were then created for each cadaver by segmenting anatomy from the CAP exam image sets, and slice-by-slice organ dose databases were created for each through the use of a Monte Carlo model of a Toshiba Aquilion ONE CT scanner. In addition to doses, average photon attenuation was calculated for each slice of anatomy in the databases, which was then used to create weighting factors by which the doses for each slice in the desired exam range were scaled. By using the reported average effective mAs delivered for each exam, simulated in-field organ doses for each cadaver were calculated and compared to those experimentally measured.

RESULTS

Simulated and measured in-field average organ doses for each cadaver and CT exam type were compared by percent difference calculations using the measured doses as the accepted standard. Average magnitudes of percent differences over all exam types were $10.6 \pm 2.5\%$, $9.2 \pm 4.0\%$, and $11.5 \pm 2.7\%$ for the cadavers of BMI 17.4, 35.2, and 43.9, respectively.

CONCLUSION

This work establishes the feasibility of a methodology by which to account for automatic tube current modulation in Toshiba patient CT examination dosimetry within the bounds of a precalculated organ dose database program. This study lays the foundation for additional work to create a more robust methodology spanning various CT makes and models.

CLINICAL RELEVANCE/APPLICATION

The tools and methodology outlined in this work are a step closer to providing accurate and clinically-feasible patient organ doses in computed tomography exams with automatic tube current modulation.

SSC13-07 • Realistic Dose Distribution in Helical Abdominal/Pelvis Scans - Fixed mA vs. Z-directional and Angular mA Modulation

Da Zhang PhD (Presenter) ; **Xinhua Li** PhD ; **Wenli Cai** PhD ; **Bob Liu** PhD

CONCLUSION

Direct dose measurements inside the Abd/Pelvis region of an anthropomorphic phantom provided realistic dose distributions, and demonstrated the significant difference between scans with fixed mA and with mA modulation.

Background

Helical CT scans with automatic tube current modulation are widely utilized clinically. However, in the regions where the preset maximum mA is reached, the scan is conducted with constant mA. Due to the complex nature of scanning motion, mA modulation, and patient shape and composition, the dose distribution inside the scanned volume is not well understood. We want to investigate and compare the dose distribution under a scan with fixed mA and a scan with both z-directional and angular mA modulation.

Evaluation

We sampled the doses experimentally inside an anthropomorphic phantom (CIRS 701 ATOM) by embedding an array of optically stimulated luminance dosimeters in it. We scanned the abdominal/pelvis region of the phantom at a GE LS 16 Pro scanner, using the routine protocol of our institution for this region (at 120 kVp, 0.5s rotation time, 16x1.25 mm beam collimation, and pitch of 1.375). The first scan employed Auto-mA and Smart-mA with a noise index of 15 and the widest available mA range, and the second scan was with a fixed 170 mA. For each scan, we acquired 16 readings along the central z-axis of the phantom, 13 readings along the peripheral z-axis near the anterior surface, and 22 readings on each of the two selected axial planes where many radio-sensitive organs are located.

Discussion

With both fixed mA and mA modulation, large fluctuations were observed on the peripheral doses along the z-direction, which was attributed to the ripple effect resulting from x-ray attenuation and beam divergence. With fixed mA, the central doses of all slices showed small fluctuation around about 85% of the reported CTDIvol. The central dose changed significantly when Auto-mA is used for compensating the change of cross-sectional shape and size of the subject. The doses on the same axial plane in both scans ranged from 70% to 160% of the reported CTDIvol, and were asymmetrically distributed.

SSC13-08 • Evaluating the Complex Relationship of Automated Tube Current Modulation, Noise Index, Image Noise and Phantom Size

Xiujiang J Rong PhD (Presenter) ; **Eric P Tamm** MD ; **Vesna Gershan** PhD ; **Dianna D Cody** PhD * ; **Xinming Liu** PhD ; **Erik K Paulson** MD ; **Vikas Kundra** MD, PhD *

PURPOSE

To determine the influence of phantom size on automated tube current modulation (ATCM) performance.

METHOD AND MATERIALS

Four tissue equivalent abdominal CT dose phantoms (CIRS 007TE) were scanned using a GE HD750 scanner. To simulate an extra-large size patient, a 5th phantom was created by wrapping a fat-ring around the Large Adult phantom. Abdominal CT protocol: 120kVp, 0.8s

rotation time, 40mm beam width, 0.984 pitch, 2.5 mm image thickness and Large Scan Field-of-View. With Auto-mA and Smart-mA enabled, Noise Index (NI) was varied resulting in various levels of image quality. Images were reconstructed using Standard algorithm. For each phantom size/NI combination, ROI (n=3/image) and noise measurements (standard deviation of ROI) in 10 consecutive images of the central portion of the phantom were performed. The relationship of average noise versus NI was plotted for each phantom size.

RESULTS

For each phantom size, noise increased linearly as NI value increased ($R^2 = 0.9898-0.9996$). However, the slopes (ranged 0.47-1.26) differed among phantom of different sizes. Using a constant NI value, and hence the same scan protocol, noise levels decreased with phantom size. For the 15 year old to medium phantom sizes (circumference of 71, 86, and 96cm), the differences in slopes (1.26, 1.21, and 1.11) were relatively minor, indicating that the measured noise values were similar as a function of NI value. The slopes (0.68 and 0.47) of the large and extra-large phantoms (circumference of 116 and 136cm) were substantially less compared to the small-medium size phantoms, and also quite different from each other, resulting in three distinct sets of lines on the noise vs NI plot. Accordingly, for large and extra-large phantoms at a given NI, image noise is less than anticipated. Counter intuitively, this suggests that for large and very large phantoms, a higher NI could be used for maintaining adequate image quality while achieving lower radiation dose.

CONCLUSION

ATCM was limited in obtaining the same noise across phantoms of different size when using the same NI. Utilization of ATCM requires NI value be optimized based on patient size for optimal performance.

CLINICAL RELEVANCE/APPLICATION

Using a fixed NI across the entire range of patient sizes will likely result in great variability in image noise. Choice of an appropriate NI therefore must take into account patient size.

SSC13-09 • Dose to Radiosensitive Organs during Routine Chest CT: Effects of Standard and Organ-based Tube Current Modulation

Federica Zanca PhD (Presenter) ; **Xochitl Lopez-Rendon** MSc ; **Walter Coudyzer** ; **Raymond H Oyen** MD, PhD

PURPOSE

To quantify the effect of standard and organ-based tube current modulation (TCM) on dose to radiosensitive organs (breasts, lungs, heart, thyroid gland) and on image quality in adult female patients of various sizes undergoing chest CT examinations.

METHOD AND MATERIALS

Four (underweight, normal, overweight and obese BMI index) female cadavers (

RESULTS

Thought the total mAs delivered per 360° is unchanged with organ-based TCM patient dose was reduced respect to the standard protocol, with a decreasing trend in function of increasing patient size ($R^2 = 95\%$, range 25% to 4% dose reduction). The dose to the breasts, lungs, heart and thyroid was also decreased, due to the lower dose to the anterior respect to the posterior side of the patients and showed an increasing trend with patient size, ($R^2 = 92$, range 23%-36% for breasts, $R^2 = 84$, range 0% to 6% for lungs, $R^2 = 92$, range 11% to 48% for the heart and $R^2 = 85$, range 0% to 21% for the thyroid). Noise was not significantly increased ($p > 0.05$) with organ-based TCM.

CONCLUSION

Organ-based TCM allows for reduction of organ doses (breasts, lungs, heart and thyroid) and the reduction increases with patient size. Indeed the higher tube current in the posterior views is contributing to the organ doses more in small (less attenuating) patients. Patient dose is also reduced but the effect is smaller for larger patients, possibly because dose to the spine and bone marrow increases.

CLINICAL RELEVANCE/APPLICATION

Compared with routine chest CT examination, CT with organ-based TCM reduces dose to radiosensitive organs in the thorax and the reduction increases with patient size. Image quality was not affected.

Physics (MRI Techniques I)

Monday, 10:30 AM - 12:00 PM • S403B

PH **MR**

[Back to Top](#)

SSC14 • AMA PRA Category 1 Credit™:1.5 • ARRT Category A+ Credit:1.5

Moderator

Gregory S Karczmar, PhD *

Moderator

Xiaohong J Zhou, PhD

SSC14-01 • Accurate Quantitative DCE-MRI of Prostate at 3T Using High-order B1 Field Correction

Kyunghyun Sung PhD (Presenter) ; **Daniel J Margolis** MD * ; **Holden H Wu** PhD ; **Yutaka Natsuaki** * ; **Steven S Raman** MD

PURPOSE

In the quantitative analysis of dynamic contrast-enhanced MRI (DCE-MRI), a critical step is to convert dynamic MR signal into contrast agent concentration, based on knowledge of the pre-contrast T1 values. We demonstrate improved T1 measurements by using a novel B1 field correction method and show more accurate quantitative DCE-MRI analysis of prostate cancer at 3T.

METHOD AND MATERIALS

Variable flip angle (VFA) imaging is commonly used for T1 mapping but known to be highly sensitive to transmit B1 field variation. We have recently developed a novel method that can simultaneously measure T1 and B1 maps, reference region VFA (RR-VFA), assuming that the fat T1 value is well characterized, and the B1 variation in the prostate is sufficiently approximated by high-order polynomials. The RR-VFA method computes B1 maps using conventional VFA images without additional scanning. Experiments were performed on 3.0T Siemens MRI systems in a total of 11 prostate cancer patients and one healthy volunteer. We used 4 flip angles (2°, 5°, 10° and 15°) for VFA imaging and compared T1 maps with and without compensating for B1 variation. Quantitative DCE-MRI analysis was performed on OsiriX using our previously developed DCE-MRI plug-in.

RESULTS

In 12 subjects, the average T1 in the prostate was 1985.8 (± 363.8) ms without B1 correction and 1557.6 (± 110.3) ms with B1 correction. The uncorrected T1 values are overestimations of the prostate T1 and vary with different subjects and MRI systems, while the corrected T1 values are consistently in a good agreement with previous observations from the literature. Figure 1 shows a representative example of the overestimation of the prostate T1 without B1 correction. The average B1 variation in the prostate was 123%. Without B1 correction, the T1 overestimations can cause underestimations of contrast agent concentration resulted in a K^{trans} map that was unsuccessful in depicting the prostate cancer (see the arrows), while the K^{trans} map with B1 correction nicely depicts two cancer regions (see the arrows). Gleason scores are 3+3 (Region 1) and 3+4 (Region 2) based on the whole mount pathology.

CONCLUSION

We have demonstrated that B1 compensation using a novel RR-VFA technique can improve the accuracy of quantitative DCE-MRI analysis of prostate cancer at 3T.

CLINICAL RELEVANCE/APPLICATION

SSC14-02 • MR-compatibility of Stents: Measuring RF Induced Heating and MR-artifact according to ASTM Standard F2182-11a and F2119-07

Felix V Guettler (Presenter) ; **Andreas Heinrich** ; **Ina Kaufhold** ; **Florian Schlesies** ; **Maximilian De Bucourt MD** ; **Ulf K Teichgraber MD**

CONCLUSION

Up to date MR-based in-stent lumen measurement is limited to a small number of systems and field-strength of 1.5 T. It does not allow accurate measures. According to ASTM RF-induced heating, depending on the antenna effect, is within acceptable ranges for the measured stent lengths.

Background

The background of this study is to measure radio frequency (RF) induced heating and artifact in MR-images at 1.5T and 3T for commonly used stents in angiography according to standardized test methods of ASTM. Furthermore the MRI-based measurability of the in-stent lumen was assessed.

Evaluation

Currently nine stents (IDEV Supera 8x100mm, Cook Medical Zilver PTX 7x80mm, Gore Tigris 6x30mm, 6x40mm, 7x30mm, 7x100mm, TERUMO Misago 8x60mm, 8x80mm, 8x100mm) were compared on a 1.5T and 3T MRI (Magnetom Avanto and Trio, Siemens, Erlangen, Germany). The signal loss was measured according to ASTM F2119 for a TSE (TR/TE 500/26ms) and Flash (TR/TE 100/15ms) sequence. The artifact border is defined as grey value shift if a pixel differs more than 30% of the reference value (solvent) to the next pixel. The visualization of in-stent lumen (inside-diameter) was determined the same way. The stents were placed parallel and antiparallel to the static magnetic field (B₀). The largest external diameters and in-stent lumen were measured at five points. For safety aspects the RF induced heating was measured according to ASTM F2182 with a TrueFISP (TR/TE 3.04/1.52ms, scan time 15min).

Discussion

With none or very limited MR-artifacts MR-based stent-lumen measurement might become feasible for a broad spectrum of clinically used MR sequences. Compared to other MR-compatible implants or instruments made from NiTi-based alloys modern stent systems show potential for further improvement.

SSC14-03 • Reduction of Susceptibility Artifacts in R2' Measurements Using Z-shimming Based Multi-echo Asymmetric Spin-Echo (Z-MASE) Sequence at High Fields

Xiaodong Zhang PhD (Presenter) ; **Yuai Hua** PhD ; **Hongtu Zhu** PhD ; **Yasheng Chen** PhD ; **Jue Zhang** ; **Xiaoying Wang** MD ; **Weili Lin** PhD ; **Hongyu An** DSc

PURPOSE

In this study, we proposed a rapid method, dubbed as Z-shimming based Multi-echo Asymmetric Spin-Echo (Z-MASE), to estimate and correct the γ B effects for an accurate estimation of R2'.

METHOD AND MATERIALS

In this method, three Z-shimming tables were applied sequentially prior to echo 1, 2 and 3 of a triple-echo ASE EPI sequence, respectively [1]. And the Z-shimming tables were only applied once for a specific 180° pulse offset t. Then a sinc function is usually assumed to characterize signal loss induced by [2]. Finally, an estimate of R2' was obtained without the effects of macroscopic field variation [3]. A small testing tube containing contrast agent was attached to a large phantom to induce γ B effect. In addition, ten normal volunteers were studied and written informed consent was obtained from all subjects. A multiple slice triple-echo ASE-EPI with Z-Shimming gradients was utilized. The imaging parameters were as follows: TR=3s; TE1=43ms, TE2 = 61ms, TE3 = 79ms; Slice Thickness =3mm, voxel size=3*3*3mm³; number of ASE offset time =23, Maximum γ TE = 26ms, 44ms, and 62ms; number of Z-Shimming gradients steps = 8, the maximum strength of Gz = 32ppm/m, the Z-Shimming-related data scan time is 24s and the total scan time is 5min 6 sec.

RESULTS

In the Phantom studies, the signal loss in the ASE images has been fully recovered as demonstrated by the almost identical line profile between the spin echo and the corrected ASE. In the volunteer studies, absolute measurements of R2' from the ten volunteers were obtained. A R2' of 12.12±4.47Hz was obtained without the γ B correction for the frontal regions of the brain. In contrast, with the γ B correction, a R2' of 2.84±0.75Hz was obtained for the frontal regions of the brain.

CONCLUSION

Unlike the conventional Z-shimming method, this method can reverse γ B effects without perfectly matching one of the Z-shimming gradients to γ B. Our approach can also be adapted as a rapid (24 sec) standalone γ B mapping method if γ B maps are needed for other DTI or fMRI studies. **REFERENCE**

- [1] Yang et al. Magn Reson Med 29, 139-144, 1998.
- [2] An H, Lin W, Magn Reson Med 47, 958-966, 2002.
- [3] An H, Lin W, Magn Reson Med 50, 708-716, 2003.

CLINICAL RELEVANCE/APPLICATION

The ability to simultaneous measurements of R2' and reduction of susceptibility artifacts may have the profound clinical application for studies of disordered brain oxygen metabolism.

SSC14-04 • Development of a Novel Multi-Atlas Method to Derive Pseudo CT from MR Image Independent of MR Sequences for PET/MR Application

June-Goo Lee PhD (Presenter) ; **Bruce R Whiting** PhD ; **Chan Hong Moon** PhD ; **H. Michael Gach** PhD ; **Jin Hong Wang** MD ; **Kyongtae T Bae** MD, PhD *

PURPOSE

To develop a multi-atlas method for deriving pseudo CT (pCT) from MR images independent of MR sequences and to evaluate the compatibility of pCT images against the reference CT (rCT) images

METHOD AND MATERIALS

We retrieved head CT images from 20 patients and used them as CT atlases. Ten of these patients also had matching MR images of the head at 4 different MR sequences: fluid attenuated inversion recovery (FLAIR), magnetization-prepared rapid acquisition with gradient echo (MPRAGE), T1 weighted (T1), and T2 weighted (T2). The MR-CT pairs were aligned using a rigid and non-rigid registration scheme. The realigned CT images were saved as the rCT images. The CT atlases were registered to each test MR image. The registration scheme was in two steps, initial alignment with affine transform and refinement with B-spline non-rigid transform. The registered atlases were sorted on basis of a Hessian analysis on MR and atlas images. After selecting the registered atlases showing more than 80% of maximum Hessian response score, the median based merging process was applied to derive pCT for each test MR image. For evaluation, pCT and rCT images were converted to attenuation value and radon transformed to generate sinograms. In these sinograms, the sinogram value was exponentiated for a correction value. The mean and standard deviation of the ratio of the correction values of pCT and rCT were calculated.

RESULTS

pCT images were successfully generated from all test MR images at different MR sequences. The mean of the ratio of correction values of pCT and rCT was close to 1 and standard deviation was small (mean, std.): (0.993±0.012, 0.062±0.016) for 10 FLAIR MRI; (0.999±0.010, 0.054±0.014) for 6 MPRAGE MRI; (0.991±0.015, 0.046±0.009) for 6 T1 MRI; and (0.987±0.012, 0.053±0.013) for 8 T2

MRI.

CONCLUSION

We have developed a multi-atlas method to derive pCT images from MR images independent of MR sequences. The pCT images of the head were in good agreement with the real rCT images.

CLINICAL RELEVANCE/APPLICATION

A robust method for deriving CT equivalent information from MRI is needed for attenuation correction in PET/MRI applications.

SSC14-05 • Peripheral Zone Prostate Cancer Sensitivity and Accuracy Using Two Different Receive Coils

Rajakumar Nagarajan PhD (Presenter) ; **Daniel J Margolis** MD * ; **Steven S Raman** MD ; **Manoj K Sarma** PhD ; **Robert E Reiter** MD ; **Michael A Thomas** PhD

PURPOSE

Magnetic resonance spectroscopy (MRS) enables recording major prostatic metabolites, such as citrate (Cit), creatine (Cr) and choline (Ch), and it has been shown to significantly improve detection of tumors in the peripheral zone, primarily by improving specificity. The external coil assembly is favored because of no image deformation and less inconvenience compared to an endorectal coil. The endorectal coil is not recommended very soon after radiation therapy, is not feasible after rectum resection. The major goal of the study is to compare the performance of 3T endorectal coil receive MR spectroscopic imaging (MRSI) of prostate with that using an external receive body array coil.

METHOD AND MATERIALS

Twenty patients (mean age 63.1yo) with prostate cancer (PCa) who underwent endorectal MR imaging and proton MR spectroscopic imaging were included in this study in 3T MRI. After the endorectal scan, patients were scanned with the external body array coil for the comparison study. MRSI parameters of endorectal and external body array were as follows: TR 750ms, TE 145ms, acquisition bandwidth 1250 Hz, 6 averages, and 512 spectral data points with the voxel resolution of 0.3ml. For the external body array, the voxel resolution was 0.35ml.

RESULTS

Peak areas for Ch, Cr, and Cit were calculated by using numeric integration. Metabolic maps of (Ch + Cr)/Cit were generated. Voxels were considered suitable if they consisted of at least 75% peripheral zone tissue, did not include periurethral tissue. Both endorectal coil and external body array metabolites ratio were significantly higher in cancer locations compared to non-cancer locations. Also the coefficient of variance was higher in external body array than the endorectal coil due to larger size of the coil and increased distance from the prostate. The sensitive and accuracy of endorectal coil is higher than (82% and 79%) the external body array (70% and 75%).

CONCLUSION

These preliminary findings confirmed that the use of endorectal coil significantly improves spectral line width and coefficient of variance of metabolite ratios when compared with external body array.

CLINICAL RELEVANCE/APPLICATION

In patients with rectal diseases or patients who could not tolerate the discomfort with insertion of an endorectal surface coil, use of the phased array coil may be recommended.

SSC14-06 • Extending Resolution Limits of Whole-heart Coronary Magnetic Resonance Angiography (MRA) Using Super-resolution Technique

Ryohei Nakayama PhD (Presenter) ; **Masaki Ishida** MD, PhD ; **Motonori Nagata** MD, PhD ; **Tatsuro Ito** MD ; **Kakuya Kitagawa** MD, PhD ; **Hajime Sakuma** MD * ; **Mio Uno** MD ; **Yoshitaka Goto** MD

PURPOSE

Coronary MRA permits noninvasive assessment of coronary artery stenoses without radiation exposure. However, several technological considerations restrict image resolution of coronary MRA. Conventionally, resolution of MRA is usually enhanced using bicubic interpolation (BCI). Recently, Super-Resolution (SR) technique has been proposed to increase MR image resolution. The purpose of this study was to investigate the value of high resolution reconstruction of coronary MRA using SR technique.

METHOD AND MATERIALS

Whole-heart coronary MRA was acquired with 32-channel cardiac coils in 35 patients at 1.5T (n=16) and 3.0T (n=19). Images with 256x256 matrices were generated as original images by down-sampling the source 512x512 images reconstructed by MR imager. The resolution of original images was restored to 512x512 matrices by using SR technique or BCI. With SR approach, the original images were further downsampled to 128x128 matrices (LR: low-resolution images). Each original and LR image was represented as a set of overlapping patches with the same number using 14x14 matrices for original and 7x7 matrices for LR images. Training dictionaries, which include the relation information in each corresponding pair of patches, were constructed using 5 slices including the target slice in the middle. Using 256x256 original image as a input, high-resolution image was generated by employing 7 pairs of patches that were the nearest neighbors in the feature vector space from training dictionaries. The source 512x512 images were used as gold standard to determine the fidelity of 512x512 images generated by SR approach in comparison with that by BCI.

RESULTS

With BCI, root mean square error, signal to noise ratio, and structural similarity index for 1.5T MRA were 3.12, 20.0dB, and 0.983, whereas those for 3.0T MRA were 3.05, 20.4dB, and 0.985. With SR approach, those for 1.5T MRA were 2.55, 21.9dB, and 0.988, whereas those for 3.0T MRA were 2.50, 22.4dB, and 0.990. The each result was significantly improved (p < .001) by SR technique as compared with BCI.

CONCLUSION

The high resolution reconstruction with SR technique developed in this study achieved highly improved image quality of coronary MRA at both 1.5T and 3.0T.

CLINICAL RELEVANCE/APPLICATION

The high resolution reconstruction generated by our SR technique may be useful for identifying coronary artery stenoses on whole-heart coronary MRA and for reducing the interpretation time.

SSC14-07 • Self-consistent Flip Angle Mapping Using Multi-spectral Synthetic MRI

Hernan Jara PhD (Presenter) * ; **Stephan W Anderson** MD ; **Jorge A Soto** MD * ; **Osamu Sakai** MD, PhD *

CONCLUSION

A self-consistent FA mapping technique has been developed that is based on image processing only. It could be useful for increasing qMRI accuracy, streamlining MRI examinations, and improving image quality at ultrahigh field strengths. 1. Wade T, McKenzie CA, Rutt BK. Flip angle mapping with the accelerated 3D look-locker sequence. Magnetic Resonance in Medicine 2013.

Background

Quantitative MRI (qMRI) accuracy can be degraded by deviations of the actual flip angles (FA) in the patient relative to the nominal-FA values of the pulse sequence. Several FA mapping techniques have been described in the literature (1): these involve a separate scan. We hypothesize that FA can be mapped as an application of multi-spectral Synthetic MRI without needing a separate scan. Because Synthetic-MRI allows for the generation of images of arbitrary contrast weighting, in particular the directly acquired (DA) images can be resynthesized and compared to the true DA reference images. If done systematically as a function of varying FA for every pixel, the actual FA will correspond to the minimum pixel value difference between the synthesized minus the true DA image.

Evaluation

We used images of the head (1.5T Achieva, Philips Healthcare) with the mixed turbo spin echo sequence, which begins with an inversion pulse. The DA images were processed qMRI algorithms for generating maps of PD, T1, and T2. Our Synthetic MRI contrast navigation algorithm was modified for automated loop operation as a function of increasing inversion pulse FA from 0-180°. The synthesized pixel values were subtracted from the corresponding DA pixel value (Fig. 1, top row), and the FA that minimizes the absolute value of the difference was found. Performing this procedure on a pixel-by-pixel basis, lead to maps of the mixed-TSE actual inversion FA (Fig. 1, bottom row).

Discussion

There is increasing need for using FA mapping for improving qMRI accuracy and for correcting B1 inhomogeneity artifacts. At the same time, because of growing financial pressures there is a need for shortening and streamlining MRI examinations. The FA mapping technique described herein could be instrumental in alleviating the above technical and financial needs.

SSC14-08 • Method of Characteristic Response Curves (CRC): An Accelerated Computational Method for Accurate Quantitative Magnetic Resonance Imaging (qMRI)

Jonathan E Scalera MD (Presenter) ; Stephan W Anderson MD ; Osamu Sakai MD, PhD * ; Hernan Jara PhD *

CONCLUSION

A twofold accelerated T1 qMRI processing algorithm based on the CRC method was developed and tested with a large imaging dataset. The methodology is very general and could be used for the computation of other qMRI parameters. CRC could be instrumental for incorporating computationally intensive qMRI algorithms into routine clinical practice.

Background

Relaxometry is often performed with intricate qMRI pulse sequences, which can lead to complicated magnetization dynamics. In some cases the magnetization dynamics is such that the Bloch equations may not have closed-form analytical solutions, and consequently the resulting qMRI relaxometry algorithms may be solvable only by iterative numerical methods, which can be very slow. For multislice high spatial resolution applications this can lead to long computational times, which may be clinically impractical. The purpose of this work was to develop a faster qMRI processing algorithm methodology whereby the most time consuming operation is performed only once for generating the Characteristic Response Curve (CRC) of the qMRI pulse sequence and this CRC model is then used as the common solution applicable by interpolation to all pixels in the imaging dataset.

Evaluation

The CRC method is very general and in principle applicable to any Bloch equation solution, nevertheless we describe here its application to T1 relaxometry with the mixed turbo spin echo (mixed-TSE) pulse sequence. A computer program was developed in MathCad (PTC, Needham, MA) and applied to MR images obtained with the mixed turbo spin echo pulse sequence using a 1.5T MRI scanner (Intera, Philips Healthcare, Cleveland, OH). The head scan of a research subject: 80 slices, 256x256 matrix, and voxel size 0.9375x0.9375x3mm³.

Discussion

T1 maps generated with the exact pixel by pixel and the CRC algorithms are shown in Fig. 1 below. Both maps are visually indistinguishable. The processing times of the standard and CRC algorithms for all 80 slices were 86s and 43s, respectively. The accuracy of the CRC algorithm relative to the standard algorithm is compared in Fig. 2 in terms of whole brain histograms revealing the same overall bimodal shape with minor differences.

SSC14-09 • A Controllable and Stable Denoising Filter for Magnetic Resonance Imaging

Xin Zhou PhD (Presenter) ; Yanli Song ; Miaofei Han ; Qiang Li PhD *

CONCLUSION

The TWE is an excellent method to control the noise reduction levels in NLM filter.

Background

Non-local means (NLM) filter is considered as one of state-of-the-art denoising methods. A big issue in NLM is that it is nearly impossible to automatically set its parameters for removing noise to a specific level, as the denoising level of NLM depends heavily on multiple parameters. We embedded a total-weight equalization technique in NLM filter (TWE-NLM) to adaptively control the denoising level by use of a single parameter of total weight. With this technique, we can automatically reduce noise standard deviation of the output image to any specific level of that of input noisy image.

Evaluation

A total of 146 magnetic resonance (MR) scans in 12 major body parts were obtained from a 1.5T MR scanner with various imaging sequences. For each body part, 4 representative images were selected for objective and subjective evaluation of image quality in the study. Standard NLM was used as a baseline method for comparison with TWE-NLM. Three denoising levels of sharp, medium, and smooth (roughly corresponding to percent noise reduction of 33%, 50%, and 66%, respectively) were specified by a radiologist. In TWE-NLM, the only adjustable parameter of total weight was automatically determined to be 1.5, 2.0, and 3.0 for the 3 denoising levels. For standard NLM, multiple parameters were manually adjusted by a physicist with a trial-and-error method in order to achieve the 3 denoising levels. Statistical analysis results show that the consistency and robustness of denoising levels achieved in TWE-NLM was markedly higher than that of NLM with manual parameter selection. A blinded subjective evaluation with more radiologists from multiple hospitals will be conducted in the coming months.

Discussion

A key issue in denoising is the easy selection of parameters and the robustness of selected parameters. We embedded a TWE approach into NLM to automatically control the denoising level through a single parameter. In addition to its simplicity for parameter selection, the TWE method also achieved a higher uniformity in noise reduction inside an images and a higher consistency across different images.

Physics - Monday Posters and Exhibits (12:15pm - 12:45pm)

Monday, 12:15 PM - 12:45 PM • Lakeside Learning Center



LL-PHS-MOA • AMA PRA Category 1 Credit™:0.5

Host
Kenji Suzuki, PhD *
Host
Jiang Hsieh, PhD *

LL-PHE-MO10A • Iron Deposition in the Brain: A Review of Current Iron Quantification Techniques

Yunhong Shu PhD (Presenter) ; Paul Bao ; Mallikarjunarao Kasam PhD ; Kirk M Welker MD

PURPOSE/AIM

There has been great interest in detecting endogenous iron in the brain as it has been shown to be correlated with aging and neurological disorders. Magnetic resonance imaging (MRI) is sensitive to iron deposition due to its abundance and high magnetic susceptibility. Given the variable appearance of cerebral iron across pulse sequences and scanner field strengths, quantitative assessment of brain iron

[Back to Top](#)

concentration is preferable to visual inspection. This presentation aims to provide an overview of several methods that have been proposed to quantitatively measure iron concentration in the brain.

CONTENT ORGANIZATION

- 1: Introduction - Tissue iron deposition forms in the brain and their relationships with specific pathology.
- 2: Review of the principles of general iron quantification methods and descriptions with specific examples
- 3: Detailed discussion on advantages and limitations of the iron quantification techniques.

SUMMARY

The ability of MRI to non-invasively measure brain iron deposition can potentially help to gain further understanding in the pathophysiology of the normal aging process and neurodegenerative diseases. Accurate analysis of iron concentration using MRI requires a good understanding of the underlying mechanism and confounding factors related to the various iron mapping techniques.

LL-PHS-MO1A • Segmentation of the Left Ventricle Using a Distance Regularized Two-layer Level Set Approach

Chunming Li PhD (Presenter) ; **Chaolu Feng** ; **Christos Davatzikos** ; **Harold I Litt** MD, PhD *

PURPOSE

Non-invasive assessment of left ventricular function is important but difficult due to poor imaging quality and complex anatomical characteristics. To overcome these challenges, we propose a distance regularized two-layer level set approach for segmentation of the left ventricle (LV) from cardiac MR (CMR) short-axis images. The segmentation results can be directly used to calculate ejection fraction (EF), which is an important indicator of the LV function.

METHOD AND MATERIALS

We propose a novel two-layer level set approach to segment the LV from CMR short-axis images. In our method, endocardium and epicardium are represented by two specified level contours of a level set function (LSF). Segmentation of the LV is formulated as a problem of optimizing the LSF such that these two level contours best fit the epicardium and endocardium. More importantly, a novel distance regularization (DR) constraint on the level contours is introduced to ensure the smoothly varying distance between them. This DR constraint leads to a desirable interaction between the level contours to maintain the anatomic geometry of the endocardium and epicardium. The negative effects of intensity inhomogeneities on image segmentation are overcome by a data term derived from a local intensity clustering property. Our method is quantitatively validated by experiments on the datasets for the MICCAI 2009 grand challenge on left ventricular segmentation, which demonstrates the advantage of our method in terms of segmentation accuracy and consistency with anatomic geometry.

RESULTS

We have validated our method using the datasets from the MICCAI 2009 challenge on LV segmentation. Comparisons with other methods show that the average perpendicular distances for our method are the smallest: 1.82 ± 0.48 mm and 1.73 ± 0.43 mm for training datasets and 1.93 ± 0.37 mm and 1.64 ± 0.42 mm for validation datasets. We have achieved much better results, giving nearly the best slope and regression coefficient: 1.04 and 0.90 for EF and 0.93 and 0.85 for the mass; and demonstrating only a small bias on the Bland-Altman plots: 3.45% for EF and -6.48 grams for LV mass.

CONCLUSION

Quantitative evaluation and comparison with other state-of-the-art methods demonstrate that our method achieves more accurate segmentation results and more reliable measurement of EF and LV mass.

CLINICAL RELEVANCE/APPLICATION

This method proposed in this paper is recommended in clinical measurement of LV function.

LL-PHS-MO2A • Factors Causing Variability of Response Classification in RECIST 1.1.

Sebastian Keil MD (Presenter) ; **Lieven Kennes** ; **Alexandra Barabasch** ; **Philipp Bruners** MD ; **Timm Dirrichs** ; **Marco Das** MD * ; **Christiane K Kuhl** MD *

PURPOSE

We conducted a systematic analysis of factors (manual vs. automated and uni- vs. three-dimensional size assessment, and impact of different target lesion selection) contributing to variability of response categorization in RECIST 1.1.

METHOD AND MATERIALS

41 female patients (58.1 ± 13.2 years) with metastatic breast cancer underwent contrast-enhanced thoraco-abdominal CT for initial staging and first follow-up after systemic chemotherapy. Data were independently and prospectively interpreted by three radiologists. In addition, response was evaluated by a CAD system that allowed automated uni- and three-dimensional assessment of target lesions.

RESULTS

Overall, between-reader-agreement was moderate (κ : 0.4-0.59), with diverging response classification observed in 19/41 patients (46%). In 25 patients, readers chose the same, and in 16, readers chose different target lesions. Selection of the same target lesions was associated with a 76% agreement rate (19/25); selection of different target lesions was associated with an 81% rate of disagreement (13/16) ($p < 0.001$). After dichotomizing response classification according to its therapeutic implication into progressive vs. non-progressive disease, disagreement was observed in 11/41 patients (27%). In 9 of these 11 patients, readers had chosen different target lesions. Disagreement rates due to manual vs. automated or uni-dimensional vs. volumetric measurements were less important (11/41 and 6/41; 27% and 15%, respectively).

CONCLUSION

Major source of variability is not the manual or uni-dimensional measurement, but the variable choice of target lesions between readers. CAD-based analysis or tumor volumetry can help avoid variability due to manual or uni-dimensional measurements only, but will not solve the problem of target lesion selection.

CLINICAL RELEVANCE/APPLICATION

Evaluation of radiological response plays a major role in oncological therapy. We investigated causes for variability of response classification in RECIST and how they might be overcome by CAD.

LL-PHS-MO3A • Coronary Artery Calcium Scoring: Comparison of Adaptive Statistical Iterative and Filtered Back Projection Reconstruction Techniques Using a Calcified Plaque Phantom

Tatsuya Umezawa RT (Presenter) ; **Fumiko Kimura** MD, PhD * ; **Masaru Morishita** ; **Itsuki Nagazumi** RT ; **Taiki Senoo** RT ; **Yasuyuki Yoshimura**

PURPOSE

Adaptive statistical iterative reconstruction (ASiR, GE Healthcare) has been used for coronary CT angiography to improve image quality and reduce radiation dose, but its influence on coronary artery calcium scoring (CACS) is unknown. In a calcified plaque phantom, we compared image noise, CT values, CACS, and coronary artery calcium volume (CACV) between filtered back projections (FBP) and ASiR to clarify if CACS differs significantly between the two and assessed factor/s influencing differences.

METHOD AND MATERIALS

We made calcified plaque models of 5 materials with different CT values, placed them into a long cylindrical phantom of 4-mm diameter that contained materials of 40 HU to simulate blood to simulate the coronary artery with calcified plaques (50% stenosis; length 5 mm), and submerged the phantom in a tank of water. We scanned it using 120 kVp and various tube currents and reconstructed images using 5 reconstruction techniques (RTs) - FBP and ASiR-FBP composites (ASiR 30%, 50%, 70%) and ASiR 100%. We measured the mean CT

values of the 5 materials in large regions of interest (ROIs; 55-265mm²) and assessed the phantom containing the calcified plaque models regarding image noise in the tank water, CT values of the small calcified plaques, and total CACS and CACV (sums of the 5 plaques). We compared these values among the 5 RTs using repeated-measure ANOVA. $P < 0.05$ was considered significant.

RESULTS

The mean CT values (large ROIs) of the 5 materials were 918, 600, 392, 177, and 110 HU without significant difference among RTs. There were significant differences among RTs in image noise ($P < 0.001$), CT values of the small calcified plaques ($P < 0.001$), total CACS ($P < 0.001$), and total CACV ($P < 0.01$), decreasing as ASiR percentage increased. Compared to FBP, total CACS decreased 6.2% in ASiR 30%, 8.8% in ASiR 50%, 13.0% in ASiR 70%, and 18.0% in ASiR 100%. ASiR decreased pixel CT values of the rim of the calcified plaques, which changed the weighted factors to calculate CACS.

CONCLUSION

Image noise, CACS, and CACV decreased as ASiR percentage increased. ASiR appeared to decrease image noise and CT pixel values of the small calcified plaque and then affect CACS.

CLINICAL RELEVANCE/APPLICATION

Compared to FBP, a blend of no more than ASiR 50% limits CACS reduction to 10%, and the same reconstruction technique should be used to assess temporal changes in CACS.

LL-PHS-MO4A • A Novel Image-based Estimation Method for Magnetic Field Inhomogeneity in Brain Echo-planar Image

Seiji Kumazawa PhD (Presenter) ; **Takashi Yoshiura** MD, PhD ; **Hiroshi Honda** MD ; **Fukai Toyofuku** PhD

CONCLUSION

We have proposed a new estimation method for the magnetic field map based on the distorted EPI image and T1WI of brain. The results demonstrate that the magnetic field inhomogeneity in EPI image can be estimated by our method, and the geometrical distortion can be reduced.

Background

Echo-planar imaging (EPI) suffers from geometrical distortion due to magnetic field inhomogeneity. Conventional methods to correct the distortion of EPI require an additional acquisition of a magnetic field map. Our purpose was to develop a new method for estimating the magnetic field map based on the distorted EPI image and T1 weighted image (T1WI) which requires no additional acquisitions.

Evaluation

Instead of an additional acquisition, our method used the segmented brain T1WI to estimate the field map. Based on MR imaging physics, our method synthesizes EPI image from tissue-objects extracted from segmented brain T1WI according to single shot EPI k-space trajectory. First, the brain T1WI was mapped by using linear transformation into EPI image based on the image orientation and position of DICOM header information. Next, the T1WI was divided into head region and air region based on the intensity histogram, and then brain extraction and tissue segmentation were applied to head region by using FSL tool. Our field inhomogeneity estimation is incorporated into the generating process of EPI image, and the estimation process is performed iteratively to minimize the cost function defined by the synthesized EPI image and the measured EPI image with geometric distortion. In this experiment, our method was applied to the EPI image with known magnetic field inhomogeneity, and was evaluated by comparing between the estimated field map and the known map.

Discussion

The magnetic field inhomogeneity map estimated by our method very accurately agreed with the filed map of the ground truth. The RMSE value between the estimated field map and ground truth was less than 0.17. In the simulated EPI image with removing the estimated magnetic field inhomogeneity map, the geometrical distortion was reduced. In visual evaluation, the brain shape in the resulting EPI was very similar to that in T1WI.

LL-PHS-MO5A • The Potential of Texture Features for Differentiation of Colonic Polyp Types for CT Colonography

Jerome Liang PhD (Presenter) ; **Bowen Song** MS ; **Guopeng Zhang** MS ; **Huafeng Wang** PhD ; **Perry J Pickhardt** MD * ; **Hongbing Lu** PhD

PURPOSE

PURPOSE: Image texture features have been widely explored for computer-aided diagnosis (CADx) on breast masses and lung nodules for malignance assessment. In our previous pilot study, we observed the discrimination in terms of image textures among different colonic polyp types, such as hyperplastic (H), tubular adenoma (Ta), tubulovillous adenoma (Va), and adenocarcinoma (A). This study aims to explore more high order spatial dependency texture features and also provide more quantitative measures on the discrimination performance of the texture features in terms of the area under the receiver operating characteristic curve (AUC).

METHOD AND MATERIALS

MATERIALS AND METHODS: The high order spatial dependency texture feature calculation is based on the Haralick's texture description with expansion in the three-dimensional image density distribution space as well as the gradient and curvature distribution domains. The database in this study includes 124 lesions (polyp and masses, confirmed by pathology) in four categories: 40 H, 45 Ta, 30 Va, and 9 A. A semi-automated segmentation was performed to extract the volume of each lesion, given the lesion's (x,y,z) coordinates, from the computed tomography colonography (CTC) image. A total of 78 features were calculated from each lesion volume. These features were fed into the support vector machines (SVM) classifier for binary classification among the four lesion categories. To avoid any bias in selection of training and testing datasets, the splitting of the training and testing datasets was repeated 100 times randomly and the outputs were averaged for AUC measure.

RESULTS

RESULTS: The binary classification for the two categories of (HandTa) and (VaandA) reached the differentiation capability of means \pm standard deviation of 0.9190 \pm 0.0363.

CONCLUSION

CONCLUSION: CADx for polyp malignance assessment is highly likely. The potential of CTC in colon cancer screening includes not only the detection of the precursor or polyps but also the diagnosis of the detected polyps for optimal polyp management for the best outcome in personalized medicine.

CLINICAL RELEVANCE/APPLICATION

Clinical Relevance/Application: Differentiation of the polyp types can render an optimal management of polyps in personalized medicine.

LL-PHS-MO6A • Experimental Quantification of the Effects of Organ-based Tube Current Modulation on Radiation Dose and SNR

Diksha Gandhi (Presenter) * ; **Dominic Crotty** PhD * ; **Grant M Stevens** PhD * ; **Taly G Schmidt** PhD

PURPOSE

To compare the radiation dose to breast, lung, heart and spine in CT chest scans, and eye lens and brain in head scans with and without organ-dose-based tube current modulation (ODM), using an anthropomorphic phantom and a clinical CT scanner. The signal-to-noise ratio (SNR) was also quantified in images reconstructed with and without ODM.

METHOD AND MATERIALS

Axial CT scans at 120 kV were performed on anthropomorphic head and chest phantoms (Rando Alderson Research Laboratories, Stanford, CA) on an ODM-equipped scanner (Optima CT660, GE Healthcare, Chalfont St Giles, England). ODM reduces the tube current for the anterior source positions, without increasing current for posterior positions. ODM has different modulation settings for chest and head exams. Dosimeters quantified radiation dose to locations in the breast, lung, heart, spine, eye lens and brain (mobile MOSFET

Dosimetry System, Best Medical, Ottawa, Canada). For both phantoms, five scans were performed with and without ODM, with all other scan parameters constant. The non-ODM chest scans were performed with two settings \diamond automA, which modulates the tube current modulation in the slice direction, and smartmA, which modulates the tube current in both the slice and angular directions. SNR was calculated in the brain and chest regions of all reconstructed images. The experimental results are now being validated with Monte Carlo simulations. In addition, 50 adult female phantoms are being simulated to study ODM in patients of varying sizes and anatomy.

RESULTS

ODM reduced the dose at all dosimeter locations, with dose changes of -31.3% in the breast, -20.7% in the lung, -24.4% in the heart, -5.9% in the spine, -10.0% in the eye and -18.7% in the brain, with respect to smartmA. The percent change in dose with respect to automA was -37.7%, -29.8%, -35.3% and -25.0% in the breast, lung, heart and spine, respectively. ODM decreased the SNR by 3.5% and 11.5% for head and chest phantoms, respectively.

CONCLUSION

Experimental studies indicate that ODM has the potential to reduce dose to sensitive organs by 5 - 38% with a decrease in SNR of less than 12%. Simulations are in progress to investigate the performance of ODM over a range of patient sizes.

CLINICAL RELEVANCE/APPLICATION

Organ-based tube current modulation has the potential to reduce the dose to radiosensitive tissues with limited degradation in SNR.

LL-PHS-MO7A • Contrast and Dose Dependencies of Resolution Property in Iterative Reconstruction CT Images

Tadanori Takata (Presenter) ; **Katsuhiko Ichikawa** PhD ; **Syoichi Terakawa** ; **Hiroyuki Hayashi** ; **Kosuke Matsubara** PhD ; **Yukihiro Matsuura** RT ; **Keita Sakuta** RT

PURPOSE

Since the iterative reconstructions (IR) are nonlinear image processing, their resolution properties are different from filtered back projection (FBP). The purpose of this study was to evaluate contrast and dose dependencies of resolution property of the IR images using a contrast adjustable cylindrical phantom.

METHOD AND MATERIALS

We evaluated an IR, sinogram affirmed iterative reconstruction (SAFIRE) provided by SIEMENS. A 100-mm diameter cylindrical acrylic phantom placed in a 200-mm diameter cylindrical case with correct centering was used. The phantom's surround was filled with diluted contrast agent, and the contrast between the phantom and the surround was set to middle contrasts of 45, 65, 85, 105 and 125 Hounsfield units (HUs). The phantom was scanned at two dose levels (75 and 150 mAs), and images were reconstructed using FBP and five strengths of SAFIRE (S1-S5). Since the image noise was obstacle for the correct resolution measurement, we added many images obtained by multi scans. The radial edge of the phantom was analyzed to determine the edge-spread function, which was differentiated to yield the line-spread function and Fourier-transformed to generate the modulation transfer function (MTF).

RESULTS

For the 45-HU contrast of S5, MTF of 75 mAs was significantly lower (up to 24%) than that of 150 mAs, while FBP offered the same MTF for both the doses. At the same dose level for S5, MTFs of 45-HU contrast were clearly lower (up to 35% and 16% for 75 and 150 mAs, respectively) than those of 125-HU contrast. The weaker strength of SAFIRE was applied, the less dose and contrast dependencies were indicated.

CONCLUSION

The degree of resolution degradation of SAFIRE significantly depended on not only the object contrast but also the scan dose. Even for objects with middle contrasts, IR degraded the resolution properties. The method using the radial edge of cylindrical phantom was effective for evaluating the resolution property of IR.

CLINICAL RELEVANCE/APPLICATION

Our results would be useful to optimal selection of IR strengths (modes) and to evaluate performances of different IR techniques.

LL-PHS-MO8A • Quantification of Hepatic Fat Using MR Imaging and Spectroscopy

Peter A Hardy PhD (Presenter) ; **Bryce Noblitt** BS ; **James T Lee** MD

PURPOSE

To develop accurate spectroscopic and imaging techniques to quantify the proton density fat fraction in livers. Additionally, we sought to understand the influence of such confounds as liver iron concentration on the accuracy of the measured fat fraction.

METHOD AND MATERIALS

Samples of a lipid nutritional supplement, IntraLipid \diamond were diluted to create a series of lipid:water standards. From each sample proton spectra were acquired with a single voxel STEAM acquisition run on a 7T Bruker ClinScan. Spectra were acquired at a variety of TE and TR times. The spectral peaks were integrated using Siemens and JMRUI software. The integrated areas were fit to standard equations to estimate the relaxation times T1 and T2 for each spectral peak. The amount of fat and water were corrected for the effects of decay before calculating the proton density fat fraction. Samples of liver were extracted from both normal wild type and obese db/db mice. Samples were heated to 37 \diamond C while they were imaged with the same spectroscopic techniques as used on the IntraLipid \diamond samples. The liver samples were then digested and assayed for iron quantification using ICP-OES spectroscopy. The measured relaxation times and spectral widths were correlated with the tissue iron concentration.

RESULTS

We used the calculated T1 and T2 values to correct the spectral areas. The calculated proton density fat fraction was then regressed against the nominal fat fraction. The correlation coefficient was 0.976 while the slope was 0.56. The true fat fraction may be much less than the nominal due to differences in density and the fraction of the lipid with hydrogens in CH2. Measured fat fraction in the livers of the mice showed a small but statistically not significant higher fat content of the livers of the db/db mice. Tissue iron measurements showed the WT had significantly elevated tissue iron concentration (325 vs 200 μ g/gm wet weight). This concentration is sufficient to increase the width of the water peak in the tissue samples.

CONCLUSION

To achieve the most accurate estimate of fat fraction in the liver it is necessary to compensate the measured peak areas of water and lipid for their relaxation times. Through the assay of iron concentration on the murine liver samples we demonstrated an additional confound.

CLINICAL RELEVANCE/APPLICATION

Fat quantitation in the liver using short TR, multi echo images will need to compensate for T1, T2 and T2* to be accurate.

LL-PHS-MO9A • Photo Acoustic Imaging of Human Peripheral Joints

Gandikota Girish MBBS (Presenter) ; **Xueding Wang** PhD

CONCLUSION

PAI technology continues to improve as we translate to human joint imaging .After reviewing this exhibit, the viewer should be aware of potential clinical role of photo acoustic imaging , its appearance , present limitations and the scope of future research .

Background

Photo acoustic imaging (PAI) is a very exciting new, non-ionizing, non-invasive, low cost, laser and ultrasound-based technology, with critical dual ability of both structural and functional imaging.PAI is sensitive to blood volume, not limited by flow (unlike ultrasound),

holding great promise for the earliest detection of increase in blood volume and angiogenesis as seen in inflammation or neoplasm.

Evaluation

After having successfully imaged animal arthritis model and human cadaver finger (images of which will also be reviewed), normal controls were imaged as a part of funded research prior to imaging patients with rheumatoid arthritis. Viewer will have the opportunity to appreciate the first ever photo acoustic images of human finger obtained demonstrating feasibility. Comparable ultrasound images will also be provided. Potential applications and limitations of PAI will be discussed.

Discussion

While ultrasound and MRI are helpful in diagnosing synovitis/synovial proliferation in a swollen joint, we hypothesize that PAI will be able to demonstrate neovascularization much earlier than ultrasound or MRI, leading to early diagnosis, earlier initiation of treatment, thereby limiting disease progression and achieving excellent outcome. Ultrasound is sensitive to neovascularity, dependent on blood flow. PAI is sensitive to blood volume, not limited by flow, holding great promise for the earliest detection of increase in blood volume and angiogenesis - a key early finding inflammation

Physics - Monday Posters and Exhibits (12:45pm - 1:15pm)

Monday, 12:45 PM - 01:15 PM • Lakeside Learning Center

[Back to Top](#)

LL-PHS-MOB • AMA PRA Category 1 Credit™:0.5

LL-PHE-MO10B • The Practicality of Ultrasound Physics in Everyday Radiology: A Case-based Review

Sarah Pittman MD (Presenter) ; Angus J Hartery MD

PURPOSE/AIM

1. To demonstrate certain fundamentals of ultrasound (US) physics, including the creation and propagation of ultrasound waves. 2. To explain several artifacts that result from the physical properties of the ultrasound beam and its interaction with soft tissue. 3. To apply an understanding of US physics and select artifacts to enhance image interpretation.

CONTENT ORGANIZATION

Selected cases will demonstrate the clinical relevance of US physics, including choice of transducer frequency and common artifacts, such as refraction and increased through-transmission.

SUMMARY

US continues to be a valuable primary diagnostic imaging modality. Due to the physical properties of the ultrasound beam and its interaction with soft tissue, several unavoidable artifacts result. A working knowledge of US physics and artifacts will improve detection, diagnosis, and management of patients.

LL-PHS-MO1B • Comparison of MS-CT and Whole-body Plethysmography: Is There Any Functional Information Available Using a Postprocessing with a Recent CAD-development?

Ansgar Malich MD (Presenter) ; Sylvia Mikulik ; Klaus Thomas ; Peter Hannemann ; Ulf K Teichgraber MD

CONCLUSION

Recently developed CAD-software has the potential to quantify and differentiate obstructive and restrictive diseases of the lung based on MS-CT data and reflect some important functional parameter of the lung.

Background

MS-CT currently does not offer functional parameter of the lung. Study aimed to analyze, whether there are parameters obtainable from CT-data reflecting functional parameters calculated by whole-body plethysmography.

Evaluation

100 patients were randomly selected who underwent MS-CT (128 row-CT) and whole body plethysmography (master-screen body, Jaeger, Germany) within < 7days. All data were analyzed using CAD (MeVISPulmo3D, Fraunhofer MeVis, Germany). Vital capacity (VC), FEV1, intrathoracic gas volume (ITGV), residual volume (RV), total lung capacity (TLC) were matched with CAD-based lung volume analysis (vol), mean low density (MLD), low and high attenuation values (LAV/HAV), lung weight (w) P15, PK (maximum of histogram) and FWHM (full width half max). Central obstruction, peripheral obstruction, restrictive diseases and emphysematic patients were analyzed.

Discussion

CAD-analysis was possible in all cases. Acquisition time was approx. 1 minute per case.

Correlation coefficients of VC were: Vol:r=.57,p ITGV correlates with Vol:r=0.71,p RV showed association to Vol.:r=0.6,p FEV1 showed a correlation to vol:r=-0.67,p Correlation coefficients of TLC vs. vol.,weight, MLD, HAV, PK and P15 were: r=0.83; r=0.51; r=-0.60; r=-0.56; R=-0.45; r=-0.52, all p-values Only moderate correlation were observed for maximum expiratory flow (PEF) and expiratory reserve volume (ERV).

Severity of obstructive and restrictive diseases showed different CAD-based data of volume, MLD, LAV and HAV (Oneway Anova, p

LL-PHS-MO2B • The Effects of Pure and Hybrid Iterative Reconstruction Techniques on Computer-aided Detection (CAD) System of Pulmonary Nodules in Dose-reduced CT Scans

Masaki Katsura MD (Presenter) ; Izuru Matsuda MD ; Masaaki Akahane MD ; Koichiro Yasaka MD ; Shouhei Hanaoka MD ; Hiroyuki Akai MD ; Jiro Sato MD ; Akira Kunimatsu MD * ; Kuni Ohtomo MD *

PURPOSE

To evaluate the effects of pure and hybrid iterative reconstruction techniques on computer-aided detection (CAD) system of pulmonary nodules using reference-, low-, and ultralow-dose chest CT.

METHOD AND MATERIALS

Fifty-nine patients(mean[SD] age, 64.7[13.4] years) gave informed consent to undergo reference-, low-, and ultralow-dose chest with 64-row multidetector CT. The reference- and low-dose CT involved the use of automatic tube current modulation with fixed noise indices(31.5and70.44 at 0.625mm, respectively) and the ultralow-dose CT was acquired with a fixed tube current-time product of 5mAs. Each 0.625-mm-thick image was reconstructed with filter-back projection(FBP), 50% adaptive statistical iterative reconstruction(ASIR)-FBP blending, and model-based iterative reconstruction(MBIR). CAD output was compared with the results of the reference standard which was established using a consensus panel of 2 radiologists, who identified 84 non-calcified nodules with diameters of 4mm or greater on reference-dose ASIR. Sensitivity in nodule detection between different radiation dose and reconstruction techniques was assessed using Cochran's Q test with post hoc McNemar test and Holm correction for multiple comparisons. The mean number of false-positive findings per examination was assessed using Friedman test with post hoc testing using Wilcoxon signed-rank test and Holm correction.

RESULTS

Compared with reference-dose CT(307.7±178.1mGy-cm), there was a 78.6% decrease in dose-length product with low-dose CT(66.0±50.8mGy-cm), and a 95.3% decrease with ultralow-dose CT(14.5±1.1mGy-cm). CAD sensitivity for nodules at ultralow-dose MBIR(26.2%) was equivalent($p=0.52-1.00$) to those at reference-(FBP,23.8%;ASIR,26.2%,MBIR;26.2%) and low-dose CT(FBP,26.2%;ASIR,25.0%,MBIR;25.0%). Mean number of false-positive findings per examination tended to increase with the use of

MBIR, particularly at low-(1.19) and ultralow-dose CT(1.32), although there were no significant differences among reconstruction techniques at both dose levels($p=0.08-1.00$).

CONCLUSION

CAD sensitivity for pulmonary nodules at ultra-dose MBIR is almost equal to that at reference-dose CT. MBIR can improve CAD performance on dose-reduced chest CT despite increased false-positive findings.

CLINICAL RELEVANCE/APPLICATION

With the use of MBIR, CAD system on ultralow-dose CT may play an equivalent role to that on regular-dose CT in helping radiologists detect pulmonary nodules.

LL-PHS-MO3B • Accurate Measurement of Airway Wall Thickness with a Model-based Line Profile Matching Technique in MDCT

Zepa Yang MS (Presenter) ; **Hyeongmin Jin** ; **Jong H Kim** PhD

PURPOSE

Accuracy of airway wall measurement has been impaired by the combined effect of partial volume and point spread blurring in CT systems. We present a novel technique which enables to determine the wall thickness of small airways by using a model-based lesion quantification technique.

METHOD AND MATERIALS

Point spread functions of a commercial CT(Sensation 16, Siemens) was acquired by using a wire phantom scanning for two different kernels(B30s and B50s). The COPDgene phantom was scanned with 120kVp, 100mAs, 1mm thickness setting and was reconstructed with the two kernels.

A set of model-derived line profiles were created by taking convolution of the point spread functions with a set of numerical airway phantoms having varying thickness ranging 0.1 - 5.0mm with 0.1mm thickness interval. These model-derived line profiles were compared with the measured line profiles across the wall from the airway phantoms in COPDgene phantoms. The wall thickness of the phantom was determined as the thickness of numerical model giving minimum error between two line profiles. Measurements were made for 4 types of airway phantoms with wall thickness of 0.6, 0.9, 1.2, 1.5 mm in 40 CT slices.

RESULTS

The mean measurement error of wall thickness with B30s kernel was 0.10 ± 0.03 mm for 0.6mm thickness, 0.06 ± 0.04 for 0.9mm thickness, 0.07 ± 0.01 for 1.2mm thickness, and 0.05 ± 0.01 for 1.5mm thickness. The error with B50s was -0.04 ± 0.07 mm for 0.6mm thickness, -0.08 ± 0.05 for 0.9mm thickness, -0.11 ± 0.05 for 1.2mm thickness, and -0.07 ± 0.06 for 1.5mm thickness.

CONCLUSION

By applying a model-based line profile matching technique, our technique could determine the airway wall thickness accurately even for the small airways.

CLINICAL RELEVANCE/APPLICATION

Our technique may allow detection of early change of airway wall thickening in early diagnosis, patient sub-typing, and therapeutic monitoring in the management of COPD disease.

LL-PHS-MO4B • Analysis of Predictive Maintenance of Linear Accelerator Beam Uniformity Using Statistical Process Control

Charles M Able MS (Presenter) * ; **Alan Baydush** PhD * ; **Michael T Munley** PhD *

CONCLUSION

PdM monitoring of beam uniformity using a new method for determining SPC control limits is more effective than using traditional control limits. SPC false alarms are reduced thereby eliminating unwarranted service intervention. We are working to develop code that will provide an SPC evaluation using the new formula.

Background

The focus of this study is to determine the effectiveness of revisions to statistical process control (SPC) chart limits for linear accelerator steering coil current (beam uniformity) predictive maintenance (PdM) monitoring

Evaluation

We have re-evaluated calculation of the limits for steering coil current (SCC) SPC charts based on our observations that the changes in SCC required for 1% change in measured beam uniformity will generally exceed the traditional limits calculated using the standard deviation of the subgroup values alone. Using empirical data obtained from controlled experiments varying the SCC while measuring the beam uniformity, we have developed a formulism that incorporates a scaling factor (Cm) in the calculation of control limits.

Discussion

SCC monitoring of an 18 MV photon beam using the new limits indicated a change in the transverse position coil operating current 2 weeks prior to multiple EXQ2 faults and unscheduled downtime. A change in beam uniformity of greater than 3% was found once the beam was scanned using a computerized water phantom and ion chamber. SPC charts of this steering coil using traditional limits would have resulted in 5 false positives prior to the first positive alarm indicated by the new limits

LL-PHS-MO5B • Tumors in the Peripheral Zone and Central Gland of the Prostate Have Different Perfusion Characteristics on Dynamic Contrast-enhanced MRI

Shoshana Ginsburg MS (Presenter) ; **Boris N Bloch** MD ; **Neil M Rofsky** MD ; **Elizabeth Genega** MD ; **Robert E Lenkinski** PhD * ; **Anant Madabhushi** MS *

PURPOSE

Pharmacokinetic (PK) perfusion parameters extracted from DCE MRI, such as the volume transfer constant and extravascular-extracellular volume fraction, are useful in cancer detection and grading. Recent studies have shown that tumors in the peripheral zone (PZ) of the prostate are more aggressive than tumors in the central gland (CG) and that the morphology of prostate cancer (PCa) differs based upon its location in the prostate. The purpose of this study is to compare PK perfusion parameters of PZ and CG tumors.

METHOD AND MATERIALS

15 endorectal 3 Tesla MRI studies, using DCE and T2W imaging, were obtained in men with biopsy proven PCa prior to radical prostatectomy (RP). The DCE MRI protocol included 2 pre-contrast images, which were acquired at 95 second intervals before the bolus injection of 0.1 mmol/kg of gadolinium-DTPA, and 5 post-contrast images that were acquired at the same temporal resolution. Following RP, surgical specimens, examined with whole mount histopathology by a trained pathologist, were evaluated for the presence and extent of PCa, which was subsequently mapped from histology to DCE MRI. The PZ and CG were manually segmented on T2W MRI by a radiologist, and each study was classified as having PCa in a particular zone when more than 70% of the tumor volume was present in that zone. Nine studies were found to have PCa in the PZ, and 6 had PCa in the CG. The iterative multiple reference tissue method was used on the DCE MRI data to estimate the volume transfer constant and extravascular-extracellular volume fraction for each prostate tumor.

RESULTS

Values for the transfer constant and extravascular-extracellular volume fraction averaged 0.27 and 0.43, respectively, for PZ tumors and 0.36 and 0.62, respectively, for CG tumors. Both the transfer constant and the extravascular-extracellular volume fraction are significantly higher in CG tumors than in PZ tumors ($p = 0.045$ for both perfusion parameters).

CONCLUSION

CG and PZ tumors manifest significantly different perfusion characteristics on DCE MRI, suggesting that vascular features of PCA depend on the tumor location in the prostate gland and that PZ and CG tumors may have distinct biologic attributes.

CLINICAL RELEVANCE/APPLICATION

Since CG and PZ tumors have different perfusion characteristics, zone-specific analysis of DCE MRI should improve assessment of PCA.

LL-PHS-MO6B • Optimal Reconstruction Filter on Observation of Periodontal Ligament Space in Dental Cone-beam CT

Yuuki Houno (Presenter) ; **Toshimitsu Hishikawa** ; **Ken-Ichi Gotoh** ; **Munetaka Naitoh** ; **Eiichiro Arijii** ; **Yoshie Kodera** PhD

PURPOSE

Diagnosis of the alveolar bone condition is important in the treatment of periodontal disease. However, visualization of the thin alveolar bone and periodontal ligament space is difficult owing to image blurring using the current imaging technique. Therefore, identification of the marginal alveolar bone level is unreliable. In this study, we try to determine high quality images of periodontal ligament space separation were obtained by changing the reconstruction filter.

METHOD AND MATERIALS

Images from 4 different areas of 2 types of head phantoms were obtained using Alphard-3030 dental cone-beam computed tomography (Asahi Roentgen Industry Co., Ltd.). The image was reconstructed from the raw data by using 5 different reconstruction filters. Post reconstruction, these reconstructed images were compared with the Alphard-3030 reconstructed images by using Thurstone's paired comparison, and a scale value was calculated. The images were evaluated limiting the clarity of periodontal ligament space boundary by 3 periodontologists and 3 radiologists with >5 years of clinical experience. To confirm the image characteristics, modulation transfer function and Wiener spectrum were calculated.

RESULTS

The best image was one reconstructed with filter that increased the high-frequency component based on Shepp and Logan's function. The Alphard-3030 reconstructed image, which is used in clinical settings, was the worst. The image reconstructed with the best filter had a higher modulation transfer factor and Wiener spectral value than the Alphard-3030 reconstructed image. These results suggest that sharp images enhance the visualization of the periodontal ligament space, and the imaging noise is insignificant. These images enable the observer to clearly view the periodontal ligament space boundary.

CONCLUSION

We determined the optimal reconstruction filter required to observe the periodontal ligament space.

CLINICAL RELEVANCE/APPLICATION

Image quality of periodontal ligament space may be improved by alternating reconstruction filter of cone-beam CT. This method can be applied to various CT apparatus without hardware replacement.

LL-PHS-MO7B • Fast and Easy Dose Estimates including Tube Current Modulation and Automatic Exposure Control

Natalia Saltybaeva ; **Martin Hupfer** PhD (Presenter) * ; **Daniel Kolditz** PhD * ; **Bernhard Schmidt** PhD * ; **Willi A Kalender** PhD *

PURPOSE

Tube current modulation (TCM) and automatic exposure control (AEC) are widely used in modern CT. The aim of this work was to include the effects of TCM and AEC in a software package for fast and easy organ and effective dose estimates.

METHOD AND MATERIALS

Measurements were carried out for a SOMATOM Definition Flash scanner (Siemens AG, Forchheim, Germany); the manufacturer provided all necessary information on their CARE Dose4D TCM/AEC product. TCM and AEC curves were derived for anthropomorphic phantoms by generating complete CT projection data sets by means of ray-tracing and predicting the flux at the detector. For all phantoms and parameter combinations studied, Monte Carlo (MC) calculations wandw/o CARE Dose4D were performed to provide tabulated dose values. These tables were included in the software package ImpactDose (CT Imaging GmbH, Erlangen, Germany) which estimates organ and effective dose depending on patient size, scan region and scan protocol. It is based on pre-tabulated dose values calculated by means of MC calculations for the ORNL family of anthropomorphic phantoms. Validation measurements were performed using thermoluminescence dosimeters (TLDs) for each of three different anthropomorphic phantoms (Rando adult, 5-y.o. and 1-y.o. CIRS) wandw/o CARE Dose4D.

RESULTS

Measured dose values were compared to MC results on a chip-by-chip basis. The mean differences for all TLD chips were 5%, 7%, and 6% for the adult, the 5-year old, and the 1-year old phantom, respectively. This deviation is in the range of the uncertainty associated with TLD measurements and indicates that TCM/AEC were correctly implemented. The derived dose values wandw/o TCM/AEC allowed for assessment of their effect on dose for different patients without the need for measurements or repeated MC calculations.

CONCLUSION

Dose estimates based on tabulated MC-derived dose distributions can provide accurate information on the effect of TCM and AEC in clinical CT if information about their implementation is provided by the manufacturer.

CLINICAL RELEVANCE/APPLICATION

The software package allows to obtain fast and accurate dose estimates when TCM/AEC is used and furthermore may serve as a learning tool.

LL-PHS-MO8B • Evaluation of Alignment Discrepancy Based on Fiducial Seeds versus Bony Anatomy or Bony Anatomy Plus Endorectal Balloon for Prostate Cancer Patients

Rui Zhang (Presenter) ; **Connel Chu** ; **Maurice L King** MD ; **John P Gibbons** PhD

ABSTRACT

Purpose/Objective(s): Fiducial seed has long been recognized as an accurate tool to correct prostate patient setup error. The alternative techniques include aligning patient using bony anatomy information and endorectal balloon. The aim of this study was to evaluate the discrepancy in prostate daily alignment based on fiducial seeds versus bony anatomy or bony anatomy plus balloon.

Materials/Methods: All alignment evaluations were carried out by using Elekta X-ray volume imaging (XVI) software. Seventeen prostate patients with both fiducial seeds and water-filled endorectal balloon and four patients with fiducial seeds only were chosen for this study. Each patient was followed for more than one month. Before each treatment fraction, a cone beam computed tomography (CBCT) was acquired and the daily shift information based on fiducial seeds was recorded for each patient as the gold standard. Then the alignment was performed again based on bony anatomy only (for patients without balloon) or based on bony anatomy plus balloon (for patients with both fiducial and balloon) using the same CBCT data. For alignment based on bony anatomy only, the auto-fusion based on bone filter was applied and the angular shifts were ignored. For alignment based on bony plus balloon, the same bone filter was applied first, then the balloon was used for anterior-posterior (AP) alignment correction. The differences between shifts determined using fiducial seeds and using the bony anatomy or bony anatomy + balloon were analyzed.

Results: In the right-left (RL) direction, discrepancies between shifts based on fiducial seeds and shifts based on bony only or bony + balloon were all less than 4 mm. In the superior-inferior (SI) direction, the discrepancies were less than 15 mm for bony only, and less than 8 mm for bony + balloon. In the AP direction, the discrepancies were all less than 11 mm for bony only or bony + balloon. Over 96% (AP) and 98% (SI) of the discrepancies were within 7 mm for bony + balloon, while over 75% (AP) and 48% (SI) of the discrepancies were within 7 mm for bony only.

Conclusions: The RL alignments are always good regardless of the alignment technique. 7 mm seems to be a reasonable setup margin for prostate patients without fiducial seeds but with balloon. Using endorectal balloon for patients without fiducial is strongly recommended since it helps alignments in both AP and SI directions.

LL-PHS-MO9B • Feasibility of 4D Endoscopic Rendering of Interventional Devices

Erick Oberstar (Presenter) * ; **Brian Davis** * ; **Martin Wagner** ; **Kevin Royalty** MS, MBA * ; **Markus Kowarschik** PhD * ; **Sebastian Schafer** * ; **Charles M Strother** MD * ; **Charles A Mistretta** PhD *

PURPOSE

Endoscopic views of devices inside the vasculature could be beneficial for navigation placement in complicated vascular anatomy. By leveraging 3D or 4D DSA, in with UW Madison's 4D Omni-Plane Fluoroscopy (4DOPF) technique for creating any desired virtual fluoroscopic views from biplane fluoroscopy, endoscopic views of vascular structures can be generated to provide additional information about the presence of complex anatomy or obstructions that would inhibit a device entering a vascular orifice or make device navigation challenging. Although 4DOPF is typically used to show the motion of a device relative to a vascular roadmap, it could be helpful to view the placement of interventional devices as they enter vascular structures from an endoscopic view.

METHOD AND MATERIALS

A 3D or 4D DSA volume is acquired in addition to orthogonal biplane fluoroscopic views. A 3D vessel lumen volume is created by subtracting a DSA volume from a dilated version of the volume to remove contrast signal inside the vessel. A device volume is generated by 4DOPF (backprojection of segmented orthogonal biplane fluoro views) and is combined with the vessel lumen volume. Endoscopic views of the vascular lumen are generated from the combined data set at each time frame.

RESULTS

The images shown were done retrospectively with parallel ray processing without correction for geometrical inconsistencies. Figure 1 shows an example of a cerebral aneurysm, and time series images of two different views of the neck of the aneurysm. Several camera views were established showing optimal device and neck visibility as indicated by the red and yellow arrows on the aneurysm in Fig 1a. Vessels obstructing the view of the aneurysm have been removed. The images surrounded by red and yellow backgrounds show four time instances of a device moving into the aneurysm from superior and inferior views Fig 1b-c.

CONCLUSION

By leveraging 3D/4D-DSA and 4DOPF, endoscopic views of an interventional device and vascular lumen can be generated to provide physicians additional information about the presence of complex anatomy or obstructions that would inhibit a device entering a vascular orifice.

CLINICAL RELEVANCE/APPLICATION

The clinical goal of our work is to develop and optimize techniques which will enhance the ability to use road mapping techniques in image guided abdominal and peripheral interventions.

Physics - Sunday Posters and Exhibits (1:00pm - 1:30pm)

Monday, 12:45 PM - 01:15 PM • Lakeside Learning Center

[Back to Top](#)

LL-PHS-SUB • AMA PRA Category 1 Credit™:0.5

LL-PHE-SU10B • Development of an Anisotropic Phantom for Quality Improvement of DTI and Tractography Algorithms in Clinical Practice

Isabelle Filipiak (Presenter) * ; **Christophe Destrieux** MD, PhD ; **Jean Philippe Cottier** MD ; **Laurent Barantin**

Background

Phantom for diffusion studies mimicking the human white fibers anatomy is still not available. To evaluate Diffusion Tensor Imaging (DTI) and tractography algorithms, we developed an anisotropic phantom representative of the human white fibers anatomy. It was composed of objects having various diffusion properties, which can be used for quality control of these sequences.

Evaluation

The 3D phantom we developed contained fiber bundles that differ in shape (5 longitudinal, 2 U-shape, and 4 angular) and material (dyneema and nylon).

It was scanned 20 times on a 3T MR scanner using the same parameters as in clinical practice: 2D single shot EPI sequence, TE/TR=96/12000 ms, voxel size = 1.7x1.7x1.7 mm³, acquisition time = 15 min.

First, fractional anisotropy (FA), mean diffusivity (MD), radial and axial diffusivity (RD and AD) were measured from region-of-interest (ROI) delineated on each fiber; differences across fiber shapes and materials were evaluated using Wilcoxon's test. In a given material (dyneema or nylon), FA, MD, RD/AD did not significantly differ with fiber shape ($p > 0.05$) and imaging session. FA measured in dyneema (0.57 ± 0.12) was higher than in nylon (0.18 ± 0.04). Then tracts were reconstructed using deterministic algorithms (Interpolated Streamline, FACT, tensorline) and propagation or position error and tractography shifts were evaluated. The tractography algorithms we used were able to reconstruct all fiber bundles. However, the number and length of fibers were twice time higher using interpolated streamline or tensorline algorithms as compared to FACT. They were also higher using dyneema.

Discussion

With this anisotropic phantom: (1) FA, MD, RD/AD values were similar across imaging sessions and the different fiber shapes representative of the human white fibers anatomy; (2) tractography was doable on the phantom ; (3) the number and length of detected fibers varied depending of the used material and algorithm.

CONCLUSION

This new anisotropic phantom significantly expands the potential of quality control in diffusion imaging to improve the accuracy of DTI data and tractography in clinical practice.

LL-PHS-SU1B • Development of Spiral Micro Holes Phantom for the Measurement of Slice Thickness in CT

Katsumi Tsujioka PhD (Presenter) ; **Rina Terauchi** ; **Ayako Gonaka** ; **Yasutomo Sato** ; **Ryoichi Kato** MD

CONCLUSION

When you evaluate the performance of multi-slice CT detector, the measurement of slice thickness is critical. However, with the small bead phantom which widely receives recommendation requires complicated operational procedures such as multiple scans and a lot of CT images. The Spiral Micro Holes Phantom we developed enables the slice thickness measurement with only one time scanning and achieves equivalent precision with the method that uses small bead. When you measure the slice thickness using conventional method such as small bead or thin plate, it requires complicated procedures such as many times of scanning and CT images. To this end, slice thickness has to be always fixed and standardized. However our phantom we developed for the purpose of measurement of slice thickness only requires one time scanning and one CT image.

Background

We development of Spiral Micro Holes Phantom for the measurement of slice thickness in CT. Artifacts, which are commonly seen with the conventional phantom with slant structure, are not seen in this new phantom. It enables helical scanning as well as slice measurement of multi slice CT with single scanning only. This time, we compared the result using this phantom and by using small bead method which had been recommended so far.

Evaluation

The Spiral Micro Holes phantom we developed has 0.5mm diameter holes on the surface of 40mm-diameter acrylic phantom. The depth

of each hole is 5mm and is placed in 5mm intervals in a spiral manner. The number of holes is 90 for an outer circumference. You can get the slice sensibility profile by measuring the CT numbers of CT images of this phantom. This time we compared the measurement precision of helical scanning and multi-slice CT with conventional small bead phantom.

Discussion

We were able to obtain SSPz with one single CT image using this new phantom designed for slice thickness measurement. No artifacts appeared which is seen in conventional methods such as slant aluminum sheet or wire method. As for the precision, the measurement result of slice thickness showed equal precision to that of conventional small bead phantom.

LL-PHS-SU2B • Towards Virtual Clinical Trials: A Framework for Clinically Relevant CT Simulations

Justin B Solomon MSc (Presenter) ; **Juan Carlos Ramirez Giraldo** PhD ; **Karl Stierstorfer** PhD * ; **Yuan Lin** PhD * ; **Ehsan Samei** PhD *

PURPOSE

To establish a framework for creating virtual anthropomorphic computed tomography (CT) images with realistic lesions, accounting for attributes of commercial CT systems.

METHOD AND MATERIALS

A detailed computer model of a commercial CT system (Siemens Somatom Definition Flash, Siemens Healthcare, Germany) was created, accounting for the system geometry, focal spot size and motion pattern, detector configuration, bowtie filter, and the contribution of quantum noise. The model was used to simulate raw projection data of a virtual anthropomorphic phantom, including lesions of varying morphology (contrast, shape, and edge profile). Both spherical and realistically shaped lesions were added. The realistic lesions were generated based on actual clinical data, using a previously validated technique. The projection data were formatted to match those of actual raw data from the scanner. This enabled CT images to be reconstructed using the manufacturer's proprietary reconstruction engine including both conventional filtered backprojection and iterative reconstruction (i.e., IRIS and SAFIRE). The reconstructed images were evaluated for noise texture realism and artifacts.

RESULTS

For all reconstruction algorithms, the proposed framework resulted in realistic images with noise properties consistent with real CT images.

CONCLUSION

It is possible to create realistic simulated CT images based on the properties of commercially available CT systems. This framework could facilitate in assessing the complex relationship between scan settings and the appearance of subtle lesions in the reconstructed images, without the need to collect clinical data. Such assessments are critical for system optimization and performance evaluation.

CLINICAL RELEVANCE/APPLICATION

Clinical trials can be difficult and costly to perform. Virtual clinical trials have the potential to reduce costs and expedite the process of evaluating new CT technologies.

LL-PHS-SU3B • Dedicated Mobile Volumetric CT for Human Brain Imaging

Jong Hyun Ryu (Presenter) ; **Kwon-Ha Yoon** MD, PhD ; **Han Ah Lee** ; **Seung Jae Byun** ; **Chang Won Jeong** ; **Jinseok Lee** ; **Kyong Woo Kim** ; **Hee-Sin Lee** ; **Kyu-Gyeom Kim** ; **Jaee Hee Kim** ; **Su Chong Joo**

PURPOSE

The cone-beam based volumetric CT is popularly applied to micro CT and dental CT. However, it is difficult to obtain human brain image of good quality because of various limitations such as artifacts when using volumetric CT with flat panel detector (FPD). We studied this work to develop a dedicated mobile volumetric CT with FPD for human brain imaging.

METHOD AND MATERIALS

Cone beam x-ray source, flat-panel detector with CMOS sensor (290.8x229.8mm), embedded PC and GPU were used in this system (Fig 1). Under the x-ray source condition of 120kV and 6mA, 360 projections were grabbed at the rate of 70 frames per seconds during 5.14 seconds for optimized human brain imaging. FOV was designed 200mm(XY) x 160mm(Z) and voxel size was 200µm in 1024³. Interface for 2D image acquisition from FPD was CAMLINK(2cable,80MHz) and it can grab 70 frames per second at 2 binning. Feldkamp back-projection algorithm was used as the base for image reconstruction, and it was used S/W filtering to sinogram for artifact reduction. Reconstruction time was less than 90 seconds for 512 cube. The CT images were obtained using a head phantom (Angiographic CT head phantom ACS, Herago, Japan). In addition modulation transfer function (MTF) and radiation dose were measured for the evaluation.

RESULTS

Using this dedicated brain volumetric CT, we could get a brain images using a head phantom with good quality. It was confirmed that artifact was reduced by S/W filtering to sinogram at image reconstruction. Based on the MTF (Modulation Transfer Function, 10%) curve, we found 20~21 lp/cm using phantom (QRM-ConeBeam, QRM GmbH, Germany) at 1024 cube. The CT images demonstrated cross sections through a reconstruction of a human head obtained with the soft tissue protocol. Various brain structures are clearly distinguishable, proving the improved contrast resolution of the system (Fig. 2). Images showed a little ring or scatter artifacts. The effective dose for this head scan was estimated to be about 1mSv.

CONCLUSION

We developed a dedicated mobile volumetric CT for brain images using cone beam x-ray and flat panel detector. This system would be perfectly suitable for intra-operative imaging and mobile imaging applications such as neurosurgery or imaging of immobilized intensive care patients.

CLINICAL RELEVANCE/APPLICATION

N/A

LL-PHS-SU4B • Automated Detection of Carotid Artery Calcifications on Dental Panoramic Radiographs: False Positive Reduction by Support Vector Machine

Ryo Takahashi ; **Chisako Muramatsu** PhD ; **Akitoshi Katsumata** DDS, PhD ; **Takeshi Hara** PhD ; **Hiroshi Fujita** PhD (Presenter)

PURPOSE

Carotid artery calcifications (CACs) are one of the indices useful in predicting the risk of arteriosclerosis. It has been suggested that CACs may be detectable on dental panoramic radiographs (DPR) obtained for dental examination. However, with the general window level for dental examination, these calcifications can be easily missed on DPRs when their purpose does not lie on arteries. The purpose of this study is to automatically detect CACs on DPRs for notifying a possible risk for arteriosclerosis.

METHOD AND MATERIALS

Our database included 100 DPRs, including 34 images with one or more CACs and 66 images without CAC. First, regions of interest including carotid arteries on the right and left sides are automatically extracted on the basis of the result of automatic mandibular contour detection. After applying top-hat filter, CAC candidates are detected by thresholding. Potential edges belonging to vertebra and hyoid bones are identified and removed from the candidates. Thirteen image features, including shape features, locational features, and intensity features, are determined. We employed a support vector machine for the reduction of false positives with an extensive search for an optimal feature set. The method was evaluated by the cross validation method, in which a half of CAC cases and a half of control cases were randomly sampled for training cases, and remaining cases were employed for testing. The sampling procedure was repeated 10 times for reducing the sampling effect.

RESULTS

The proposed method obtained the 90% sensitivity with average false positive marks of 2.5 per images. Considering some calcifications are hardly detectable on DPRs, the sensitivity of 90% is satisfactory with a relatively small number of false positives. An optimal feature set included 8 features. It was found that the shape-related features are not so useful, except for circularity, indicating the variations in size and shape of CACs. Locational features may be useful for removing false positives due to normal structures. Intensity-related features were considered most useful.

CONCLUSION

The proposed method can be useful for automatic detection of CACs on DPRs obtained in general dental examinations.

CLINICAL RELEVANCE/APPLICATION

Automated detection of carotid artery calcifications on dental panoramic radiographs may contribute for early diagnosis of arteriosclerosis.

LL-PHS-SU5B • A Dose Finding Cadaver Study Using Model-based Iterative Image Reconstruction (MBIR) in CT Imaging of the Chest

Kathrin Weber (Presenter) ; **Fabian Mueck** ; **Lucas L Geyer MD *** ; **Maximilian F Reiser MD** ; **Stefan Wirth MD ***

PURPOSE

To compare image quality (IQ) of 64-row CT scans of the chest, respectively acquired at varying dose levels and reconstructed with model based iterative reconstruction (MBIR), to standard baseline examinations at full dose and using adaptive statistical iterative image reconstruction (ASIR).

METHOD AND MATERIALS

12 human cadavers were included. A full-dose baseline reference (FBR) was acquired (CT HD750; GE Healthcare, Waukesha, IL) using a standard-of-care protocol (0.625mm helical, 0.984 pitch, 120kV, 10-400mA modulation, noise index NI=39 VS=0.625; NI = allowed proportional level of noise in a water phantom in virtual slices of varying thickness (VS in mm); raw data were reconstructed in soft tissue kernel using ASIR 50%). These baseline raw data were also reconstructed with MBIR (D0). Additionally, each cadaver was scanned with varying dose levels D1-D5 by changing NI and VS (D1: NI=35, VS=2.5; D2: NI=70, VS=0.625; D3: NI=35, VS=5; D4: NI=70, VS=2.5; D5: NI=70, VS=5; all reconstructed with MBIR). Except for NI, VS and MBIR, all other parameters were identical to the FBR, all series reformatted in 3mm axial, coronal and sagittal slices. Two radiologists, blinded to the dose level, independently compared IQ for soft tissue evaluation of D0-D5 to the full-dose FBR (IQ: -2:diagnostically inferior, -1:inferior, 0:equal, +1:superior, +2:diagnostically superior; respectively). For statistical analysis ICC and Wilcoxon's test were used.

RESULTS

Mean values were (CTDIvol in mGy: D0 = 8.6±4.0, D1 = 4.8±3.7, D2 = 4.2±3.1, D3 = 2.6±2.1, D4 = 1.3±1.0, D5 = 0.7±0.5); (IQ: D0 = +2.0±0.3, D1 = +1.54±0.5, D2 = +1.0±0.5, D3 = +0.6±0.4, D4 = +0.0±0.5, D5 = -1.2±0.6). All values were significant different from one another; p

CONCLUSION

Data reconstruction with MBIR instead of ASIR allows for significant dose reduction of 85% in non contrast enhanced CT imaging of the chest without impairment of the image quality, resulting in a calculated mean effective dose of 0.71±0.63 mSv.

CLINICAL RELEVANCE/APPLICATION

For non contrast enhanced standard chest exams MBIR allows for diagnostic CT of the chest markedly below 1mSv without loss of image quality and significant image improvement at higher dose levels.

LL-PHS-SU6B • Numerical Modeling of the Dynamics of Ultrasound Contrast Agents in a Vascular Network: Validation Study

Laure D Boyer (Presenter) ; **Pauline Le Notre MSc** ; **Stephen Randall Thomas PhD** ; **Ingrid Leguerney** ; **Nathalie B Lassau MD, PhD *** ; **Stephanie Pitre-Champagnat**

CONCLUSION

The NM with the Fluent software and with the modeling of realistic injection of CA by bolus was validated for studying the dynamics of blood and CA in a simple geometry. Results obtained with a more realistic vascular network composed of 30 vessels will be presented.

Background

Dynamic Contrast-Enhanced Ultrasonography (DCE-US) is a particularly attractive method to assess tumor microvasculature from the concentration quantification of ultrasound contrast agents (CA) within lesions. This method does not yet benefit from methodological tools imported from physics to characterize the ability of the quantification methods to evaluate the tumor microcirculation. In this context, we developed the first numerical model (NM) based on Computational Fluid Dynamics software for studying the quantification methods to describe tumoral perfusion in a complex vascular network and to apprehend their variations according to the tumor growth, hemodynamic configuration and CA injections. The aim of this study is to validate this approach in comparison with DCE-US experiments on simple geometrical configuration composed of 1 fluids bifurcation.

Evaluation

The NM was developed with Fluent software (ANSYS, France), which modeled blood and CA flows in a vascular network with laminar flow described by Poiseuille's law. Geometry of the numerical and experimental phantom was a 31cm length tube with a diameter of 2mm with 1 bifurcation giving 2 parallel tubes located 23cm from the input. The volume of injected CA was 0.1mL with blood flows of 26, 34, 41 and 56mL/min. Realistic injection of CA by bolus was implemented in the NM. DCE-US experiments were performed with an Aplio scanner (Toshiba Medical Systems, Japan) and a 12MHz probe with SonoVue (Bracco, Italy) as CA. Areas under the curve (AUC) from the time-CA concentration curves were extracted and compared between experimental data and the NM.

Discussion

The numerical curves of CA concentration versus time were similar to those obtained experimentally, with a decrease of AUC values according to the blood flow, in agreement with the indicator-dilution theory.

LL-PHE-SU8B • Metal Artifact Reduction in MRI: Update on Conventional and Emerging Techniques

Michael N Hoff PhD (Presenter) ; **Paxton Smith MEng** ; **San Xiang**

PURPOSE/AIM

1. Review the mechanisms responsible for MRI artifacts caused by metallic implants.
2. Review standard and emerging techniques used to reduce metal-induced MRI artifacts.
3. Show examples of artifact reduction using emerging MRI methods.

CONTENT ORGANIZATION

- * Describe the common types of embedded metal hardware found in post-surgical patients.
- * Review the presentation of metal artifacts in MRI and describe the physical mechanisms of signal loss, signal pile-up, and distortion.
- * Review the efficacy of metal artifact reduction in standard imaging practice using spin echo, STIR, high readout bandwidth, thin slice selection, and increased matrix image size.
- * Present advanced techniques for metal artifact reduction, such as MARS, 3D-PLACE, MAVRIC, SEMAC, and XS-bSSFP.

SUMMARY

1. Metal artifacts in MRI impair the Radiologists' evaluation of structures adjacent to the metal implants.
2. Clinicians can minimize metal artifacts using standard scanner parameters.
3. Emerging techniques show great promise to further reduce metal artifacts in MRI.

LL-PHE-SU9B • Changes in Tumor Shadows and Microcalcifications on Mammography in Elderly Patients with Stage I/II Breast Cancer Following KORTUC II, a New Radiosensitization Treatment
Akira Tsuzuki MS (Presenter); Yasuhiro Ogawa MD, PhD; Akihito Nishioka MD, PhD; Kei Kubota MD, PhD; Shin Yaogawa RT; Kenji Itoh RT; Youko Yamada RT; Toshikazu Sasaki; Norikazu Yokota RT; Shiho Tokuhira MS; Ryo Akima MS, RT; Naoya Hayashi MS, RT

AAPM/RSNA Basic Physics Lecture for the Radiologic Technologist: Digital Imaging Exposure Indicators-Implications for Image Quality and Dose

Monday, 01:30 PM - 02:45 PM • S102D

[Back to Top](#)

QA PH

SPPH21 • AMA PRA Category 1 Credit™:1.25 • ARRT Category A+ Credit:1.5

Moderator

Douglas E Pfeiffer, MS *

Eric L Gingold, PhD

Charles E Willis, PhD

LEARNING OBJECTIVES

1) Understand why exposure indicators are necessary for computed radiography and digital radiography. 2) Provide examples of how exposure indicators can be used for quality control of an imaging operation. 3) Explain the relationship between the amount of radiation used to perform the examination, the radiation dose to the patient, and the quality of the resulting image. 4) Discuss the importance of establishing and managing target values. 5) Appreciate the practical limitations of exposure indicators.

ABSTRACT

URL

Physics Symposium: Uncertainties in Radiation Therapy 2

Monday, 01:30 PM - 05:45 PM • S102C

[Back to Top](#)

QA PH RO

SPPH22 • AMA PRA Category 1 Credit™:4 • ARRT Category A+ Credit:4.5

LEARNING OBJECTIVES

1) Describe the limitations of traditional QA/QM programs in radiation oncology. 2) Understand the rationale for establishing risk-based QA/QM programs in radiation oncology. 3) Learn how to apply FMEA methodology in radiation oncology.

SPPH22A • New Paradigms of QA/QM

Jatinder R Palta PhD (Presenter)

LEARNING OBJECTIVES

View learning objectives under main course title.

ABSTRACT

The increasing complexity, functionality, and site-to-site variability of modern radiation therapy planning and delivery techniques challenge the traditional prescriptive quality assurance/quality management (QA/QM) programs that ensure safety and reliability of treatment planning and delivery systems under all clinical scenarios. The manufacturing industry has historically relied on extensive testing and use of techniques such as probabilistic reliability modeling for developing and maintaining new products. Among the most widely used method of risk analyses are Failure Modes and Effects Analysis (FMEA). This is a methodology for analyzing potential reliability problems early in the development cycle where it is easier to take actions to overcome these issues, thereby enhancing reliability through design. FMEA is used to identify potential failure modes, determine their effect on the operation of the product, and identify actions to mitigate the failures. From a manufacturer's perspective, FMEA is a valuable method to systematically evaluate a device design's potential for inducing use errors. User errors are defined as a pattern of predictable human errors that can be attributable to inadequate or improper design. When these risk analyses are done early in the development cycle, potential faults and their resulting hazards are identifiable and much easier to mitigate with error-reducing designs. These risk management methods are excellent complements to other important user-centered design best practices. Risk analysis, or hazard analysis, is a structured tool for the evaluation of potential problems which could be encountered in connection the use of a device. The early and consistent use of FMEAs in the design process allows the engineers to design out failures and produce reliable and safe products. FMEAs also capture historical information for use in future product improvement. Such an approach should result in a QA/QM program in Radiation Oncology that has

URL

SPPH22B • QA/QM of the Reference Dosimetry

Larry A DeWerd PhD (Presenter) *

LEARNING OBJECTIVES

View learning objectives under main course title.

SPPH22C • QA/QM of the Treatment Planning Process

Jeffrey V Siebers PhD (Presenter) *

LEARNING OBJECTIVES

View learning objectives under main course title.

SPPH22D • QA/QM of the Treatment Delivery Process

Thomas R Mackie PhD (Presenter) *

LEARNING OBJECTIVES

View learning objectives under main course title.

SPPH22E • QA/QM of the Treatment Guidance Process

Lei Dong PhD (Presenter) *

LEARNING OBJECTIVES

View learning objectives under main course title.



SSE22 • AMA PRA Category 1 Credit™:1 • ARRT Category A+ Credit:1

Moderator
Hiroyuki Yoshida, PhD *
Moderator
Hiroshi Fujita, PhD

SSE22-01 • Digital Breast Tomosynthesis (DBT): Computerized Detection of Clustered Microcalcifications in Planar Projection from Multiscale Bilateral Regularized Simultaneous Algebraic Reconstruction

Ravi K Samala PhD (Presenter) ; **Heang-Ping Chan** PhD ; **Yao Lu** PhD ; **Lubomir M Hadjiiski** PhD ; **Jun Wei** PhD ; **Mark A Helvie** MD *

PURPOSE

To develop computer-aided detection (CADe) methods for microcalcification clusters (MCs) in DBT.

METHOD AND MATERIALS

With IRB approval and informed consent, DBTs were acquired from human subjects using a GE prototype DBT system. The data set was divided into a training set (127 views from 64 breasts with MCs) and an independent test set (104 views from 52 breasts with MCs and 76 views from 38 breasts without MCs). The biopsy-proven cluster location was marked by an MQSA radiologist. DBT volume is reconstructed using our recently developed simultaneous algebraic reconstruction technique (SART) with multiscale bilateral regularization that reduces noise, enhances MCs, and preserves the sharpness of tissue structures. A planar projection (PPJ) image is generated by selectively extracting the high-frequency information including potential MCs from the 3D volume and projecting it to a plane. Cluster centroid objects and individual seed points are then detected from the PPJ image using iterative adaptive thresholding in combination with segmentation guided by the local contrast-to-noise ratio (CNR). The cluster centroid objects are further screened using a neural network trained for recognizing true signals and false positives (FPs). Dynamic clustering embedded with machine learning rules based on CNR, size and number of signals is used to detect MCs. FP clusters are further reduced using the size, skewness and kurtosis properties of the CNR histogram of the cluster. The detection on PPJ images was compared with that in the 3D volumes using jackknife free-response receiver operating characteristic (JAFROC) analysis.

RESULTS

For the test set, the FP rate decreased by 50% at 85% sensitivity for both the view-based and case-based performance (0.81 and 0.54 FPs/view, respectively) on the PPJ images compared to that in the 3D volumes (1.92 and 1.01 FPs/view). The case-based sensitivity reached 95% at 0.82 FPs/view in the PPJ images. JAFROC analysis showed a significant improvement with a figure-of-merit of 0.65 and 0.58 for PPJ and 3D, respectively (p -value=0.006).

CONCLUSION

Computerized MC detection on PPJ images outperforms that in 3D reconstructed volumes. Further study is underway to improve the PPJ method.

CLINICAL RELEVANCE/APPLICATION

CADe can be an adjunct to radiologist reading and has the potential to improve detection of subtle microcalcification clusters and increase the workflow in DBT interpretation.

SSE22-02 • Benchmarking Computer-aided Detection of Pulmonary Nodules on the Recently Completed Publicly Available LIDC/IDRI Database

Colin Jacobs MSc * ; **Bram Van Ginneken** PhD (Presenter) ; **Stephan Fromme** * ; **Mathias Prokop** MD, PhD * ; **Eva M Van Rikxoort** PhD

PURPOSE

The recently completed LIDC/IDRI database provides by far the largest public resource to assess the performance of algorithms for the detection of pulmonary nodules in thoracic CT scans. We report the performance of two detection systems, and address the issue of completeness of the reference standard.

METHOD AND MATERIALS

The LIDC/IDRI database contains 890 thoracic CT scans with section thickness of 2.5mm or lower, one per patient, from 7 centers acquired with 17 different scanner models from 4 manufacturers. Cases have been annotated in an extensive reading process comprising a blinded and an unblinded review by four radiologists who indicated all nodules 3mm effective diameter. We define nodules >3mm indicated by all four observers as positive findings. We applied two pulmonary nodule detection systems: Herakles, an industry research prototype (MeVis Medical Solutions, Bremen, Germany) and ISICAD (Image Sciences Institute, Utrecht, The Netherlands), a system trained with data from the Dutch-Belgian NELSON lung cancer screening trial. We report sensitivity at 1, 2, and 4 false positive (FP) detections per scan and analyze the FPs.

RESULTS

The 890 scans contained 775 positive findings. At 1, 2, and 4 FP/scan, Herakles had a sensitivity of 69%, 75%, and 79%, respectively. For ISICAD this was 51%, 63%, 72%. We analyzed the FPs of Herakles at an operating point of 2 FP/scan. Of these, 31% were annotated by at least one radiologist as a nodule >3mm. An additional 17% were indicated by at least one radiologist as a nodule

CONCLUSION

The LIDC/IDRI data set is an excellent benchmarking tool for nodule detection algorithms. Automated detection can identify pulmonary nodules that have not been annotated in an extensive reading process with blinded and unblinded review by four human observers.

CLINICAL RELEVANCE/APPLICATION

Algorithms for automatic detection of pulmonary nodules can be compared and improved through the availability of a common database for benchmarking.

SSE22-03 • Independent Combination of Multiple Readers for the Detection of Lung Nodules in Chest Radiographs: Setting a Benchmark for Computer-aided Detection

Steven Schalekamp MD (Presenter) * ; **Nico Karssemeijer** PhD * ; **Cornelia M Schaefer-Prokop** MD * ; **Bram Van Ginneken** PhD

PURPOSE

The detection performance for lung nodules in chest radiography shows a large interreader variability. High miss rates of lung cancer have been reported though judged as being visible in retrospect. History has proven that computer intelligence is able to surpass human performance also for complex tasks (e.g., Watson). Purpose of our study was to explore the potential gain in performance by independent combination of multiple observers. That way we aimed to define the upper boundary of visual detectability that ideally should be achieved by a computer aided detection (CAD) system.

METHOD AND MATERIALS

111 digital chest radiographs (CXR) containing a single small nodule (average diameter 16mm.) and 189 normal controls served as study

group. Nodules had to be visible on the frontal radiograph with 42% of them judged as being of low and very low conspicuity. Twelve observers were asked to localize the lung nodules in the CXRs with help of bone suppressed images. Location based ROC was used for analysis. Mean sensitivity in a false positive fraction range between 0 and 0.2 was used to measure nodule localization performance. This was done for all observers separately and subsequently for the combination of multiple observers (up to 12). Observer findings were averaged when findings were located within 1.5 cm of each other. When no finding was present at the location of another observers finding a zero-score was assigned in the averaging calculation.

RESULTS

The mean sensitivity at a false positive fraction range between 0 and 0.2 was 64.0% for single reading (range 45.5% - 78.2%). Combining the readings of two observers improved lung nodule detection on average to a mean sensitivity of 73.1%. Adding more observers lead to a further performance increase up to a mean sensitivity for 12 observers of 82.3%. On average, 26 nodules were missed by single observers, 15 nodules by a combination of 2 observers, and only 5 nodules were missed when combining 12 observers.

CONCLUSION

The variable and partially low baseline performance underlines the limitation of the single observer. If CAD is able to reach the combined performance of multiple readers, a dramatic increase of nodule localization performance can be expected with drastic reduction of missed rates.

CLINICAL RELEVANCE/APPLICATION

An independent combination of multiple readers for the detection of lung nodules in chest radiographs should be used as measure for achievable CAD performance.

SSE22-04 • Computer-aided Detection of Epidural Masses in Computed Tomography Using a Constrained Gaussian Mixture Model

Sanket Pattanaik BS ; **Jiamin Liu** PhD ; **Jianhua Yao** PhD * ; **Weidong Zhang** PhD ; **Evrin B Turkbey** MD ; **Ronald M Summers** MD, PhD (Presenter) *

PURPOSE

Although epidural masses detection is often accomplished using MRI, the more routine use of CT imaging makes early detection in this modality advantageous. Our preliminary Computer-Aided Detection (CAD) framework addresses the dearth of work focusing explicitly on the detection of epidural masses. We supply a spatially-constrained Gaussian Mixture Model (CGMM), using tissue classes informed by the spinal canal composition, to localize candidate detections and reduce false positives.

METHOD AND MATERIALS

40 patients with chest-abdomen-pelvis CT scans were examined. 23 patients were selected with MRI reports confirming an epidural mass. 17 patients without epidural masses were randomly selected to serve as controls. Two radiologists manually demarcated the centroids of each epidural mass identified in the CT scans to serve as ground truth. The CAD system segments the whole spine using a watershed algorithm and directed graph search. It isolates the spinal canal using a four-part vertebra medial model, boundary dilation, and intensity thresholding. Four tissue classes were generated using K-means clustering to represent normal intradural tissue, fat/vasculature, the epidural mass, and a partial volume region between the bone and soft tissue. CGMM was employed to refine classification, taking advantage of both spatial and intensity parameters. Detections were limited to masses extending from the canal boundary. These detections were then submitted for feature extraction and support vector machine classification (SVM).

RESULTS

Before classification with SVM, our CAD system detected 44 out of 47 detections. Missed detections resulted from undersegmentation of the canal in the L5-S1 regions. A sensitivity of 80% with 7.2 false positives per patient was attained following classification and ten-fold cross-validation, which compared favorably with the sensitivity of 76% with 7.4 false positives per patient attained by restricting CAD to intensity based K-Means clustering.

CONCLUSION

Our CAD system lays the groundwork for detection of epidural masses in CT scans and points to the importance of using a combination of spatial and intensity based parameters to localize masses in the canal.

CLINICAL RELEVANCE/APPLICATION

Epidural masses in the spinal canal can cause pain or paralysis and can indicate metastasis. Alerting radiologists of the presence of these masses in CT can speed response to underlying pathologies.

SSE22-05 • A Fully Automatic Registration Algorithm for Multiparametric Prostate MRI

Valentina Giannini (Presenter) ; **Anna Vignati** ; **Simone Mazzetti** ; **Filippo Russo** MD ; **Christian Bracco** PhD * ; **Michele Stasi** ; **Daniele Regge** MD

PURPOSE

Multiparametric (mp) MRI has been proposed as a potential alternative screening method for prostate cancer (PCa) diagnosis. One of the most challenging problems is to correctly align different types of images so that features coming from different sequences can be extracted from the same group of pixels. The aim of this study is to present a fully automatic registration system capable of correcting for movements generated during the dynamic acquisition (DCE) and for DW image distortion.

METHOD AND MATERIALS

The dataset includes 21 men with histologically proven PCa (age 65 [7], mean[SD]) that underwent endorectal 1.5T MRI with the following scanning protocol: axial T2-w, DW imaging (b-values 0,600, 1000 and 1400 s/mm²) and a 13-s time resolution DCE sequence. All patients underwent radical prostatectomy within 3 months from MRI. A radiologist manually outlined regions of interest on the T2-w images in areas corresponding to the tumoral foci at histology and in a non-tumoural region located in the contralateral peripheral zone (PZ).

First a multi-resolution rigid registration algorithm, based on the mutual information similarity measurement, corrected misalignment between T2-w and DCE images. Afterward, a linear deformation field decaying along the vertical axis was applied on the DW images. Pharmacokinetics and ADC parameters coming from registered and non-registered images were fed into a Bayes classifier, and the area under the receiver operating characteristic curve (AUC) was computed before and after registration. The one-tailed paired t-test was used to evaluate differences between AUC, sensitivity e specificity obtained by the classifier before and after registration.

RESULTS

With registration AUC and sensitivity increased from 0.59(0.15) (mean [SD]) to 0.88(0.11) (p

CONCLUSION

This study demonstrated the feasibility of a fully automatic registration framework on a MRI prostate CAD system. The proposed method seeks to have all the MRI dataset registered to the T2-w image, thus allowing a more reliable multiparametric analysis.

CLINICAL RELEVANCE/APPLICATION

An automatic registration algorithm, integrated in a CAD for PCa, can reduce observer variability and reading time, and can be used to guide targeted prostate biopsy directly on the suspected region.

SSE22-06 • Computer-aided Detection of Prostate Cancer Based on Automatic Multi-parametric Magnetic Resonance Image Analysis

Simone Mazzetti (Presenter) ; **Valentina Giannini** ; **Anna Vignati** ; **Filippo Russo** MD ; **Michele Stasi** ; **Daniele Regge** MD

CONCLUSION

The application of a CAD system based on mp-MRI information that automatically highlight cancer suspicious regions will improve the diagnostic accuracy of the radiologist, reducing reader variability and speeding up the reading time.

Background

Prostate cancer (PCa) is the most common malignancy affecting men in the world and represents the third cause of cancer death in industrialized countries. Diagnosing PCa using multi-parametric (mp) magnetic resonance imaging (MRI) is increasingly being used in the diagnostic pathway, also in combination with computer-aided diagnosis (CAD) systems, in order to automatically detect and localize the disease.

Aim of this study is to present a CAD system based on T2-w imaging, diffusion (DW) and dynamic contrast-enhanced (DCE) acquisitions to produce a pixel-wise malignancy probability map of the prostate gland.

Evaluation

The dataset included 20 men, with PSA > 4 ng/ml and confirmed PCa by transrectal ultrasonography guided biopsy. Patients underwent MRI at 1.5T using an endorectal coil and radical prostatectomy within 3 months of imaging. The pathologist contoured foci of cancer on prostate sections, to create the standard of reference. Then a radiologist compared imaging with histopathology and reported both malignant and benign regions of interest (ROI) on the T2-w images.

The first step for the CAD system was the registration between T2-w, DW and DCE-MRI. Then each pixel belonging a ROI was represented as a vector containing values of T2-w signal intensity, of the apparent diffusion coefficient and of quantitative physiological parameters (e.g. k_{ep} , k^{trans}) from DCE. Selected features were fed into a support vector machine classifier in order to provide a classification that maximized the detection of true positives, minimizing the false positive cases.

The area under the ROC curve for the classifier was equal to 0.93, sensitivity 0.84 and specificity 0.85.

Discussion

The CAD performed automatic mp-MRI analysis, supported by a preliminary registration step between the three MRI datasets. The results are objective and reproducible, providing a unique information for clinicians summarized in a malignancy probability map.

Physics (Image Reconstruction)

Monday, 03:00 PM - 04:00 PM • S403B



[Back to Top](#)

SSE23 • AMA PRA Category 1 Credit™:1 • ARRT Category A+ Credit:1

Moderator

Xiangyang Tang, PhD *

Moderator

Stanislav Zabic, PhD *

SSE23-01 • Design and Evaluation of an Interactive MPR Viewer for Real-time Filtering of Large High-resolution Breast CT Data

Ronny Hendrych * ; Marcel Beister (Presenter) * ; Willi A Kalender PhD *

PURPOSE

In clinical breast CT it is of interest to calculate low-noise CT volumes for soft-tissue lesion (STL) detection from noisy high-resolution (HR) images for micro-calcification diagnosis to avoid multiple reconstructions. A viewer for multi planar reformatting (MPR) was developed and evaluated to offer a continuous adjustment of spatial resolution, to reduce the time necessary for the diagnostic procedure and to improve the workflow.

METHOD AND MATERIALS

Simulations of mathematical breast phantoms were performed (ImpactSim, CT Imaging GmbH, Erlangen, Germany) with average glandular dose levels varied from 1.5 up to 6 mGy. Furthermore, a breast CT prototype (CT Imaging GmbH, Erlangen, Germany) was used to scan an ACR Phantom (CIRS, Norfolk, VA, USA). Volumetric images were reconstructed in HR mode and subsequently 3D filtered using the following techniques: Gaussian, median and box filters and an iterative impulse detector using a weighted median filter. The visibility of lesions was assessed by calculating the effective contrast-to-noise ratio (CNR_{eff}), combining the usual CNR with the diameter of the lesion in question.

RESULTS

The MPR viewer allowed for continuous interactive real-time filtering of large HR volumes in an interactive fashion. In the simulated breast CT volumes the applied filters improved the CNR_{eff} for lesions of 2 mm from 1.4 unfiltered in the HR volumes up to 39.2, 23.7, 40.5 and 8.5 for box filter, median, Gaussian and impulse detector. For the ACR phantom the Gaussian filter achieved the best results with an increased CNR_{eff} from 7.6 to 51.4 for the smallest lesion. Thereby all filters help to surpass the Rose criterion which states that values of 5 or higher are necessary to distinguish objects from the surrounding area.

CONCLUSION

The MPR viewer eliminates the need for multiple reconstructions in breast CT. It allows adjusting interactively the spatial resolution and thereby changing the effective CNR continuously.

CLINICAL RELEVANCE/APPLICATION

MPR viewers may help to avoid multiple image reconstructions, increase the effective CNR of lesions and improve the workflow for breast CT exams.

SSE23-02 • Evaluation of Sinogram Affirmed Iterative Reconstruction Using the XCAT Phantom in a Model Observer Study

Fatma Elzahraa A Elshahaby (Presenter) ; Benjamin Tsui PhD * ; Matthew K Fuld PhD * ; Pamela T Johnson MD * ; Elliot K Fishman MD * ; Jingyan Xu PhD

PURPOSE

The study was designed to compare the performance of Siemens♦ Sinogram Affirmed Iterative Reconstruction (SAFIRE) and the Weighted Filtered BackProjection (WFBP) reconstruction methods using realistically simulated CT images from the 3D Extended Cardiac-Torso (XCAT) phantom and the Channelized Hotelling Observer (CHO) in a lesion detection study.

METHOD AND MATERIALS

Five simulated spheres (dia.=5mm, attenuation ratio of sphere:background= 1%) were placed at 5 locations in the liver of the XCAT phantom. Noisy CT projection data, 50 sets of lesion-present and 50 lesion-absent, at 11.5 mAs/rotation were generated using the DRASIM/XCAT simulation software. They were reconstructed on a Siemens Definition Flash scanner using WFBP with kernels B31F, B41F, B50F, B70F, and SAFIRE at strengths 1, 3, 5, and each with kernels I31F, I41F, I50F, I70F. A total of 250 lesion-present and 250 lesion-absent images were generated for each reconstruction + kernel combination. The central 64x64 pixels centered on the lesion was extracted and processed using 5 octave-wide rotationally symmetric frequency channels. 125 CT images were used for CHO training and 125 images for CHO testing. The receiver operating characteristic (ROC) curve and the area under the curve (AUC) from each reconstruction + kernel combination, and the statistical significance of the AUC difference were analyzed by LABROC4 and CLABROC programs.

RESULTS

The mean AUC did not change much for different kernels of WFBP, but it varied for SAFIRE especially at strengths 3 and 5. Using the sharp kernel I70F, the AUC decreased as the images became noisier which reduced the lesion detectability. For this detection task, the

kernels giving the highest AUCs were B50F for WFBP and I41F for SAFIRE. At these kernels, SAFIRE-3 outperformed WFBP and SAFIRE-1 and the AUC differences were statistically significant. The AUC difference between SAFIRE-3 and SAFIRE-5 was statistically insignificant indicating similar performance in lesion detection.

CONCLUSION

By appropriate choices of the filter strength and kernels, SAFIRE outperformed the WFBP method in a lesion detection task using realistically simulated CT images. The results remain to be confirmed using clinical data.

CLINICAL RELEVANCE/APPLICATION

The advanced Sinogram Affirmed Iterative CT reconstruction (SAFIRE) method has the potential to improve lesion detectability in the clinical setting.

SSE23-03 • Quantitative Assessment of Metal Artifact Reduction in C-arm Cone-beam CT Guidance of Neurovascular Interventions

Carolina Cay (Presenter) ; **Marta Wells** ; **Adam S Wang** PhD * ; **Jeffrey H Siewerdsen** PhD * ; **Tina Ehtiati** PhD * ; **Christopher Rohkohl** * ; **Bernhard G Scholz** MD * ; **Martin G Radvany** MD *

PURPOSE

To evaluate the performance of a metal artifact reduction (MAR) algorithm in C-arm cone-beam CT guidance of neurovascular interventions.

METHOD AND MATERIALS

Preclinical studies were conducted using a robotic C-arm (Artis Zeego; Siemens AG) for 3D imaging and MAR prototype developed by the manufacturer. The MAR algorithm involves semi-automatic segmentation of metal components, sinogram correction, and 3D image reconstruction. A head phantom was developed involving a natural skull in tissue-equivalent plastic and the intracranial space filled with brain-equivalent gelatin. Plastics representing low-contrast brain, vessels, and CSF were incorporated along with a 3D prototype vascular tree and aneurysm (~9 mm diameter). Metal components were successively introduced: steel, titanium, and tungsten spheres (3.2, 6.4, and 12.8 mm diameter); an intravascular stent (Enterprise; DePuy); and coils (Deltamax; DePuy) the last two with and without iodine contrast in the vascular tree. 3D images were reconstructed with and without MAR, and artifact magnitude was quantified in terms of the voxel value standard deviation from streaks in a region about the metal component.

RESULTS

The MAR algorithm demonstrated strong reduction in artifact in each scenario and restored image quality to a level sufficient for visualization of the metal component and surrounding structures. Artifact magnitude without and with MAR was, respectively: 427 vs 35 HU (3.2 mm steel); 506 vs 44 HU (6.4 mm steel); 384 vs 49 HU (12.8 mm steel); 451 vs 35 HU (coil only); and 455 vs 50 HU (stent + coil). Similar improvement (~8 to 13x reduction in artifact magnitude) was evident in Ti and W spheres (3.2 to 12.8 mm). Even under the most severe scenario examined, MAR restored visualization of the component and did not visibly degrade the fidelity of surrounding structures.

CONCLUSION

The MAR algorithm provided excellent reduction of artifact magnitude even under challenging scenarios of large and multiple metal components. This quantitative performance assessment indicates that the method warrants investigation in clinical studies. Ongoing work includes streamlining the semi-automatic segmentation step and analysis of tolerance to MAR parameters.

CLINICAL RELEVANCE/APPLICATION

3D imaging in neurovascular intervention is challenged by artifacts arising from stents, coils, and clips. The MAR algorithm diminishes such artifacts for improved guidance and verification.

SSE23-04 • Diagnostic Performance Assessment of an Iterative Reconstruction Algorithm Using a Model Observer: Correlation with Human Observers for a Low Contrast Detection Task with Unknown Lesion Locations

Shuai Leng PhD (Presenter) ; **Lifeng Yu** PhD ; **Yi Zhang** ; **Michael R Bruesewitz** ; **Thomas J Vrieze** RT ; **Cynthia H McCollough** PhD *

PURPOSE

To investigate the ability of a Channelized Hotelling Observer (CHO) to predict human observer performance for the task of low contrast lesion detection for unknown lesion locations, where CT images were reconstructed using an iterative reconstruction (IR) algorithm.

METHOD AND MATERIALS

Two cylindrical rods (3 mm and 5 mm diameters) were placed in a 35 x 26 cm torso-shaped water phantom to simulate lesions with -15HU contrast at 120 kV. The phantom was scanned 100 times on a 128-slice CT scanner at each of 4 dose levels (CTDIvol = 22.8, 17.1, 11.4, and 5.7 mGy). Images were reconstructed with the system's IR algorithm (SAFIRE, Siemens). A total of 100 signal-present images were generated by placing regions of interest (ROIs) around each lesion and 50 background images were generated from images without lesions, with each ROI containing 128x128 pixels. The location of the lesion (rod) in each ROI was randomly distributed by moving ROIs around each lesion. Three trained observers identified the presence or absence of lesions, indicated the lesion location in each image, and scored their confidence for the detection/localization task on a 6-point scale, from which localization ROC (LROC) curves were generated. The same images were analyzed using a CHO with Gabor channels. Internal noise was added to the decision variables for the model observer study. Area under the LROC curve (AUC) was calculated using a non-parametric approach for both human and model observers. The correlation between the performance of human observers and the CHO model observer was calculated.

RESULTS

The performance of human and model observers was highly correlated at all dose levels for both lesion sizes, with Pearson product-moment correlation coefficients of 0.994 and 0.994 for 3mm and 5mm diameter lesions, respectively.

CONCLUSION

The performance of CHO with Gabor channels was highly correlated with human observer performance for the detection and localization of low contrast lesions with uncertain locations in CT images reconstructed with the SAFIRE IR algorithm.

CLINICAL RELEVANCE/APPLICATION

The ability of a CHO to objectively assess the performance of iterative reconstruction algorithms for detection tasks may provide an efficient mechanism for optimizing CT image quality and dose.

SSE23-05 • Do We Need to Model the Ray Profile in Iterative Clinical CT Image Reconstruction?

Christian Hofmann (Presenter) ; **Michael Knaup** PhD ; **Marc Kachelriess** PhD

PURPOSE

To find out whether clinical CT images benefit from modeling the geometric properties of each x-ray.

METHOD AND MATERIALS

Iterative image reconstruction promises to reduce image noise (and thereby patient dose), to reduce artifacts, or to improve spatial resolution. Among vendors and researchers, however, there is no consensus of how to best achieve these aims. We here focus on the aspect of geometric ray profile modeling (RM) which is realized by some algorithms while others model the ray as a straight line. To independently analyze whether RM is of advantage we implemented several iterative reconstruction algorithms without RM (SART, OSC, OSEM) and with RM (SART-RM, OSC-RM, OSEM-RM). In all cases noise was matched to be able to focus on comparing spatial resolution. A thorax phantom with additional bar and circular resolution patterns was simulated using the geometry of a typical clinical CT system

(0.6 mm detector element size at isocenter, 1024 projections per rotation). The size of the focal spot ranges from realistic 0.5 mm to unrealistic 5.0 mm. To quantify image quality we analyze line profiles through the resolution patterns to define a contrast factor (CF) for contrast-resolution plots, and we compare the normalized cross-correlation (NCC) with the ground truth for the circular resolution patterns.

RESULTS

For the unrealistic case of 5.0 mm focal spot the CF can be improved by a factor of 2 due to RM: the 4.2 lp/cm bar pattern, which is the first bar pattern that cannot be resolved without RM, can be easily resolved with RM. For the realistic case of a 0.5 mm focus all results show approximately the same CF. The NCC shows no significant differences between with and without RM when the source width is smaller than 2.0 mm (as in clinical CT). From 2.0 mm to 5.0 mm improvements can be observed with RM, increasing with increasing focus size.

CONCLUSION

Geometric RM in iterative reconstruction helps to improve spatial resolution if the ray cross-section is much larger than the ray sampling distance. In clinical CT, however, the ray is not much thicker than the distance between neighboring ray centers. Therefore RM appears not to be necessary in clinical CT.

CLINICAL RELEVANCE/APPLICATION

Geometric RM is of high computational cost. Clinical CT will benefit if the focus of iterative reconstruction is noise, dose and artifact reduction rather than resolution improvement.

SSE23-06 • A Novel Iterative-reconstruction Algorithm for Metal Artifact Reduction: Comparison with Filtered Back Projection and Linear-interpolation

Siva P Ramam MD (Presenter) ; Pamela T Johnson MD * ; Matthew K Fuld PhD * ; Elliot K Fishman MD *

PURPOSE

Iterative reconstruction algorithms offer a new option for the reconstruction of images with decreased metal-related artifacts. The goal of this study is to quantitatively and qualitatively compare CT scans performed in patients with metallic hardware when reconstructed with three different reconstruction algorithms: (1) Traditional weighted filtered back-projection (WFBP), (2) a novel iterative reconstruction algorithm (IR-MAR) designed for metal artifact reduction (Siemens, Germany), and (3) a linear interpolation metal artifact reduction algorithm (LI-MAR).

METHOD AND MATERIALS

20 different consecutive pelvic CT scans in patients with unilateral or bilateral metallic hip arthroplasties were identified. These data sets were reconstructed in the axial plane using the three different reconstruction algorithms (WFBP, IR-MAR, and LI-MAR). An abdominal radiologist with 2 years of experience evaluated the images (on a scale of 1-10) with regards to image quality, providing separate scores for the overall image and individual appearances of the bladder, prostate/uterus, and pelvic side walls. ROI analysis was performed of the bladder lumen and subcutaneous fat (ipsilateral to hardware) with mean Hounsfield attenuation values and standard deviation (as a surrogate for noise) recorded.

RESULTS

Subjective quality ratings for the overall image (p

CONCLUSION

A novel metal artifact reduction algorithm based on iterative reconstruction offers significant improvements in subjective image quality compared to both traditional filtered back projection and older linear interpolation algorithms. Moreover, quantitative decreases in image noise are at least equivalent to linear interpolation MAR algorithms.

CLINICAL RELEVANCE/APPLICATION

A novel iterative reconstruction algorithm (IR-MAR) offers considerable qualitative and quantitative advantages over older reconstruction techniques when dealing with metal artifacts on CT.

Physics (Image-guided Radiation Therapy I)

Monday, 03:00 PM - 04:00 PM • S404AB

PH RO

[Back to Top](#)

SSE24 • AMA PRA Category 1 Credit™:1 • ARRT Category A+ Credit:1

Moderator

David A Jaffray, PhD *

Moderator

Sandy Napel, PhD *

SSE24-01 • PET Image-guided Dose Escalation Study for Cervical Cancer Patients Receiving HDR Brachytherapy

James W Anderson PhD (Presenter) ; Krystyna D Kiel MD ; Yixiang Liao ; Rui Yao PhD ; Damian Bernard PhD ; Julius Turian ; James C Chu PhD *

PURPOSE

To study the feasibility and benefit of boosting dose to active regions of cervical cancer identified by positron emission tomography (PET) imaging during brachytherapy.

METHOD AND MATERIALS

5 patients imaged with both MRI and PET/CT were retrospectively studied. An experienced physician contoured the GTV and HR-CTV using the MRI scan alone, and then contoured the region of PET-hot activity using a PET/CT image. The MRI and PET/CT images were then fused, and a PET-HR-CTV volume was constructed from the union of the HR-CTV and PET-GTV.

Each patient had been treated using a Syed or TandR applicator with 4-20 interstitial needles. Two new plans were optimized using Oncentra's IPSA package with the following objectives: 1) a plan using only the MRI contours in which the HR-CTV-D90 received the prescription dose (Rx), and 2) a plan where the HR-CTV D90 received Rx and the PET-GTV D90 was boosted to 1.5Rx. In both cases the EQD2 D2cc dose to the bladder and rectum were kept below the GEC-ESTRO guidelines of 90 and 75 Gy, including the contribution from external beam therapy. Dose-volume parameters calculated for the all volumes.

RESULTS

Significant differences were seen between the MRI-GTV and PET-GTV contours (average size difference 21.8cc, average overlap 50%, see Figure 2). The PET-GTV boost to 150% was possible in four out of five cases, with the last case reaching 127% before reaching the rectal D2cc limit (Table 1). In 3 of the test cases, the PET-GTV also received about 150% of the Rx dose in the MRI-only plans the two other cases were those in which the PET-GTV volume extended the most outside of the HR-CTV.

CONCLUSION

PET imaging modality has the potential to identify residual cervical cancer otherwise not visible on MRI and CT studies. This work has found that MRI target contouring regularly does not include regions of PET activity, and PET-based planning can lead to improved coverage over plans using MRI alone without sacrificing OAR sparing.

CLINICAL RELEVANCE/APPLICATION

SSE24-02 • An Evolutionary Algorithm for the Optimization of Parameters in Radiation Beam Profile Modeling for the CyberKnife X-band Linear Accelerator

Matthew R Witten PhD (Presenter) ; **Owen Clancey** PhD

ABSTRACT

Purpose/Objective(s): To optimize parameters for the modeling of the beam profile of the CyberKnife X-band linear accelerator, and to investigate the dependencies of the parameters on depth and collimator size.

Materials/Methods: The measured data for the CyberKnife linear accelerator were acquired using the M3000-RS scanning system (Advanced Radiation Measurements, Inc., Port Saint Lucie, FL) and two 60012 p-type stereotactic dosimetry diodes (PTW, Inc., Freiburg, DE). The scanning system was used to precisely and accurately position the diodes to acquire both depth-dose data (the variation in radiation dose as the beam penetrates the surface of the water and interacts deeper and deeper in it), as well as beam profile data (the variation in dose in the plane perpendicular to the direction of travel of the beam). The beam profile shape is a consequence of the circular collimators, which range in diameter from 5 mm to 60 mm. The dose is at the maximum at the central axis of the beam. The dose is then relatively constant until the beam meets the physical edge of the collimator. Near the edge, the dose precipitously decreases, from nearly 100% of the maximum just inside the field, through 50% at the field edge, and finally to approximately 1-3% far from the field edge, where the dose is primarily attributable to scatter, as there is no primary irradiation outside the collimator. Accurately modeling the penumbra can be difficult, as the shape of the curve used to model the penumbra needs to be finely tuned to reflect the reality of the physical decrease in dose. The model used to calculate the beam profile assumed that there were three Gaussian scattering kernels which contributed to the dose, and the convolution of the kernels in the dose calculation formalism produced an analytical form of the off-center ratio involving the sum of error functions. Associated with each scattering kernel is an amplitude and standard deviation. The amplitudes and standard deviations associated with the scatter kernels were optimized with an evolutionary algorithm, where each individual was represented by a sextuple of real numbers. No a priori assumptions were made regarding the functional dependence of the scatter kernel amplitudes and standard deviations upon these variables.

Results: The optimization was able to produce an acceptable agreement, to within 2%, with measurement for the off-center ratio (OCR) values for full range of collimator sizes and at all depths (15 mm, 50 mm, 100 mm, 200 mm, 300 mm). There were depth- and collimator size-dependencies of the scatter kernel amplitudes, and the standard deviations possessed a dependence upon depth.

Conclusions: An evolutionary algorithm can be successfully used to optimize scatter kernel parameters in the modeling of the beam profile of the CyberKnife x-band linear accelerator.

SSE24-03 • Volumetric Modulated Arc Therapy for Intracranial Stereotactic Radiosurgery with Multiple Lesions: Image Guidance and Dosimetric Analysis

Zhiheng Wang (Presenter)

SSE24-04 • Effect of a Low-strength Magnetic Field on Ionization Chamber Reference Dosimetry

Eric Pepin PhD (Presenter) ; **Olga Green** PhD *

PURPOSE

To evaluate the impact of a 0.32-Tesla magnetic field present in the first commercial MRI-IGRT system on various ionization chamber dosimetry correction factors and to discover any directional dependence thereon.

METHOD AND MATERIALS

Various ionization chambers were evaluated to determine polarity, ion recombination, and stem effect correction factors using a Cobalt-60 MRI-IGRT system. Correction factors were determined using techniques outlined in the AAPM Task Group 51 report and various other publications. Correction factors were determined as a function of ion chamber orientation in the magnetic field and compared to readings taken on a linear accelerator in the absence of a magnetic field.

RESULTS

The various ionization chambers with a central anode were within prescribed tolerance limits for P_{pol} and P_{ion} in the presence of a magnetic field. Parallel plate ionization chambers exceeded tolerance limits for P_{pol} , but were within tolerance for P_{ion} in the presence of a magnetic field. There are no established tolerance limits for a stem correction factor, but several ionization chamber of both design types showed significantly different stem correction factors in the presence of a magnetic field compared to when not in a magnetic field. All ionization chambers showed a directional dependency in the stem correction factor in the presence of a magnetic field.

CONCLUSION

The ability of central anode ionization chambers to satisfy TG-51 correction factor tolerance limits seems uninhibited by the presence of a magnetic field, however parallel plate chambers were strongly affected by the presence of a magnetic field. Chambers of all design types may require bi-directional commissioning due to variations in the stem correction factor when in the presence of a magnetic field.

CLINICAL RELEVANCE/APPLICATION

Certain designs of ionization chambers seem unaffected by a magnetic field and are suitable for use with the first MRI-IGRT machine.

SSE24-05 • Analysis of Predictive Maintenance of Linear Accelerator Beam Uniformity Using Statistical Process Control

Charles M Able MS (Presenter) * ; **Alan Baydush** PhD * ; **Michael T Munley** PhD *

CONCLUSION

PdM monitoring of beam uniformity using a new method for determining SPC control limits is more effective than using traditional control limits. SPC false alarms are reduced thereby eliminating unwarranted service intervention. We are working to develop code that will provide an SPC evaluation using the new formula.

Background

The focus of this study is to determine the effectiveness of revisions to statistical process control (SPC) chart limits for linear accelerator steering coil current (beam uniformity) predictive maintenance (PdM) monitoring

Evaluation

We have re-evaluated calculation of the limits for steering coil current (SCC) SPC charts based on our observations that the changes in SCC required for 1% change in measured beam uniformity will generally exceed the traditional limits calculated using the standard deviation of the subgroup values alone. Using empirical data obtained from controlled experiments varying the SCC while measuring the beam uniformity, we have developed a formulism that incorporates a scaling factor (C_m) in the calculation of control limits.

Discussion

SCC monitoring of an 18 MV photon beam using the new limits indicated a change in the transverse position coil operating current 2 weeks prior to multiple EXQ2 faults and unscheduled downtime. A change in beam uniformity of greater than 3% was found once the beam was scanned using a computerized water phantom and ion chamber. SPC charts of this steering coil using traditional limits would have resulted in 5 false positives prior to the first positive alarm indicated by the new limits

SSE24-06 • Forcing Lateral Electron Disequilibrium to Spare Lung Tissue: A Novel Technique for Stereotactic Body Radiation Therapy of Lung Cancer

Brandon Disher (Presenter) ; **George Hajdok** ; **Stewart Gaede** ; **Matthew Mulligan** ; **Jerry J Battista**

PURPOSE

Stereotactic Body Radiation Therapy (SBRT) is a treatment option for inoperable early stage lung cancer patients. SBRT uses tightly conformed megavoltage (MV) x-ray beams to ablate the tumour in only a few treatment sessions. Small MV x-ray fields may cause lateral electron disequilibrium (LED) to occur within lung tissue, which can reduce the dose to the tumour to a variable extent. These dose effects may be challenging to predict using commercially-available dose calculation algorithms. Thus, to avoid LED, previous authors suggested using low energy photons and larger fields for lung cancer patients. We propose a new form of SBRT, named LED-optimized SBRT (LED-SBRT), which utilizes RT parameters designed to exploit LED to advantage. It will be shown that LED-SBRT can be used to reduce the dose within healthy lung tissue while enabling escalation of tumour dose levels.

METHOD AND MATERIALS

The DOSXYZnrc Monte Carlo software was used to calculate dose within a typical SBRT patient. To mimic a 360° SBRT arc, 36 equally weighted fields were focused onto the small tumour (~1 cm). 6 or 18 MV x-ray energies were used to simulate different plans of various field sizes. The LED-optimized plan, 18MV(3x1cm²), was compared to a clinical standard arc using 6MV(3x3cm²) beam parameters. A planning target volume (PTV) was generated by considering the extent of tumour motion over the patient's breathing cycle. All dose results were normalized such that at least 95% of the PTV received at least 54 Gy (i.e. D95).

RESULTS

The LED-optimized plan produced a hot spot at the tumour center equal to 169Gy, which was approximately twice as large as the maximal dose found within the conventional plan. Despite escalated tumour dose levels, normal lung dose was still decreased. For example, the mean lung dose and V20 decreased by ~ 0.5 Gy and 1.1%, respectively, comparing the LED-optimized plan to the clinical standard.

CONCLUSION

This article introduces a novel SBRT technique, LED-SBRT, which exploits the LED phenomenon to reduce normal lung dose levels and permit tumour dose escalation.

CLINICAL RELEVANCE/APPLICATION

These results are significant as tumour dose escalation correlates well with tumour control (and overall survival), while lower lung dose metrics reduce the risk of lung toxicities (e.g. pneumonitis).

Medical Physics 2.0: Nuclear Imaging

Tuesday, 08:30 AM - 10:00 AM • S102D

[Back to Top](#)



RC321 • AMA PRA Category 1 Credit™:1.5 • ARRT Category A+ Credit:1.5

Co-Director

Ehsan Samei, PhD *

Co-Director

Douglas E Pfeiffer, MS *

RC321A • Nuclear Imaging Perspective

Douglas E Pfeiffer MS (Presenter) *

LEARNING OBJECTIVES

1) Understand the history and development of nuclear imaging. 2) Become introduced to the advances of hybrid imaging. 3) Understand the impact of equipment development on medical physics support.

ABSTRACT

Nuclear imaging has not received the attention or development enjoyed by other imaging modalities. Nevertheless, our understanding of nuclear imaging and development of protocols and hybrid systems has led to new requirements for testing and other medical physics support. This presentation will discuss these developments and the impact they have had on the medical physics support needed by nuclear imaging departments.

RC321B • Nuclear Imaging 1.0

Osama R Mawlawi PhD (Presenter)

LEARNING OBJECTIVES

1) Learn acceptance testing and commissioning of gamma cameras/SPECT / and PET-CT systems. 2) Describe routine quality control procedures and their frequencies. 3) Become familiar with ACR accreditation of planar, SPECT, and PET systems. 4) Learn about various potential image artifacts of gamma camera, SPECT and PET systems.

ABSTRACT

The aim of this lecture is to provide the audience with an overview of the current medical physics testing procedures that are performed on gamma cameras, SPECT and PET systems. The lecture will be divided into 3 main parts; the first part will describe the tests performed for acceptance testing of these systems while the second part will describe the routine quality control and assurance tests and their frequencies. The last part of the lecture will focus on the ACR accreditation process and the necessary phantom imaging for gamma cameras, SPECT and PET systems. Throughout the lecture, examples of potential image artifacts will be presented.

RC321C • Nuclear Imaging 2.0

Jeffrey Nelson (Presenter)

LEARNING OBJECTIVES

1) Become familiar with new physics metric and analytics in nuclear imaging. 2) Determine testing implication of emerging technologies in nuclear imaging. 3) Envision the clinical implementation of new physics metrics and analytics.

ABSTRACT

Uncertainties in Imaging for Radiation Oncology: Sources and Mitigation Techniques-Incorporation of Imaging as a Biomarker in RT

Tuesday, 08:30 AM - 10:00 AM • E261

[Back to Top](#)



RC322 • AMA PRA Category 1 Credit™:1.5 • ARRT Category A+ Credit:1.5

Co-Director, Moderator

Robert Jeraj

LEARNING OBJECTIVES

1) Anatomical imaging in treatment response (RECIST, volumetrics). 2) PET in treatment response assessment (PERCIST etc) with

uncertainties. 3) MRI in treatment response assessment. 4) Imaging biomarkers.

RC322A • Introduction to Biomarkers

Robert Jeraj (Presenter)

LEARNING OBJECTIVES

1) Imaging biomarkers and surrogate endpoints. 2) Prentice's criteria vs real world. 3) Imaging biomarker characteristics. 4) Imaging biomarker validation and qualification.

RC322B • PET Assessment/Uncertainties

Paul E Kinahan PhD (Presenter) *

LEARNING OBJECTIVES

1) Understand the advantages and disadvantages of PET/CT as a biomarker for radiation oncology. 2) Understand sources of bias and variance in PET/CT imaging, both in data acquisition and analysis. 3) Understand the limitations of functional PET/CT techniques currently being used to evaluate treatment effect.

RC322C • MRI Assessment/Uncertainties

Edward F Jackson PhD (Presenter)

LEARNING OBJECTIVES

1) Understand the physical principles of functional MR techniques currently being used to evaluate treatment effect. 2) Understand selected applications of each of these techniques to the assessment of radiation therapy. 3) Understand current limitations of each of the techniques.

URL's

web.me.com/efjackson

Minicourse: Current Topics in Medical Physics-Radiation Dose Reduction in Medical Imaging

Tuesday, 08:30 AM - 10:00 AM • S404AB



[Back to Top](#)

RC323 • AMA PRA Category 1 Credit™:1.5 • ARRT Category A+ Credit:1.5

Moderator

Mahadevappa Mahesh, MS, PhD *

ABSTRACT

This mini-course will include discussions on how to reduce radiation dose and clinical management in the areas of CT, Fluoroscopy and Radiography (CR and DR). Discussion will include dose-reducing strategies applicable due to technological advances, and also include practical steps on how to manage patient and staff safety clinically.

RC323A • CT Dose Reduction and Clinical Management

Mahadevappa Mahesh MS, PhD (Presenter) *

LEARNING OBJECTIVES

1) To identify various radiation dose reduction strategies in CT. 2) To assess impact of technological advances on reducing CT dose. 3) To describe ways to optimize radiation dose in CT.

ABSTRACT

RC323B • Fluoroscopy dose reduction and Clinical Management

Pei-Jan P Lin PhD (Presenter)

LEARNING OBJECTIVES

1) To identify that there are two basic schools of fluoroscopy operation logic design (FOLD). Discussion of FOLD enables us to understand how the modern fluoroscopy systems are able to. 2) Provide a wider dynamic range of patient thickness and reduce the patient exposure at the same time. 3) And, to identify there is a need to establish a hospital wide radiation monitoring and tracking system (HWRM).

ABSTRACT

There are two basic schools of fluoroscopy operation logic design (FOLD). Discussion of FOLD enables us to understand how the modern fluoroscopy systems are able to (1) lower radiation dose to the patient, (2) maintain the image quality required and (3) provide a wider dynamic range of patient thickness. While equipment based reduction of patient dose is effective, there is a need to monitor the overall radiation dose as the patient receives various types of radiological examinations. A hospital wide radiation monitoring (HWRM) is ever increasing as public-at-large becomes aware of potential radiation injuries from some of the radiological examinations. A sample monitoring system that is designed to monitor various patient dose data generated from CT and RF equipment will be discussed.

RC323C • CR and DR Dose Reduction and Clinical Management

Charles E Willis PhD (Presenter)

LEARNING OBJECTIVES

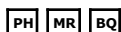
1) Appreciate why dose reduction efforts are necessary in projection radiography using CR and DR. 2) Identify the meaning of vendor-specific receptor exposure indicators and the new standardized receptor exposure indicators, and their indirect relationship to patient dose. 3) Assess the role of output indicators, DAP, KAP, and EAP, in estimating patient dose. 4) List simple operational methods for managing radiation doses in clinical radiography.

ABSTRACT

Computed Radiography (CR) and Digital Radiography (DR) are key technologies that enable the electronic practice of radiology. Both CR and DR are capable of producing acceptable diagnostic quality images over a wide range of exposures. A combination of traditional and new methods is necessary to manage the concomitant radiation dose to patients undergoing projection radiography examinations.

Quantitative Imaging: Functional MRI (fMRI)

Tuesday, 08:30 AM - 10:00 AM • E353A



[Back to Top](#)

Director
Michael F McNitt-Gray, PhD *

RC325A • Quality Assessment and Quantitation of Language and Motor fMRI

James T Voyvodic PhD (Presenter)

LEARNING OBJECTIVES

1) Understand the major sources of variance in fMRI results. 2) Be aware of post-processing approaches for reducing variance and improving reproducibility. 3) Understand the quality assessment methods used to measure sources of variance within individual patient scans. 4) Appreciate how to evaluate whether a particular patient fMRI scan meets the quality assessment criteria necessary for obtaining quantitative fMRI measurements within clinically useful reproducibility margins.

ABSTRACT

Many different variables affect clinical fMRI mapping of language and motor function, including behavioral task performance, head motion, tissue pathology, physiological variables, scanner performance, and software analysis methods. In order to achieve reproducible quantitative clinical fMRI results it is important to assess each of the major sources of variability, and to reduce unwanted signal variability where possible. This presentation will focus on identifying specific quality assessment criteria necessary to obtain reproducible quantitative fMRI results. It will also discuss the quantitative precision that can be expected for clinical fMRI results if the quality assessment criteria have been met. By establishing objective quality assessment criteria and validated reproducibility constraints, clinicians should be able to evaluate the quantitative confidence (i.e. margin of error) of the fMRI results for individual patient scans. Such guidelines are essential to enable quantitative measurements of the laterality, location, and spatial extent of clinically important functional brain areas. <http://hawking.biac.duke.edu/RSNA>

RC325B • More Quantitative fMRI Paradigms for Presurgical Mapping of the Visual System

Edgar A Deyoe PhD (Presenter) *

LEARNING OBJECTIVES

1) Review the functional organization of the human visual cortex. 2) Become familiar with state-of-the-art methods for presurgical mapping of the visual system with fMRI. 3) Learn of new methods for visualizing and interpreting fMRI brain maps of the visual system. 4) Become aware of interpretational issues such as neurovascular uncoupling that can significantly affect interpretation in a presurgical mapping context.

ABSTRACT

The complexity of MRI technology and the wealth of new information it provides can leave clinicians hard pressed to stay abreast of the latest developments and applications, especially since the field continues to evolve at a brisk pace. The goal of this session will be to review clinically relevant aspects of fMRI methods and their use in mapping the visual system to aid diagnosis of vision-related CNS diseases and to assist treatment planning, delivery and followup. The session will include a review of fundamental organizational principles of the human visual system with an emphasis on those properties that may be particularly relevant for clinical applications. Some principles, such as retinotopic organization may be generally familiar, but the ability to map this organization in detail quantitatively in individual patients and its utility in specific clinical applications is likely to be novel. Unique methods will be described for visualizing this organization both within the brain and as it relates to the patient's visual field and scotomata. The session will describe specific clinical applications of visual system mapping with fMRI and will present case studies to highlight such applications. Also, included is a description of methodology aimed at streamlining the clinical workflow and highlighting practical issues that should be considered to obtain high quality data with clinical patients. The overall goal is to show how it is possible to spend as little as 10 minutes of fMRI scan time yet obtain information that can be invaluable for diagnosis and treatment of patients with brain tumors, arteriovenous malformations, epilepsy and other pathologies that can impact central visual pathways.

RC325C • BOLD Cerebrovascular Reactivity Mapping as Applied to Brain Tumor fMRI

Jay J Pillai MD (Presenter) *

LEARNING OBJECTIVES

1) Understand the role of breath hold cerebrovascular reactivity (BH CVR) mapping in the assessment of neurovascular uncoupling potential. 2) Appreciate how neurovascular uncoupling may affect the reliability of BOLD fMRI activation maps. 3) Describe how BH CVR mapping can be performed in brain tumor patients.

ABSTRACT

The phenomenon of neurovascular uncoupling (NVU) is an important limitation of blood oxygen level dependent (BOLD) functional MRI (fMRI). One effective and practical method for assessment of risk of NVU is BOLD breath hold cerebrovascular reactivity (BH CVR) mapping. BH CVR mapping, similar to MR perfusion methods, allows assessment of regional hemodynamic impairment that may result in NVU and thus may lead to false negative activation on task-based sensorimotor or language fMRI that may be used for presurgical mapping in patients with brain tumors and other resectable brain lesions. However, unlike MR perfusion imaging, which assesses static or baseline perfusion to brain tumors and peritumoral regions, BOLD BH CVR mapping enables a dynamic assessment of cerebrovascular response, and its results can be applied to any task-based activation map. This lecture will describe the technique of BH CVR mapping, some of its strengths and limitations, and include cases in which interpretation of clinical fMRI exams has been affected by the additional information provided by these maps.

Physics (Quantitative Imaging I)

Tuesday, 10:30 AM - 12:00 PM • S403A

PH CT BQ

[Back to Top](#)

SSG13 • AMA PRA Category 1 Credit™:1.5

Moderator
Robert M Nishikawa, PhD *
Moderator
Marc Kachelriess, PhD

SSG13-01 • Characterization of Carotid Atherosclerotic Plaque Components Based on Quantitative Phase-contrast Hounsfield Units

Tobias Saam MD (Presenter) * ; Marian Willner ; Sandra Fill ; Julia Herzen ; Ulrich Schueller ; Holger Hetterich MD ; Alexander C Hipp ; Maximilian F Reiser MD ; Franz Pfeiffer ; Fabian Bamberg MD, MPH *

PURPOSE

Conventional CT can distinguish between soft, mixed and calcified plaques but has difficulties to further differentiate soft plaques due to an overlap in Hounsfield units (HU) of fibrous and lipid tissue. Phase-contrast imaging is a novel X-ray based imaging technique that relies on the X-ray phase-shift rather than its absorption, yielding a higher contrast in biological soft tissue. The purpose of our study was to evaluate whether plaque components can be differentiated based on their phase-contrast HU (HU-P), which can be calculated in analogy to absorption-contrast HU.

METHOD AND MATERIALS

Four ex-vivo human carotid arteries were imaged at a laboratory-based set-up using a conventional X-ray tube (35kV) and grating-interferometer. Tomographic images were reconstructed with an effective pixel size of 100 μ m and correlated with histopathology sections. Regions corresponding to fibrous, lipid or calcified tissue based on histopathology were manually traced. Mean HU-P were calculated for all analyzed regions.

RESULTS

A total number of 80 cross-sections with 72 fibrous, 19 lipid and 24 calcified tissue containing regions were assessed. Fibrous, lipid and calcified tissues were associated with significant different mean HU-P (52.6 \pm 7.0, 21.0 \pm 9.8 and 371.5 \pm 158.0, p no overlap of HU-P between fibrous (range 44.9 \diamond 63.3) and lipid tissue (3.1-30.1). Similarly, no overlap of HU-P was observed between calcified tissue (range 174.4 \diamond 593.7) and the other tissue components. Figure 1 demonstrates axial phase contrast CT images (A) and corresponding histology sections (B, C, Fib=fibrous, Lip=lipid and Cal=calcified tissue; length of the scale bar = 2 mm).

CONCLUSION

In an ex-vivo experimental set-up grating-based phase contrast CT can reliably differentiate between calcified, fibrous and fatty tissue based on quantitative HU-P, indicating its high potential for improved assessment of carotid atherosclerotic disease.

CLINICAL RELEVANCE/APPLICATION

Phase-contrast computed tomography might improve characterization of carotid atherosclerotic plaque morphology compared to conventional absorption CT.

SSG13-02 • Quantitative Image Analysis of MRI for Treatment Response Assessment of Multiple Myeloma

Chuan Zhou PhD (Presenter) ; **Qian Dong** MD ; **Daniel R Couriel** ; **Heang-Ping Chan** PhD ; **Lubomir M Hadjiiski** PhD ; **Jun Wei** PhD

PURPOSE

It is challenging for radiologists to visualize early changes in multiple myeloma (MM) within 3-6 months after autologous bone marrow transplant (BMT) due to small amount of marrow infiltration evident on MR images. This pilot study investigated the feasibility of using quantitative image analysis to evaluate early changes of BM in MRI for assessing treatment response.

METHOD AND MATERIALS

With IRB approval, 29 cases with MM requiring BMT were evaluated retrospectively. 31 pairs of spine MRI scans performed pre- and post-BMT (3-6 months), including 2 patients underwent second BMT after 4 and 6 months of the first BMT, respectively, were collected. The vertebral body volumes in sagittal views of T1-weighted sequence were manually outlined and their adjacent disc volumes were automatically extracted using morphological operations. A 3D dynamic intensity energy transformation (DIET) method was developed to characterize BM infiltration after BMT. DIET transformed the voxel intensity of a vertebral body to an energy enhancement value (EEV), defined as the ratio of the intensity entropy at the voxel to the median intensity entropy in the adjacent discs. Treatment response was quantified by an EEV response index (EEV-RI) calculated as the percentage of vertebrae with an increase in the mean EEV over the vertebral body in the post-BMT scan. In addition, the EEV heat map accentuated the intensity distribution pattern of the vertebral body and facilitated radiologist's visual assessment of the pre-to-post changes of BM infiltration.

RESULTS

Of the 31 follow up MRI scans, 25 were clinically diagnosed as good responders to BMT. The DIET method correctly identified 22 good responders using a decision threshold of > 40% for the EEV-RI. The agreement reached 0.903 \pm 0.14 with a kappa value of 0.74. The mean EEV increased by an average of 35.4 \pm 36.7% for the 22 good responders and decreased by 14.6 \pm 10.0% for the 6 non-responders. The mean EEV decreased by 19.0 \pm 20.5% for the 3 cases that were mistakenly identified as no response.

CONCLUSION

The substantial agreement between computer and clinical outcomes demonstrated the feasibility of using the quantitative image metric (EEV) for assessing treatment response for MM.

CLINICAL RELEVANCE/APPLICATION

Quantitative image-based biomarker may improve the accuracy and efficacy for staging and assessing treatment response for MM, allowing clinicians to optimize therapy of individual patients.

SSG13-03 • Use of a Dedicated Extremity Cone-beam CT Scanner for Evaluation of the Weight-bearing and Non-weight-Bearing Knee

Gaurav K Thawait MD (Presenter) ; **Abdullah Muhit** PhD ; **Wojciech Zbijewski** PhD * ; **Joseph W Stayman** PhD * ; **John Yorkston** PhD * ; **Shadpour Demehri** MD ; **John A Carrino** MD, MPH * ; **Jeffrey H Siewerdsen** PhD *

PURPOSE

To prospectively compare cone-beam CT (CBCT) examination of the knee in sitting (non-weight-bearing, NWB) position versus upright (weight-bearing, WB) position as a potential indicator of osteoarthritis (OA).

METHOD AND MATERIALS

A prototype CBCT scanner dedicated to extremity imaging was previously reported and assessed in terms of spatial resolution, contrast resolution, radiation dose, and optimal imaging protocols. An IRB approved study was performed in which 13 patients (8 females, 5 males; 31-78 yo, mean 56 yo) were prospectively enrolled for CBCT exams in NWB and WB positions using the prototype scanner. 11 were previously diagnosed with knee OA. 2 musculoskeletal radiologists measured the medial tibiofemoral (TF) joint space width and meniscal protrusion (MP) in coronal plane in consensus. Differences in such morphology were analyzed between NWB and WB images using paired Wilcoxon signed-rank test.

RESULTS

The scanner exhibited spatial resolution of ~15-17 lp/cm, depending on reconstruction technique, with high-contrast bone detail judged comparable or superior to conventional CT. Optimal scan protocol was 80 kVp, 120 mAs, imparting 9.0 mGy (dose at the center of a CTDI phantom). Isotropic sub-mm spatial resolution facilitated precise measurement of joint space morphology. For the 2 non-OA patients, the change in joint space between NWB vs WB exams appeared minor (2.67 mm vs 2.41 mm, respectively), and there was no evidence of meniscal protrusion. A greater difference in medial TF joint space was observed in OA patients: 1.91 \pm 0.85 mm for the NWB setup versus 1.23 \pm 0.8 mm for the WB setup, and the results were statistically significant (p=0.003). 4 of the OA patients exhibited no MP, 4 exhibited MP in both the NWB and WB exams, and 3 exhibited MP only in the WB exam (MP_{NWB} = 2.09 \pm 2.26 mm, MP_{WB} = 5.16 \pm 1.46 mm, p=0.016).

CONCLUSION

The TF joint space width and MP in OA patients was found to change significantly in sitting (NWB) versus upright (WB) exams. The ability to conduct NWB and WB exams in CBCT with a favorable dose profile and image quality sufficient for such morphological analysis could provide a valuable tool for OA diagnosis and treatment assessment.

CLINICAL RELEVANCE/APPLICATION

Weight-bearing CBCT of the knee can provide functional information and precise morphological analysis in cross sectional imaging not achieved by projection radiographs.

SSG13-04 • Comparison of Estimation of Patient Size Specific Dose Estimates (SSDE) Using Attenuation-based Estimation of Patient Size versus Geometrical Diameter for CT Examination of Thorax

Shima Aran MD (Presenter) ; Laleh Daftaribesheli MD ; Bob Liu PhD ; Hani H Abujudeh MD, MBA *

PURPOSE

The attenuation-based estimation of patient size and geometrical diameters are 2 methods introduced for the purpose of converting displayed CTDI volume to patient Size Specific Dose Estimates (SSDE). We assessed feasibility of applying the AAPM TG 204 for estimating patient SSDE using water equivalent diameter (Dw) and anteroposterior (DAP), lateral (DL), Sum (DSum= DAP +DL) and effective (DEff) diameters for chest CT.

METHOD AND MATERIALS

In an IRB-approved study, we evaluated 100 consecutive adult chest CT exams (M:F 60:40, mean age 61.5±12.8 years). Patients were classified into 2 groups of

RESULTS

Complete skin to skin measurements were possible in 6% the patients. Geometrical diameters (DLat, DSum and DEff) were significantly different and larger compared with Dw except for DAP (p0.92). However, SSDE values were significantly lower (p

CONCLUSION

The attenuation values measured from axial CT can be feasibly used to estimate SSDE. These values are significantly larger compared with Geometrical diameters derived SSDE for chest CT. The lack of specific levels of measurement (along the z axis) of attenuation or geometrical diameters has profound effect on SSDE variability.

CLINICAL RELEVANCE/APPLICATION

SSDE estimations are different using attenuation-based vs. geometrical diameters for chest CT. An optimal level of measurements should be defined for best use of SSDE estimations from CTDIvol.

SSG13-05 • Evaluating Proximal Femur Bone Strength Prediction by Advanced Characterization of Trabecular Microarchitecture Using Scaling Index Computation and Support Vector Regression

Chien-Chun Yang (Presenter) ; Mahesh Nagarajan ; Markus B Huber PhD ; Felix Eckstein MD * ; Thomas M Link MD, PhD * ; Axel Wismueller MD, PhD ; Julio Carballido-Gamio PhD ; Thomas Baum MD ; Sharmila Majumdar PhD * ; Jan S Bauer MD ; Eva-Maria Lochmueller MD

PURPOSE

Biomechanical bone strength prediction in proximal femur is important for osteoporosis diagnosis and fracture risk estimation. Our study proposes using advanced geometrical scaling index bone structure characterization in combination with statistical bone mineral density (BMD) features extracted from multi-detector computed tomography (MDCT) images of proximal femur specimens, with subsequent prediction of bone strength through support vector regression (SVR). The performance of this system is compared with a standard approach that uses mean BMD and multi-regression models.

METHOD AND MATERIALS

Axial MDCT images were acquired from 146 proximal femur specimens using a 16-row scanner and a calibration phantom. Adaptive spherical volumes of interest (VOI) were positioned in the femoral head (Huber et al., Radiology 2008) for BMD conversion and image analysis. VOIs of these BMD images were characterized through statistical moments as well as advanced geometrical features extracted with the Scaling Index Method (SIM) (Huber et al., IEEE-TBME 2011). The specimens were then biomechanically tested through a lateral fall on the greater trochanter, and failure load was recorded. All features were analyzed by multi-regression and SVR for predicting bone strength. The performance for different combinations of feature groups was compared using root-mean-square error (RMSE) and coefficient of determination (R^2). A Wilcoxon signed-rank test was used to compare two RMSE distributions and test for statistically significant differences in performance.

RESULTS

Combination of SIM features and mean BMD, when used in conjunction with SVR, exhibited the best prediction performance (RMSE = 0.95 ± 0.13 ; $R^2 = 0.62$). This was significantly better than the standard approach of using BMD and multi-regression (RMSE = 1.11 ± 0.141 ; $R^2 = 0.490$).

CONCLUSION

Our results show that the performance of predicting biomechanical strength in proximal femurs can be significantly improved by including SIM-derived geometrical features in addition to mean BMD, and through the use of support vector regression.

CLINICAL RELEVANCE/APPLICATION

Complementing BMD characterization on MDCT images with advanced geometrical features and machine learning can contribute to improved osteoporosis diagnosis and disease progression monitoring.

SSG13-06 • A New Method for Automated Anatomic Landmark Detection to Aid Automated Patient-specific Radiation Dosimetry in Tube-current Modulated CT Scans

Tim O'Connell MD, MEng (Presenter) * ; Maryam Khatonabadi * ; Michael F McNitt-Gray PhD * ; Aaron D Sodickson MD, PhD

PURPOSE

To develop an automated method of body part determination and body landmark detection for the purpose of characterizing regional variations in X-ray tube output and enabling regional radiation dose estimation.

METHOD AND MATERIALS

Software was created that extracts the image data from CT scans, detects the body contours, and performs thresholding to determine image tissue characteristics. The software then performs analysis on the tissue-specific attenuation curves along the Z-axis to determine body part scanned and anatomic landmarks. If the images are from a chest CT, the software computes the position (image number) of the lung apices, and the start of the right and left hemidiaphragms. If the images are from an abdomen/pelvis CT, the software computes the position of the start of the right and left hemidiaphragms, and the position of the iliac crests. Transaxial images from 100 CT scans (50 chest, 50 abdomen/pelvis) were retrieved from PACS for automated body part determination and landmark detection. These scans were also evaluated by a radiologist and the position of the relevant landmarks was recorded manually for comparison with the computed values.

RESULTS

100% of scans were correctly identified as being either chest (50/50) or abdomen/pelvis (50/50). In the chest CT group, there was no significant difference between the measured and computed location of the lung apices, right, and left diaphragm (t-test p = 0.42, 0.93, and 0.19 respectively); the mean difference between measured and computed position of the lung apices was 0.14 ± 1.02 cm, the right diaphragm was 0.05 ± 2.60 cm and the left diaphragm was 0.40 ± 2.06 cm. In the abdomen/pelvis CT group, there was no significant difference between the measured and computed location of the right diaphragm (p = 0.051) or the iliac crests (p = 0.19), but there was a significant difference in left diaphragm detection (p = 0.03). In this group, the mean difference between measured and computed position of the right diaphragm was -0.13 ± 0.51 cm, the left diaphragm was -0.24 ± 0.62 cm, and the iliac crests were -0.06 ± 0.98 cm.

CONCLUSION

This study demonstrates a new method of body part determination and body landmark detection that has high reliability and can provide crucial information needed for automated CT radiation dosimetry calculations.

CLINICAL RELEVANCE/APPLICATION

Relevant for improving radiation dosimetry through automated image analysis.

SSG13-07 • Fully-automated Segmentation of Cartilage from the MR Images of Knee Using a Multi-atlas and Local Structural Analysis Method

June-Goo Lee PhD (Presenter) ; **Serter Gumus** MD ; **Chan Hong Moon** PhD ; **Cheng Tao** MD ; **Sonu K Bae** ; **Kyongtae T Bae** MD, PhD *

PURPOSE

To develop a fully-automated method to segment cartilage from the magnetic resonance (MR) images of knee and to evaluate the performance of the method on a public open dataset.

METHOD AND MATERIALS

For the development and testing of a fully-automated program for cartilage segmentation, we used 100 cases of knee MR images from a public open dataset (available at www.ski10.org). MR images were acquired in the sagittal plane with gradient-echo T1-weighting sequence and fat suppression at 0.4*0.4mm in-plane and 1mm slice-thickness resolution. The dataset also includes the segmentation result by experts to label and delineate the bone and cartilage of the femur and tibia. We randomly divided the 100 cases into the training set (60 cases) and the test set (40 cases).

The segmentation process was carried out in two steps, atlas-building and local-adjustment. In the atlas-building step, all training cases were registered to a test case via a non-rigid registration scheme. The final metric values from each registration were recorded for sorting. Nine best matched results were selected and merged to generate the atlas-based segmentation mask by majority voting. In the local-adjustment step, the statistical information of bone, cartilage and surrounding regions was computed from the atlas-based segmentation result. This information was used to determine seed points for a graph-cut algorithm to segment bone regions. Structurally similar points from the registered multiple atlases were identified via a Hessian analysis. Finally, a locally-weighted voting process was applied for a local adjustment. The performance of the segmentation program was evaluated in terms of dice similarity coefficient (DSC), sensitivity and specificity of segmented femoral and tibial cartilages against the reference cartilage segmentation of the test cases from the dataset.

RESULTS

The cartilages were segmented successfully in all test cases. The DSC was 0.67 ± 0.07 for femoral and 0.53 ± 0.08 for tibial cartilage. The segmentation performance was according to (sensitivity, specificity): ($57.5 \pm 9.6\%$, $99.9 \pm 0.04\%$) for femoral and ($53.0 \pm 8.4\%$, $99.9 \pm 0.02\%$) for tibial cartilage.

CONCLUSION

We have developed a fully-automated segmentation program for knee cartilage from MR images. The performance of the program on 40 test cases was highly promising.

CLINICAL RELEVANCE/APPLICATION

The fully-automated segmentation method will facilitate the quantification of cartilage.

SSG13-08 • Iodine-density Analysis Using Spectral CT Imaging in Differentiating Benign and Malignant Serous Cavity Effusion

Ye Ju (Presenter) ; **Ailian Liu** MD ; **He Qing Wang** MSc ; **Yijun Liu** ; **Renwang Pu** MBBCh, FRCPC ; **Wenjun Cui**

PURPOSE

To assess the value of quantitatively iodine concentration measurement of enhanced spectral CT imaging in the differential diagnosis of malignant and benign serous cavity effusion.

METHOD AND MATERIALS

Approval for this retrospective HIPAA compliant study was obtained from the institutional review board, and informed consent was waived. From August 2012 to February 2013, totally 45 patients, including 13 cases of benign serous effusion and 32 cases of malignant serous effusion proven by histopathological diagnosis or laboratorial examination, underwent plain and three-phase enhanced spectral CT imaging through fast kVp-switching technique. 140 kVp polychromatic images and iodine-based material density images were reconstructed. The mean CT value (M-CT) was measured at plain and three-phase enhanced 140 kVp images, and the difference of CT values (D-CT) was calculated. The iodine concentration (M-I) was also quantitatively measured at iodine-based material density images and the difference (D-I) was calculated. The difference of these parameters was evaluated statistically by independent-samples t test.

RESULTS

CONCLUSION

The nature of the serous cavity effusion was difficult to be identified only by the CT values on conventional enhancement scanning. The iodine-density images of spectral CT imaging at venous phase and delayed phase play an important role in identifying malignant and benign effusion.

CLINICAL RELEVANCE/APPLICATION

The iodine-density images of enhanced spectral CT scanning provides a sensitive approach for identifying benign and malignant serous cavity effusion.

SSG13-09 • Quantitative Measures of Normal Lung Texture Change during Respiration: Analysis of Variation Using 4-dimensional CT

Shane P Krafft MS, BS (Presenter)

PURPOSE

While image quality is often considered the main barrier to achieving valid, reproducible quantitative image biomarkers, anatomic motion during CT acquisition presents another unique challenge. The implementation of 4-dimensional CT allows us to reconstruct the lung volume at equally spaced phases of the breathing cycle and, as a result, we can estimate the impact of anatomic variability on quantitative analysis of lung parenchyma. The purpose of this study was to demonstrate the variation of lung texture features with the phase of the respiratory cycle.

METHOD AND MATERIALS

4DCT scans were acquired for 10 patients with non-small-cell lung cancer prior to radiotherapy. Normal lung volumes were segmented with a semi-automatic 3D region-growing algorithm on each of the 10 binned phase reconstructions (0-90%). The original 12-bit CT images were reduced to a bit depth of 8 and gray-level co-occurrence and run length matrices were used to extract 17 non-directional 2D texture features from the segmented total lung volume. The extracted features were evaluated for phase dependence relative to the end exhalation phase (50%). For each patient, Spearman's rank correlation (R_s) was used to determine the relationship between feature and the calculated lung volume from each phase image set.

RESULTS

Within an individual 4DCT scan, change in texture relative to the end exhale phase varied up to 75.3%. Over the entire patient population, 8 of the 17 metrics showed an average change due to respiratory phase of less than 5%; however, the range of measured changes was 0.9-31.2% over all of the considered texture features. 5 of 17 features were highly correlated ($|R_s| > 0.7$) to lung volume.

CONCLUSION

Using 4DCT the phase dependence of texture measures was demonstrated. While some of the extracted texture features may be reasonably independent of respiratory phase, large differences were observed for others. The correlation of features to the lung volume

highlights the periodic phase dependence of some of the considered texture metrics.

CLINICAL RELEVANCE/APPLICATION

As the respiratory phase influences extracted texture measures of lung parenchyma, anatomic variability must be considered in attempts to standardize quantitative imaging biomarkers.

Physics (Multi-energy CT)

Tuesday, 10:30 AM - 12:00 PM • S403B



[Back to Top](#)

SSG14 • AMA PRA Category 1 Credit™:1.5 • ARRT Category A+ Credit:1.5

Moderator

Michael D Silver, PhD *

Moderator

Katsuyuki Taguchi, PhD *

SSG14-01 • Cone-beam CT with Sparse Arrays of Photon Counting Silicon Strip Detectors: Reconstruction, Performance Characterization, and Application to Dual-energy Imaging

Wojciech Zbijewski PhD (Presenter) * ; **Jennifer Xu** ; **Steven W Tilley** BS ; **Grace Gang** ; **Joseph W Stayman** PhD * ; **Katsuyuki Taguchi** PhD * ; **Erik Fredenberg** MSc, PhD * ; **Mats Lundqvist** PhD * ; **John A Carrino** MD, MPH * ; **Jeffrey H Siewerdsen** PhD *

PURPOSE

Silicon strip (Si-strip) photon counting detectors (PCDs) entering use in mammography provide advantages of reduced electronic noise and dose, spectral imaging, and coincidence detection for reduction of charge sharing. We present a new implementation of PCDs configured for CT, investigate the design and 3D reconstruction algorithms to address sparse detector coverage, and evaluate performance in single and dual-energy (DE) CT.

METHOD AND MATERIALS

The PCD was a 5x25 cm² Philips MicroDose Si-strip detector, consisting of a 21-row sensor array at 50 μ m pixel pitch (~100,000 pixels) in a sparse matrix with inter-sensor gaps up to 5 mm matched to pre-patient collimation. A benchtop CT system was configured with source-detector distance ~65 cm. Imaging was performed at 70 kVp (+0.2 mm Cu, +2 mm Al) at 0.06-0.12 mAs per frame. To overcome effects of sparse sampling, translate-rotate orbits were studied, ranging from single axial scan (1x360°) to six axially staggered scans (6x360°). Penalized-likelihood (PL) reconstruction was employed to address the complex sampling of the system through the built-in forward model and to provide noise reduction in DE decomposition through Total Variation (TV) regularization. Reconstruction-based DE decomposition of an ~8 cm diameter water phantom with inserts of iodine (10 mg/mL), calcium (200 mg/mL), and oil was performed from data collected in two energy windows.

RESULTS

The fraction of voxels sampled by less than one ray decreased from 65% for the 1x360° orbit to 18% for the 6x360° orbit for an 80x80x15 mm³ volume, with corresponding reduction in artifacts. DE CT images with TV regularization exhibited accurate decomposition with only slight variation with exposure; the fraction of correctly identified iodine voxels (true-positive fraction) increased from 73% to 77% and 83% for exposures of 0.06 mAs/frame, 0.09 mAs/frame and 0.12 mAs/frame, respectively; the false-positive fraction for iodine decreased from 5% and 0.06 mAs to 3% at 0.12 mAs.

CONCLUSION

The feasibility of volumetric CT with Si-strip PCDs in both single- and DE modes was established, demonstrating accurate DE classification of iodine and calcium in a single scan.

CLINICAL RELEVANCE/APPLICATION

High-performance PCDs translated to a benchtop CT platform enables single- and DE imaging from a single kVp scan and permits investigation of benefits in CT image quality, dose, and new applications.

SSG14-02 • Dual Energy Breast CT for Tissue Composition Measurement

Sabee Y Molloi PhD (Presenter) * ; **Huanjun Ding** ; **Travis Johnson** ; **Justin Ducote**

PURPOSE

Studies have suggested the possibility to differentiate a malignant lesion from benign tissue by characterizing them according to their water, lipid and protein composition. The purpose of this study is to investigate the feasibility of a three-material compositional measurement of water, lipid and protein content of breast tissue with dual kVp cone-beam CT.

METHOD AND MATERIALS

40 postmortem breasts were imaged with a flat-panel based dual kVp cone-beam CT system at 50 and 120 kVp, followed by image-based tissue decomposition into water, lipid and protein contents. The mean glandular dose (MGD) from the dual kVp scans was approximately 6 mGy. The optimal imaging protocols, in terms of dual kVp tube voltages and dose distributions were first simulated with an analytical model which maximized the dual energy signal-to-noise ratio (SNR) with respect to MGD. A three-material phantom, consisting of water, vegetable oil and polyoxymethylene plastic was used for dual energy calibration for water, lipid and protein, respectively. The expected errors due to the calibration materials were also estimated by simulation. The breasts were then chemically decomposed into their respective water, lipid and protein contents after imaging to allow direct comparison with data from dual energy decomposition.

RESULTS

The dual energy breast tissue decomposition in terms of the volumetric percentages of water, lipid and protein contents exhibited strong correlation with data from the chemical analysis, which is considered to be the gold standard. As compared with the chemical analysis, the average root-mean-square (RMS) percentage error in tissue decomposition for all 40 breasts was calculated to be 3.6%.

CONCLUSION

The results of this study suggest that the water, lipid, and protein contents can be accurately measured using dual energy breast CT. The tissue compositional information can potentially improve the sensitivity and specificity for breast cancer diagnosis.

CLINICAL RELEVANCE/APPLICATION

Accurate compositional analysis of breast tissue may potentially improve the sensitivity and specificity of breast cancer detection and reduce the number of biopsies needed for suspicious lesions.

SSG14-03 • Clinical Dual Energy CT (DECT): Can Monoenergetic Imaging Remove Metal Artifacts?

Stefan Kuchenbecker MENG (Presenter) ; **Sebastian Faby** DIPLPHYS ; **Soren Schuller** ; **Matthias Baer** DiplPhys ; **Michael M Lell** MD * ; **Marc Kachelriess** PhD

PURPOSE

DECT provides so-called monoenergetic images based on a linear combination of the original polychromatic images. At certain

patient-specific energy levels $E \approx 130$ keV, corresponding to certain linear combination weights $w \approx 1.6$, a significant reduction of metal artifacts is observed. We aim at analyzing the method to identify its limitations.

METHOD AND MATERIALS

DECT can be used to exactly calculate virtual monochromatic images (neglecting scatter). This calculation has to be done in rawdata domain before image reconstruction. Clinical CT, however, uses a simplified version of monochromatic imaging by linearly combining the low and the high kV images, and by assigning a keV-value to that linear combination. Those pseudo monochromatic images are used by radiologists to obtain images with reduced metal artifacts. We analyzed the underlying physics and carried out a series expansion of the polychromatic attenuation equations. The resulting non-linear terms are responsible for the artifacts, but they are not linearly related between the low and the high kV scan: A linear combination of both images cannot eliminate the non-linearities, it can only reduce their impact. Scattered radiation yields additional non-cancelling non-linearities. To quantify the artifact reduction potential of pseudo monochromatic images we simulated the Forbild abdomen phantom with metal implants and we measured a semi anthropomorphic abdomen phantom with inserts of high iodine concentration using a clinical dual source CT system (100 kV, 140 kV Sn). In each case we manually selected an optimal w , and we automatically computed an optimal w by minimizing the standard deviation S of the voxel values of the smoothed (to minimize the impact of image noise) soft-tissue regions around the metal implants.

RESULTS

For the initial images $S=150$ HU (100 kV) and 59 HU (140 kV Sn). The manually setting yields $w=1.62$ with $S=18.2$ HU, while the automatic setting yields $w=1.60$ and $S=18.1$ HU. A complete artifact reduction corresponding to $S=3.71$ HU (image noise only), as achieved with rawdata-based processing, was not possible with pseudo monochromatic imaging.

CONCLUSION

Pseudo monochromatic imaging is able to reduce metal artifacts (at the cost of contrast-to-noise ratio) but it cannot remove them.

CLINICAL RELEVANCE/APPLICATION

Artifact reduction through pseudo monochromatic imaging is helpful. But it should be avoided if alternative dedicated artifact reduction approaches are available.

SSG14-04 • Effectiveness of Synthesized Monochromatic Imaging Generated with a Fast Kilovoltage Switching Dual Energy CT Scanner for Improved Patient-to-Patient Uniformity of Aortic Enhancement during Abdominal CT Angiography: An In-Vivo and In-Vitro Study

Ghaneh Fananapazir MD (Presenter) ; Rendon C Nelson MD * ; Joshua Wilson PhD ; Kingshuk Choudhury PhD ; Daniele Marin MD

PURPOSE

To investigate whether virtual monochromatic imaging (VMI) generated from a fast kilovoltage-switching single-source dual-energy CT (DECT) acquisition may correct for beam hardening artifacts, improving uniformity of abdominal aortic enhancement across different body sizes.

METHOD AND MATERIALS

A proprietary tapered hollow phantom with a bone-mimicking insert and a hollow tube mimicking the aorta was developed. The tube was filled with different iodine solutions simulating various degrees of aortic enhancement. The phantom was filled with water. Single-source DECT was performed and VMIs were synthesized at different energies (40-140keV, @ 20keV increments). The phantom was also scanned using conventional polychromatic kV settings (80-140kVp, @ 20kV increments). CT numbers in the aorta and water (noise) were measured along the entire length of the phantom. 62 consecutive patients (38 M; mean age 60 years \pm 13 SD; mean BMI 30kg/m² \pm 6 SD) underwent DECT scans. Aortic attenuation was measured at polychromatic 140kVp and VMI 80keV datasets. The relationship between aortic attenuation and signal-to-noise (SNR) as a function of body diameter was assessed for the phantom and clinical patients.

RESULTS

There was a significant negative correlation between both aortic attenuation/SNR and phantom diameter using polychromatic energy beams (-15.7HU/cm @ 80kVp to -6.8HU/cm at 140kVp) or VMI at energies equal or lower than 60keV (\approx 18.7HU/cm @ 60keV to -53.5HU/cm @ 40keV). Aortic attenuation and SNR were nearly independent of phantom diameter at 80keV VMI (-4.3HU/cm; P

CONCLUSION

The 80keV VMI improved consistency of aortic enhancement across different body sizes, although this could come at the cost of decreased magnitude in aortic enhancement.

CLINICAL RELEVANCE/APPLICATION

Lower susceptibility to beam-hardening effects using VMI increases consistency in aortic attenuation measurements across different patient body sizes.

SSG14-05 • A Fast and Noise-efficient Estimator for Material Decomposition in Multi-bin Photon Counting X-ray Detectors

Paurakh L Rajbhandary BS (Presenter) ; Scott S Hsieh MS ; Norbert J Pelc ScD *

PURPOSE

We present a fast, noise-efficient, and accurate targeted least squares estimator (TLSE) for material separation using PCXDs with multiple energy bin capability. The proposed estimator uses a novel method of incorporating dynamic weighting that allows noise to be homogenous and close to the Cramer-Rao Lower Bound (CRLB) throughout the operating range.

METHOD AND MATERIALS

The TLSE estimator uses a non-iterative and adaptive least squares method followed by bias correction based on a calibration phantom. In the initial step, a generalized weighted least squares linearized at the center of the operating region is used. The second step utilizes the output from the first estimate as a pointer to localize a region in a 4-by-4 grid of operating range to extract noise-weighting statistics. This dynamically adjusts the weights of the energy bins to optimize noise properties. After this adaptive step, a localized least squares and error correction process akin to A-table method (Alvarez et al) is applied to produce the final estimate. The variance and bias of this estimator between 0 to 6 cm of aluminum and 0 to 50 cm of water is simulated with Monte Carlo methods and compared to alternative estimators.

RESULTS

The proposed estimator produced an average bias of $(2.59 \pm 4.66) \times 10^{-5}$ cm and variance-to-CRLB ratio of 1.039 ± 0.039 . Using the same protocol, the gold standard Maximum Likelihood Estimator (MLE) showed average bias and variance-to-CRLB ratio of $(2.77 \pm 2.25) \times 10^{-5}$ cm and 1.035 ± 0.037 but was 50.1 times slower in our simulation. Compared to a previous non-iterative estimator (Alvarez et al), the variance-to-CRLB of TLSE is more homogenous and its average value is reduced from 9.7% to 3.9%. Average variance-to-CRLB ratio for TLSE is lower by as much as 19% in the peripheral region.

CONCLUSION

The TLSE is a computationally efficient method for implementing material decomposition technique using multi-bin PCXDs that offers noise parameters comparable to the gold standard MLE method.

CLINICAL RELEVANCE/APPLICATION

The proposed estimator is a practical method of material decomposition that can be used in clinical applications (such as angiography, virtual pre-contrast imaging) using PCXDs.

SSG14-06 • Value of Monoenergetic Low-kV Dual Energy CT Datasets for Improved Image Quality of CT Pulmonary Angiography

Paul Apfaltrer MD (Presenter) ; Sonja Sudarski ; John W Nance MD ; Christian Fink MD ; Stefan O Schoenberg MD, PhD * ;

Thomas Henzler MD ; Holger Haubenreisser ; David Schneider

PURPOSE

High vessel attenuation and high contrast-to-noise ratio (CNR) are prerequisites for high diagnostic confidence in CT pulmonary angiography (CTPA). This study evaluated the impact of reconstructed monoenergetic dual-energy (DE) CTPA datasets on vessel attenuation and CNR.

METHOD AND MATERIALS

RESULTS

CONCLUSION

Virtual 70-keV monoenergetic CTPA image datasets significantly increase vessel attenuation and CNR of DE-CTPA studies, suggesting that clinical application of low-keV monoenergetic reconstructions may allow a decrease in the amount of iodinated contrast required for adequate image quality in DE-CTPA examinations.

CLINICAL RELEVANCE/APPLICATION

DE-low-keV monoenergetic imaging may allow reductions in iodinated contrast material without compromising image quality; this may be particularly relevant in patients with impaired renal function.

SSG14-07 • Half and Quarter Dose Dual Energy CT Enabled by Prior Image Constrained Compressed Sensing

John W Garrett MS (Presenter) * ; Stephen T Brunner BS ; Jie Tang PhD ; Guang-Hong Chen PhD *

PURPOSE

The dose in dual-energy CT (DE-CT) studies is often high due to the decomposition of the CT images, as well as the need to acquire a high and a low energy data set. The Prior Image Constrained Compressed Sensing (PICCS) algorithm may enable half or even quarter dose acquisitions in DE-CT while retaining spatial resolution and diagnostic information.

METHOD AND MATERIALS

The PICCS reconstruction technique was adapted for use in DE-CT. It was then applied to a porcine DE-CT study (0.625 x 0.625 x 5 mm³) acquired using a GE Discovery CT750 HD scanner (GE Healthcare, Waukesha, WI) at full, half, and quarter dose using a 50/50 dose partition. Bone/water decomposition images as well as virtual monochromatic images (40-102 keV) were reconstructed using the conventional filtered backprojection (FBP) and PICCS techniques. For each technique, the background noise in the bone/water decomposition images and the contrast-to-noise ratio (CNR) for the gall bladder in the 50 keV virtual monochromatic images were measured. In addition, the images were subjectively reviewed by a diagnostic radiologist.

RESULTS

At half dose, the background noise in the PICCS bone/water images was lower than that of the full dose FBP by 24%, while the half dose FBP background noise was 44% higher. At a quarter dose, the background noise of the PICCS bone/water images was found to be within 1% of the full dose FBP images, while the quarter dose FBP was higher by 92%. In the 50 keV virtual monochromatic images, the CNR of the PICCS images was higher than that of the full dose FBP by 22% and 9% at half and quarter doses respectively. For the reduced dose FBP images the CNR was lower by 34% and 40% at the same dose levels. Radiologist review determined that the half dose PICCS bone/water and virtual monochromatic images were diagnostically equivalent to the full dose FBP images, and the quarter dose PICCS was comparable the half dose FBP.

CONCLUSION

DE-CT images reconstructed at half or quarter radiation dose with the PICCS algorithm are similar to the full dose FBP reconstruction in terms of noise and diagnostic information. As a result, the application of the PICCS framework in DE-CT enables half or quarter dose studies to be performed with no significant loss of diagnostic information.

CLINICAL RELEVANCE/APPLICATION

This study is clinically relevant because it offers the possibility of performing dual-energy CT studies at half or quarter dose in a clinical setting.

SSG14-08 • Application of Photon-counting CT: Metal Artifact Reduction

Radin A Nasirudin DIPLENG (Presenter) ; Kai Mei ; Petar Penchev DIPLENG, PhD ; Ernst J Rummeny MD ; Martin Fiebich ; Peter B Noel PhD

PURPOSE

Photon-counting detectors (PCD) have the ability to discriminate photons based on their energies, thus providing information on the composition of the scanned object. This work presents an algorithm called Spectral-driven Iterative Reconstruction (SPIR) that utilizes spectral information to reduce metal artifact in Computed Tomography (CT).

METHOD AND MATERIALS

A Monte-Carlo simulator was used to simulate CT acquisitions of a jaw phantom. The phantom consists of teeth, jawbone and bone marrow. One tooth was substituted with a gold implant (density 19g/cm³). The CT simulation is setup as follows: Cone-beam geometry, photon-counting detector with 6 energy bins and an X-ray source of 125 keV. In the first step of the algorithm, the simulated projection data were decomposed to determine the spatial location and density of the gold. The information of the gold implant was then incorporated into a penalized maximum likelihood reconstruction algorithm as a prior. The result from the algorithm was objectively and subjectively assessed.

RESULTS

The algorithm was able to distinguish the gold implant from other components of the phantom. The incorporation of prior information into the reconstruction algorithm delivers a notably improved image: streaking artifacts were reduced significantly without compromising the anatomical information, while the dark shadings around the dental implant were eliminated. The signal-noise-ratio (SNR) was significantly improved (13.6), when compared to FBP (2.2) or conventional iterative reconstruction (5.8). Especially the regions surrounding the implant show extreme improved diagnostic quality when using our approach (see Figure)

CONCLUSION

The incorporation of spectral information into statistical reconstruction significantly improves the diagnostic quality, while providing more information on the composition of the scanned object. Thus the implementation of PCDs does not only offer significant dose reduction but also the improvement of diagnostic image quality.

CLINICAL RELEVANCE/APPLICATION

The imminent clinical introduction of PCDs is a promising extension. It will lead to new clinical relevant applications, while also minimizes radiation exposure to the general population.

SSG14-09 • Effective 120 kV CT Images from Dual-energy CT Scans

Yongshuai Ge (Presenter) ; Jie Tang PhD ; Guang-Hong Chen PhD *

PURPOSE

Dual-energy CT (DECT) scans provide monochromatic CT images at different energies and effective atomic number based on the material information acquired from scanned projection data at 80kV and 140kV. However, many conventional clinical diagnostic tasks are performed based on the CT number of materials in 120 kV CT images. There are many potential benefits of generating equivalent 120 kV

CT images from DECT scans.

METHOD AND MATERIALS

Using a 64-slice GE Discovery CT750HD scanner, dual energy CT imaging was performed on both a Catphan phantom and human subject studies with IRB approval. From GSI dual energy scans, monochromatic images from 40keV to 140keV were generated at 1keV intervals. A normalized effective x-ray spectrum was generated from the vendor provided 120 kV x-ray spectrum with additional filtration of a 20cm (30cm for human subjects) thick water equivalent slab. The normalized effective x-ray spectrum was used to weight and combine the GSI produced monochromatic images to generate equivalent 120 kV CT images for evaluation. The method was validated using the 120kV phantom results and 120 kV scan of the same subject. In the phantom study, CT numbers were measured in ROIs of 8 different materials with nominal CT numbers ranging from -1000 to 1000 HU. In human subject studies, CT numbers were measured from 21 ROIs in fat and soft tissue.

RESULTS

For the phantom study, the relative errors of the synthesized and 120 kV CT images are 5%, 4%, 2%, 1%, 1%, 2%, 1%, 0%, for Polystyrene, LDPE, PMP, air, Teflon, Delrin, Acrylic and the background material respectively. In the Bland-Altman analysis of human subject results, the bias of CT numbers between the synthesized effective 120 kV and acquired 120 kV CT images is 0.5 HU and the limits are within 1.7 HU.

CONCLUSION

Effective 120kV CT images can be generated from a GSI dual energy CT scan with high accuracy.

CLINICAL RELEVANCE/APPLICATION

The synthesized 120 kV CT images can help clinicians make routine diagnosis together with quantitative imaging enabled by GSI imaging.

Physics (X-ray Imaging)

Tuesday, 10:30 AM - 12:00 PM • S404AB

[Back to Top](#)



SSG15 • AMA PRA Category 1 Credit™:1.5 • ARRT Category A+ Credit:1

Moderator

Martin J Yaffe, PhD *

Moderator

Joseph Manak *

SSG15-01 • Developments to a Rapid In-clinic Peak Skin and Organ Dose Algorithm for Improved Patient Risk Management During High-dose Fluoroscopically Guided Interventions

David Borrego MS (Presenter) ; **Daniel A Siragusa** MD ; **Wesley E Bolch** PhD

PURPOSE

Data from a detailed parameterization of over 23,763 exposure conditions from high frequency and/or high-dose fluoroscopically guided interventions reveal the dynamic nature of these procedures. As such, simple point calibrations of the KAP meter and spectral data assumptions may lead to gross errors in skin and organ dose calculations. This work seeks to investigate new methods and calibrations for improved accuracy gains over previous iterations of the University of Florida's Rapid In-Clinic Peak Skin Dose Algorithm (RIPSA).

METHOD AND MATERIALS

Calibration factor maps were developed that accounted for copper filtration, tube voltage, and current. The calibration factor maps were then coded into the RIPSA software for improved accuracy. Organ doses are further dependent on x-ray energy spectra. A first order estimation of the energy spectra was generated along with an energy spectra to match measured first and second HVLs to within $\pm 3\%$ with an in-house spectrum generator based on the TASMIP database. Organ doses were then calculated with the use of MCNPX transport code.

RESULTS

The only statistically significant variables affecting the calibration factor are tube voltage within each filtration based on a one-way ANOVA ($F(10,97)=3.18$, $p=0.001$, $\eta^2=0.05$). The KAP meter is highly dependent on the quality of the x-ray spectra, which can introduce errors of up to 40% without the use of the calibration factor maps. Matching spectral data to the first and second HVLs yielded a 17% improvement in organ doses within in-field organs. These additional steps in calculating organ and skin doses have a negligible computational burden on the RIPSA software, with an average time of less than two seconds to calculate skin doses following an irradiation event.

CONCLUSION

This work represents robust improvements to the University of Florida's RIPSA software by incorporating detailed x-ray energy spectra and calibration curves for the KAP meter while also overcoming the challenges of characterizing: 1) a dynamic radiological exam and 2) the variability of a patient population when conducting a dose reconstruction that can provide the interventional physician information needed to modify behavior when clinically appropriate.

CLINICAL RELEVANCE/APPLICATION

This work is an innovative effort, overcoming previous challenges, to equip interventional radiologists with accurate organ and real-time skin dose distributions to help guide clinical decisions.

SSG15-02 • Development of a New Image Operation System with Hand Movements Using a Kinect Sensor for Angiography

Yuki Ishida (Presenter) ; **Toshihiro Ogura** PhD ; **Norio Hayashi** PhD ; **Mitsuru Sato** ; **Mika Okajima** ; **Kunio Doi**

PURPOSE

During angiographic examinations, interventional radiologists need various image manipulation such as paging, roaming, enlarging and fusion in order to assess vessels and sources of bleeding. However, radiologist could not touch screen by hand, because of his/her gloves to be kept clean. Usually, radiologists provide verbal instructions to technologists, who may operate to display appropriate images with various image processing. However, if technologist may not be at the console due to the preparation of the catheter or contrast agent, quick operation may not be performed. Therefore, we developed a new image operation system using a motion sensor for angiography. With this system, radiologists could operate various image processing only with movements in hands.

METHOD AND MATERIALS

We used the Kinect technique which is a gesture recognition technology to read the movement of radiologists. The Kinect sensor consisted of an infrared laser emitter, an infrared camera and an RGB camera for gesture recognition. Measurements of depth were made by triangulation using the infrared camera. For initialization, radiologist's hands were recognized by computer for right palm forward protrusion.

RESULTS

CONCLUSION

With the image operation system using a motion sensor for angiography, various image processing can be performed with our hand movements, which would be a new technology for angiography in operating rooms.

CLINICAL RELEVANCE/APPLICATION

This system can be implemented as a useful tool to radiologists for control of image viewing without touching the workstation in existing angiography system in operating rooms.

SSG15-03 • Stationary Chest Tomosynthesis System Using Distributed CNT X-ray Source Array

Jing Shan (Presenter) ; **Andrew Tucker** ; **Yueh Z Lee MD, PhD *** ; **Michael D Heath *** ; **Xiaohui Wang PhD *** ; **David Foos MS *** ; **Jianping Lu *** ; **Otto Zhou PhD ***

PURPOSE

The purpose of this work is to investigate the feasibility of constructing a stationary chest tomosynthesis system using a stationary CNT source array, and to evaluate the relationship between source geometry configurations and the tomosynthesis image quality.

METHOD AND MATERIALS

A bench-top chest tomosynthesis system using a CNT source array (XinRay Systems, NC) and a flat panel detector (Carestream Health Inc. NY) was built. The source array contains 75 focal spots operating at 80kVp and 5mA anode current. The tube output and entrance dose were measured. Projection images were reconstructed using commercial software (Realtime Tomography, Pa). System in-plane resolution and in-depth resolution were measured using a 100um cross-wire phantom at different source configurations including linear-source geometry with different angular coverage and a square-source geometry. In addition, anthropomorphic chest phantom images were acquired and reconstructed for image quality assessment.

RESULTS

CONCLUSION

The experimental results demonstrate the feasibility of stationary chest tomosynthesis. This can lead to improved system design, potentially faster imaging speed, and reduced patient motion blur. The CNT source array is capable of delivering sufficient x-ray flux and dose required for chest tomosynthesis. The square source geometry shows comparable in-plane and in-depth resolutions as linear geometry.

CLINICAL RELEVANCE/APPLICATION

Stationary tomosynthesis system can improve image quality and reduce image acquisition time, which can improve the workflow and benefit the detection of small lung nodules and other chest pathology.

SSG15-04 • Comparison of Microcalcification Detection in Digital Mammography and Breast Tomosynthesis Using a Hybrid Technical-clinical Test Method

Lesley Cockmartin (Presenter) ; **Gwen Aerts** ; **Federica Zanca PhD** ; **Nicholas Marshall** ; **Eman Shaheen** ; **David Dance PhD** ; **Kenneth C Young PhD** ; **Hilde Bosmans PhD ***

PURPOSE

To compare the detectability of microcalcifications in patient images for digital mammography (2D) and breast tomosynthesis (BT) using a hybrid technical-clinical method.

METHOD AND MATERIALS

Spherical microcalcifications (CaCO₃), in groups of 5 in the Voxmam phantom (Leeds Test Objects, UK), were imaged in 2D and BT mode. Templates of microcalcifications embedded in different thicknesses of polymethyl methacrylate (PMMA), were created for 2D and BT projections by dividing exposures of the Voxmam phantom containing microcalcifications in PMMA by images of homogeneous PMMA. The templates were multiplied into projection images of patients with equivalent breast thicknesses and then processed/reconstructed. Four groups of microcalcification diameters were used: 354-224, 283-180, 226-150 and 177-106 μ m. All microcalcifications were imaged at 2 different heights (z-positions) above the detector. For the detection study, 511 2D images and 511 BT series were viewed: 355 with microcalcifications and 156 without. Seven observers scored the presence or absence of the microcalcification group in the center of a highlighted area via a 5 point confidence rating scale and counted how many microcalcifications were visible. Detection performance of 2D and BT was compared via ROC analysis with sub-analyses for microcalcification size, breast thickness and z-position.

RESULTS

Peak contrast in the projections ranged from 1.3% to 16% for 2D and from 0.8% to 11% for BT templates. Preliminary ROC results showed a better detection of microcalcifications in 2D compared to BT (*p* with an area under the curve (AUC) of 0.95 compared to 0.85. A statistically significant difference was found for the two intermediate size groups only. The AUC in 2D and BT were significantly different only for higher breast thicknesses (>5cm). Higher z-positions (>3cm) showed higher significant differences between 2D and BT. Finally, the Wilcoxon matched pairs test indicated a significant difference (*p* between the counts for 2D and BT).

CONCLUSION Detection performance of 2D and BT for all microcalcification sizes depends on breast thickness and z-position, suggesting the need for further optimization of acquisition and reconstruction in BT for thicker breast and higher z-positions.

CLINICAL RELEVANCE/APPLICATION This hybrid method can quantify detectability differences between 2D and BT and allows investigation of influential parameters using real clinical backgrounds.

SSG15-05 • Digital Breast Tomosynthesis: Reader Study of the Effects of Acquisition Geometry on the Perception of Contrast-detail Test Objects

Mitchell M Goodsitt PhD (Presenter) * ; **Heang-Ping Chan PhD** ; **Lubomir M Hadjiiski PhD** ; **Emmanuel G Christodoulou PhD** ; **Sandra Larson PhD** ; **Paul L Carson PhD *** ; **Scott Zelakiewicz *** ; **Andrea Schmitz *** ; **Mark A Helvie MD *** ; **Chintana P Paramagul MD** ; **Colleen H Neal MD ***

PURPOSE

A reader study was performed to evaluate the impact of acquisition geometry (total angle and number of projection views (pv)) on the perception of contrast-detail (CD) objects in digital breast tomosynthesis (DBT).

METHOD AND MATERIALS

Modular breast phantoms consisting of slabs that mimic the composition and parenchymal pattern of breast tissue were imaged using a GE prototype DBT system. Two slabs, one with a homogeneous and one with a heterogeneous background were machined to include CD arrays of 25 holes, 1-5 mm in diameter and 0.2-1 mm in depth. Slabs were arranged to create 4 different 5cm thick phantoms with the heterogeneous CD slab and 1 with the homogeneous CD slab. Each phantom was imaged with 12 different acquisition geometries (total angles: 16-64°, pv: 9-21). Two acquisitions were repeated to study reproducibility. Identical x-ray technique factors were used with a mean glandular dose of a digital mammogram (~1.2mGy). Focal slices of the SART-reconstructed CD arrays were selected. 91 image pairs (IPs) were formed from the 14 geometries for each phantom, resulting in a total of 455 IP comparisons in a reader preference study. The IPs were randomized and evaluated by 4 trained readers on a 3 point scale (1= preferred image, 0.5=similar, 0=not preferred). The total % scores for all images and readings for each geometry were compared.

RESULTS

For the heterogeneous CD slab, the 3 highest scoring geometries and percent preferred were: 60°21pv(98%), 64°17pv(80%), and 48°17pv(71%). The lowest scoring were: 16°17pv(10%), 24°9pv(18%), and 24°13pv(35%). For the homogeneous CD slab, the highest scoring were: 60°21pv(87%), 32°17pv(82%), and 48°17pv(77%). The lowest scoring were: 16°17pv(1%), 40°11pv(18%), and 24°9pv(20%). Average % scores for repeat scans were within 4% in the homogeneous CD images and 7% in the heterogeneous CD images.

CONCLUSION

In general, CD objects are better perceived with wide-angle than narrow-angle DBT. For this study, the 60°21pv acquisition geometry yielded the best perception of CD objects. These results may be applicable to mass perception. The optimal acquisition geometry should be a compromise that accounts for perception of calcifications and soft tissue lesions and scan time.

CLINICAL RELEVANCE/APPLICATION

DBT systems can be designed with a range of acquisition angles and angle increments. This study demonstrates the perception of contrast-detail objects and possibly masses is best with wide-angle DBT.

SSG15-06 • Cascaded-systems Analyses for Describing the DQE of Low-Z, High-Z and Double-Z Detectors

Seungman Yun ; Jesse Tanguay ; Ho Kyung Kim ; Ian A Cunningham PhD (Presenter) *

PURPOSE

The development of theoretical models of x-ray interaction physics is a critical step in optimal detector design and assessment. While cascaded-systems analyses (CSA) are often used to describe image signal and noise in many systems, past work has considered detectors consisting of a single element (single Z) even though most commonly used and promising candidates are compound materials. In addition, the effects of coherent and incoherent scattering on image quality are usually ignored which can be a poor assumption in low-Z materials.

METHOD AND MATERIALS

A parallel-cascade approach is used to describe photoelectric, coherent and incoherent interactions in low-Z, high-Z and double-Z detectors. This is achieved using an energy-labeled reabsorption process introduced to describe incoherent scatter and allowing for reabsorption of the high-Z characteristic emission by the low-Z atom. Analytic expressions of signal and noise transfer are developed to describe the detective quantum efficiency (DQE) in terms of the modulation transfer function (MTF) and Wiener noise power spectrum (NPS). The model was validated using Monte Carlo calculations for Si, Se, CsI and PbI₂ and by experimental measurements of the DQE using narrow spectra above and below the K-edge energies with a high-resolution CMOS-based CsI detector. Results were compared with a simpler single-Z model to determine the need for the complex double-Z model in each case.

RESULTS

Excellent agreement was obtained with both Monte Carlo and experimental results for all conditions tested. It is shown that a combination of two single-Z models, weighted by the atomic weight of each material, gave equivalent results to the comprehensive double-Z model within a few percent. Incoherent interactions have the potential to produce a substantial low-frequency drop in the MTF and DQE of low-Z detectors.

CONCLUSION

These results show that combining two simple single-Z models is adequate for a description of the double-Z detectors and the effect of incoherent scatter must be considered for low-Z materials. We believe that this CSA model of the DQE is useful for an optimal design of conventional radiography detectors and the estimation of x-ray imaging performance of novel photoconductor materials.

CLINICAL RELEVANCE/APPLICATION

Development of comprehensive models of the DQE is necessary to ensure high quality images and low patient exposures with new detector designs.

SSG15-07 • Volumetric Breast Density Quantification Using Spectral Mammography

Sabee Y Molloy PhD (Presenter) * ; Huanjun Ding ; Elin Moa MS * ; Stephen A Feig MD *

PURPOSE

Breast density is a significant risk factor in developing breast cancer. Breast density is currently reported by radiologists using BI-RADS categories, which is known to have a large inter-observer variability. The purpose of this study is to evaluate spectral mammography for quantification of breast density.

METHOD AND MATERIALS

Four-view mammograms for 93 women from a previous study using a prototype Philips MicroDose Mammography SI system were used and all images were arranged in a random order for a blind comparison study. The system uses a photon counting detector to acquire energy resolved images in a single exposure with no additional dose to the patient. Four-category BI-RADS rankings were assigned independently by 10 radiologists based in the USA and the UK. The four-category ranking was converted to breast density scales (0 ~ 100%) using a linear relationship. Area-based breast density measurements were also performed by a physicist using Cumulus 4 and by an automatic image segmentation method based on a fuzzy C-mean clustering (FCM) technique. Volumetric breast density was calculated with a dual energy decomposition technique using the available spectral information. For all four techniques, the linear regression analysis was performed to investigate the correlation of the breast densities from the right and left breasts.

RESULTS

The breast densities from the right and left breasts showed a reasonably good linear correlation. The normalized variance about the best-fit line, which reflects the precision of the techniques, was estimated to be 8.4, 13.4, 6.1, and 1 for BI-RADS, Cumulus, FCM, and dual energy decomposition, respectively. This indicates that the variability in estimation of breast density is substantially lower using spectral mammography as compared with using BI-RADS, Cumulus and FCM in conjunction with standard mammography.

CONCLUSION

Spectral mammography may offer quantification of volumetric breast density with excellent precision during standard screening mammography. This will largely eliminate the inter- and intra-observer variability in the currently used BI-RADS ranking.

CLINICAL RELEVANCE/APPLICATION

Breast density quantification is useful for assessing the risk of developing breast cancer. Spectral mammography can be used for accurate quantification of breast density in screening mammography.

SSG15-08 • Clinical Potential of High-energy Phase Sensitive Mammography

Hong Liu PhD (Presenter) ; Xizeng Wu PhD

PURPOSE

The objective of this study is to demonstrate the potential clinical benefits of high kVp phase sensitive x-ray breast imaging through a comparison with conventional mammography.

METHOD AND MATERIALS

A contrast-detail phantom was imaged by an in-line phase sensitive x-ray imaging prototype and by a commercial digital mammography unit. The phase contrast prototype utilizes a microfocus x-ray source (50 um focal spot) operating at 120kVp and 4.5 mAs, and a CsI coated CMOS digital detector with a 50 um pixel pitch. In order to generate phase contrast, sufficiently large source to object and object to detector distances of 68.6 cm and 100 cm were used respectively. An innovative phase retrieval algorithm was applied to the acquired phase contrast images to generate phase-map images of the phantom. For a comparison, the same contrast-detail phantom was also imaged with a clinical GE Senographe DS flat panel digital mammography system, at 28 kVp and 54 mAs as well as 27 kVp and 131 mAs. The mean glandular doses with all images were calculated based on the measured exposure parameters and Monte Carlo simulations. The signal to noise ratio (SNR) of the target disks were measured, and observer-based subjective evaluations were also conducted to compare the disks detectability and absorbed doses of the high energy phase sensitive images and low energy conventional images.

RESULTS

For almost equal mean glandular doses, the measured disk SNR values were about three-times higher for the phase-map images than the images acquired with the clinical mammography system. Observer based contrast-detail analyses also demonstrated improved detectability by the high-energy phase sensitive images for both a similar and a reduced dose, as compared to the low energy conventional images.

CONCLUSION

This preliminary phantom study demonstrates the clinical potential of high-energy in-line phase sensitive mammography in improving the lesion detectability and reducing radiation dose to patients.

CLINICAL RELEVANCE/APPLICATION

The study demonstrates the technical feasibility and potential clinical benefits of high-energy phase sensitive x-ray imaging as compared to conventional digital mammography.

SSG15-09 • The Comparison between 2D Digital Mammography and Digital Breast Tomosynthesis for Morphological Assessment of Microcalcification Clusters: A Simulation Study

Eman Shaheen (Presenter) ; **Chantal Van Ongeval MD** ; **Federica Zanca PhD** ; **Lesley Cockmartin** ; **David Dance PhD** ; **Kenneth C Young PhD** ; **Hilde Bosmans PhD** *

PURPOSE

The detection and characterization of microcalcifications play an important role in the early diagnosis of breast cancer. Morphology and number of microcalcifications are two important determinative factors of the differential diagnosis between benign and malignant calcifications. Therefore, we focused on describing microcalcification clusters based on these parameters in a comparative study between 2D full field digital mammography (FFDM) and breast tomosynthesis (BT).

METHOD AND MATERIALS

Image data was collected from 46 patients. Fifty microcalcification clusters were simulated into raw projection images of 2D and BT at the same insertion positions for the same patient. The projections were then processed (2D) or reconstructed (BT). The simulated clusters were validated for realistic appearance by radiologists in a previous study where no significant difference was found between real and simulated clusters. In this study, six radiologists evaluated the clusters using the following parameters: morphology in terms of the Le Gal classification determining the dominant type, and the number of calcifications counted in the cluster. The 2D and BT images were read in separate sessions. The observed agreement and a corresponding p-value were reported for the dominant Le Gal type for every observer. The Wilcoxon rank test and linear regression were applied to compare the number of microcalcifications. P-value < 0.05 indicates significant difference.

RESULTS

For the dominant Le Gal, the observed agreements ranged from 0.34 to 0.84 and p-values from 0.076 to 0.611 indicating no statistically significant difference between 2D and BT for all observers. The Wilcoxon test showed significant differences, regarding the number of calcifications in 2D compared to BT, for all observers (p-values

CONCLUSION

Our results show that no significant difference was found comparing 2D FFDM and BT for the morphological description based on the Le Gal classification, but 2D outperformed BT in the number of microcalcifications. Further development in BT will address this.

CLINICAL RELEVANCE/APPLICATION

No systematic change in Le Gal classification was found between 2D and BT but the number of counted calcifications was lower in BT suggesting future clinical studies examine microcalcifications in BT.

Physics - Tuesday Posters and Exhibits (12:15pm - 12:45pm) Tuesday, 12:15 PM - 12:45 PM • Lakeside Learning Center

[Back to Top](#) [PH](#) **LL-PHS-TUA** • AMA PRA Category 1 Credit™:0.5 **Host Gregory S Karczmar**, PhD *

Host Xiaohong J Zhou, PhD

LL-PHS-TU10A • Statistical Analysis of Breathing Track Recorded with RPM Varian System of Patients Undergoing Gated SBRT

Dariusz Michalski (Presenter) *

ABSTRACT

Purpose: To statistically quantify the breathing track recorded during gated Stereotactic Body Radiation Therapy (SBRT), evaluate its spectral composition, entropy and signal complexity.

Method: Breathing track recorded with RPM gating (Varian Medical Systems) is used as tumor motion surrogate and controls gated SBRT. This methodology assumes the tumor and the surrogate motion correlation and the reproducibility of the breathing pattern. The time frame of gated SBRT might span even 30 minutes per fraction. This can introduce adverse changes in patients breathing, which is equivalent to changes in lung kinematics and tumor motion. 20 consecutive pairs of breathing tracks of 10 patients were evaluated. They were preprocessed before the analysis. Spectral content above 1 Hz was removed since this time scale do not correspond to breathing in a standard sense of respiratory lung's dynamics. The moving average filter spanning 1 second further smoothed the signal. The base line shift of the signal was equated with the signal spectral content below 0.1 Hz. The breathing track spectral Shannon entropy was computed for the 0.1-1.0 Hz range. The breathing track complexity was evaluated with Lempel-Ziv complexity (LZC) measure.

Results: Base line shift is the main source of variability in the breathing pattern of patients undergoing gated SBRT. Excluding sporadic bursts of the signal with analysis of its 95 percentile the base line shifts can exceed 0.5 cm. The signal is stationary. The normalized spectral Shannon entropy is at the level of 0.5. The breathing pattern does not exhibit random characteristics. It is deterministic. The normalized LZC starts around 0.15 for two symbol encoding. Increasing number of encoding symbols saturates this measure at 0.5-0.6. The variability of the end of inhalation can cause spectral perturbation that can be viewed as base line shifts.

Conclusions: Base line shifts are the main risk of affecting prolonged phase-based gated SBRT. The risk of their occurrence can be viewed as a time dependent systematic error. Deterministic characteristics of breathing patterns can help in its prevention.

Elements of irregularity in breathing can be caused by a chaotic component in the deterministic signal. This indicates that a new approach in tumor motion management can consider these features.

LL-PHS-TU1A • ECG Pad for Efficient Cardiac MR Gating

Nanda Deepa Thimmappa MD, MBBS (Presenter) ; **Mitchell Anthony Cooper** ; **Silvina P Dutruel MD** ; **Keigo Kawaji PhD** ; **Thanh D Nguyen PhD** ; **Yi Wang PhD**

PURPOSE

To assess the feasibility and reliability of ECG gated cardiac MRI with a simplified reusable electrode design that does not touch the skin.

METHOD AND MATERIALS

A silicon positioner holding up to 4 ECG leads was developed to allow detection of ECG signals from the back without requiring shaving, adhesive or even removal of the gown. The patient lies down on the device such that the patient's weight ensures good contact of the leads against the patient's gown and electrode Gel diffusing through the gown provides electrical contact with the skin (figure). Leads were tested at 1.5 T (GE Signa EXCITE) using axial double IR, SSFP, fgret perfusion, delayed IR. 12 subjects (Females: 5), mean age: 41 years (27-81yrs) were evaluated with both traditional disposable leads and this reusable ECG pad. Comparison of electrical signals and time for set up was recorded.

RESULTS

The total set up time (initial set up before the scan and time to take off the leads after scanning) was 7:24 minutes with the leads compared to 4:56 minutes with the pad with a mean difference of 2:28 minutes (31%, $p=0.005$). The ECG signal and image quality was comparable for the two techniques. Volunteers preferred the ECG pad, finding it to be comfortable and convenient.

CONCLUSION

This simplified approach to ECG gating is more convenient and comfortable for patients without sacrificing ECG signal quality.

CLINICAL RELEVANCE/APPLICATION

Robust and comfortable ECG gating with this reusable silicon lead holder that does not require skin contact improves cardiac gated MRI by eliminating uncomfortable disposable adhesive ECG leads.

LL-PHS-TU2A • Does the MR of Culture Negative Disc Space Infection Differ from Culture Positive Infections?

Shaoyin Duan (Presenter) ; **Gina Diprimio** ; **Mark E Schweitzer MD**

CONCLUSION

Conclusion: Patients with the culture negative disc space infection have obvious marrow edema and endplate erosion, more frequency of disc fluid and long complaint days and less frequency of facet fluid. Follow up MR at more than 1 month can find these lesions with significant absorption or shrinkage, while within 1 month follow-up maybe not.

Background

Objective: As many disc space infections are culture negative, as there is increasing evidence that a subgroup of end plate reactive changes actually represent indolent infections, we sought to compare the MR findings of disc space infections with and without positive cultures

Evaluation

Methods: the clinical and MR imaging of 26 patients with disc space infections, of which 9 cases (15 discs) who were blood and local tissue culture negative, and 17 cases (21 disc) who were culture positive, were retrospectively evaluated by two radiologists. All patients had the histological confirmation, the negative group have the follow up MR, performed within 1 month in 5 cases, 1-3 months in 7 and more than 3 months in 5 and responded appropriately to antibiotic treatment; the positive group were histological diagnosis as the acute inflammation. MR findings , epidemiology were compared. Statistical analysis consisted of T and chi squared tests

LL-PHS-TU3A • Pre-processing within a Breast MRI CADx System for the Initial Separation of Mass and Non-mass-like Lesions Prior to Computer Characterization

Hui Li PhD (Presenter) ; **Maryellen L Giger PhD *** ; **Li Lan** ; **Sunny Y Duan** ; **Stephan Hu** ; **Gillian M Newstead MD *** ; **Hiroyuki Abe MD** ; **Michelle Lindgren MD**

PURPOSE

To develop a pre-processing method for automatically identifying mass and non-mass-like lesions on breast MRI for subsequent separate analysis in the task of distinguishing between malignant and benign lesions

METHOD AND MATERIALS

Our dataset included 123 biopsy-proven lesions from 103 MRI studies acquired between January 2009 and April 2010, including 35 benign mass, 50 malignant mass, 11 benign non-mass-like and 27 malignant non-mass-like lesions. Each MRI underwent computerized 3D lesion segmentation and feature extraction to extract lesion characteristics of morphology, texture, and kinetics. Output from the system yielded the probability of the lesion being a mass (as opposed to a non-mass-like lesion) from a Bayesian artificial neural network (BANN). Classification performance was evaluated with a leave-one-case-out method using ROC analysis with area under the ROC curve as the figure of merit.

RESULTS

The classifier's performance gave an AUC value of 0.93 ($SE=0.02$) in the task of differentiating mass lesions from non-mass-like enhancement breast lesions. The main lesion features incorporated into the classifier included Sphericity (shape), Time to Peak (kinetic), Variance (texture), Sum Entropy (texture), and Average Gray-Level (texture). Also, incorporation of the pre-processing step in our CADx algorithm yielded a statistical significant improvement in the malignant and benign classification task. AUC values of 0.88 ($SE=0.03$) and 0.95 ($SE=0.02$) were obtained in the task of distinguishing between malignant and benign lesions on the entire dataset and mass lesions only (p -value=0.04).

CONCLUSION

Automated quantitative image analyses of breast MRI can yield features sufficient for identifying lesions as mass or non-mass-like lesions prior to application of CADx algorithms.

CLINICAL RELEVANCE/APPLICATION

In order to improve CADx diagnostic accuracy, computer algorithms (as do radiologists) should recognize lesions as mass or non-mass-like lesions prior to assessing likelihood of malignancy.

LL-PHS-TU4A • Metal Artifact Reduction in Computed Tomography for Assessment of Lead Extraction in Patients with Implantable Cardiac Defibrillator (ICD)

Aaron So PhD (Presenter) ; **Simon Modi** ; **James White MD** ; **Raymond Yee** ; **Aashish Goela MD** ; **Ting-Yim Lee MSc, PhD ***

PURPOSE

Patients with ICD may require lead extraction if there is presence of lead fibrosis and calcification but such procedure requires specialist equipment and skills and is associated with high mortality. We investigated the effectiveness of several image acquisition, reconstruction and processing methods for metal artifact reduction in CT to facilitate its use for pre-procedural identification of lead calcification.

METHOD AND MATERIALS

A dual coil ICD lead (St Jude Medical) with radiopaque beads attached was inserted into the right ventricle of an excised pig heart. The heart was filled with water and scanned in approximately the same orientation as in patients with a single energy CT (SECT) protocol using 120 kV, 120 mAs and 0.625 mm collimation on a Discovery 750HD scanner (GE Healthcare). The scan was repeated with a dual energy CT (DECT) protocol using 140/80 kV alternating every 0.2 ms and 210 mAs. Three sets of 0.625-mm-thick cardiac images were generated using the DECT scan data: (1) monochromatic 70 keV, (2) 70 keV plus ASIR (Adaptive Statistical Iterative Reconstruction), (3) 70 keV plus MARS (Metal Artifact Reduction Software, GE). Image set (1) to (3) were used to reduce artifacts from beam hardening, projection noise and projection truncation induced by the lead respectively. Artifacts in each image set were compared against those in the 0.625 mm and 10 mm averaged SECT images.

RESULTS

DECT 70 keV and 70keV+ASIR images manifested intense shading and streaking artifacts that were minimally different from those of the 0.625 mm SECT image and the lead was not visible in all these images. 70keV+MARS image exhibited less artifacts but the lead region was invisible. The 10 mm averaged SECT image showed the least artifacts while the lead with the attached beads was clearly seen.

CONCLUSION

DECT+MARS showed better artifact removal than DECT without MARS or with ASIR suggesting projection truncation was the dominant cause of the lead artifacts. However, MARS is unable to restore the lead image adequately. The averaging method cancelled out the artifacts while restoring the lead image with minimal compromise of the axial resolution.

CLINICAL RELEVANCE/APPLICATION

Lead extraction is complicated and associated with significant mortality and morbidity. The proposed method facilitates the use of CT for assessing lead calcification and the need of lead extraction.

LL-PHS-TU5A • Does Iterative Reconstruction Lower CT Radiation Dose: Evaluation of 15000 Examinations

Peter B Noel PhD (Presenter) ; **Bernhard C Renger** MSc ; **Martin Fiebich** ; **Alexander A Fingerle** MD ; **Daniela Muenzel** MD ; **Martin Dobritz** MD ; **Ernst J Rummeny** MD

PURPOSE

Evaluation of 15000 computed tomography (CT) examination to investigate if iterative reconstruction (IR) reduces sustainably radiation exposure.

METHOD AND MATERIALS

Information from 15000 CT examination were collected, including all aspects of the exams such as scan parameter, patient information, and reconstruction instructions. The examinations are acquired between January 2010 and December 2012, while after 15 month a first generation IR algorithm was installed on a 256-slice MDCT. To collect the necessary information from PACS, RIS, MPPS and structured reports a Dose Monitoring System (DMS) was developed. To harvest all possible information an optical character recognition system was integrated, for example to collect information from the screenshot CT-dose-report. The tool transfers all data to a database for further processing such as the calculation of effective dose and organ doses. To evaluate if IR provides a sustainable dose reduction the effective dose values were statistically analyzed with respect to protocol type, diagnostic indication, and patient population.

RESULTS

CONCLUSION

Iterative reconstruction algorithms reduce sustainably and significantly radiation dose in the clinical routine. The amount of radiation dose reduction cannot be generalized to a fixed amount since the initial dose depends on the diagnostic indication and protocol design.

CLINICAL RELEVANCE/APPLICATION

The dose aspect remains a priority in CT research. Our results illustrate that not only in studies with a limited number of patients but in the clinical routine IRs provide long-term dose saving.

LL-PHS-TU6A • Artifact Analysis in Digital Breast Tomosynthesis (DBT)

Paola Enrica Colombo (Presenter) ; **Lorenzo Radici** ; **Stefano Pasetto** ; **Annalisa Trianni** ; **Alberto Torresin** MPH

PURPOSE

Digital Breast Tomosynthesis (DBT) systems have been recently introduced. Limited angular sampling is responsible for ghost artifacts in off-focus planes: an object is visible very far from the in-focus plane. In this work a methodology and special designed phantom for full characterization of DBT artifacts are presented and applied to three commercial systems (Hologic, Siemens, IMS).

METHOD AND MATERIALS

The methodology proposed describes the artifacts behaviour in off-focus planes by means of:

- artifact punctual propagation in z-direction using the Artifact Spread Function (ASF) (WU (2004));
- integral information of the dishomogeneity produced by artifact evaluating standard deviation of a suitable ROI containing both ghost feature and background.
- artifact geometric extension in tube-motion direction by measuring artifact line profiles;

A gel phantom containing spherical features of various materials and diameters is developed. Parameters are expressed as function of vertical plane position.

RESULTS

ASF depends linearly on sphere diameter but not on sphere material (contrast) and it is affected on system's angular range. The Standard Deviation parameter depends on sphere diameter but also on contrast and the trend is different for the three systems. Profiles extension shows different behaviour for the three systems and doesn't depend on sphere diameter and contrast.

CONCLUSION

ASF, standard deviation of a suitable ROI and profile analysis are an adequate set of measurements to describe artifact behaviour, which depends mainly on systems design.

CLINICAL RELEVANCE/APPLICATION

Artifacts are always visible in Digital Breast Tomosynthesis images. Their extent depend mainly on system design.

LL-PHS-TU7A • MR-T2-weighted Signal Intensity: A New Imaging Marker of Prostate Cancer Aggressiveness

Anna Vignati (Presenter) ; **Valentina Giannini** ; **Simone Mazzetti** ; **Filippo Russo** MD ; **Christian Bracco** PhD * ; **Michele Stasi** ; **Daniele Regge** MD

PURPOSE

Improving accuracy of risk assessment in prostate cancer (PCa) patients represents today a compelling clinical need. While it is well known that PCa usually shows a lower signal intensity (SI) than non-neoplastic prostatic tissue on T2-weighted (T2w) magnetic resonance imaging (MRI), its value in differentiating PCa aggressiveness is unknown. The propose of this study is to investigate if T2w SI correlates with the pathological Gleason Score (pGS), the reference standard for measuring the biological activity of PCa.

METHOD AND MATERIALS

The study dataset comprises 31 men (64 y, mean age) with biopsy proven PCa including: 9 men with pGS 3+3 tumours, 11 with pGS 3+4, 5 with pGS 4+3, and 6 with pGS 4+4. All patients underwent multiparametric MRI with a 1.5 T scanner and endorectal coil, including a T2w axial scan (TR/TE, 2960/85 ms; FOV, 16 cm; slice thickness, 3 mm; acquisition matrix, 384 x 288). Data were processed with in-house developed software packages based on C++ algorithms and ITK libraries. First, intensity inhomogeneity correction field was performed by the combination of a phantom intensity profile and a proper median smoothing of the original T2w image. Second, from the central 2D image of the T2w volume, the coil was segmented by a Hough transformation. Finally, a k-means algorithm and morphological operations were performed to automatically extract the obturator muscles (OBT). The T2w volume was then normalized by the median value of the OBT. The Pearson correlation coefficient (R) was calculated to assess if there was a correlation between tumour aggressiveness, based on pGS, and T2w signal.

RESULTS

Mean value \pm SD of T2 values for the different pGS group were: 2.63 \pm 0.67 for pGS 3+3; 2.19 \pm 0.57 for pGS 3+4; 1.74 \pm 0.31 for pGS 4+3; 1.81 \pm 0.13 for pGS 4+4. R showed a moderate correlation (R=-0.63) between tumours with pGS 3+3 and those with 4+4.

CONCLUSION

Preliminary findings suggest that T2 SI could be a reliable imaging marker to predict PCa risk of progression. T2 SI may be

considered as an additional feature in computer-aided diagnosis (CAD) schemes.

CLINICAL RELEVANCE/APPLICATION

An imaging marker of cancer aggressiveness, measurable before surgery, could contribute to stratify patients with PCa according to their progression risk, thus improving individual treatment strategy.

LL-PHS-TU8A • In Ovo Serial Monitoring of Different Organ or Tissue's Structural Evolvement in Developmental Chicken Embryo Using DTI

Zien Zhou MD (Presenter) ; Weiwei Ma ; Lei Li ; Jia Hua ; Jianrong Xu ; Jiani Hu ; Wenjin Wang ; Yunqi Yan

PURPOSE

The purpose of this study is to monitor different organ or tissue's structural evolvement(hind limb, gizzard, heart, brain and eye) serially in chicken embryo during development using DTI.

METHOD AND MATERIALS

Eight fertile Hy-Line White eggs were placed into an automatic digital incubator with temperature (37.8°C) and humidity (60%). From days 6 to 18, five normally developing eggs were scanned every 24 hours(T2WI and DTI). The dual-cooling technique(eggs were cooled at 4°C for one hour before imaging and wrapped in a piece of Techni-Ice during imaging) was used to suppress motion artifact. MR scans were performed using the 3.0 T Philips Achieva System(Philips Medical Systems, Best, Netherlands) with a four-channel dedicated animal coil. The sequence parameters of T2WI and DTI are shown in table 1. All imaging planes were sagittal. Different organ and tissues(hind limb, gizzard, heart, brain and eye) were recognized according to the anatomical position and signal difference in T2WIs, which were also used to guide the placement of ROIs for DTI analysis. FA was automatically calculated using the Dti-Studio v2.4 software (Johns Hopkins University, USA). Three ROIs were put in each organ or tissue, and the average FA was used as the structural anisotropy of that organ or tissue. The incubation day-dependent changes in structural anisotropy of these organs were obtained according to the average data of all five embryos in every experimental day.

RESULTS

The average FAs of the five eggs in hind limb, gizzard, heart, brain and eye from day 6 to 18 are shown in table 2. The gizzard in day 6 and the heart in day 6,7,8,9 is too small to be discriminated in DTI. The incubation day-dependent linear regression of structural anisotropy in these organ or tissues is shown in figure 1. The FA value shows a progressive linear increase in hind limb, gizzard, heart and brain with the increasing days of incubation, and the FA value in eye shows no change. Figure 2 is an example of ROIs drawing in hind limb, gizzard, heart, brain and eye according to T2WI and corresponding FA maps of DTI at incubation day 12, 14,17.

CONCLUSION

MRI has the potential to observe the structural development of different organ of tissue in chicken embryo without sacrifice for histological examination.

CLINICAL RELEVANCE/APPLICATION

A widely-available (3.0 T) MRI system can be used as a powerful investigative tool to evaluate embryonic development with DTI.

LL-PHS-TU9A • Impact of Breast Glandular Description on Average Glandular Dose and Radiation Risk Assessment in Mammography

Nausikaa Geeraert MSc, DiplPhys (Presenter) * ; Remy Klausz DiplEng * ; Lionel Desponds PhD * ; Serge L Muller PhD * ; Isabelle Bloch ; Hilde Bosmans PhD *

PURPOSE

Originally introduced by Hammerstein in 1979 for comparing doses delivered with different radiographic techniques to the average breast in mammography, Average Glandular Dose (AGD) is the dosimetry quantity generally recommended for collective risk assessment. Conversion factors from Entrance Surface Air Kerma (ESAK) to AGD were computed by different authors using Monte Carlo computation on reference breast models of homogeneous glandularity. We want to investigate more in detail AGD applicability to individual risk assessment and in particular the influence of the breast glandular quantity and distribution.

METHOD AND MATERIALS

Four semi-cylindrical phantoms are defined. Phantom 1 is the reference breast model used by Dance (1990), i.e. 8 cm radius, 45 mm thick, 10 mm skin, 50% homogeneous glandularity intra-skin. Phantom 2 differs from 1 by a doubled surface (11.3 cm radius). Phantom 3 glandularity is 0%, Phantom 4 has 50% average intra-skin glandularity, but contains a 75cm² x 3.5cm region with 59% glandularity embedded in 0% glandularity resulting in a surfacic glandularity (SG) of 75%, a peak glandularity (PG) as used by the automatic exposure control of 46%, a thickness-based glandularity (TG) from tables in Dance (2000) of 41% and an image-based VG of 34% including skin. AGDs are compared for the same exposure (0.45 mm Al Half-Value-Layer) resulting in an AGD of 1mGy for phantom 1.

RESULTS

AGDs are 1mGy (phantoms 1 and 2), 1.2mGy (phantom 3). AGD for phantom 3 is the highest in spite there is no glandular tissue at risk. AGD for phantom 2 is the same as phantom 1; however the quantity of glandular tissue at risk is doubled. AGD of phantom 4 depends on the selected glandularity: 0.90 mGy (SG), 1.03 mGy (PG), 1.05 mGy (TG) and 1.08 mGy (VG).

CONCLUSION

As shown by our phantom studies, AGD does not reflect the individual risk. For AGD computation the glandular content is not correctly described by a single quantity. Recently developed mammographic image-based glandularity computation methods could be used to improve the AGD computation. Moreover access to the description of glandular quantity and distribution will make the practical development of metrics for individual risk assessment possible.

CLINICAL RELEVANCE/APPLICATION

Demonstrate limitations of the current use of AGD and propose improvements to individual radiation risk assessment using image-based volumetric glandularity computations.

Physics - Tuesday Posters and Exhibits (12:45pm - 1:15pm) Tuesday, 12:45 PM - 01:15 PM • Lakeside Learning Center

[Back to Top](#) **LL-PHS-TUB** • AMA PRA Category 1 Credit™:0.5

LL-PHE-TU10B • New Generation Coronary and Aortic CT Scanners: What the Radiologist Needs to Know

Anand Narayan MD, PhD (Presenter) ; Pamela T Johnson MD * ; Mahadevappa Mahesh MS, PhD * ; Elliot K Fishman MD * ; Stefan L Zimmerman MD

PURPOSE/AIM

State of the art MDCT technology to evaluate coronary arteries and the aorta include high pitch CT scanners and wide area detectors. These two technologies use different strategies to capture a fast moving heart in a single rotation or a single heart beat. The aim of this exhibit is to review the physics underlying these new CT scanners and familiarize readers with information necessary to guide scanner selection and protocol optimization to best take advantage of these new systems.

CONTENT ORGANIZATION

1. Introduction

- Review of relevant basic CT physics
- Technological challenges in evaluating coronaries and aorta

2. Next generation CT scanners- review of scanner hardware and physics

- High pitch CT scanners
- Wide area detector scanners
- Dual energy CT

3. Relative advantages and disadvantages of next generation scanners

- Temporal and spatial resolution optimization
- Dynamic perfusion imaging
- Radiation dose reduction
- Dual energy cardiovascular applications

4. Imaging protocols

SUMMARY

After reviewing this exhibit, readers will gain an understanding of the principles behind the newest generation CT technology for evaluating the coronary arteries and the aorta, the advantages and disadvantages of these technologies, as well as protocol optimization to maximize utility of these new scanners.

LL-PHS-TU1B • Development of Cranial MRI-Phantom for Assessing Perfusion, Diffusion, and Fluctuation

Tomohiro Chigusa ; Tosiaki Miyati PhD ; Naoki Ohno MS ; Hikari Usui ; Shinnosuke Hiratsuka (Presenter) ; Hirohito Kan ; Toshifumi Gabata MD ; Osamu Matsui MD

PURPOSE

To clarify relations and mechanisms among blood-perfusion, water-diffusion, water-fluctuation, and biomechanics of the intracranial tissue, we developed an original cranial phantom for magnetic resonance imaging (MRI).

METHOD AND MATERIALS

The new cranial phantom consisted of a high-density polypropylene filter (filtration accuracy of 0.5 μ m, apparent diffusion coefficient [ADC] of 1.3×10^{-5} mm²/s) with intra- and extra-filter spaces, and a capacitor space, which were filled with water at 17 degrees centigrade. These correspond to a brain parenchyma, artery and vein, and cerebrospinal fluid space, respectively. Then, volume loading was periodically applied to the cranial phantom by a pulsation flow (simulated cerebral blood flow) pump. Under these conditions, on a 3.0-T MRI, we determined the regional phantom flow and the ADC change (water-fluctuation) in the pulsation period using pseudo-continuous arterial spin labeling and ECG-triggered multi-phase single-shot diffusion echo planer imaging with multi-b (16 points), respectively. Moreover, we compared those values with trans-cranial phantom flow obtained with phase contrast cine MRI and actual pressure wave in the phantom.

RESULTS

The ADC change during the pulsation period in the filter was synchronized with the trans-cranial phantom flow and actual pressure wave in the phantom, indicating water-fluctuation are affected by biomechanical properties. The regional phantom flow agreed with the trans-cranial phantom flow and the ADC change. Moreover, ADC calculated with lower b-values (0 to 160 s/mm²) depended on the regional phantom flow.

CONCLUSION

Our original phantom makes it possible to clarify relations and mechanisms among blood-perfusion, water-diffusion, water-fluctuation, and biomechanics of intracranial tissue. Perfusion, diffusion, fluctuation, and biomechanics of the intracranial tissue interact in diverse ways.

CLINICAL RELEVANCE/APPLICATION

Our original phantom makes it possible to clarify relations and mechanisms among blood-perfusion, water-diffusion and fluctuation, and biomechanics of the intracranial tissue.

LL-PHS-TU2B • Improvement of CAD Scheme for Detection of Silent Lacunar Infarcts on MR Images by Using Template Matching on Eigen Space

Yoshikazu Uchiyama (Presenter) ; Chisako Muramatsu PhD ; Takeshi Hara PhD ; Junji Shiraishi * ; Hiroshi Fujita PhD

PURPOSE

The detection of asymptomatic lacunar infarcts is important because their presence indicate an increased risk of severe cerebral infarction. However accurate identification of lacunar infarcts on MR images is often hard for radiologists because of the difficulty in distinguishing lacunar infarcts and enlarged perivascular spaces. Therefore, we have been developing CAD schemes for the detection of lacunar infarcts. Our previous method was applied to 132 patient cases and the sensitivity of 96.8% with 0.71 FP per slice was obtained. However, further reduction of FPs was remained as an issue to be solved for the clinical application. The purpose of this study is to improve our CAD scheme for detection of lacunar infarcts by use of a template matching technique on eigen space.

METHOD AND MATERIALS

Our database consisted of T1- and T2-weighted images obtained from 132 patients, which included 93 lacunar infarcts. The images were acquired on a 1.5 T MR scanner. Using our previous method, almost all lacunar infarcts were detected accurately. However, 753 FPs were obtained. For reduction of these FPs, we employed template matching technique. Although the conventional template matching is useful for the reduction of FPs, it has 2 pitfalls. (1) It needs to keep a large number of templates for improving the detection performance. (2) The calculation of the cross-correlation coefficient with these templates takes much time. To solve these problems, we used template matching in the lower dimension space made by a principal component analysis.

RESULTS

Our computerized method was evaluated by using 2-fold cross validation. By using the proposed method, 34.1 % of FPs were eliminated. The final performance indicated that the sensitivity of the detection of lacunar infarcts was 96.8% (90/93) with 0.47 FP per slice.

CONCLUSION

By using the proposed method, the quantity of the template became 1.9 % of conventional template matching. The computation time could be shortened largely. Moreover, the number of FPs was decreased from 0.71 to 0.47 per slice while keeping the same sensitivity of 96.8 %. Therefore, the proposed method is useful technique in the CAD scheme for the detection of lacunar infarcts on MR images.

CLINICAL RELEVANCE/APPLICATION

Our CAD scheme can output locations of lacunar infarcts with a small number of FPs, and would be useful in assisting radiologists for identifying lacunar infarcts on MR images.

LL-PHS-TU3B • Fully Automated Segmentation of Whole Breast in MR images Using Dynamic Programming

Luan Jiang PhD ; Yanyun Lian ; Yajia Gu MD ; Xiaoxin Hu ; Qiang Li PhD (Presenter) *

PURPOSE

We are developing a computer-aided diagnostic (CAD) scheme for breast cancer diagnosis, risk assessment, and density analysis in

magnetic resonance (MR) image. This study is to develop a key technique in the CAD for accurate segmentation of the whole breast.

METHOD AND MATERIALS

We obtained 37 clinical transverse breast MR scans from Shanghai Cancer Hospital in China. All images were fat-suppressed T1-weighted MR acquired with an Aurora 1.5-T MR scanner. The image size was 512×512×256 and the resolution in x, y, z axis was 0.7031 mm after linear interpolation in z axis. Sixteen breasts in 8 cases were manually delineated by a physicist and confirmed by a radiologist for objective evaluation of three-dimensional (3-D) segmentation method. We first developed techniques to determine a bounding box for a breast and to extract the major part of the breast by use of a 3-D spiral scanning method and dynamic programming. A small portion of the breast around the pectoral muscle was not included in the initial segmentation result. We then further developed a technique to delineate the chest wall and to add the missing small portion of the breast back to the major portion. A sectional dynamic programming method was designed in each 2-D slice of a 3-D MR scan to trace the upper and/or lower boundaries of the chest wall. Our method also took advantages of the continuity of chest wall across adjacent slices. The performance level of the whole breast segmentation method was subjectively observed by human readers, and was evaluated by objective indices of Dice overlap measure and volume agreement.

RESULTS

By subjective observation of the 37 cases, we found that the proposed method obtained good segmentation of the whole breasts. By comparing with the manually delineated region of 16 breasts in 8 cases, an overlap index of 90.5% ± 2.6% (mean ± SD), and a volume agreement of 96.2% ± 3.5% were achieved, respectively.

CONCLUSION

The fully automated method for accurate segmentation of the whole breast would be useful for developing CAD systems for risk assessment and early diagnosis of breast cancer in MRI.

CLINICAL RELEVANCE/APPLICATION

Our CAD scheme could help the radiologists to quantitatively analyze breast cancer risk and to improve the accuracy and efficiency of breast cancer diagnosis.

LL-PHS-TU4B • Type Discrimination of Calcifications by Phase Images of Magnetic Resonance Imaging Using a Breast Phantom

Katsuhiko Kida (Presenter) ; **Sachiko Goto** ; **Tomoka Doi** RT, BS ; **Masaki Ikeda** RT, BS ; **Tsutomu Kajitani** ; **Yoshiharu Azuma** PhD

CONCLUSION

It was suggested that the discrimination between calcium oxalate and phosphate is possible by measuring the slope of linear approximation of phase values of calcifications obtained by changing TE on high-pass filtered phase images.

Background

In mammography, the presence of microcalcifications in breast tissues is of great importance since microcalcifications are mammographic characteristics of early breast cancer. The microcalcifications in breast disease have two distinct types, calcium oxalate and phosphate. It has been reported that microcalcifications with calcium oxalate were found only in benign cysts, whereas microcalcifications with calcium phosphate were associated with benign or malignant lesions. We previously reported the detection of clam shell (as simulating calcification) using high-pass filtered phase images of MRI. In this study, we furthermore discriminated the two types of calcifications of known components.

Evaluation

A cup shaped gel phantom, containing calcium materials of known components which are 4 kidney stones of calcium oxalate, a kidney stone of calcium phosphate and a tooth, was made to simulate calcification in the breast. A tooth was employed as a comparison since its enamel has a high content of calcium phosphate. The slopes of linear approximation of phase values obtained by changing from 4.6 to 20.7 msec at 2.3 msec in-phase intervals were newly employed for type discrimination of calcifications in 3.0-T MR system.

Discussion

On the high-pass filtered phase image, calcium oxalate and phosphate were detected as hyperintense area. Furthermore, the phase values became higher as TE became longer. The slope of linear approximation of the calcium oxalate was larger than the calcium phosphate. The result indicates that calcium oxalate and phosphate are distinguishable with the slope of linear approximation. The diameters of stones were about 5 mm to 10 mm. This method might be useful for the discrimination between benign and malignant breast disease, although we need to discriminate smaller sizes of calcifications.

LL-PHS-TU5B • Improvement on Chest Digital Tomosynthesis Using Dual-view Geometry

Yuncheng Zhong PhD (Presenter) ; **Chao-Jen Lai** PhD ; **Youtao Shen** ; **Chris C Shaw** PhD *

PURPOSE

Digital tomosynthesis (DTS) is able to crudely separate the overlapping anatomical structures on chest radiography. However, the resolution in the posterior-anterior (PA) view is quite limited due to the nature of DTS. Furthermore, the spillover of high-contrast objects from off-fulcrum planes generates artifacts. We demonstrate that by applying a dual-view DTS on chest imaging, the spatial resolution in PA direction is improved and the artifacts are alleviated.

METHOD AND MATERIALS

We proposed a dual-view DTS technique in which projection images are acquired in two orthogonal views and reconstructed using an iterative method. We acquired cone beam CT images of an anthropomorphic chest phantom with 300 projections and an angular step size of 1.2°. The experiment was carried out using 120kVp, 40mA continuous mode x-ray, with source-to-detector distance of 180cm. The flat panel detector had a pixel size of 0.2mm. The dual-view DTS images were extracted from the CBCT images with different angular ranges and step sizes to investigate the effects of these parameters. We extracted the DTS data with the angular ranges of 30° and 60° respectively, each of which was using 1.2° and 2.4° angular step sizes. Single-view DTS images were also extracted and reconstructed for comparison. Visual inspection as well as the quantitative analysis of root-mean-squared-deviation (RMSD) and the thick slice thickness were used for evaluation.

RESULTS

The dual-view DTS images were fairly accurate in depicting the shape and dimensions of the anatomy in the fulcrum, especially for the sagittal views. The RMSD values calculated on different regions demonstrated the improvement of the image quality in dual-view DTS over single-view DTS. The thick slice thickness was greatly reduced for dual-view DTS. Our results also demonstrated that the RMSD and thick slice thickness with 60° angular range was better than with 30° angular range, and the a smaller angular step size with the same angular range resulted better quality images.

CONCLUSION

With a similar number of projections, dual-view DTS can render more accurate 3D images than single-view DTS does. This work was supported in part by research grants CA124585 and CA138502 from NIH-NCI.

CLINICAL RELEVANCE/APPLICATION

The applying of dual-view DTS technique provides better image quality and spatial resolution in chest imaging.

LL-PHS-TU6B • ICRP103 Effective Dose vs DLP vs SSDE: Which Is a More Clinically Useful and Sensitive Tool for Identifying Radiation Dose Outliers?

PURPOSE

Comparing the ability of ICRP 103 effective dose (ED), dose-length product (DLP) and size-specific dose estimate (SSDE) to identify patients scanned with above-expected radiation dose.

METHOD AND MATERIALS

Abdominopelvic CTs from July 2012 to March 2013 performed on 64-slice (Sensation 64, Siemens) scanners were reviewed. All scans were acquired using standard departmental protocol with tube current modulation. Parameters (mean mAs, kVp, scan length, effective patient diameter) and dose metrics (CTDIvol, ED, SSDE, DLP, organ doses) for these scans were extracted using commercial software (eXposure, Version 1). All patients who underwent the CT scan with doses = or = 2 standard deviations (SD) beyond the mean DLP, ED and SSDE were identified and assessed. The mid slice effective diameter was also manually calculated using $vAP*Lat$ (where AP=anteroposterior diameter and Lat=transverse diameter) for a subset of patients.

RESULTS

1685 exams were included in the study. The mean DLP, ED and SSDE for these studies were 734.7 ± 338.5 mGy-cm, 13.2 ± 6.4 mGy-cm and 15.6 ± 3.8 mGy. The scans with dose = 2 SD [DLP 1411.6 (35; 6M, 29F); ED 25.9 (29; 12M, 17F); and SSDE 23.1 (47; 7M, 40 F)] or = 2 SD [DLP 57.8 (none); ED 0.5 (none); and SSDE 8 (4; 1M, 3 F)] were identified. The effective diameter for the subset of patients with dose = 2 SD of mean SSDE was statistically similar to the automated values ($p=0.34$). The 4 patients with = 2 SD of mean SSDE were very small patients. For dose = 2 SD, DLP (12/29) and ED (11/35) mostly identified patients with repeat series while the SSDE mostly identified patients scanned with arms by the side (24/47) or off centering (17/47) as the cause of high radiation dose. The organ specific ED for liver and urinary bladder demonstrated best correlation with ED (0.99, 0.98) followed by DLP (0.95, 0.97). SSDE showed the least correlation (0.86, 0.86) which dropped as the SSDE increased (for = 2 SD, correlation dropped to 0.26 and 0.32 for liver and bladder organ dose respectively).

CONCLUSION

SSDE identified the largest number of patients with above-average radiation dose and is a more sensitive indicator of patient positioning and attenuation in the field of view. DLP and ED are more sensitive indicators of scan length.

CLINICAL RELEVANCE/APPLICATION

SSDE, DLP and ED are influenced by different scanning parameters, and should be used appropriately to study the influence of a particular parameter.

LL-PHS-TU7B • A Novel Implementation of X-ray Differential Phase Contrast CT Imaging without Talbot-Lau Interferometer: Principles and In Vivo Animal Studies

Ke Li MS (Presenter) ; Stephen T Brunner BS ; Yongshuai Ge ; John W Garrett MS * ; Guang-Hong Chen PhD *

PURPOSE

The recently proposed method to achieve X-ray differential phase contrast CT (DPC-CT) imaging using a grating Talbot-Lau interferometer has not had success in achieving in vivo DPC-CT scans. A novel method is proposed to achieve DPC-CT imaging without grating interferometer and used for in vivo imaging.

METHOD AND MATERIALS

A calibration phantom (12.7 cm diameter) containing several insertions with known electron density was scanned using a 64-slice Discovery CT 750HD scanner to obtain electron density imaging of the phantom. The same phantom was scanned using a tabletop DPC-CT data acquisition system with grating interferometer to obtain DPC-CT imaging. The DPC-CT image values were calibrated to generate the corresponding electron density imaging. The calibration coefficients (at the effective energy of 28 keV) obtained from the benchtop grating based DPC-CT system were used to calibrate the electron density obtained from the dual energy CT scan into the corresponding DPC-CT image values. In vivo canine and porcine studies were performed to generate DPC-CT images at 28 keV effective energy.

RESULTS

DPC-CT image values measured from grating based DPC-CT system and the proposed method are given as the following pairs: Polymethyl methacrylate ($3.32e-7$, $3.33e-7$); Polytetrafluoroethylene ($5.49e-7$, $5.19e-7$); Polyoxymethylene ($3.94e-7$, $3.91e-7$); GAMMEX Adipose ($2.72e-7$, $2.74e-7$); GAMMEX Liver ($3.16e-7$, $3.22e-7$). Linear regression of the DPC-CT image values obtained from the two methods has a coefficient of determination of 0.998. The slope of the regression was used to calibrate the electron density imaging from animal experiments to generate DPC-CT imaging in vivo.

CONCLUSION

DPC-CT imaging can be achieved in vivo from a clinical dual energy CT scanner with high accuracy and at any target X-ray beam energy.

CLINICAL RELEVANCE/APPLICATION

DPC-CT images generated from DECT may provide immediate new diagnostic information for soft tissues without the complication of modifying hardware. This may open up a new venue for cancer detection.

LL-PHS-TU8B • Diffusion Kurtosis in the Vertebral Bone Marrow

Tomohiro Noda (Presenter) ; Tosiaki Miyati PhD ; Naoki Ohno MS ; Harumasa Kasai MSc ; Nobuyuki Arai MS ; Risa Yorimitsu ; Makoto Kawano ; Yuta Shibamoto MD, PhD

PURPOSE

To assess the structure of cancellous tissue in the vertebral bone marrow, we analyzed the restricted diffusion using diffusion kurtosis.

METHOD AND MATERIALS

On a 1.5 T MRI, single-shot diffusion echo planar imaging was used with b values of 0, 20, 120, 500, 1200 and 2200 s/mm², and a sensitivity encoding technique. Apparent diffusion kurtosis (K_{app}) and apparent diffusion coefficient (D_{app}) were calculated from diffusion kurtosis analysis based on non-Gaussian diffusion theory. K_{app} and D_{app} were determined in the lumbar vertebral body of seven normal subjects, and then compared with the bone mineral density (BMD) obtained with dual-energy X-ray absorptiometry (DXA). Moreover, fat fraction (FF) of the bone marrow was measured with spectral presaturation with inversion recovery in the same subject.

RESULTS

A strong positive correlation was found between K_{app} and BMD in the vertebral bone marrow ($R^2=0.76$, P_{app} and FF in this region, showing the dependence on trabecular architecture. However, there was no significant correlation between D_{app} and BMD, indicating the greater utility of the K_{app} than that of the D_{app} .

CONCLUSION

Water-restricted diffusion analysis with diffusion kurtosis makes it possible to obtain more detailed information on the structure of cancellous tissue and the bone metabolism.

CLINICAL RELEVANCE/APPLICATION

Diffusion kurtosis analysis increases the amount of bone metabolic information, and may be useful for assessing bone aging, early degeneration in the cancellous tissue and diagnosis of osteoporosis.

Lukas Havla (Presenter) ; **Michael Peller** DPhil ; **Konstantin Nikolaou** MD * ; **Maximilian F Reiser** MD ; **Olaf Dietrich** PhD

CONCLUSION

The transformation of DECT attenuation data into polar coordinates exhibits the potential to improve tissue visualization and material decomposition.

Background

Dual-energy computed-tomography (DECT) allows for patient examination with two different x-ray spectra at the same time. Thereby, independent data on material-specific attenuation properties are obtained. The separate evaluation of both datasets can be difficult and non-conclusive; particularly, for DECT data with contrast media enhancement, material decomposition in the relevant scale of ± 200 HU is challenging due to similar attenuation coefficients of calcium and iodine. We hypothesize that the transformation of dual-energy data into polar coordinates can ease analysis and help to distinguish between concentration and kind of matter.

Evaluation

Given two corresponding DECT images, first, the attenuation values ($a_i(U1)$, $a_i(U2)$) in Hounsfield units (HU) of both energies ($U1$, $U2$) are displayed as scatter plot in Cartesian coordinates for all voxels i . Then, the polar coordinate transformation is applied; i. e., the distance, r_i , of every data point ($a_i(U1)$, $a_i(U2)$) to the coordinate origin and the angle, F_i , to the abscissa is calculated. Depending on the examined tissues and/or materials, different characteristic polar angles can be observed in the spectrum-like scatter plot of (r_i , F_i). For example, typical polar angles for fat, calcium, and iodine-based contrast agent are -125° , 62° , and 71° , respectively. Alternatively, it is possible to display the parameter map $F(x,y)$ (x,y : coordinates in image space) which allows assessing the spatial distribution of specific materials in an image with preserved anatomic and morphologic structure and details.

Discussion

The advantage of our method is the possibility to display the energy dependence of the attenuation coefficient in a function of a single variable (polar angle F) which contains the additional relevant information on material attenuation. Material decomposition becomes possible by selecting only data corresponding to certain polar angles.

Physics (Population-Dose Survey) Tuesday, 03:00 PM - 04:00 PM • S403A [Back to Top](#) [QA](#) [PH](#) **SSJ22** • AMA PRA Category 1

Credit™:1 • ARRT Category A+ Credit:1 **Moderator Mitchell M Goodsitt**, PhD *

Moderator Dianna D Cody, PhD *

SSJ22-01 • ACRIN PA 4006: Characterization of Mean Glandular Dose Adjusted to Volumetric Breast Density in a Prospective Digital Breast Tomosynthesis Screening Trial

Mathew Thomas BS (Presenter) ; **Yohei Matsutani** ; **Jae Y Choi** DPhil ; **Despina Kontos** PhD ; **Emily F Conant** MD * ; **Andrew D Maidment** PhD *

PURPOSE

To characterize the effect of breast density and thickness on mean glandular dose (MGD) in digital mammography (DM) and digital breast tomosynthesis (DBT).

METHOD AND MATERIALS

Participants in this prospective screening trial were imaged with 2-view DM and 2-view combined DM/DBT obtained at 15% reduced dose. The MGD was calculated from exposure parameters for the combination-DM/DBT. Area (PD) and volumetric (VD) percent breast density was estimated using fully-automated, FDA-cleared software (Hologic R2 Quantra). PD and VD in each image was averaged for each breast. MGD unadjusted for glandularity was calculated from exposure factors in the DICOM header on a per-acquisition basis. MGD was adjusted for patient glandularity by Dance coefficient conversions. Statistical comparisons were made by paired t-test and regression analysis.

RESULTS

Data was available for analysis on 330 patients with 1320 images. Compressed breast thickness was 54.6 mm and 56.0 mm for CC and MLO, respectively. VD was 11.9% and 12.5% for LCC and RCC, respectively; PD was 23.4% and 21.6%, respectively. Volumetric density was 45.7% lower than area density (p

CONCLUSION

MGD for mammography is dependent upon thickness and glandularity, while MGD in tomosynthesis is predominately thickness-dependent. The VD was lower than the PD, and both were substantially below 50% in all images. Reporting MGD without adjusting for glandularity underestimates actual dose delivered to the breast tissue per acquisition.

CLINICAL RELEVANCE/APPLICATION

This work characterizes key factors affecting MGD in combination-DM/DBT screening and provides more accurate estimates of MGD for prospective screening.

SSJ22-02 • Fetal Radiation Doses in Computed Tomography Examinations of Pregnant Patients: A Comparison between Whole-body and Individual Organ Doses at Three Different Gestational Ages

Nelia Long MS (Presenter) ; **Matthew Maynard** MS ; **Roger Y Shifrin** MD ; **Nash S Moawad** MD, MS ; **Wesley E Bolch** PhD

PURPOSE

The purpose of this study was to compare values of whole fetal averaged absorbed dose to that for individual fetal organs following CT examination of the adult pregnant female. These differences were compared across three gestational ages and with variations in maternal perimeter at a given gestational age.

METHOD AND MATERIALS

In this study, the University of Florida (UF) series of anatomic computational models of the adult pregnant female were employed which provided detailed anatomical modeling of the developing fetus at 10, 25, and 38 weeks gestation to determine the fetal size range at which the average whole-body fetal dose would be sufficient to approximate the dose to specific fetal organs. Monte Carlo simulations were used to calculate individual fetal organ doses as well as whole-body doses for a Toshiba Aquilion ONE scanner at 100 mAs per rotation. Variations in radiation dose to the fetus with changes in maternal size as given by the maternal abdominal perimeter were also explored.

RESULTS

Calculated CT doses for abdomen-pelvis CT exams for soft-tissue organs differed by up to 26% from whole body averaged fetal doses. However, skeletal tissue doses were at most 110% larger than whole-body doses within the 25- and 38-week models. Skeletal doses were as high as 25 mGy per 100 mAs per rotation. Skeletal doses within the 10-week model were no more than 30% larger than the calculated whole-body dose. At greater gestational ages, the significant differences in results between the average whole-body dose and the skeletal dose during abdomen-pelvis CT exams should be considered when prospectively assessing stochastic risks to these tissues.

CONCLUSION

Although whole-body fetal dose is often the only quantity quoted in CT dosimetry, the imaging community should be aware that although soft-tissue organ doses are very similar to this number, the skeletal dose can be more than twice as large as the whole-body dose. These differences should be taken into consideration when making projections of stochastic risks resulting from exposures to the fetal skeletal tissues.

CLINICAL RELEVANCE/APPLICATION

Stochastic risk estimates to the skeletal tissues following in utero exposures during CT imaging of pregnant patients may be under reported if approximated using estimates of whole-body fetal dose.

SSJ22-03 • Radiation Dose from 3D Rotational Neurovascular Studies vs. Conventional 2D DSA

Elena Tonkopi MS (Presenter) ; Ahmed H Al-Habsi MD ; Jai Shankar

PURPOSE

To compare patient effective dose resulting from two alternative imaging methods for pre-intervention assessment of intracranial aneurysms: a series of Digital Subtraction Angiography (DSA) runs taken at different positions, and a 3D RA technique.

METHOD AND MATERIALS

In a retrospective analysis, we investigated the planning studies of 44 patients who underwent endovascular coiling in our institution between January and October 2012. Images were acquired on a bi-plane II-based system (Siemens Axiom Artis) not equipped with a DAP meter. Conventional 2D projection DSA images were simulated with an anthropomorphic head phantom using 12 s runs with a rate of 2 f/s. Entrance skin exposure was measured with a 60 cc ionization chamber (Radcal, Accu-Pro) for AP, LAT, and Oblique projections. A commercially available Monte Carlo simulation program PCXMC was used to calculate patient effective dose. The second technique involved acquisition of 128 images during a 200° rotation of the C-arm around the patient's head resulting in the 3D reconstruction. A 16 cm CT dosimetry phantom and a 100 mm pencil ion chamber were used to measure the CT dose index resulting from the RA. The ImPACT patient dosimetry software was employed for patient effective dose calculations. Scatter radiation was measured at 152 cm from the head phantom during both acquisitions. An unpaired two-tailed t-test was used to determine the significance of differences between patient doses in each group.

RESULTS

The sixteen patients underwent 2D projection DSA with a mean number of cine runs of 5.1 (minimum 4, maximum 8). Twenty eight patients were assessed using the 3D RA protocol, which included an AP/LAT run and one rotational spin. In the 2D DSA group the mean effective dose was 2.11 mSv (range 1.69-3.43 mSv), and in the 3D RA group effective dose was 1.29 mSv ($p=0.00028$). Scatter to the staff was 2.2 times higher during the cine run than from the one spin RA ($p=0.00016$).

CONCLUSION

Our study demonstrated that the patient effective dose and scatter radiation to the staff were significantly lower from the 3D RA than that from the 2D projection DSA runs used in the planning of cerebral aneurysm coiling.

CLINICAL RELEVANCE/APPLICATION

3D rotational angiography (RA) has the potential to decrease radiation dose and to improve the efficiency of the procedure.

SSJ22-04 • Predictive Models for Estimating Organ Dose from Fixed and Tube Current Modulated CT Scans Using Regional CTDIvol and Water Equivalent Diameter

Maryam Khatonabadi (Presenter) * ; Grace Kim MD ; Dianna D Cody PhD * ; Gary Arbique PhD * ; S. Bruce Greenberg MD ; Christopher H Cagnon PhD ; John J Demarco PhD ; Michael F McNitt-Gray PhD *

PURPOSE

To create predictive models that estimate organ doses from fixed mA or tube current modulated CT scans and that were applicable to both chest and abdomen exams. These models employ water equivalent diameter (WED) to describe patient size and a regional descriptor of scanner output, regional-CTDIvol.

METHOD AND MATERIALS

A total of 334 CT exams (188 chest and 146 abdomen/pelvis) of adult females, adult males and pediatric patients, were collected from 64-slice CT scanners from three different manufacturers (Siemens Healthcare, GE Healthcare and Toshiba Medical); all scans were performed with TCM. Voxelized patient models were created from image data from each exam and organs were identified by semi-automated segmentation to obtain: liver, spleen, and kidneys for abd/pel exams and lungs and glandular breasts tissue for chest exams. For patient size, WED was calculated for each image. For all patients, regional landmarks were manually identified and used to calculate regional CTDIvol. A validated Monte Carlo based CT dosimetry simulation package was used to estimate dose to all segmented organs, once using TCM data and once simulating fixed mA scans. Predictive models based on WED and regional CTDIvol values were developed to estimate organ dose using 60% of cases as a training set. The model was evaluated using the remaining 40% of cases as a test set and compared the predicted values to detailed simulated results for each case. RMS of absolute percent errors between simulated and estimated organ doses were reported across all organs, scanners and scan types as well as for individual organs.

RESULTS

The overall RMS of absolute percent error was 6.7% for fixed mA and 13.9% for TCM simulations. RMS errors were less than 10% for all organs in fixed mA simulations and range from 11-14.8%, for TCM CT scans. Smaller sized patients tended to have larger percent errors.

CONCLUSION

Predictive models were generated based on regional information of the scanner output and size and agreed with detailed simulations to within 7% for fixed and 14% for TCM across all scanners, organs, and exam types. The TCM predictive model could possibly be further improved by tailoring it to smaller patients.

CLINICAL RELEVANCE/APPLICATION

Organ doses can be estimated in a robust fashion for patients undergoing CT exams using predictive models based on regional descriptors of scanner output and patient size.

SSJ22-05 • Decreased Radiation Dose and Preserved Diagnostic Accuracy with Iterative Reconstruction at Coronary Computed Tomography Angiography: Intra-Individual Comparisons

Wei-Hua Yin (Presenter) ; Bin Lu MD ; U. Joseph Schoepf MD * ; Zhi-Hui Hou MD ; Run-Ze Wu ; Nan Li ; Lei Han ; Yang Gao ; Fang-Fang Yu

PURPOSE

Iterative reconstruction techniques show promise to decrease radiation requirements at coronary CT angiography (CCTA). No study performed a direct head-to-head, intra-individual comparison of iterative reconstruction algorithms with traditional filtered back projection (FBP) vis-à-vis diagnostic accuracy and radiation dose at CCTA.

METHOD AND MATERIALS

RESULTS

Sensitivity and specificity for diagnosing =50% coronary artery stenosis on a per-segment level were 88.5% and 92.1% with FBP and 84.2% and 93.4% with iterative reconstruction ($p>0.05$). The area under the receiver-operating characteristic curve on a per-segment level was 0.903 [95% confidence interval (CI), 0.875-0.932] and 0.888 (95%CI, 0.856-0.920) with FBP and iterative reconstruction, respectively ($p = 0.290$). Compared with FBP, iterative series showed no significant ($p>0.05$) differences in image quality analyses. Median effective radiation dose was 52% lower for the iterative reconstruction protocol compared with FBP [0.73mSv (interquartile range, 0.55-1.18) vs. 1.53mSv (1.15-2.42), p

CONCLUSION

Compared with a routine *FBP* protocol, 50% reduced dose acquisition using iterative reconstruction preserves image quality and diagnostic accuracy at CCTA.

CLINICAL RELEVANCE/APPLICATION

Iterative CT image reconstruction techniques have potential to further reduce already low radiation requirements associated with CCTA.

SSJ22-06 • Quantifying the Spread in Deviation Index (DI) - An Initial Experience for a Tertiary Health Care Center and Its Affiliated Community Hospital

Jaydev K Dave PhD, MS (Presenter) ; Eric L Gingold PhD

CONCLUSION

Only 15%-18% of DI values fall within the target range of -0.5 to 0.5, and the SD ranged from 1.8 to 2.7. Thus, the range recommended in AAPM Report 116 is not being achieved in the current practice. This audit of DI values indicates the need for quality improvement projects and perhaps a re-evaluation of target values.

Background

Deviation Index (DI) expresses the deviation in image receptor dose utilized for a digital radiograph relative to a target value. The AAPM Report 116 recommends a desirable operating range of the DI to be between ± 0.5 . The goal of this work was to quantify the spread in the DI for radiographs under real-world clinical conditions.

Evaluation

IRB exemption was obtained. The DI values were evaluated for radiographs obtained using storage phosphor and flat-panel digital radiography systems at a tertiary medical center and an affiliated community hospital (Jan-2012 to Mar-2013). Descriptive statistics for the DI and percent cases within ranges listed in AAPM Report 116 were computed as a function of exam location and type.

Discussion

The mean \pm standard deviation (SD) for all DI values ($n=283141$) was 1.4 ± 2.7 . For neonatal ($n=1877$) and adult ($n=32785$) radiographs with mobile equipment and manual exposure parameters the mean \pm SD for the DI were -1.1 ± 2.4 , and 0.3 ± 2.4 , respectively. The most common radiographic exposure using manual technique was anterior-posterior chest for the neonatal (45%) and adult (60%) populations with mean \pm SD for the DI to be -1.2 ± 2.2 , and 0.1 ± 1.8 , respectively. For radiographs obtained with automatic exposure control ($n=90272$) the mean \pm SD for the DI were 0.7 ± 2.5 ; amongst these, radiographs of the chest were most frequent (58%) with a mean \pm SD for the DI of 0.9 ± 2.2 . The mean \pm SD of the DI for radiographs acquired with the flat-panel digital radiography system were 1.5 ± 2.3 . Only 15% to 18% of the cases were in the target exposure range for the entire data set and the subsets considered. Overall, 23% radiographs were in the underexposed category (5%: DI < -3.0 and 18%: DI from -3.0 to -0.6) and 62% radiographs were in the overexposed category (37%: DI from 0.6 to 3.0 and 25%: DI > 3.0). The DI values followed a gaussian distribution for the subsets considered in this study.

Physics (Non-Conventional CT Imaging) Tuesday, 03:00 PM - 04:00 PM • S403B [Back to Top](#) [PH](#) [CT](#) **SSJ23** • AMA PRA Category 1 Credit™:1 • ARRT Category A+ Credit:1 **Moderator Jeffrey H Siewerdsen**, PhD *

Moderator Stephen Rudin, PhD *

SSJ23-01 • Imaging-task-Optimized, Source-detector Trajectory Design and Reconstruction in 3D Interventional Imaging

Joseph W Stayman PhD (Presenter) * ; Adam S Wang PhD * ; Wojciech Zbijewski PhD * ; Yoshito Otake * ; Jeffrey H Siewerdsen PhD *

PURPOSE

Interventional cone-beam CT differs greatly from diagnostic CT not only in highly flexible positioning of the source and detector, but also in that interventional imaging tasks typically involve well-posed detection and localization of targets which have been identified in pre-operative 3D imaging and planning. We propose to leverage this wealth of patient- and task-specific prior knowledge to design customized source-detector trajectories for subsequent intraoperative CBCT acquisitions to maximize imaging task performance.

METHOD AND MATERIALS

Task-based performance in 3D imaging is predictable using analytical models of the imaging chain. Task-based detectability index, for example, can be computed upon specification of a task function, acquisition geometry, trajectory, detector physics, reconstruction process; and the patient anatomy. Using a preoperative CT volume to integrate patient-dependence, we compute a marginal detectability index related to individual rotation angle/obliquity pairs of an interventional C-arm. A task-based trajectory is formed by successively finding the angle pair yielding the greatest detectability (e.g., the \blacklozenge next best view \blacklozenge) and adding it to a growing collection of angles. The trajectory design approach was applied to a simulated pulmonary nodule detection task where the data from a task-driven noncircular orbit was reconstructed using a model-based iterative approach.

RESULTS

The task-based trajectories designed for the pulmonary nodule detection task were largely continuous despite the lack of a continuity constraint and tended to avoid long radiological path lengths (e.g., avoiding projections involving overlap of the nodule with bone or a surgical tool). Image reconstructions using the task-based orbit show excellent visualization of the nodule. By comparison, the nodule was obscured in reconstructions from sub-optimal orbits due to noise/limited spatial resolution.

CONCLUSION

Leveraging patient-specific information and analytical model for task-based imaging performance within the 3D image acquisition process allowed the design of customized orbits that maximize task performance in image-guided interventions.

CLINICAL RELEVANCE/APPLICATION

Task-based trajectories yield improved imaging performance over standard orbits and can potentially automatically overcome challenging imaging scenarios near high-density objects and bone.

SSJ23-02 • Bipolar Contrasts Generated by Microbubbles in Grating-based X-ray Phase Contrast CT

Xiangyang Tang PhD (Presenter) * ; Yi Yang PhD

PURPOSE

We propose to utilize microbubbles as the contrast agent in grating-based x-ray phase contrast CT. Via a phantom study, we investigate the bipolar contrasts generated by microbubbles in grating-based x-ray phase contrast CT and its variation over the size of microbubble targets and detector cells.

METHOD AND MATERIALS

The phantom consists of seven targets that are clusters of microbubbles at diameters $2.5\ \mu\text{m}$. To simulate the small lesions in advanced clinical and preclinical applications, microbubbles are deployed along a spiral locus in each cluster with its outer dimension from the smallest to largest equal to 50, 75, 100, 250, 500, 1,000 and $2,500\ \mu\text{m}$. To assure a random deployment that mimics a chaotic distribution, half of the microbubbles in each cluster are randomly removed. The projection data are acquired at a 1° angular interval over 360° range. In data acquisition, a 31.6 keV monochromatic x-ray source with infinitesimal focal spot is assumed. At each angular position, grating G shifts 8 steps, and the x-ray exposure is gauged as a summation over all the 8 steps of grating shifting and equal to 5.0×10^7 photon/cm². To investigate the contrast generated by microbubbles over spatial resolution, we conduct the study at detector cell sizes 48, 96, 128 and $256\ \mu\text{m}$, respectively.

RESULTS

The preliminary data show that the contrast generated by microbubbles in grating-based x-ray phase contrast CT is bipolar: the one generated by the differential phase contrast mechanism is negative, while that by the dark-field mechanism is positive. Moreover, the microbubbles' bipolar contrasts in x-ray phase contrast CT are significantly larger than its counterpart in the conventional attenuation CT.

CONCLUSION

Using microbubbles as the contrast agent, the grating-based x-ray phase contrast CT may outperform the conventional attenuation CT significantly, especially in the scenarios where small lesions are to be detected at high spatial resolution.

CLINICAL RELEVANCE/APPLICATION

The preliminary results reported in this study may be of relevance to the preclinical and eventually clinical applications of grating-based x-ray phase contrast CT.

SSJ23-03 • Novel Results from a First Preclinical X-ray Phase-contrast CT Scanner

Astrid Velroyen (Presenter) ; **Andre Yaroshenko** ; **Arne Tapfer** ; **Martin Bech** ; **Mark Muller** ; **Bart Pauwels** ; **Jeroen Hostens** ; **Peter Bruyndonckx** ; **Xuan Liu** ; **Alexander Sasov** ; **Franz Pfeiffer**

PURPOSE

In the last years, x-ray phase-contrast and dark-field imaging have been proven to provide superior soft-tissue contrast and complementary information in comparison to conventional attenuation-based imaging, thus great potential for medical imaging is anticipated. As a first step towards clinical implementation, we have developed a grating-based compact preclinical phase-contrast CT scanner with rotating gantry [1], from which we present novel results.

METHOD AND MATERIALS

Our preclinical phase-contrast CT scanner is the first one to comprise a laboratory x-ray source, a detector and a three-grating interferometer installed on a rotating gantry. The interferometer is used to transfer minimal, sample-induced directional changes of the x-rays into intensity variations on the detector. From those measurements, the two new contrast modalities, i. e. phase-contrast, which is based on the refraction of x-rays, and dark-field contrast, which indicates microstructured regions that scatter x-rays, are obtained in addition to the attenuation-based image. [2, 3] By acquiring reference CT scans we studied thermal and rotation-induced instabilities that compromise the precise alignment and relative movement of the fine interferometric structures and thus cause image artifacts. Newly developed software tools are presented that allow to regain accurate images despite those instabilities. Also, technological advances that improve visibility and scanner performance in general are shown.

RESULTS

We show CT scans of several biological samples and phantoms to demonstrate the possibilities of the new system. First planar radiographic images of a living mouse in differential phase, dark-field and attenuation contrast are presented, as well as phase-contrast ex-vivo mouse CT images made possible by the software and hardware improvements introduced to the scanner.

CONCLUSION

Our measurements clearly show the improved soft-tissue contrast and complementary information that can be obtained by phase and dark-field imaging in comparison to the conventional attenuation image. [1] Tapfer et al. PNAS 2012. [2] Pfeiffer et al. Nat Phys 2006. [3] Pfeiffer et al. Nat Mater 2008.

CLINICAL RELEVANCE/APPLICATION

By proving the feasibility of phase-sensitive imaging with a compact rotating gantry, this work represents an important milestone in translating phase-contrast from bench to bedside.

SSJ23-04 • Grating-based Phase-Contrast Computed Tomography of Benign and Malignant Breast Tumors at Polychromatic X-ray Sources-An Ex-vivo Study

Susanne Grandl MD (Presenter) ; **Marian Willner** ; **Julia Herzen** ; **Doris Mayr** ; **Sigrid Auweter** ; **Alexander C Hipp** ; **Aniko Sztrokay** MD ; **Franz Pfeiffer** ; **Maximilian F Reiser** MD ; **Karin Hellerhoff** MD

PURPOSE

Weak soft tissue contrast is a limiting factor in conventional X-ray based breast imaging. Grating-based phase-contrast computed tomography (PC-CT) using synchrotron sources provides an improved differentiation between non-invasive and invasive breast carcinoma and healthy breast tissue. Due to the limited availability of synchrotron sources the clinical implementation of phase-contrast imaging will rely on the translation of the technique into polychromatic X-ray sources.

METHOD AND MATERIALS

Grating-based PC-CT of 6 ex-vivo formalin fixed breast specimens containing benign and malignant breast tumors (3 fibroadenomas, 1 cystosarkoma phyllodes and 2 invasive carcinomas) was conducted using a Talbot Lau interferometer run at a polychromatic X-ray source of 40 kVp. Phase-contrast and co-registered absorption-contrast images were compared to corresponding histological slices. The visualization of selected findings in phase contrast was compared to absorption contrast.

RESULTS

Grating-based PC-CT is able to depict the 3-dimensional structure of dilated ducts; high phase contrast is found as a correlate to thickened fibrous ductal walls. Phase- but not absorption contrast differentiates between fibrous and less fibrous breast tissue and reflects the extension of compact tumor components of lobular carcinoma. PC-CT provides an excellent depiction of the characteristic dilated, branched ductuli of fibroadenomas and a clear demarcation of the tumor boundaries of fibroadenomas and cystosarkoma phyllodes.

CONCLUSION

On the basis of selected findings in benign and malignant breast tumors, we demonstrate that grating-based PC-CT provides additional information to the conventional absorption contrast even when using polychromatic X-ray sources. Even though the spatial resolution is inferior to synchrotron-based imaging, the technique might serve as complementary diagnostic tool for in-vivo as well as ex-vivo breast diagnostics.

CLINICAL RELEVANCE/APPLICATION

The study represents an important step towards clinical implementation of PC-CT, as it demonstrates the potential of the technique in the absence of synchrotron radiation.

SSJ23-05 • Artifact-suppressed, Low-dose C-arm CBCT Imaging of Low-contrast Cerebral Lesions

Xiao Han MSc (Presenter) ; **Satoru Oishi** PhD * ; **Tetsu Satow** MD ; **Hirokichi Yokoyama** RT ; **Masanobu Yamada** RT ; **Michael D Silver** PhD * ; **Yu-Bing Chang** ; **Emil Y Sidky** PhD ; **Xiaochuan Pan** PhD *

PURPOSE

Three-dimensional images of a patient brain can be obtained by use of a C-arm-based CBCT system for clinical evaluation of cerebral lesions of low-contrast such as Intracranial Hemorrhage (IH) to surrounding soft tissues. Current CBCT systems employ FDK-based algorithms for yielding brain images, which require data acquired at a large number of projection-views and thereby incur a high level of radiation dose. In addition, FDK-based reconstructions may be susceptible to noise and shading artifacts, which can mimic or obscure low-contrast lesions. In this work, we develop an optimization-based algorithm for reconstructing C-arm CBCT brain images, with specific objectives of suppressing artifacts and significantly lowering radiation dose.

METHOD AND MATERIALS

A clinical C-arm CBCT system was used for collecting brain data of patients at 607 views over 200 in 20 seconds. We refer to the acquired data as the full-view data, from which we formed a half-view data set by removing one projection frame at every other view. An iterative algorithm, referred to as ASD-POCS, was adapted to fully incorporate calibration information characterizing the actual scan geometry, which deviates from a circular trajectory due to gantry wobble. We applied the adapted ASD-POCS algorithm to the half-view data, and compared the reconstructions to the FDK reconstructions from full- and half-view data sets.

RESULTS

The half-view ASD-POCS reconstructions show suppressed artifacts than both full- and half-view FDK reconstructions. The soft-tissue contrast of the half-view ASD-POCS reconstruction is superior to the half-view FDK reconstruction, and is visually comparable to that of the full-view FDK reconstruction.

CONCLUSION

Our new algorithm is capable of reconstructing from half-view data patient-brain images with reduced artifacts and comparable soft-tissue contrast than the full-view FDK reconstruction.

CLINICAL RELEVANCE/APPLICATION

We have demonstrated a C-arm CBCT imaging technique with improved image quality at considerably lowered imaging dose for clinical evaluation of low-contrast lesions such as IH.

SSJ23-06 • Dynamic Range Extension in Flat Detector CT Using a Compressed Sensing-based Multi-exposure Technique

Ludwig Ritschl (Presenter) ; **Jan Kuntz** ; **Michael Knaup** PhD ; **Marc Kachelriess** PhD

PURPOSE

To increase the dynamic range of flat detectors in CT without increasing dose or scan time.

METHOD AND MATERIALS

The dynamic range R of x-ray detectors is the ratio between the highest detectable signal (just before overexposure) and the lowest detectable signal (where x-ray quantum noise = electronic noise). Achieving low contrast resolution (e.g. 5 HU contrast of 5 mm objects) in human beings requires $R = 10^6$ which includes two factors: the accuracy of attenuation measurements in each ray and the capturing of significant attenuation differences between different rays due to differences of ray position (peripheral vs. central rays). Flat detectors, however, operate at $R \approx 10^3$ and avoiding underexposure for central rays typically means accepting overexposure for peripheral rays and thus truncation artifacts. Dual or multi-exposure techniques could be a remedy if dose and scan time did not increase. We propose a new multi-exposure technique that performs dense sampling with high exposure levels interrupted from time to time by a sparse low exposure sampling (e.g. every 16th projection). We generalized the compressed sensing-based iTV algorithm [Phys. Med. Biol. 56:1545] to optimally combine the highly sampled high exposure data with the interleaved sparsely sampled low exposure data. The generalized iTV method was verified using simulated as well as measured data, acquired with a Varian flat detector, and was compared to a situation where two exposures were made in a conventional way and with the standard situation of having only one exposure while accepting overexposure in the peripheral patient areas (e.g. in the skin).

RESULTS

The images with extended dynamic range and generalized iTV reconstruction are nearly undistinguishable from those with double exposure. Minor differences are visible only in the peripheral areas where only very sparse information was available for iTV. Dose and scan time remain the same as with today's single exposure scans.

CONCLUSION

Sparsely sampling the low exposure CT scan and interleaving many high exposure projections combined with compressed sensing reconstruction is sufficient to provide images nearly equivalent to a CT scan with a high dynamic range detector.

CLINICAL RELEVANCE/APPLICATION

Flat detector CT, in particular images in interventional CT and in image-guided radiation therapy, can significantly benefit from the dynamic range extension and the improved low contrast resolution.

Physics (MRI Techniques II) Tuesday, 03:00 PM - 04:00 PM • S404AB [Back to Top](#) PH MR **SSJ24** • AMA PRA Category 1 Credit™:1 • ARRT Category A+ Credit:0.5 **Moderator Geoffrey D Clarke**, PhD

Moderator Dennis L Parker, PhD *

SSJ24-01 • Feasibility and Accuracy of a New Virtual Real-time Navigation Option for MRI-guided Interventions in the Prostate

Harald F Busse PhD (Presenter) ; **Gregor Thormer** * ; **Josephin Otto** ; **Nikita Garnov** ; **Arno Schmitgen** * ; **Axel Winkel** PhD * ; **Thomas K Kahn** MD ; **Michael Moche** MD

PURPOSE

To determine the targeting accuracy of a virtual real-time navigation option for MRI-guided interventions and to estimate the feasibility for transrectal prostate biopsies at 3 T.

METHOD AND MATERIALS

A standard MR-compatible interventional device (DynaTRIM, Invivo) was modified to provide real-time feedback of the virtual needle path. Interventional instruments are tracked by a digitizer that measures the 3D offset between a set of reflective markers attached to the instrument manipulator and reference markers mounted in a fixed geometry to the MR table. Device-to-MRI transformation was determined in a one-time calibration step. Prior to the intervention, the device was registered by a custom-made 3D localization of reference MR markers. The navigation system (Localite, Germany) then provided MRI views centered at the position of the instrument tip and reformatted along either the axis or standard radiological planes. The accuracy was estimated in a 3-T MRI trial (Trio, Siemens) by targeting 30 invisible peas (mean diameter 8.5 mm) without any control imaging. Clinical application under IRB approval involved 18 patients (52-72 y.o., mean 65) that had negative biopsies under TRUS guidance. MRI intervention times and biopsy findings were documented.

RESULTS

The add-on components did not affect image quality or patient comfort. Device registration was successful and fast (< 30 s). Experimental biopsy samples contained pea material in 28/30 cases corresponding to a maximum 3D error of 4.3 mm in 93% of the cases. Median clinical intervention time was 55 (36-89) minutes and involved two lesions in 7/18 patients (39%). No procedure-related complications were observed. The obtained specimens were diagnostic in all cases. In 8 patients (44%), histopathology revealed prostate cancer of Gleason Score 6 and 7.

CONCLUSION

Virtual real-time MRI navigation was found to be feasible and accurate in combination with an existing interventional device for the prostate. Potential stereotactic errors, in particular from prostate motion, can be rapidly detected and corrected for by updating the 3D navigation dataset. The underlying technique can be modified to work with other devices, scanner models and clinical applications as well.

CLINICAL RELEVANCE/APPLICATION

The presented virtual real-time navigation solution is a convenient and accurate add-on option to facilitate interventional instrument guidance in organs like the prostate.

SSJ24-02 • 4D Flow MRI Assessment of Cerebral Blood Flow after Extracranial-intracranial Bypass

Tetsuro Sekine (Presenter) ; **Yasuo Amano MD** ; **Ryo Takagi MD** ; **Yoshio Matsumura RT** ; **Yuriko Suzuki BS *** ; **Shinichiro Kumita MD**

CONCLUSION

The hemodynamics after EC-IC bypass is assessed by 4D Flow comprehensively.

Background

Extracranial-intracranial (EC-IC) bypass is performed to maintain blood flow in the brain of patients with internal carotid artery (ICA) occlusion. However, hemodynamics after EC-IC bypass is not well known. The aim of this study was to comprehensively assess the hemodynamics in patients after EC-IC bypass using time-resolved 3D phase contrast MRI (4D Flow).

Discussion

4D Flow shows that the type of bypass affects flow direction and BFV, and that ΔP correlates with ΔBFV . 4D Flow can quantify BFV and ΔP after EC-IC bypass as well as visualize flow direction.

SSJ24-03 • Diffusion Analysis with Triexponential Function in Liver Steatosis

Tatsuya Hayashi (Presenter) ; **Tosiaki Miyati PhD** ; **Junji Takahashi** ; **Yoshinori Tsuji** ; **Masakatsu Tano** ; **Satoshi Saito**

PURPOSE

Our previous study has shown that triexponential function analysis noninvasively obtains more detailed information on diffusion in liver; however, the influence of fat accumulation to liver quantitative diffusion analysis is not clear. The purpose of this study was to assess the influence of liver steatosis on diffusion and perfusion by using the triexponential function analysis.

METHOD AND MATERIALS

On a 1.5 T MRI, navigator-echo triggered single-shot diffusion echo planar imaging was used with multiple b values of 0 to 1500 s/mm^2 , TE of 77 ms, TR of 1 respiratory cycle, and an imaging matrix of 128×74 . Thirty-three patients underwent diffusion-weighted magnetic resonance imaging (DWI) with multiple b -values to obtain perfusion-related diffusion, fast free diffusion, and slow restricted diffusion coefficients (D_p , D_f , D_s) and fractions (F_p , F_f , F_s) with triexponential function analysis. They also underwent dual-echo gradient echo imaging for measurement of hepatic fat fraction (HFF). Of these, 13 patients were included in the control group and 20 in the fatty liver group with HFF >5%. Parameters of two groups were compared using the Mann-Whitney U test. The relationships between each diffusion coefficient and HFF were assessed using the Pearson correlation.

RESULTS

Perfusion-related diffusion coefficient D_p and fast free diffusion coefficient D_f were significantly reduced in the steatotic liver group compared with in the control group ($D_p = 27.72 \pm 6.61 \times 10^{-3} \text{ mm}^2/\text{sec}$ vs. $33.33 \pm 6.47 \times 10^{-3} \text{ mm}^2/\text{sec}$, $P = .0072$; $D_f = 1.70 \pm 0.53 \times 10^{-3} \text{ mm}^2/\text{sec}$ vs. $2.06 \pm 0.40 \times 10^{-3} \text{ mm}^2/\text{sec}$, $P = .0224$). There were no significant differences in other parameters between both groups. Furthermore, D_p and D_f were correlated with HFF ($P < .0001$, $r = -0.64$ and $P = .0008$, $r = -0.56$, respectively).

CONCLUSION

Decreased liver perfusion in steatosis cause the reduction in D_p , and extracellular fat accumulation and intracellular fat droplets in steatosis lead to the reduction in D_f . Thus, the influence of hepatic steatosis should be taken into consideration when the triexponential function analysis is used to assess diffuse liver disease.

CLINICAL RELEVANCE/APPLICATION

Steatosis can act as a potential confounder in quantitative diffusion analysis and to know the influence of steatosis on diffusion and perfusion parameters is important.

SSJ24-04 • Quantitative Comparison of Varying Combinations of MRI Metal Artifact Compensation Techniques (HBW-TSE, VAT and SEMAC) for Hip Prosthesis Imaging

Chen Lin PhD (Presenter) * ; **Trenton D Roth MD** ; **Larry Friggle ARRT** ; **Eric Tarkowski MD** ; **Kenneth A Buckwalter MD**

PURPOSE

The goal of this study is to quantify and compare the reduction of metal artifacts using combinations of high transmit and receive bandwidth (HBW-TSE), View Angle Tilting (VAT) and Slice Encoding for Metal Artifact Correction (SEMAC) in order to derive an appropriate MRI protocol for hip prosthesis imaging that maximizes artifact reduction in a clinically realistic scan time.

METHOD AND MATERIALS

A hip phantom was constructed using human cadaveric bones and a total hip prosthesis (Biomet Orthopedics). The acetabular cup (titanium) and femoral stem (titanium with a cobalt chrome ball) were implanted during a simulated total hip arthroplasty. The prosthesis was placed in a bath of fat, agar, and water to simulate the soft tissues. The inclusion of fat allows the evaluation of artifacts resulting from failure of fat suppression.

2D Coronal STIR images (FOV=38cm, matrix=384x307, TR/TE/TI=5000ms/36ms/145ms, SI Thk=3.5mm, ETL=23) were acquired with a HBW-TSE sequence and with the addition of the VAT and SEMAC using slice encoding steps of 2, 4, 6, 8, 10, 12 and 14 (SEMAC x2-14) on a 1.5T MR scanner (Siemens Aera). Parallel imaging acceleration factor (iPAT) of 2 and 4(max) were applied with SEMACx2 and SEMACx4-14 to compensation for the increase of acquisition time. The dimension of the artifact along the short and long axis in the same middle slice was measured independently by three reviewers and blinded to the metal artifact compensation techniques and parameters.

RESULTS

As shown in the plot, the measured dimension of in-plane artifact initially decreases with the addition of VAT ($p=0.004$, 0.0003 for long and short axis) and SEMAC x2 ($p=0.045$, 0.16 for long and short axis). However, there is no further reduction with higher SEMAC (ANOVA $p=0.95$, 0.98 for long and short axis). The results from three reviewers are in good agreement, suggesting that the measurements are reproducible and reliable.

CONCLUSION

The combination of HBW STIR with VAT and SEMAC reduces metal artifact from a phantom metal hip prosthesis, but approaches a limit with VAT and SEMAC x2 where further increases of SEMAC steps increase the acquisition time without significant reduction of the artifact.

CLINICAL RELEVANCE/APPLICATION

In the presence of a hip prosthesis, VAT and SEMAC slice encoding steps of 2 should be applied on high bandwidth coronal STIR images for optimal metal artifact reduction and minimal scan time.

SSJ24-05 • Time-resolved Quantitative Ventilation and Perfusion Imaging in Free Breathing without ECG Triggering Using Non Contrast Enhanced DC Gated FLASH MRI Imaging

Andre Fischer DIPLPHYS, PhD (Presenter) ; **Christian O Ritter MD** ; **Dietbert Hahn MD** ; **Thorsten A Bley MD** ; **Herbert Koestler PhD ***

CONCLUSION

Quantification of time-resolved ventilation/perfusion datasets using DC gated ^1H FLASH imaging is feasible and in accordance with

literature. This technique offers high patient comfort since data are acquired without applying contrast agents in free breathing and without ECG triggering.

Background

Recently, a non contrast enhanced technique acquiring quasi-randomly MRI data of the human lung in free-breathing and without ECG triggering was introduced [1]. To prevent artifacts due to respiratory/cardiac motion, these data are simultaneously acquired with the DC self gating signal. The DC signal enables accurate determination of the respiratory/cardiac phase. Thereby, complete respiratory/cardiac cycles without motion artifacts can be reconstructed. From these datasets qualitative functional lung maps can be obtained [2]. In this abstract we describe a way to quantify the reconstructed time-resolved respiratory/cardiac cycles.

Evaluation

A quantification method for time-resolved ventilation data has been presented earlier [3]. For perfusion, the main task is to find a relationship between the FLASH signal equation in dependency on the number of applied excitation pulses and v_{blood} which is related to the perfusion rate. This concept is abbreviated AQUAPICSS (Absolute QUantification of Perfusion-Induced Changes in the Steady-state Signal). Using AQUAPICSS and [3], we successfully obtained quantitative time-resolved ventilation/perfusion maps of the human lung from 7 healthy volunteers (5m/2f, age 20-25). Imaging parameters:

3.0T, $T_R=2.5ms$, $T_E=0.7ms$, $\gamma=8$, $192 \times 192, 450 \times 450 mm^2, 10mm, t_{meas}=4min$. The quantitative perfusion maps were additionally compared to SEEPAGE [4]. Figure 1a demonstrates that perfusion values are in good accordance between SEEPAGE and AQUAPICSS. Figure 1b shows an exemplary quantitative ventilation map.

Discussion

The observed perfusion/ventilation values were in accordance with literature values [5,6]. Furthermore, the AQUAPICSS perfusion maps correspond well to quantified rates from additionally acquired SEEPAGE datasets. Since simultaneous quantification of ventilation and perfusion is feasible, this technique enables the determination of the V/Q ratio without applying contrast agents.

SSJ24-06 • Evaluation of Short Term Reproducibility of Apparent Diffusion Coefficients for Diffusion-weighted Imaging of the Prostate

Meredith Sadinski BA (Presenter) ; **Milica Medved** PhD ; **Ibrahim Karademir** MD ; **Yahui Peng** PhD ; **Gregory S Karczmar** PhD * ; **Aytekin Oto** MD * ; **Yulei Jiang** PhD ; **Steffen Sammet** MD, PhD * ; **Shiyang Wang** PhD *

PURPOSE

To evaluate the short term reproducibility of DW-MR imaging of the prostate through consistency in ADC maps between subsequent scans of the same patient using the same scanner and identical imaging parameters.

METHOD AND MATERIALS

14 patients with biopsy proven prostate cancer were evaluated under an IRB-approved protocol. Each patient underwent two, identical DW-MRI scans gathered back-to-back with the patient remaining on the table between acquisitions. ADC maps for each scan were generated using a least squares fit and a deformable registration was performed on the scan pairs using the Plastimatch software employing a Demons algorithm. The prostate and ROIs within cancer lesions were delineated on each scan per patient by two radiologists using the b=0 images. The prostate volume was divided into sextants (anterior apex, posterior apex, anterior medial, posterior medial, anterior base, posterior base) and absolute and magnitude percentage difference in ADC per voxel was calculated and compared across sextants. Voxel-based as well as ROI-based variation in ADC was also calculated for cancerous ROIs.

RESULTS

The absolute difference in ADC per voxel within the prostate ranged from 2.33×10^{-10} to $1.60 \times 10^{-3} mm^2/sec$ (per voxel magnitude percentage difference of 0.00%-200%, mean 10.52%). Variation in ADC was found to be largest in the posterior apex (0.00%-200%, mean 11.55%) although difference between sextants was not statistically significant. Cancer ROIs showed a voxel-based difference in ADC per voxel of 1.07×10^0 to $8.41 \times 10^{-4} mm^2/sec$ (0.00%-67.37%, mean 11.16%). ROI-based analysis showed that the difference in mean ADC of a cancerous ROI between the two scans ranged from -4.22×10^{-4} to $4.63 \times 10^{-4} mm^2/sec$ with mean absolute difference $3.63 \times 10^{-5} mm^2/sec$.

CONCLUSION

DW-MRI has strong potential to become a powerful quantitative imaging biomarker for prostate cancer but it is necessary to characterize the reproducibility of DW-MRI when using it in the clinic or developing new approaches for its use. Our data demonstrates that ADC variation within the prostate is modest, on the order of 10%.

CLINICAL RELEVANCE/APPLICATION

DW-MRI is a mainstay of MRI of prostate cancer, but although a fundamental limitation of its use in the clinic or as a potential quantitative biomarker, reproducibility has not been well established.

Medical Physics 2.0: Radiography Tuesday, 04:30 PM - 06:00 PM • E351 [Back to Top](#) **PH** **RC421** • AMA PRA Category 1 Credit™:1.5 • ARRT Category A+ Credit:1.5 **Co-Director Ehsan Samei**, PhD *

Co-Director Douglas E Pfeiffer, MS *

LEARNING OBJECTIVES 1) To gain an appreciation for the broad developments in radiography technology and operation from film to digital, CR to DR, and the implications. 2) To understand the major challenges to optimized radiography that can be addressed by physics input and expertise. **ABSTRACT** Radiography continues to be the mainstay of medical imaging practice worldwide. The last 30 years have witnessed a number of major technological transitions in radiography, in particular from analogue to digital technologies, and from CR to DR. While these and newer advances have addressed a number of prior shortcomings, they have introduced new challenges. Image post-processing, for example, while praised as an asset of digital operation, has often been underutilized and suboptimal. This lecture aims to provide a historical perspective on these topics and to offer topics that worth the focus of the medical physics community.

RC421A • Radiography Perspective

Ehsan Samei PhD (Presenter) *

LEARNING OBJECTIVES

View learning objectives under main course title.

RC421B • Radiography 1.0

Aaron K Jones PhD (Presenter)

LEARNING OBJECTIVES

1) Review the testing philosophies, tests, and foci of current quality control programs in radiography. 2) Understand the motivation and basis for these current foci. 3) Investigate the limitations, shortcomings, and relevancy of these current foci in the modern radiography era.

RC421C • Radiography 2.0

Eric L Gingold PhD (Presenter)

LEARNING OBJECTIVES

1) Identify the likely changes in medical physics services for radiographic systems over the next 5-10 years. 2) Recognize the value of data logging capabilities of modern digital radiographic systems. 3) Understand how to utilize data to identify quality issues and recommend changes that can improve performance in digital radiography. 4) Understand how to employ modern image

performance metrics to analyze image quality and assist facilities in optimizing the capabilities of radiographic systems. 5) Utilize modern process control methods to monitor stability.

ABSTRACT

Uncertainties in Imaging for Radiation Oncology: Sources and Mitigation Techniques-Imaging for Target Definition Tuesday, 04:30 PM - 06:00 PM • S102D [Back to Top](#) [PH](#) [RO](#) RC422 • AMA PRA Category 1 Credit™:1.5 • ARRT Category A+ Credit:1.5 Co-Director, Moderator Robert Jeraj RC422A • Uncertainties in Physical Target Definition Using PET

Assen S Kirov PhD (Presenter) *

LEARNING OBJECTIVES

1) PET segmentation requirements for target definition. 2) Types of PET auto-segmentation approaches. 3) Challenges for PET segmentation.

URL's

<http://www.mskcc.org/staff/assen-kirov>

RC422B • Practice and Uncertainties in Biological Target Definition

Robert Jeraj (Presenter)

LEARNING OBJECTIVES

1) Dose painting definitions. 2) Dose painting workflow. 3) Uncertainties in dose painting. 4) Dose painting studies.

Minicourse: Current Topics in Medical Physics-Nuclear Cardiac Imaging for Physicists Tuesday, 04:30 PM - 06:00 PM • S403B [Back to Top](#) [PH](#) [NM](#) [CA](#) RC423 • AMA PRA Category 1 Credit™:1.5 • ARRT Category A+ Credit:1.5 Moderator G. Donald Frey, PhD

LEARNING OBJECTIVES 1) The participant will understand the role of nuclear cardiology in the diagnosis of cardiac disease. 2) The participant will understand the role of the medical physicist in PET imaging of the heart. 3) The participant will understand the role of SPECT imaging of the heart.

RC423A • Introduction

G. Donald Frey PhD (Presenter)

LEARNING OBJECTIVES

1) The participant will have an overall orientation to the role of medical physics in nuclear cardiology.

ABSTRACT

This section of the course will provide an overall introduction

RC423B • SPECT Imaging of the Heart

Mark T Madsen PhD (Presenter)

LEARNING OBJECTIVES

1) Understand how cardiac SPECT studies are acquired. 2) Understand how cardiac SPECT studies are reconstructed and what corrections are required. 3) Understand how cardiac SPECT studies are analyzed. 4) Become familiar with cardiac SPECT instrumentation.

ABSTRACT

Cardiac SPECT is the most common nuclear medicine procedure and it contributes nearly 85% of the radiation dose associated with nuclear medicine imaging. In this presentation, the instrumentation and algorithms associated with cardiac SPECT will be reviewed. We begin with conventional general purpose SPECT systems that rely on parallel collimation along with the associated special purpose cardiac SPECT systems that are based on the conventional approach. Recent advances in SPECT instrumentation have made available cardiac systems that rely on novel collimation and detector systems and these will also be reviewed. SPECT reconstruction approaches will be discussed including methods for motion, scatter and attenuation correction. Commercially available resolution recovery software for improving image quality and potentially reducing patient dose will round out the presentation..

RC423C • PET Imaging of the Heart

Sameer Tipnis PhD (Presenter)

LEARNING OBJECTIVES

1) To understand the basic physics of cardiac PET imaging and the differences with cardiac SPECT. 2) To learn the proper way of acquiring data, including ECG gating, choice of bins, list mode data acquisition. 3) To understand the factors that affect image quality. 4) To learn tips for acquiring good clinical images. 5) To understand the role of dynamic PET imaging for determination of coronary flow reserve (CFR).

ABSTRACT

Quantitative Imaging: Dynamic Contrast Enhanced MRI (DCE-MRI) Tuesday, 04:30 PM - 06:00 PM • S404AB [Back to Top](#) [PH](#) [MR](#) [BQ](#) RC425 • AMA PRA Category 1 Credit™:1.5 • ARRT Category A+ Credit:1.5 Director Michael F McNitt-Gray, PhD *
RC425A • The Physical Principles and Challenges of Dynamic Contrast Enhanced MRI Applications

Edward F Jackson PhD (Presenter)

LEARNING OBJECTIVES

1) Understand selected applications of quantitative MR imaging biomarkers, particularly DCE-MRI applications. 2) Understand the factors that currently limit widespread acceptance and use of such quantitative MR imaging biomarkers, including sources of bias and variance. 3) Understand some of the current initiatives focused on the standardization, qualification, and validation of selected quantitative MR imaging biomarkers.

ABSTRACT

Clinical and clinical research applications of quantitative anatomical and functional MR imaging biomarkers, including those focused on treatment assessment, have continued to dramatically expand. Studies at single centers have clearly demonstrated the potential of such applications. However, sources of bias and variance of quantitative MR imaging biomarkers have not previously been adequately investigated, thus limiting the implementation of robust methods to mitigate their effects. Therefore, when it comes to applications of such techniques across vendor platforms, centers, and time, challenges arise due to lack of standards, appropriate phantoms, and protocols. During the past few years, several quantitative MR imaging initiatives have been instigated. This symposium presentation will review selected applications of quantitative MR imaging biomarkers, illustrate some of the current challenges in broadening the use of such biomarkers, and discuss some of the current initiatives of various scientific and federal

organizations that are focused on the standardization, qualification, and validation of MR quantitative imaging biomarkers. Specific examples of DCE-MRI applications and standardization efforts will be provided.

URL's
web.me.com/efjackson

RC425B • Clinical Applications of Quantitative DCE-MRI

Michael V Knopp MD, PhD (Presenter)

LEARNING OBJECTIVES

1) To apply the concepts and pathophysiology of quantitative DCE MRI in clinical applications. 2) To review technical and procedure considerations for clinical applications. 3) To familiarize with current and evolving clinical applications of qDCE-MRI. 4) To utilize qDCE-MRI in and interpret clinical applications.

ABSTRACT

Dynamic contrast enhanced MRI has evolved over the last two decades into a readily available MRI add-on procedure that enables a spatial and time resolved insight into the microcirculation of tissues, both neoplastic as well as benign. While the cinematic display of the temporal contrast enhancement as well as the visual inspection of a signal intensity curve placed over a region of interest enables a ready visual perception of the characteristics of contrast enhancement, a methodological data reduction to a quantitative readout has been more challenging to validate, implement and interpret. Today, the fundamental pathophysiology, appropriate MRI acquisition and post-processing approach are well understood. Quantification is a key enabler to use imaging more as a disease (bio) marker especially for monitoring disease response or progression, as well as putting a more structured interpretation of the dynamic imaging findings into the patient care process. The clinical applications that benefits the most are those where the extent and/or intensity of tissue microcirculation can serve as a marker of biologic characteristics, guide the further diagnostics (tissue biopsies) and/or therapy management. The most common use of applying the fundamental methodologies of DCE-MRI is MR Mammography which is further evolving from a purely morphologic to a semi-quantitative or quantitative imaging procedure. Characterizing malignant tissues, inflammation or angiogenic processes with quantitative approaches is expanding our radiologic toolbox and ability to provide outcome impacting information. Quantitative DCE MRI is evolving to be an increasingly meaningful, clinically relevant and obtainable functional readout of the underlying tissue microcirculation and it will depend on our expansion of radiologic disease insight to truly capitalize on its capabilities.

RC425C • Oncologic Applications of Quantitative DCE-MRI

Anwar R Padhani MD (Presenter) *

LEARNING OBJECTIVES

1) To show that DCE-MRI can be analyzed using qualitative to quantitative methods. 2) To illustrate that routine clinical use of DCE-MRI makes use of qualitative assessments. 3) To indicate that early drug development requires quantification including reproducibility assessments. 4) To realize that complex DCE analysis has roles in validation, drug development, and is needed for multiparametric assessments.

ABSTRACT

Using DCE-MRI in oncologic clinical practice should not be delayed/hindered by the complexities of the technique. The last 20 years of validation work allows us to be confident that DCE-MRI (morphology, subtraction maps, curve shapes and semi-quantitative methods) work in the clinic. Complex quantitative DCE analysis has roles in validation, drug development, and is needed for multiparametric assessments. Future work should now focus on incorporating mpMRI imaging for directing personalized medicine.

Medical Physics 2.0: Fluoroscopy Wednesday, 08:30 AM - 10:00 AM • E451A [Back to Top](#)   **RC521** • AMA PRA Category 1 Credit™: 1.5 • ARRT Category A+ Credit: 1 **Co-Director Ehsan Samei**, PhD *
Co-Director Douglas E Pfeiffer, MS *
RC521A • Fluoroscopy Perspective

Ehsan Samei PhD (Presenter) *

LEARNING OBJECTIVES

1) To become familiar with major trends in fluoroscopy technology. 2) To understand transitions in technology that requires new and advanced evaluations. 3) To appreciate how a medical physicist is to effectively engage with clinical practice.

ABSTRACT

Just like other medical imaging modalities, fluoroscopy has been undergoing a number of technological transitions. Those include transitions from II to flat panel detectors and from 2D to 3D imaging. While these advances offer improvements and new possibilities, they challenge the conventional way a system is to be tested. In addition, given the interventional nature of the modality, there is an increasing need for the medical physicist to be more operationally engaged with the use and optimization of the technology. This lecture aims to offer a historical perspective on these topics and an outline of major priorities for fluoroscopic physics service.

RC521B • Fluoroscopy 1.0

Beth A Schueler PhD (Presenter)

LEARNING OBJECTIVES

1) Review basic fluoroscopy imaging system performance evaluation tests. 2) Compare measurement procedures for fluoroscopic exposure assessment. 3) Become familiar with test procedures designed to assess fluoroscopic image quality. 4) Learn about implementation of patient dose management processes for fluoroscopic procedures.

ABSTRACT

This segment will provide a review of customary medical physics support activities for fluoroscopic imaging systems. Quality control testing procedures for image quality evaluation, radiation dose measurement and other mechanical performance characteristics are essential for optimizing equipment performance and ensuring patient and staff safety. Test equipment, phantoms, measurement methods and recommended performance criteria for these tests will be summarized as they apply to different types of fluoroscopic equipment, from angiographic imaging systems to radiographic-fluoroscopic (RF) tables and mobile C-arms. In addition, the medical physicist's role in clinical implementation of fluoroscopic systems will be discussed, including ensuring appropriate configuration of anatomical program settings, recommendations for patient dose management and methods for patient dose estimation.

RC521C • Fluoroscopy 2.0

Keith J Strauss MS (Presenter)

LEARNING OBJECTIVES

1) Understand need for and advantages of quantitative (as opposed to qualitative) analysis of image quality. 2) Identify and understand new tools becoming available for evaluating fluoroscopic equipment performance. 3) Identify appropriate configuration of acquisition parameters as a function of patient size. 4) Be able to configure the radiation dose to the detector to ensure diagnostic image quality at properly managed patient dose.

ABSTRACT

Abstract Steps that are required to turn physics support of fluoroscopy from a compliance focused to operationally focused program will be discussed. New metrics and analytics to better quantify high contrast resolution, low contrast resolution, temporal resolution, and 3D imaging will be examined. Changes in testing protocols necessary to address new hardware technologies, new acquisition methods, state-of-the-art image processing and analysis will be reviewed. A recently developed "physics testing mode" that the vendors will provide in the near future will be described. Proper management of patient dose metrics will be reviewed. The presentation concludes with clinical implementation of these new strategies. Proper training and communication is critical. Proper configuration of acquisition parameters (focal spot size, voltage and added filter, tube current, pulse width, pulse rate, scatter removal) as a function of patient size from the smallest neonate to the largest bariatric patient is key to providing diagnostic image quality at properly managed radiation doses. In addition, one must ensure that the detector dose as a function of filter type and thickness, pulse rate, field of view, and complexity of the examination is properly configured.

Uncertainties in Imaging for Radiation Oncology: Sources and Mitigation Techniques-Site-specific IGRT Applications: Impact of Different Approaches on Uncertainties Wednesday, 08:30 AM - 10:00 AM • N229 [Back to Top](#) [PH](#) [RO](#) RC522 • AMA PRA Category 1 Credit™:1.5 • ARRT Category A+ Credit:1.5 **Co-Director, Moderator Laurence E Court**, PhD
LEARNING OBJECTIVES 1) Impact of different approaches on uncertainties for specific sites, including pelvis, HandN, thorax, and abdominal sites.
RC522A • Pelvis

Emilie Soisson PhD (Presenter)

LEARNING OBJECTIVES

1) Be able to describe the sources and magnitude of positional uncertainty in irradiation of the pelvis. 2) Understand the role of image guidance in localizing pelvic targets. 3) Be able to compare the imaging strategies employed in the pelvis and understand residual uncertainties associated with each system. 4) Be able to compare published results with their own clinical practice.

ABSTRACT

Detection of organ motion is required for accurate targeting in radiation therapy of the pelvis. It is well known that pelvic targets change size, shape, and location as a result of changes in bladder and rectal filling and the size and location of these organs on the planning CT cannot be easily reproduced at treatment. While organ filling can be partially controlled through dietary regulation, complete immobilization is not possible. Image guidance (IGRT) provides the opportunity to monitor inter- and intra-fraction anatomical changes to better ensure plan delivery accuracy. In turn, IGRT has allowed for margin reduction and dose escalation, especially in the case of the prostate. The potential reduction in margin is then dependent on several factors including the ability to visualize the target and the frequency of imaging. Since target anatomy is generally not rigid with respect to bony landmarks, images used for localization must provide adequate soft tissue contrast or be used in combination with implanted surrogates. Due to the variety of IGRT approaches available and the possibility of having more than one imaging system in each treatment vault, it is now possible to inter-compare different localization methods to determine the uncertainty of a particular approach. Results of these studies are surprising and suggest that even though we think we can see the prostate with our chosen image guidance strategy, back-to-back imaging with different modalities will likely reveal that the prostate not only a different size but also often in a different place. In addition, intra-fraction motion is considerable in the prostate indicating that significant margins are might be required in the absence of intra-fraction tracking.

RC522B • Head and Neck

Laurence E Court PhD (Presenter)

LEARNING OBJECTIVES

1) Be able to describe the uncertainties in head and neck radiation therapy. 2) Appreciate the different approaches used. 3) Have an understanding of the range of margins used for head and neck treatments clinically, and the rationale for these. 4) Be able to logically compare published margins with their own clinical practice.

ABSTRACT

Head and neck cancer is a difficult site for radiation therapy because of the complexity in target delineation, normal tissue sparing and treatment planning. Typically, head and neck patients are immobilized using thermoplastic masks, which are custom-made to fit the individual patient. Generic, or patient-specific neck supports may be used. In many institutions IGRT is considered standard of care for these patients. Thus, many of the uncertainties in head and neck treatments are minimized. However, it is important to understand the residual uncertainties. The immobilization devices are good at minimizing intrafraction movement, but the complex motions of the head and neck region mean that there can be day-to-day variations in the relative positions of different regions, such as between the neck and head. The extent of these variations has been well studied, and will be described in this presentation. There are also different approaches to the IGRT process, including the use of 2D or 3D imaging. This session will explore the uncertainties in head and neck radiation therapy, including inter-fraction variations and also variability in contouring. Mitigation strategies will be discussed. We will describe the treatment margins used by different including their respective rationale.

RC522C • Thorax and Abdomen

Sonja Dieterich PhD (Presenter)

LEARNING OBJECTIVES

1) Be able to describe the sources of uncertainties in the thorax and abdomen. 2) Learn how different respiratory motion management influence margins. 3) Gain an understanding what typical ranges of margins are for the respective methods. 4) Be able to determine appropriate margins for their respective clinical practice.

ABSTRACT

The uncertainties thorax and abdominal regions in the human body consists of overall patient setup uncertainty, respiratory motion, and organ deformation. Depending on the location of the target, a site-specific combination of these three components make up the total uncertainty. Respiratory motion compensation methods are increasingly used in clinical practice to minimize uncertainties. The most commonly used respiratory motion compensation methods are: breath-hold, abdominal compression, gating, and real-time tracking. Each method has a different impact on uncertainties. The simulation imaging also contributes to variations in uncertainties. CT artifacts which may change the contouring margins used depend on the data acquisition technology used during simulation. Free breathing, deep inspiration or expiration breath-hold, gated 4D-CT (both phase-gated and amplitude gated), scanner speed, pitch, and number of slices per revolution all influence the uncertainties. In addition to uncertainties in the position of the target, the relative position of organs at risk (OAR) to the target area may also change intra- or inter-fractionally. The concept of using OAR margins in the planning phase to anticipate potential relative shifts of OAR to target position will be discussed. Assessing OAR dose during daily image-guided patient setup can help identify setup variations exceeding OAR safe margins. Strategies to address setup variations exceeding uncertainty limits based on clinical experience will be discussed.

Minicourse: Recording and Reporting Radiation Dose: National and International Perspectives and Activities Wednesday, 08:30 AM - 10:00 AM • N226 [Back to Top](#) [QA](#) [PH](#) RC523 • AMA PRA Category 1 Credit™:1.5 • ARRT Category A+ Credit:1.5
Director J. Anthony Seibert, PhD
URL's www.imp.uni-erlangen.de/RSNA2012

RC523A • The American College of Radiology Dose Index Registry

Richard L Morin PhD (Presenter)

LEARNING OBJECTIVES

1) Understand how registries perform. 2) Understand the way in which registries have altered physician behavior and improve patient care. 3) Identify the parameters involved in optimizing radiation dose in clinical practice. 4) Apply this knowledge by participating in a dose index registry and utilizing these techniques in Maintenance of Certification.

ABSTRACT

RC523B • The European Perspective

Willi A Kalender PhD (Presenter) *

LEARNING OBJECTIVES

1) Understand that CTDI is merely a technical concept for scanner acceptance and constancy testing, but not a measure for patient dose. 2) Learn about concepts for patient- and scanner-specific patient dose estimates. 3) Learn about the concept of diagnostic reference levels and its strengths and weaknesses.

ABSTRACT

There is no major debate regarding the validity of the computed tomography dose index (CTDI) in Europe because it is considered as a tool for scanner acceptance and constancy testing. Its use for that purpose is undisputed. Measures for patient dose have been a major topic for decades. There are no common regulations valid for all of Europe, but there are a number of initiatives and concepts in place already which originated here. Among these are primarily the generation of conversion coefficients k for estimating values of the effective dose E from the dose length product (DLP) by $E = k \times DLP$ and the concept of dose reference levels (DRL). DRLs for radiological examinations in the European Union were demanded by law already in 2000.

Patient dose assessment relies predominantly on pre-tabulated values generated for anthropomorphic and voxel phantoms. Efforts are underway to provide more patient-specific dose estimates (PSDE) independent of CTDI phantom measurements. The lecture will review the above concepts and will point to both strengths and weaknesses.

RC523C • Informatics Tools for Recording/Tracking Dose

Kevin O'Donnell (Presenter) *

LEARNING OBJECTIVES

1) Understand how DICOM Radiation Dose SR (RDSR) captures procedure dose information, the modalities and details covered. 2) Understand how the IHE Radiation Exposure Monitoring Profile (REM) coordinates the capture and management of RDSR objects and how it can be applied in a radiology practice. 3) Understand how 'CT dose screens' from legacy scanners can be ported into RDSR. 4) Understand how to apply the pre-scan dose pop-ups on the CT console specified in the MITA CT Dose Check (XR-25) standard. 5) Understand how to specify the above standards and features when purchasing and integrating radiology systems.

Quantitative Imaging: Quantitative Imaging in FDG-PET Wednesday, 08:30 AM - 10:00 AM • S102AB [Back to Top](#) PH NM BQ
RC525 • AMA PRA Category 1 Credit™:1.5 • ARRT Category A+ Credit:1.5 **Director Michael F McNitt-Gray**, PhD *
RC525A • Lessons Learned from Drug Development Trials Using Molecular Imaging

Jeffrey L Evelhoch PhD (Presenter) *

LEARNING OBJECTIVES

1) Understand how pharma uses the information provided by FDG-PET. 2) Become familiar with site qualification and quality control methods used in clinical trial of an investigational therapeutic agent. 3) Understand why specific clinical trial imaging protocols may differ from clinical practice and importance of adhering to the clinical trial imaging protocol. 4) Realize which issues confound attempts to achieve more quantitative FDG-PET in the context of a clinical trial of an investigational therapeutic agent.

RC525B • Examples of Multi-Center Molecular Imaging Trials: Trial Design and Quantitative Approaches

David A Mankoff MD, PhD (Presenter)

LEARNING OBJECTIVES

1) Describe applications of molecular imaging as a biomarker for cancer drug therapy. 2) Discuss elements of clinical study design for molecular imaging. 3) Contrast molecular imaging versus conventional imaging and therapy trials.

RC525C • Understanding and Controlling Sources of Variability in Multi-Center PET Imaging

Paul E Kinahan PhD (Presenter) *

LEARNING OBJECTIVES

1) Identify the importance of quantitative imaging principles in the setting of clinical trials. 2) Identify the role of standards, including DICOM and others, in the successful application of quantitative imaging principles. 3) Analyze quantitative imaging techniques and apply this knowledge to protocol development in the setting of clinical trials.

Physics (CT-Imaging Phantoms) Wednesday, 10:30 AM - 12:00 PM • S403A [Back to Top](#) PH CT **SSK19** • AMA PRA Category 1 Credit™:1.5 • ARRT Category A+ Credit:1.5 **Moderator Guenter Lauritsch**, PhD *
Moderator Rebecca Fahrig, PhD *

SSK19-01 • Objective Assessment of Low-contrast Performance in the ACR CT Accreditation Phantom Using a Channelized Hotelling Observer and Its Correlation with Human Observers

Lifeng Yu PhD (Presenter) ; **Shuai Leng** PhD ; **Yi Zhang** ; **Zhoubo Li** ; **James M Kofler** PhD ; **Cynthia H McCollough** PhD *

PURPOSE

Despite its current use as a metric in the low-contrast resolution test for the American College of Radiology (ACR) CT Accreditation Program, contrast to noise ratio is not appropriate for iterative reconstruction (IR). The purpose of this study was to develop and validate a quantitative metric using a channelized Hotelling observer (CHO) that can be used to assess low-contrast resolution in the ACR phantom for IR methods.

METHOD AND MATERIALS

The proposed metric is based on a CHO model, which predicts an index of detectability from a number of 2-alternative forced choice (2AFC) trials, in this case generated from repeated CT scans of the ACR phantom. To test this metric, the low-contrast module of the ACR phantom was scanned on a 128-slice scanner (Definition Flash, Siemens) and a 64-slice scanner (Lightspeed VCT, GE). Routine abdomen protocols were used at three dose levels (CTDIvol=16, 12, and 8 mGy), each scanned 100 times. On each scanner, images were reconstructed with one filtered-backprojection kernel and 2 IR settings: B40 and I40 with strengths of 3 and 5 for Siemens; Standard and ASIR with a mix ratio of 50% and 100% for GE. Three board-certified medical physicists blindly evaluated images in a random order (totally 1800 images = 2 vendors x 3 doses x 3 reconstructions x 100 images), and recorded a quality score for detecting all four 6-mm rods using a 6 point scale. Percent correct of the 2AFC was calculated using CHO. The correlation between the index of detectability predicted by CHO and the scores by human observers was tested.

RESULTS

A strong correlation between CHO and human observer scores was observed. Pearson correlation coefficients were 0.932 (95% CI: [0.70, 0.99]) for Siemens and 0.926 (95% CI: [0.68, 0.98]) for GE. Both IR methods improved low-contrast performance, with one

more significantly than the other (p
CONCLUSION

The proposed task-based low-contrast detectability metric may provide an objective measure of low-contrast performance in ACR CT evaluation.

CLINICAL RELEVANCE/APPLICATION

Use of IR methods challenges existing low-contrast performance tests, such as with the ACR phantom. The proposed metric provides an objective and reliable measure of low-contrast performance.

SSK19-02 • Moving Forward with the AAPM-ICRU CT Dose Phantom

Donovan M Bakalyar PhD (Presenter) ; **John M Boone** PhD * ; **Michael F McNitt-Gray** PhD * ; **Robert L Dixon** PhD * ; **Erin Angel** PhD * ; **Kirsten L Boedeker** MS * ; **Kish Chakrabarti** PhD ; **Heather Chen-Mayer** PhD ; **Dianna D Cody** PhD * ; **Wenzheng Feng** ; **Shuai Leng** PhD ; **Sarah E McKenney** BS, BA * ; **Richard L Morin** PhD ; **J. Thomas Payne** PhD ; **Jeffrey H Siewerdsen** PhD * ; **Keith J Strauss** MS ; **Paul B Sunde** * ; **Thomas L Toth** * ; **Zhitong Yang** PhD

CONCLUSION

The AAPM-ICRU phantom and proposed measurement techniques are robust, simple and readily applied to the ever growing variety of CT design geometries.

Background

$CTDI_{vol}$ and DLP are universally used members of the CTDI family of radiation dose indices. However, the phantoms and measurement techniques used for determining these values suffer from limitations that are especially evident for the growing number of cone beam and very wide fan beam CT machines. In accordance with the recommendations of AAPM Task Group 111, Task Group 200 (TG200) has designed a phantom and tested procedures which are suitable over a broader range of machines and conditions than the current methodology.

Evaluation

The phantom is 30 cm in diameter and is constructed of polyethylene; it is of sufficient length (60 cm) so that virtually no scatter from scanning near the ends of the phantom will reach the central plane. A small detector is placed in the central plane at the center, near the edge, or at an intermediate radius and a helical scan through the entire phantom is performed. For this scan the dose recorded by the chamber approaches D_{eq} , the value that would be reached for an infinite scan. By recording the dose rate as a function of position during the scan, the dose $D(L)$ at the central plane can be determined for any scan length L . From this record, the approach to equilibrium function $H(L)$, defined as the ratio $D(L)/D_{eq}$, is determined. These concepts can be extended to axial scans on stationary tables and are not limited by the width of the beam. Testing has been performed on a Philips Brilliance 64 scanner and a Toshiba Aquilion One.

Discussion

$H(L)$ is a robust function and displays only a weak dependence on tube potential and z-axis collimation. Our measurements show that the central plane dose is substantially more uniform than that for the CTDI body phantom. The phantom design is easily and transparently scalable, making it readily adaptable to the size specific dose estimates described by the report of AAPM Task Group 204 resulting in an index that remains simple but accounts for both girth and scan length. Correlations to air and small phantom measurements can be used for verification in the field.

SSK19-03 • A Comprehensive Study of Single- and Dual-source Coronary CT Angiography with Stents Using an Anthropomorphic Phantom with a Beating Heart Model

George S Fung PhD (Presenter) * ; **Karl Stierstorfer** PhD * ; **Satomi Kawamoto** MD * ; **Katsuyuki Taguchi** PhD * ; **Matthew K Fuld** PhD * ; **Thomas G Flohr** PhD * ; **Elliot K Fishman** MD * ; **Benjamin Tsui** PhD *

PURPOSE

The object is to study the effect of coronary stents and heart motion on the quantification accuracy of lumen diameter and lumen attenuation of coronary stents using an anthropomorphic phantom with a beating heart model and a CT projection simulator in single- and dual-source CT (SSCT and DSCT) angiography.

METHOD AND MATERIALS

The digital 4D phantom with a beating heart model, coronary arteries and stents, was developed and used in simulating coronary CT angiography (CTA) image data with different heart rates (HRs), i.e., 50-110bpm. Clinical stainless steel coronary stent models of different diameters, i.e., 2.5-4mm, were deployed at 3 coronary locations, i.e., LAD, LCX and RCA. Single and dual-source CTA images of the phantom were generated using an instrumental-accurate CT projection simulator at mid-diastolic phase and reconstructed using standard clinical protocols. Artificial in-stent lumen narrowing (ALN) and lumen attenuation (ALA) were calculated from the reconstructed CTA images using both SSCT and DSCT systems at the different HRs.

RESULTS

In the static heart study, CTA images from all 3 stents suffered similar degradation, as ALN increased from 28% to 48% and ALA increased from 2% to 68% as the stent diameter decreased from 4mm to 2.5mm, due to partial volume (PV) and metal beam-hardening (BH) artifacts. In the beating heart study using SSCT, there were minor degradations for LAD stent at all HRs and for LCX stent at 50-70bpm. For LCX stent at 90-110bpm and for RCA stent at all HRs, lumen diameter and attenuation could not be robustly measured due to the high variation of in-stent attenuation and deformed structure of the stents in the CTA images. In the beating heart study using DSCT, CTA images of LAD and LCX stents at all HRs and RCA stent at 50bpm had minor motion artifacts. The RCA stent in CTA images suffered from significant motion artifacts at 70bpm and above. When compared to SSCT, DSCT achieved comparable ALA for LAD stent at all HRs and over 30% of improvement in ALA for LCX and RCA stents at low HRs.

CONCLUSION

High temporal resolution provided by DSCT overcomes most of the motion artifacts for the stents at the LAD and LCX over large range of HRs in CTA images. Additional research is needed to reduce artifacts due to the large motion of RCA, and PV and BH effects.

CLINICAL RELEVANCE/APPLICATION

DSCT overcomes most of the motion artifacts for the stents at the LAD and LCX over large range of HRs in CTA.

SSK19-04 • Size-specific Organ Dose Calculation Using Age and Gender Specific Computational Human Phantoms in Patients Undergoing Computed Tomography Examinations

Choonsik Lee PhD (Presenter) ; **Jenifer W Siegelman** MD, MPH ; **Mark P Supanich** PhD * ; **Les R Folio** DO, MPH

PURPOSE

To develop a method to estimate organ doses for patients with different torso diameters that can be readily used in clinical settings without the need for Monte Carlo simulation. CT Dose Index ($CTDI_{vol}$) and Dose Length Product (DLP) are available from the dose report for patients undergoing computed tomography (CT) examinations but are based on CTDI phantom measurements that do not represent patient organ dose. As direct measurement is not feasible, intensive Monte Carlo simulation coupled with computational human phantoms is used to calculate patient organ doses; more important measure.

METHOD AND MATERIALS

We employed a set of computational human phantoms in six age groups (newborn to adult) based on ICRP reference data to pre-calculate an organ dose library using the known x-ray spectra of a reference CT scanner (Siemens Sensation 16). $CTDI_{vol}$ -normalized doses to major organs included in (or close to) the scan coverage was calculated for head, chest,

abdomen-pelvis (AP), and chest-abdomen-pelvis (CAP) scans using head and body filters and 120 kVp. Effective diameters at the middle level of the scan range were measured and exponential regression curves were derived between organ doses and the effective diameters. Illustrative organ doses were calculated for a given CT scanner and patients with different effective diameters by multiplying the organ dose library by the $CTDI_{vol}$ of the given CT scanner.

RESULTS

Exponential regression coefficients were established for male and female patients scanned for head, chest, AP, and CAP examinations for a range of effective diameters. Illustrative organ doses were calculated for hypothetical male patients with the effective diameters of 10, 20, 30, and 40 cm scanned for a CAP exam ($CTDI_{vol}$ of 11.1 mGy). Exponential fitting coefficients for CAP scan normalized by body phantom were used for the calculation.

CONCLUSION

A convenient method to calculate doses for patient organs included in or close to scan coverage was developed for major examinations. Once the effective diameter of a patient and the $CTDI_{vol}$ measurement (or from dose report) are available, organ dose may be calculated using the proposed method with the exponential fitting coefficients.

CLINICAL RELEVANCE/APPLICATION

The proposed method will be useful for calculating patient organ dose using the effective diameter of the patient and $CTDI_{vol}$ measurement without performing intensive Monte Carlo simulation.

SSK19-05 • Validation of Monte Carlo Simulation Dosimetry Method Using In-Vivo Measurements in Patients Undergoing CT Examinations

Maryam Khatonabadi (Presenter) * ; **Jonathon Mueller** ; **Kyle McMillan** * ; **Maria Zankl** PhD ; **Dianna D Cody** PhD * ; **Christopher H Cagnon** PhD ; **John J Demarco** PhD ; **Michael F McNitt-Gray** PhD *

PURPOSE

The purpose of this study was to validate Monte Carlo (MC) simulation based dose estimates by generating voxelized models of patients for the purpose of simulations and comparing simulated values with in-vivo dose measurements from clinical CT scans.

METHOD AND MATERIALS

In-vivo rectal TLD dose measurements were performed for 9 patients undergoing CT Colonography on an MDCT (LightSpeed VCT, GE Healthcare), with IRB (Institutional Review Board) approval. For each patient, two scans, prone and supine, were acquired; both using a fixed mAs technique. In-vivo dose measurements were obtained from TLDs that were affixed to the inner lumen of rectal catheters. Dose from the TLDs were determined taking into account their energy response. For each patient, voxelized models from CT images were generated based on a tissue-Hounsfield Unit (HU) look-up table. In a small validation study using the Visible Human (VH) GSF voxelized model, doses calculated using the tissue-HU look up table from CT image data were within 10% of those obtained using the voxelized model in which each voxel is identified with a tissue type. A previously developed and validated MC based dosimetry package was used with the voxelized colonoscopy patient models to simulate dose to the TLDs. Measured and simulated in-vivo TLD doses were compared for all 9 patients, calculating a Root Mean Square of absolute percent error between measured and simulated values.

RESULTS

The RMS of absolute percent error between TLD measurements and MC simulations was 12.2% with a maximum of 20.3% and minimum of -19.7%.

CONCLUSION

The results of this study demonstrated that MC simulations using voxelized patients and equivalent source model result in reasonably accurate doses compared to actual measurements. Simulations mostly overestimated measurements due to small FOV of the images used to create voxelized models, which resulted in cutoff of anatomy, i.e. less tissue for simulated photons to penetrate through, and therefore higher dose to segmented TLDs than actual TLD dose measurements.

CLINICAL RELEVANCE/APPLICATION

In-vivo validation of MC methods used to estimate dose is crucial for implementation of MC simulations in the clinic. This study showed that these estimations reasonably agree with measurements.

SSK19-06 • Lower Bound on Detectable Lung Nodule Growth Using Phantom CT Data

Marios A Gavrielides PhD (Presenter) ; **Qin Li** ; **Rongping Zeng** PhD ; **Kyle J Myers** PhD ; **Berkman Sahiner** PhD ; **Nicholas Petrick** PhD

PURPOSE

To determine the minimum detectable growth in lung nodules of various sizes.

METHOD AND MATERIALS

Four different combinations (layouts) of synthetic nodules were placed in the vasculature insert of an anthropomorphic phantom and scanned with a 16-detector row CT scanner (Philips, MX8000). Each layout included four nodules of different shapes (spherical, elliptical, lobulated, and spiculated) but with the same size (5, 8, 9, or 10mm) each placed in a fixed location. For each layout, ten repeat scans were acquired at 20, 100, and 200 mAs; 1.2 pitch; thin or thick slice collimations (16x0.75mm and 16x1.5mm, respectively); and reconstructed to 0.8, 1.5, and 3mm for the thin slice collimation, and 2, 3, and 5mm for the thick slice collimation. Nodule volume estimates were determined using a previously developed 3D matched filter estimator. For each nodule size, the pooled distribution of volume estimates was shifted by a percentage c to simulate a growing nodule. The standard deviation of the shifted distribution was also accounted for. Analysis of nodule growth was then conducted as a detection problem, where the shifted distribution was considered the signal present distribution and the baseline (non-shifted) distribution was considered signal absent. The area under the receiver operating characteristic curve (AUC) was used as a detectability metric, where c was varied until a target AUC was reached. The resulting value of c was the minimum detectable change for that AUC value. Bootstrap re-sampling was used to derive 95% confidence intervals on the value of c .

RESULTS

Both nodule size at baseline and choice of slice collimation protocol had an effect in the value of minimum detectable growth. For $AUC=0.95$, the minimum detectable nodule growth (volume increase) across all protocols and shapes was {45% [42-48], 21% [20-21] and 16% [16-17]} for nodule sizes of 5, 8, and 9 mm respectively. Minimum detectable growth fell to {17% [16-17], 19% [19-21] and 15% [15-16]} when the thin slice collimation protocol (16x0.75mm) was used.

CONCLUSION

Our phantom study indicates that the lower bound for detectable nodule growth in subcentimeter nodules is relatively small, on the order of 20% or less in volume for a thin slice CT acquisition protocol.

CLINICAL RELEVANCE/APPLICATION

These results could complement findings from theoretical and clinical studies to determine a potentially useful role for volume as a surrogate metric of nodule size change.

SSK19-07 • Iterative Reconstructions and Low Contrast Resolution Measurements: Are ACR Accreditation Threshold Values Still Valid?

James M Kofler PhD (Presenter) ; **Lifeng Yu** PhD ; **Shuai Leng** PhD ; **Yi Zhang** ; **Zhoubo Li** ; **Cynthia H McCollough** PhD *

PURPOSE

The ACR recently switched from visual analysis of low contrast resolution (LCR) to quantitative measurement of contrast-to-noise ratio (CNR). This study compares the use of CNR threshold values as pass/fail criteria with use of visual impressions of LCR by human observers for the task of evaluating iteratively reconstructed (IR) phantom images.

METHOD AND MATERIALS

Two scanner models from 2 manufacturers (Lightspeed VCT, GE; Definition Flash, Siemens) were used to acquire data of the low contrast resolution section of the ACR CT accreditation phantom at CTDIvol levels of 8, 12, and 16 mGy. Images were reconstructed at 5mm image thickness using 3 different algorithms (1 FBP and 2 IR (at different strength settings). Image acquisition and reconstruction were repeated 100 times for each, yielding a total of 1800 images. All images were blindly reviewed by 3 board-certified physicists using a 6-point scale to rate the detectability of the four 6-mm rods. CNR measurements were recorded, with a CNR = 1.0 indicating pass, which is the CNR threshold value used by the ACR accreditation program for adult abdominal protocols.

RESULTS

CNR measurements for nearly all of the IR images, at all dose levels, passed the ACR accreditation criteria. Visual analysis, using previous ACR criteria, showed a marked decrease in the pass rate with decreasing dose levels for all reconstruction methods. At an arbitrary pass rate of 20% (i.e., 20% of the 100 images passed), visual analysis showed 1 IR strength (vendor 1) and 2 IRs strengths (vendor 2) as passing at 12 mGy (all IRs pass at 16 mGy; all fail at 8 mGy). Using a CNR threshold of 1.0, all IR images pass at all dose levels.

CONCLUSION

CNR threshold values currently used by the ACR CT accreditation program are misleading with respect to the visual assessment of LCR for IR images.

CLINICAL RELEVANCE/APPLICATION

The established quality assured by ACR CT accreditation will not be maintained with IR images. Very poor quality images, as rated by observers, pass the ACR CNR criteria by a wide margin.

SSK19-08 • Patient-specific Whole-body Voxel Models for Accurate Organ and Effective Dose Estimation

Natalia Saltybaeva (Presenter) ; **Daniel Kolditz** PhD * ; **Willi A Kalender** PhD *

PURPOSE

Monte Carlo (MC) simulations can be performed on patient CT image data. However, this data is limited to the scanned volume and does not allow estimating dose for organs outside the directly exposed range. Standard mathematical phantoms do not have this limitation, but they do not reflect individual patient anatomy. The aim of this work was to generate whole-body patient-specific voxel models for accurate organ and effective dose estimations.

METHOD AND MATERIALS

Three anthropomorphic phantoms representing an adult (Alderson Research Laboratories, New York, USA) and 5 and 1 y.o children (CIRS, Norfolk, VA, USA) were considered as patients and scanned with thorax routine protocols (SOMATOM Definition Flash, Siemens, Forchheim, Germany) with tube voltages of 80, 100 and 120 kV. The absorbed dose was measured using 90 calibrated TLD chips. Whole-body voxel models were generated by amending the patient CT volume by size-adapted versions of the ICRP Reference Male phantom in case of the adult and ORNL voxel phantoms in the case of the pediatric patients. Organ definitions provided with these phantoms were transferred to the combined models and adapted interactively. MC simulations were performed using the validated tool ImpactMC (CT Imaging GmbH, Erlangen, Germany) for a) the unamended patient volumes, b) the combined whole-body models. Simulated 3D dose distributions were compared with TLD measurements chip by chip.

RESULTS

The mean difference between measurements and simulations based on the unamended CT volumes was 19%; using the whole-body model reduced the difference to 6%. In contrast to unamended CT volumes, whole-body models intrinsically also provided the dose values for organs outside the scanned volume. These organs contributed 17%, 34% and 36% to effective dose for the adult, 5y.o. and 1 y.o. phantom, respectively.

CONCLUSION

Patient-specific whole-body models allow to increase accuracy of dose estimation and to calculate dose for all relevant organs.

CLINICAL RELEVANCE/APPLICATION

The approach is useful for individual patient dose estimation, especially for clinical studies.

SSK19-09 • A Single Phantom for Objective Quality Control of Both CT and Dental CBCT

Hugo De Las Heras PhD, MSc (Presenter) * ; **Felix Schofer** PhD * ; **Wilhelm J Van Der Putten** PhD *

CONCLUSION

The QUART phantom (with software) is an objective, reliable, time and cost-efficient alternative to perform the tests required for the quality control of both dental CBCT devices and CT scanners.

Background

The latest developments in quality control for dental cone beam CT (CBCT) devices have a much more objective and efficient approach than traditional QC phantoms for CT scanners. We present a phantom and software that recently became the German and Italian standard for dental CBCT (QUART DVT AP). The phantom is designed to evaluate all test parameters required in national and international protocols for CT quality control (IAEA publication 19, EU criteria publication 162 and ACR QC manual), as well as to test noise reduction algorithms and tube current modulation. In order to evaluate its application to whole body CT scanners, evaluations were performed using it and a standard Catphan phantom.

Evaluation

Both phantoms were scanned in a CT scanner using the same settings. Consecutive scans were obtained at 130 kVp with exposures varying from 50 to 300 mAs. Both phantoms could evaluate uniformity, imaged slice width, position accuracy, noise and CT number accuracy. However, in addition, the QUART phantom and software presented here enabled the direct, automatic evaluation of contrast (between 120 and 150), limiting resolution (0.6 lp/mm at 10 % of the modulation transfer function) and contrast-to-noise ratio (CNR, increasing from 128 to 290) in less than 20 seconds per image.

Discussion

The CNR is an objective, straight-forward and time-efficient measure that releases equivalent results to traditional low contrast-detail tests and increases the reliability of quality control tests. As an example, the attached figure shows a comparison of contrast and CNR for both phantoms. The observed sensitivity (score range divided by uncertainty) of the CNR evaluation ($0.013 \pm 0.002 \text{ mAs}^{-1}$) was twice the one obtained with the Catphan contrast-detail evaluation method ($0.007 \pm 0.002 \text{ mAs}^{-1}$).

Physics (Quantitative Imaging II) Wednesday, 10:30 AM - 12:00 PM • S403B [Back to Top](#) [PH](#) [CT](#) [BQ](#) **SSK20** • AMA PRA Category 1 Credit™: 1.5 • ARRT Category A+ Credit: 1.5 **Moderator John N Aarsvold**, PhD

Moderator Mats Danielsson, PhD *

SSK20-01 • Stability of Iodine Density Measurements with Spectral Detector CT in an Anthropomorphic Phantom of Varying Size: Comparison of Conventional and Virtual Mono-energy Images

PURPOSE

Simultaneous dual-energy CT (DECT) data can be used to generate virtual mono-energy images at varying keV levels. These images include in-plane and object-size beam-hardening corrections. We aimed to evaluate the stability of iodine density measurements in virtual mono-energy images, using a phantom of two sizes.

METHOD AND MATERIALS

A customized water-equivalent anthropomorphic CT phantom (QRM, Moehrendorf, Germany) was scanned with and without a 2.5 cm extension ring to enable measurements at 2 phantom sizes (20x30 cm and 25x35 cm). The phantom included 8 tubes of 11.1 mm diameter, 2 tubes of 7.9 mm diameter, and 2 tubes of 6.4 mm diameter, all filled with 7 mg/ml iodine solution. The tubes were arranged 3 ϕ 11 cm from the phantom center (Fig. 1). Conventional and 65 keV mono-energy images for both phantom sizes were obtained at 120 kVp and 500 mAs using a novel Spectral Detector CT (SDCT) prototype (Philips Healthcare, Cleveland, OH, USA). Variation between HU values of the iodine tubes was analyzed (paired T-test) for tube location, tube diameter, image type, and phantom size.

RESULTS

Mono-energy image HU values for the iodine tubes were independent of tube location, tube diameter, or phantom size. There was no significant difference ($p=0.39$) in the standard deviation (SD) of HU values at different tube locations in the small-size phantom ($SD=0.76\%$) vs. the large-size phantom ($SD=0.88\%$). Variation of the HU values between tubes with different diameters was even smaller, 0.46% in the small-size and 0.64% in large-size phantom. Compared to mono-energy images, in the conventional images the variation of HU values at different tube locations was significantly higher (p

CONCLUSION

The quality of virtual mono-energy images at 65 keV was superior to that of conventional images, with no beam-hardening effect. Mono-energy images demonstrated stable iodine density measurements, independent of phantom size, tube location, and tube diameter.

CLINICAL RELEVANCE/APPLICATION

Stable density measurements of contrast material, independent of patient size and ROI location, are important for integration of Spectral Detector CT into clinical practice.

SSK20-02 • The Size-based Emphysema Quantification Using Length Scale Analysis in 3D Volumetric Chest CT

Minho Lee PhD (Presenter) ; Namkug Kim PhD ; Joon Beom Seo MD, PhD ; Sang Young Oh MD ; Sang Min Lee MD ; Jae Seung Lee ; Yeon-Mok Oh MD, PhD ; Yongjun Chang

PURPOSE

To propose a quantification method to classify emphysema clusters by size using length scale analysis in volumetric chest CT.

METHOD AND MATERIALS

Volumetric CT scans of twenty patients with chronic obstructive pulmonary disease (COPD) were performed by a 16-multi detector row CT scanner (Siemens Sensation 16) with in 0.75mm collimation. Using thresholding by -950 HU, emphysema index (EI) of low attenuation area (LAA) mask was evaluated. Based on these LAA masks, a length scale analysis to estimate each emphysema cluster's size was performed as follows. At first, Hole filling algorithm was performed on the emphysema mask and Gaussian low pass filter (LPF) with various size of kernel (15mm) was performed from large to small size, iteratively. Maximum density voxel in the each filtered volume was selected and dilated by the size of the kernel, which was regarded as the specific size emphysema mask. In this way, emphysema cluster with specific size range was classified and evaluated from the LAA mask. The accuracy of this classification result was evaluated and compared by an expert thoracic radiologist with 10 scale visual evaluation to determine size classifying accuracy and to determine probabilities for incorrect estimation. In addition, an artificial phantom study for mimicking emphysema and a COPD patients study were performed to evaluate the accuracy of this algorithm.

RESULTS

In phantom study, in case of sphere-like the shape of emphysema with various sizes from 1mm to 15mm, the method shows exact estimation on every case. In the COPD patients, size based EI were $3.48 \pm 1.97\%$, $12.85 \pm 7.07\%$, $7.07 \pm 7.88\%$, and $4.11 \pm 8.22\%$, (size : 15mm), respectively. In addition, association study between blind visual evaluations of size based EI by an expert thoracic radiologist and our method showed all significant correlations r values : 0.499, 0.725, 0.768, 0.939, respectively) and probabilities for incorrect estimation were $0.0 \pm 0.0\%$, $0.67 \pm 0.2\%$, $0.5 \pm 0.41\%$, and $1.17 \pm 0.26\%$ (size : 15mm), respectively. Overall underestimation and overestimation probabilities are 1.17% and 1.17%, respectively.

CONCLUSION

The methods proposed a robust emphysema clustering method, which could lead to new implication and progress of COPD

CLINICAL RELEVANCE/APPLICATION

This method is especially useful in measuring size based emphysema analysis and could be possible to evaluate etiology and progress of COPD using 3D volumetric chest CT.

SSK20-03 • Virtual Non-contrast CT Using Dual Energy Spectral CT: Reproducibility of Calcium Mass for Coronary Calcium Scoring

Myung Jin Chung MD * ; Wan-Youk Kim (Presenter) ; Dong Ik Cha MD ; Sung Mok Kim MD ; Moon C Kim RT ; Kyung S Lee MD, PhD

PURPOSE

To create virtual non-contrast CT, two-material decomposition is allowed from Spectral CT based on sinogram space, instead of three-material decomposition method allowed in image space. However, various virtual non-contrast images can be made from various material decomposition (MD) methods in spectral CT. We evaluated the feasibilities of three different virtual non-contrast (VNC) images derived from single source dual energy spectral CT compared to true non-contrast (TNC) image.

METHOD AND MATERIALS

This HIPAA-compliant study was approved by institutional review board and informed consent was provided from all patients. Twenty-four patients prospectively underwent non-contrast CT followed by contrast enhanced chest CT using single source fast kVp switching dual energy scan. Iodine eliminated images so called as VNC were reconstructed using two kinds of 2-material decomposition algorithms (MDW, material density-iodine/water; MDC, material density-iodine/calcium) and material suppression algorithm (MSI, iodine suppression image). Using third party workstation, semiautomatic calcium measurements were performed.

RESULTS

Quantified calcium scores (AJ score) from all three VNCs correlated well with that of TNC ($R^2 = 0.95, 0.88, \text{ and } 0.88$ for MDW, MDC, and MSI, respectively). However correlation coefficients were less than 0.9 ($C = 0.83, 0.62, \text{ and } 0.63$ for MDW, MDC, and MSI, respectively). Measured calcium volumes on VNCs also correlated well with that of TNC ($R^2 = 0.94, 0.87, \text{ and } 0.90$ for MDW, MDC, and MSI, respectively), with correlation coefficients of 0.78, 0.59, and 0.63 for MDW, MDC, and MSI, respectively. Among the three VNCs, MDW correlated best with TNC.

CONCLUSION

VNC image from contrast enhanced CT using dual energy material decomposition/suppression is feasible for coronary calcium scoring. However, among various methods to make virtual noncontrast image from spectral CT, material quantifications are different depending on the decomposition methods. Furthermore, the absolute value on VNC tends to be smaller than that on TNC and should be considered with calibration.

CLINICAL RELEVANCE/APPLICATION

Absolute values of calcium scoring on VNC tend to be smaller than that on TNC and should be considered with calibration.

SSK20-04 • Reproducibility of Imaging Features Computed from Same-day Repeat CT Scan Images Reconstructed at Different Acquisition Parameters

Binsheng Zhao DSc (Presenter) ; **Yongqiang Tan** PhD ; **Mingshi Wang** ; **Hyun-Ju Lee** MD, PhD ; **Chuanmiao Xie** ; **Jing Qi** ; **Ross C Ehmke** BA ; **Lawrence H Schwartz** MD

PURPOSE

Radiogenomics promises the genetic assessment of cancer patients with non-invasive radiographic imaging studies. To date, little attention has been paid to the sensitivity of imaging features to repeat scans and acquisition parameters. This study explored the reproducibility of imaging features computed on repeat CT scans reconstructed at different parameters.

METHOD AND MATERIALS

This study included a retrospective dataset containing 32 lung cancer patients, each having two same-day repeat CT scans and reconstructed into 6 image series, i.e., a combination of 3 slice intervals (5, 2.5 and 1.25mm) and 2 reconstruction algorithms [Lung (L) and Standard (S)]. Three radiologists independently used an in-house algorithm to segment 32 tumors (= 1 cm; one per patient) in all image series. 261 imaging features describing tumor size, histogram, shape, edge and texture were computed from the final tumor volumes, based on the common volumes obtained by 2 out of the 3 radiologists. The concordance correlation coefficient (CCC) was used to measure the agreement between each feature computed from two repeat scans reconstructed at the 6 series, i.e., 1.25L (first scan) and 1.25L (second scan), 1.25Sand1.25S, 2.5Land2.5L, 2.5Sand2.5S, 5Land5L and 5Sand5S.

RESULTS

Out of the 261 features, CCC of 32 features were = 0.95 and of 169 features were = 0.75 for all 6 series. Size and histogram features were highly reproducible for all parameter settings; shape index and boundary gradient strength were the least reproducible. For 2.5Sand2.5S re-scans, all run-length, GTDM and spatial correlation features had CCC=0.95; surprisingly, many features showed inferior reproducibility with 1.25Land1.25L re-scans, possibly due to noise.

CONCLUSION

Imaging parameters and repeat scans affect the reproducibility of imaging features to various degrees. Generally, the reproducibility of size, histogram, GTDM, run-length, spatial correlation, Laws', Gabor, wavelet, LoG and GLCM features (except 1.25Land1.25L for several features) at all parameter combinations ranged from acceptable (CCC=0.75) to excellent (CCC=0.95). The correlation of these features to gene expression warrants further investigation.

CLINICAL RELEVANCE/APPLICATION

Precautions should be taken with regard to CT imaging acquisition parameters when conducting radiogenomics studies.

SSK20-05 • Improving CT Perfusion Image Quality Using Principal Component Analysis

Timothy Pok Chi Yeung BSc (Presenter) ; **Nathan De Haan** ; **Mark Dekaban** ; **Laura Morrison** ; **Lisa Hoffman** ; **Slav Yartsev** ; **Glenn S Bauman** MD * ; **Ting-Yim Lee** MSc, PhD *

PURPOSE

Many CT perfusion (CTP) studies of small animal tumor models are performed using clinical CT scanner due to its availability, but the tradeoff between spatial resolution and image noise affects the quality of CT perfusion images. This study aimed to evaluate the ability of principal component analysis (PCA) in improving the contrast-to-noise ratio (CNR) of CTP images in a preclinical model of malignant glioma.

METHOD AND MATERIALS

Wistar rats (n = 8) implanted with C6 glioma cells were scanned using CTP. Each CTP image set was filtered using 2, 4, 6, 8, and 10 principal components from PCA to result in 40 additional image sets. The noise level and CNR were used to quantify image quality in all 48 unfiltered and filtered image sets. The fractional residual information (FRI) was used to evaluate the amount of information loss after PCA filtering. Blood flow (BF), blood volume (BV), and permeability-surface area product (PS) before and after filtering were calculated. Noise level, CNR, BF, BV, and PS in the normal brain and tumor were expressed as mean ± standard error of the mean. These metrics before and after filtering with different numbers of principal components were compared to evaluate the differences between the filtered and the unfiltered image sets.

RESULTS

PCA filtering significantly decreased noise level and increased CNR (p = 0.01). An average of 26% (range, 11 to 49%) of pixels in the tumor had information loss of = 5% when filtering with only two principal components; this percentage decreased to an average of 1% (range, 0 to 3%) with four or more components. Normal brain BV and PS were significantly different than the values in the tumor (p < 0.01) without or with PCA filtering (using 4 or more principal components). Normal brain and tumor BF values were not significantly different without PCA filtering, but they became significantly different after filtering with 4 principal components (p = 0.03).

CONCLUSION

PCA filtering improved the CNR in CTP studies. Four or more principal components are required to filter the CTP source images without substantial loss of information leading to higher contrast between tumor and normal brain tissue in BF maps.

CLINICAL RELEVANCE/APPLICATION

Lowering radiation exposure can lead to deterioration of CNR in CTP studies. PCA improves CNR to allow repeated ultralow dose CTP studies for assessing treatment response in the clinical setting.

SSK20-06 • Image Registration for Prostate MR Guided Biopsy Using Automated Biomechanical Modeling

Wendy Van De Ven MSc (Presenter) ; **Nico Karssemeijer** PhD * ; **Jelle O Barentsz** MD, PhD ; **Henkjan Huisman** PhD *

PURPOSE

To investigate the effect of extending a non-rigid surface-based registration method with biomechanical modeling for prostate MR guided biopsies on the target registration error (TRE) using internal reference landmarks. The method is fully automated and we compare accuracy to previous results obtained with manual optimization of parameters in every patient.

METHOD AND MATERIALS

The accuracy of a novel non-rigid registration method involving biomechanical modeling to account for deformations inside the prostate was determined. While MR-TRUS registration is the ultimate goal, we used MR guided MR biopsy imaging data from six consecutive patients for this evaluation. The data included T2-weighted images (0.8x0.8x3.0 mm) before and after insertion of a needle guide causing deformation of the prostate. The needle guide had an orientation and dimension comparable to a transrectal ultrasound (TRUS) probe. The prostate in the two images was segmented and corresponding surface meshes were generated in both images by assuming identical prostate orientations. Next, a tetrahedral volume mesh was generated from the image before needle insertion. Prostate deformations due to needle insertion were simulated using the surface displacements as boundary condition. A 3D thin-plate spline deformation field was calculated by registering the mesh vertices. The TRE was defined as the Euclidean distance between registered and reference landmark position and was calculated for 45 reference landmarks manually annotated in both T2-weighted images. The results of this automated method were also compared to previous results obtained with manual optimization.

RESULTS

The median TRE of the automated surface-based registration method with biomechanical regularization was 2.21 mm (range 0.55-7.32 mm), which was significantly lower than a median TRE of 3.02 mm (range 0.85-7.95 mm) obtained without biomechanical regularization (PP = 0.10).

CONCLUSION Non-rigid surface-based image registration extended with biomechanical modeling can be automated and improves the registration accuracy for prostate MR guided biopsies.

CLINICAL RELEVANCE/APPLICATION The automated surface-based registration method extended with biomechanical modeling is applicable to MR-TRUS registration and can help to improve effectiveness of MR guided TRUS biopsy procedures.

SSK20-07 • Validity of Myocardial Perfusion Asynchrony Measurements

Andrew Van Tosh MD *; **Nathaniel Reichel MD**; **Christopher J Palestro MD**; **Kenneth Nichols PhD (Presenter) ***

PURPOSE

Left ventricular (LV) asynchrony can be quantified by both gated blood pool (BP) and myocardial perfusion (MP) tomography. A concern regarding MP phase measurements is their reliance on tracking myocardial walls in cases of severely reduced MP, for which counts are low. PET data are acquired in gated list mode and both BP and MP data are available for the same pts. To test validity of MP phase measurements for severely decreased MP we compared MP to BP phase measurements, which are not affected by decreased MP.

METHOD AND MATERIALS

Data were analyzed retrospectively for 67 pts (42 males; 23 females; 71±12 yrs) with suspected heart disease evaluated by ⁸²Rb PET/CT. Data were collected in gated list mode and rebinned into BP tomograms of tracer imaged during the first pass transit through the heart chambers, and separately into MP tomograms of tracer imaged during equilibrium. For BP PET data LV contraction phases were computed for each of 17 LV segments. Excluding the 3 most basal-septal segments to ensure LV cavity sampling the bandwidth (BW) of contraction phases were computed, defined as % of the R-R interval accounting for 95% of LV regional contractions. MP tomograms were analyzed by commercial algorithms, which computed summed rest scores (SRS) indicating severity of MP defects, and MP phase BW derived from phases of maximum count brightness corresponding to regional end-systole at each voxel at locations identified by algorithms as corresponding to the myocardial wall.

RESULTS

37 pts had negligible defects (SRS = 4) with BP phase BW = 16±8%, lower than the 30 pts with significant MP defects (SRS > 4) (33±22%, p = 0.0001). BP and MP phase BW were similar for all pts (24±% versus 26±16%, p = 0.49), pts with SRS = 4 (16±8% versus 19±9%, p = 0.15), and pts with SRS > 4 (33±23% versus 36±19%, p = 0.50). BP and MP phase BW correlated significantly and similarly with SRS (r = 0.59, p < 0.0001 and r = 0.61, p < 0.0001), consistent with greater amounts of asynchrony being related to more severe myocardial damage. Differences between BP and MP phase BW had no correlation to SRS (r = 0.04, p = 0.75). Thus, severe MP defects had no deleterious effect on MP phase quantitation.

CONCLUSION

Detection of LV asynchrony by phase measurements derived from gated ⁸²Rb PET/CT tomograms are robust and reliable, regardless of severity of MP defects.

CLINICAL RELEVANCE/APPLICATION

It is justifiable to include scintigraphic asynchrony measurements in forming clinical impressions for pts exhibiting severe MP defects.

SSK20-08 • Classification of Osteoarthritic and Healthy Chondrocyte Patterns in Human Patellar Cartilage on Phase Contrast Computed Tomography through Topological and Geometric Features

Mahesh Nagarajan (Presenter); **Paola Coan**; **Markus B Huber PhD**; **Paul C Diemoz PhD**; **Christian Glaser MD**; **Axel Wismueller MD, PhD**

PURPOSE

Phase-contrast X-ray computed tomography (PCI-CT) has been demonstrated at achieving soft-tissue contrast with micrometer scale resolution while imaging cartilage. This study proposes to quantitatively evaluate the performance of topological and geometrical approaches in characterizing chondrocyte patterns as observed in PCI-CT of human patellar cartilage as healthy or osteoarthritic.

METHOD AND MATERIALS

Five osteochondral cylinders (7 mm diameter, 3 osteoarthritic, 2 healthy) extracted from post-mortem human patellae were subject to PCI-CT at 26 keV (European Synchrotron Radiation Facility, Grenoble, France). From reconstructed CT images of the cartilage, 842 regions of interest (ROI) of size 51x51 pixels capturing chondrocyte patterns were then annotated in the radial zone of the cartilage matrix from high resolution images (voxel size: 8 x 8 x 8 μm³). Two texture analysis techniques - (1) Scaling Index Method (SIM), that estimates local scaling properties and (2) Minkowski Functionals (MF), that evaluates topological properties, were used to extract features from the ROIs. Random sub-sampling cross-validation was utilized in optimizing a support vector regression model with a radial basis function kernel for the classification task. Performance was measured using area under the Receiver-Operator Characteristic (ROC) curve (AUC) for each feature.

RESULTS

With the experimental conditions used in this study, the best classification performance was observed with the SIM histogram (0.95 ± 0.06) which was significantly better than the performance achieved by all Minkowski Functionals ♦ Area (0.61 ± 0.07), Perimeter (0.85 ± 0.10) and Euler Characteristic (0.88 ± 0.09).

CONCLUSION

Our study investigates the use of advanced texture analysis techniques in images acquired with PCI-CT to quantitatively evaluate their ability in distinguishing between healthy and osteoarthritic cartilage. Our results show that geometrical features derived from SIM can capture differences in chondrocyte patterns annotated in the radial zone of knee cartilage matrix extracted from healthy and osteoarthritic specimens with high accuracy, and significantly outperform topological features derived from MF at the same task.

CLINICAL RELEVANCE/APPLICATION

Computer-aided feature analysis can distinguish between osteoarthritic and healthy chondrocyte patterns in knee cartilage as seen on Phase Contrast CT imaging studies with micrometer scale resolution.

SSK20-09 • Analysis of Treatment Response of Bladder Cancers on CT Scans: Comparison of Computerized Volume Estimation with WHO and RECIST Criteria

Lubomir M Hadjiiski PhD (Presenter); **Alon Z Weizer MD**; **Ajjai S Alva MD**; **Elaine M Caoili MD, MS**; **Richard H Cohan MD ***; **Heang-Ping Chan PhD**; **Kenny H Cha BEng**; **Stephen Dailey**

PURPOSE

To evaluate the accuracy of our Auto-Initialized Cascaded Level Set (AI-CALS) 3D segmentation system, the WHO and the RECIST criteria in estimation of treatment response of bladder cancer using CT scans.

METHOD AND MATERIALS

The AI-CALS system is designed to extract 3D lesion boundary based on level sets. The system uses as input an approximate bounding box for the lesion of interest. With IRB approval, pre- and post-chemotherapy treatment CT scans of 20 patients with

bladder cancers were collected retrospectively for this preliminary study. For all cases, cystectomy was performed after treatment and the disease outcome was available as reference standard of treatment response. 35% of patients had pT0 disease (complete response) at cystectomy. A radiologist marked 20 temporal pairs of primary site cancers and also manually outlined full 3D contours on both the pre- and post-treatment scans using a GUI. For all cancers, following WHO and RECIST criteria two radiologists measured the longest diameter and its perpendicular on the pre- and post-treatment scans. Receiver operating characteristic (ROC) analysis was performed and the area under the ROC curve (AUC) was calculated to estimate the accuracy for prediction of pT0 stage (complete response) at cystectomy by the manual (3D), AI-CALS (3D), WHO (2D), and RECIST (1D) methods.

RESULTS

For the 20 cancers, the average pre- and post-treatment volumes from radiologist's segmentation were 36.0 and 17.6 cm³, respectively. The AUC for prediction of pT0 disease at cystectomy was 0.68±0.13 for the AI-CALS compared to 0.72±0.11 for the manual segmentation. The difference was not significant. Prediction of pT0 disease using the RECIST criteria by two radiologists was lower than the two 3D methods with AUCs of 0.59±0.14 and 0.66±0.12, respectively. Prediction of pT0 disease using the WHO criteria by the two radiologists had AUCs of 0.50±0.14 and 0.56±0.12, respectively, which were lower than all other methods.

CONCLUSION

The 3D pre- and post-treatment volume estimates obtained by manual radiologist segmentation and AI-CALS provided more accurate depiction of the irregular 3D tumor shapes and volume changes compared to the 1D (RECIST) and 2D (WHO) estimates.

CLINICAL RELEVANCE/APPLICATION

For tumors with irregular shape such as bladder cancers the 3D automated segmentation has the potential to accurately and efficiently determine tumor volume and response to treatment.

Physics (Molecular Imaging) Wednesday, 10:30 AM - 12:00 PM • S404AB [Back to Top](#)   **SSK21** • AMA PRA Category 1 Credit™:1.5 • ARRT Category A+ Credit:1.5 **Moderator Georges El Fakhri**, PhD

Moderator Scott Metzler, MD

SSK21-01 • Intravoxel Incoherent Motion Perfusion MRI: A Sensitive Imaging Biomarker of Tumor Oxygenation

Zhongwei Zhang MD, PhD (Presenter); **Rami R Hallac** MS; **Qing Yuan** PhD; **Peter Peschke** PhD; **Ralph P Mason** PhD *

PURPOSE

The overall poor perfusion rate caused by abnormal vascular architecture and increased flow resistance is an important contributor to hypoxia and resistance to therapies. The intravoxel incoherent motion (IVIM) effect observed by diffusion-weighted MRI offers a non-invasive, quantitative method to measure perfusion. In this study, we investigate the feasibility of using the perfusion parameters derived from IVIM MRI as a sensitive imaging biomarker of tumor oxygenation.

METHOD AND MATERIALS

Small pieces of tumor tissue (Dunning R3327- AT1 and MAT-Lu rat prostate sublines) were implanted subcutaneously in the thigh of six male Copenhagen rats. MRI was performed at 4.7 T with a 35 mm volume coil, tunable to 1H or 19F. Each animal breathed air followed by 100% oxygen and then carbogen (95% O₂, 5% CO₂), all delivered at 2 L/min. A multi-shot FSE DWI sequence was performed with TR/TE_{eff} = 2000/56ms, 40mm × 40mm FOV, 128×64 matrix, ETL = 8, and 2 NSA. Diffusion gradients were applied in 3 orthogonal directions with 10 b-values (0-1500s/mm²). ADC was computed by fitting all b-values to a monoexponential model and IVIM parameters were calculated using a biexponential model: $S/S_0 = fp \cdot \exp(-bDp) + (1-fp) \cdot \exp(-bDt)$. ADC_{iv} = ADC - Dt was also defined to quantify intravascular space. pO₂ (mmHg) was estimated using 19F FREDOM method through injection pO₂ reporter. Pearson correlation coefficients (r) between IVIM parameters and pO₂ were calculated.

RESULTS

The pO₂ measured in air correlated strongly and significantly with the mean of $fp \cdot Dp$ ($r=0.88$), as well as Dp in air ($r=0.84$), which indicates fp and $fp \cdot DP$ are sensitive to pO₂ in air. When gas challenge was given, Strong correlation with fp was found for $?pO_2cb$ (pO₂ in carbogen-pO₂ in air) ($r=0.80$) and $?pO_2o_2$ (pO₂ in oxygen-pO₂ in air) ($r=0.89$). A similar strong and significant correlation was found between ADC_{iv} and $?pO_2cb$ and $?pO_2o_2$ ($r=0.86$ and $r=0.92$). It suggests that the baseline fp as well as ADC_{iv} determines the size of tumor response to gas challenge.

CONCLUSION

This study indicates that the perfusion parameters derived from IVIM MRI serve as a sensitive imaging biomarker of tumor oxygenation. IVIM Perfusion MRI may also be of value in the assessment of tumor microenvironment, monitoring tumor radiation therapy response.

CLINICAL RELEVANCE/APPLICATION

The IVIM Perfusion MRI provides a unique tool for assessment of tumor oxygenation and tumor microenvironment without the use of exogenous contrast.

SSK21-02 • Establishing Cell Structure-based Biomarkers of Disease Using Label-free Optical Quantification of Cell Mass, Volume, and Density in Early and Late Stage Colorectal Cancer Cell Lines

Sophia Bornstein MD, PhD; **Eric Anderson** MD, PhD; **Melissa Wong** PhD; **Owen McCarty** PhD; **Kevin Phillips** (Presenter)

ABSTRACT

Purpose/Objectives

Metastasis, the leading cause of all cancer-related deaths, is facilitated by the hematogenous transport of circulating tumor cells (CTCs) from the primary tumor site to distant organs. We have developed label-free optical tools to quantify the basic physical features of CTCs including their total dry mass content and subcellular density distribution. To interpret these biophysical signatures of cancer at the single cell level, we investigated these quantitative features as a function of tumorigenic potential in the patient-matched SW480/SW620 colorectal cancer cell lines as a model of early and late stage disease.

Materials/Methods

Using non-interferometric quantitative phase microscopy (NIQPM), a technique that can be carried out on commercial microscopes, we quantified the dry mass content and sub-cellular density distribution of cultured cell lines plated on microscope slides. The density distribution was fit with a bi-modal Gaussian distribution whose size parameters quantified the contributions of small and large density structures to the overall composition of the cells. The Jarque-Bera test was used to evaluate normality of all parameters. One-way analysis of variance with Bonferonni post hoc analysis was used to assess statistical significance among parameters across multiple normally distributed cell parameters.

Results

SW620 cells demonstrated a morphology-dependent total dry mass content. The relative amount of small and large micron-scale density contributions to cellular density was found to be morphology-dependent among SW480 cells. SW620 cells possess significantly denser small-scale structures in comparison to SW480 cells. The density contributions from large-scale structures are conserved across all the SW cell types.

Conclusions

Micron scale characterization of the SW cell types with NIQPM demonstrated a systematic bimodal distribution of the subcellular density distribution whose small-scale peak was sensitive to tumorigenic potential of the SW620 cells. Total mass was also specific to SW620 cells. This work quantitatively elucidates distinct cellular architectural phenotypes of early and late stage colorectal cancer in an in vitro setting. These results provides a rational for the use of label-free optically derived metrics to be tested clinically as biomarkers capable of monitoring responses among CTCs to radiological interventions.

SSK21-03 • Comparison of Quantitative Approaches to Identify Patients with Parkinsonism Using Dopamine Transporter Scans

PURPOSE

Presynaptic dopamine transporter ^{123}I -ioflupane (DaT) SPECT imaging facilitates the differentiation of Parkinsonism from essential tremor (ET). Some groups advocate quantitative analyses of caudate (C) or putamen (P) counts for improved differentiation of these two entities, while others recommend applying normal limits to background-corrected counts. This investigation was undertaken to determine which data analysis approach agrees most strongly with a final diagnosis of Parkinsonism.

METHOD AND MATERIALS

We performed a retrospective analysis of ^{123}I -FP-CIT SPECT data for 50 pts (age 64 ± 12 years; 28 F; 22 M) who were evaluated for movement disorders. Data were reconstructed by OSEM (12 iterations, 8 subsets) and corrected for attenuation by the Chang method. BASGAN software (Eur J Nucl Med Mol Imaging 2007;34:1240-53) generated ratios of automated caudate (AC) and automated putamen (AP) counts per pixel versus background counts per pixel, and dichotomous abnormal values for caudate (DC) and putamen (DP) by applying recently updated age- and sex-adjusted normal limits (Eur J Nucl Med Mol Imaging 2013;40:565-73). In separate processing sessions, a medical physicist manually drew regions of interest to determine maximum caudate (MC) and maximum putamen (MP) counts, without knowledge of other clinical or quantitative results. The diagnosis of the patient's official report served as the reference standard. ROC analysis determined optimal discrimination thresholds and kappa statistics evaluated strength of agreement.

RESULTS

Twenty-seven pts had Parkinsonism and 23 had ET. Highest agreement with final diagnoses was found for MP ($\kappa = 0.72$), followed by DC, MC, AC, AP and DP ($\kappa = 0.67, 0.64, 0.64, 0.63$ and 0.41 , respectively). MP also had highest accuracy (86%), with sensitivity of 78% and specificity of 96%. Pixel averaging and statistical noise of background counts were likely reasons that automated output from BASGAN software underperformed manual determinations of maximal counts.

CONCLUSION

We conclude that, in the analysis of presynaptic dopamine transporter SPECT scans, a straightforward detection of abnormally suppressed putamen counts is the single quantitative measure that agrees most strongly with a diagnosis of Parkinsonism.

CLINICAL RELEVANCE/APPLICATION

While quantitation of DaT scans can bolster visual determinations of disease states, use of quantitative measures should be applied judiciously in influencing final diagnoses.

SSK21-04 • Spectral CT with K-edge Detection of Targeting Gold-nano-Particles: An Experimental Study

Thorsten R Fleiter MD (Presenter) ; **Marie-Christine Daniel** PhD ; **Omer Aras** MD

PURPOSE

To determine the specific detectability of targeting Gold-Nano-particles using K-edge CT imaging for the selective and quantitative imaging of the Gold cores.

METHOD AND MATERIALS

Mice with over-expression of the Angiotensin - converting Enzyme (ACE) were prepared with Lisinopril-Gold-Nano-particles. The Gold core diameter of the conjugates was measured with 10-15 nm. The animals were euthanized and frozen at 2, 4, 6 and 10 min after the injection of the conjugates. A control group of mice was prepared with conventional Lisinopril ahead of the injection of Lisinoprol-Gold-Nano-particles to block the binding sites for the conjugate and therefore to analyze the targeting capabilities of the Conjugate. The mice were scanned with a photon counting full spectral CT with data sampling 5KeV above and below the K-edge of Gold at 80.7 KeV. The difference of these two measurements was used to reconstruct images that contained the Gold signal only. Additional data sampling was performed over the residual x-ray spectrum and used for the reconstruction of the anatomical background for the Gold specific images.

RESULTS

The highest signal to noise and Gold to anatomical background ratios were achieved at 10 min after the injection of the Lisinopril-Gold-Nano-particles. The highest signal was measured in the heart muscles and the lung parenchyma. The anatomical background was completely eliminated in the k-edge images of the Gold. The signal to noise ratio in these images was $>5:1$. An overlay of the anatomical images and the Gold images better demonstrated the distribution of the Gold particles. There were no gold signals detectable in mice that were pre-treated with Lisinopril prior to the conjugate injection.

CONCLUSION

K-edge imaging to detect targeting Gold-Nano-Particles with Computed Tomography is feasible. The specific Gold-images can be used for a fast assessment of the distribution of the particles and therefore the density of the bindings sites for the molecule.

CLINICAL RELEVANCE/APPLICATION

K-edge imaging with Spectral CT can be used to track Nano-particles with high Z cores like Gold that could be designed to specifically display e.g. tumors or cardiac scars.

SSK21-05 • Direct Visualization of miRNA-22 Biogenesis in Isoproterenol-induced Cardiac Hypertrophy by Bioluminescence Imaging In Vitro and In Vivo

Yingfeng Tu (Presenter) ; **Bao-Zhong Shen**

CONCLUSION

These findings elucidate the feasibility of using our constructed miRNA reporter imaging system to monitor the location and magnitude of expression level of miRNA-22 in CH and to appraise the function of antagomir-22 in silencing the cardiac endogenous miR-22 expression in vitro and in vivo.

Background

Evidence from recent studies has shown that miRNAs play key roles in cardiac hypertrophy (CH). To measure the expression level of endogenous miRNAs is very conducive to understanding the importance of miRNAs in CH. However, current methods to monitor endogenous miRNA level, such as northern blotting, quantitative real-time polymerase chain reaction (qRT-PCR), and miRNA microarrays can not provide real-time information of miRNA biogenesis in CH. Here, we constructed a novel miRNA reporter imaging system to monitor the miR-22 expression in CH in which three copies of the antisense of miR-22 (3 \times PT_miR-22) was cloned immediately into the downstream region (3'UTR region) of the gaussia luciferase (Gluc) reporter genes, driven by a cytomegalovirus (CMV) promoter.

Evaluation

In this current study we found that with prolongation of isoproterenol (ISO) stimulation in vitro and in vivo, the expression level of miR-22 in cardiomyocytes was gradually increased. Accordingly, the bioluminescence imaging analysis revealed that the fluorescence signals of the miRNA reporter imaging system (CMV/Gluc/3 \times PT_miR-22) gradually decreased under conditions where miRNA-22 was up-regulated by ISO stimulation. However, the firefly luciferase (Fluc) activity of CMV/Fluc, as a positive control, was not affected with ISO treatment. Furthermore, knockdown of miR-22 by antagomir-22 could reverse the repressed Gluc activities in vitro and in vivo.

Discussion

The development of imaging strategies related to miRNAs will be critical to advance our understanding of the interactions of miRNAs with their target genes and signaling pathways, and eventually to evaluate the use of miRNAs as a novel class of diagnostics and

SSK21-06 • Volume of Drug Distribution as a Function of Time for Adaptive Gamma Variate Fits to Plasma Concentrations Curves

Michal J Wesolowski PhD, MSc (Presenter) ; **Surajith N Wanasundara** PhD, MSc ; **Richard C Puetter** PhD ; **Maria T Burniston** PhD ; **Paul S Babyn** MD ; **Carl A Wesolowski** MD, FRCPC

CONCLUSION

While it is often assumed that the distribution of a drug in the body is complete after 1-2 hours, this does not appear to be the case for patients having a GFR marker study and a high incidence of ascites for whom it may take several days to reach 95% of the final volume of distribution.

Background

In studies of renal function and glomerular filtration rate (GFR) it is commonly assumed that the distribution of drug in the body is complete within the first 1-2 hours after a single injection or institution of a continuous infusion of a GFR marker. If incorrect, this may lead to inaccuracy in the calculation of plasma clearance and affect patient care. To test the validity of this assumption, a time dependent volume of drug distribution term was derived from the mass conservation equation in the Tikonov adaptively fit gamma variate (TK-GV) model of plasma clearance.

Evaluation

Following a single intravenous injection, the plasma concentration of a radioactively labeled glomerular filtration marker, $^{51}\text{Cr-EDTA}$, was monitored over 24 hours (up to 16 samples) in thirteen patients being evaluated for liver transplantation. For each patient, the volume of drug distribution as a function of time, from adaptive gamma variate fits to plasma concentration versus time curves, was obtained. Plasma clearance and the time required to reach 95% of the final GFR marker volume of distribution were calculated.

Discussion

In these patients, the time required to reach 95% of the final volume of distribution ranged from 0.79 to 11.08 days, which is significantly longer than is commonly assumed. In fact, the GFR marker appears to be eliminated faster than the completion of the volume distribution expansion implying that a steady state volume cannot be reached in practice. Finally, it is shown that on average, 7% of the value of plasma clearance can be attributed solely to this volume expansion. We therefore propose that extrarenal clearance, which has often been invoked to explain discrepancies observed between plasma and urinary clearance values, may largely originate in this time dependent volume expansion term.

SSK21-07 • Prognostic Value of Metabolic Tumor Volume Measured by Differing Methods on Staging ^{18}F -fluorodeoxyglucose Positron Emission Tomography in Esophageal Cancer

Vinod Malik MBBCh, MA (Presenter) ; **Ciaran J Johnston** MD ; **Julie A Lucey** PhD ; **John V Reynolds** MD

PURPOSE

Metabolic tumor volume (MTV) a volumetric parameter obtained on ^{18}F -fluorodeoxyglucose positron emission tomography/computed tomography (^{18}F -FDG PET/CT) has been shown to be an independent prognostic factor for survival in patients with esophageal cancer. This study ascertained if different methods of calculating MTV would have an effect on its utility as a prognostic factor.

METHOD AND MATERIALS

From December 2008 to May 2011, 150 patients with biopsy-proven cancer of the esophagus or esophagogastric junction underwent staging ^{18}F -FDG PET/CT. Maximum standardized uptake value (SUVmax) and MTV of the primary tumor was recorded at different thresholds (absolute cut-offs of SUV 2.5 and 3.5, threshold values of 42% and 50% SUV max and a variable method depending on the SUV max of the primary tumor). Survival analysis was performed using Kaplan-Meier and independent prognostic factors determined using Cox regression multivariate analysis.

RESULTS

^{18}F -FDG PET/CT SUVmax < 4.1 ($p=0.0014$), ^{18}F -FDG PET/CT MTV (absolute cut-off SUV 2.5 method) < 14.5cm³ ($p=0.001$), ^{18}F -FDG PET/CT MTV (absolute cut-off SUV 3.5 method) < 7.5cm³ ($p=0.0013$), ^{18}F -FDG PET/CT MTV (threshold value of 42% method) < 5.9cm³ ($p=0.0005$), ^{18}F -FDG PET/CT MTV (threshold value of 50% method) < 4.4cm³ ($p=0.0004$), ^{18}F -FDG PET/CT MTV (variable method) < 4.7cm³ ($p=0.0008$) were all significantly associated with outcome on analysis.

CONCLUSION

Regardless of the method used to measure MTV, it consistently was able to predict survival even when simple quantitative analysis only is performed.

CLINICAL RELEVANCE/APPLICATION

MTV is a valuable prognostic factor in patients with esophageal cancer even when performed with simple quantitative analysis which is available on all clinical scanners.

SSK21-08 • Determining the Minimal Required Radioactivity of F-18 FDG for Reliable Semi-quantification in PET-CT Imaging: A Phantom Study

Ming-Kai Chen MD, PhD (Presenter) ; **David H Menard** ; **David W Cheng** MD, PhD *

PURPOSE

The aim is to investigate minimal required radioactivity of F-18 FDG and corresponding imaging time for reliable semi-quantification in PET-CT imaging in an effort for dose reduction

METHOD AND MATERIALS

We performed F-18 FDG PET-CT study using an ECT phantom containing various spheres (diameter: 3.4, 2.1, 1.5, 1.2, 1.0 cm) filled with a fixed concentration of 165 kBq/ml and background 23.3 kBq/ml (total 156.8 MBq) at multiple time points up to 20 hrs of radioactive decay. The images were acquired for 10 min/bed at each time point using 3-D mode in a hybrid GE Discovery 690 scanner equipped with LYSO detectors and a 64-slice CT. The images were reconstructed in 1, 2, 3, 4, 5, and 10 min per bed using ordered-subset expectation maximum (OSEM) algorithm with 24 subsets and 2 iterations. The standardized uptake values (SUV) of the spheres with both maximal and average were measured by applying volume of interests (VOI) in serial PET images. The minimal required activity concentrations at various acquisition time were determined as well as the minimal product of activity concentration and acquisition time.

RESULTS

The minimal required activity concentration for precise SUVmax quantification in spheres (

CONCLUSION

Our phantom study provided guidance for minimal required activity and acquisition time for precise semi-quantification in F-18 FDG PET imaging. We can further reduce dose and radiation exposure to patients at reasonable acquisition time in clinical studies.

CLINICAL RELEVANCE/APPLICATION

(dealing with PET-CT) Based on the data, we can further reduce the administrative dose of F-18 FDG in clinical studies.

SSK21-09 • Detecting Osteoporosis Using Photoacoustic Spectroscopy

CONCLUSION

Photoacoustic spectroscopy is technically for detecting the osteoporosis at no radiation cost. This method may be sensitive to the micro structural changes in the bone. In addition with multi spectral imaging, it is possible to analyze different components of the bone tissue such as calcium by decomposing the photoacoustic spectrum to the standard tissue absorbers optical spectrums.

Background

Osteoporosis, is the most common metabolic bone disorder. Monitoring the micro architectural deterioration of the bone tissue and the decrease of the bone mineral density are necessary for early detection the osteoporosis. Broadband attenuation of ultrasound signal is correlated with bone mineral density and its microstructure. In addition, the optical absorption spectrum of the bone tissue analyzes its mineral, water, lipid and oxy-deoxy hemoglobin content. Therefore photoacoustic spectroscopy as a hybrid functional method that combines both optical and ultrasound information is a promising technique for determination of osteoporosis in early stages.

Evaluation

In this study, the quantitative ultrasound calcaneal phantoms of normal and osteoporotic bone were imaged in the transmission mode and the corresponding photoacoustic spectrums were obtained. Our photoacoustic imaging system includes a tunable Q-switch Nd:YAG laser followed by an OPO system generating pulses at the wavelength range of 690 nm-950 nm. The photoacoustic signal is detected with the FDA approved Sonix RP ultrasound system including a data acquisition device for recording the raw data. Multiple points of each phantom were evaluated using a linear US probe with 128 elements. Finally the maximum raw data was extracted from the elements and the value was normalized to the illuminating laser energy.

Discussion

The result revealed a general decrease in the spectrum of the osteoporotic phantom compared to the normal one. The trend matches the optical spectrum of the calcaneus bone tissue. In this test, there was about two times contrast between the normal and osteoporotic case. These phantoms were modeling the bone microstructure and more contrast is expected in the real bone tissue including other tissue absorbers.

Physics - Wednesday Posters and Exhibits (12:15pm - 12:45pm) Wednesday, 12:15 PM - 12:45 PM • Lakeside Learning Center [Back to Top](#) [PH](#) **LL-PHS-WEA • AMA PRA Category 1 Credit™:0.5 Host Samuel G Armato, PhD**

Host Bruce R Whiting, PhD

LL-PHE-WE10A • Current and Novel Imaging Technologies in Coronary Computed Tomography: What the Radiologist Needs to Know

Haruhiko Machida MD (Presenter) ; **Isao Tanaka** ; **Rika Fukui** ; **Yun Shen PhD *** ; **Yue Dong** ; **Eiko Ueno MD** ; **Takuya Nishino** ; **Etsuko Tate**

PURPOSE/AIM

1. To review standard coronary computed tomography (CCT) and its limitations
2. To illustrate current and novel imaging technologies in CCT
3. To demonstrate optimal strategies using these technologies by presenting experimental data and clinical images

CONTENT ORGANIZATION

1. Standard CCT and its limitations

- retrospective ECG-gated helical scan/ECG mA modulation
- radiation/contrast medium (CM) dose
- limited spatial/temporal resolution
- calcification/stent/beam-hardening (BH) artifact

2. Current and novel imaging technologies

- step-and-shoot (SAS) scan
- iterative reconstruction (IR)
- high definition CT (HDCT)
- motion correction algorithm
- dual-energy CT (DECT): BH correction/monochromatic imaging/material density imaging

3. Optimal strategies using these technologies

SUMMARY

To overcome the limitations of standard CCT, SAS scan and IR can reduce radiation dose, and HDCT and motion correction algorithm can improve spatial and temporal resolution. DECT can reduce CM dose and BH effect, remove vessel calcification, improve vessel contrast and delineation, and provide unique information about plaque composition. Optimal strategies using these technologies in CCT are essential for appropriate patient management.

LL-PHS-WE1A • Validation of Commercial Software's Reported SSDE Values

Dustin A Gress MS (Presenter) ; **Jenifer W Siegelman MD, MPH** ; **Mark P Supanich PhD *** ; **Alphonso Magri PhD**

CONCLUSION

Calculation of the derivative metric of effective diameter is accurate within the stated error of the SSDE calculation method (10-20%,TG-204). It is acceptable to use the effective diameter and SSDE outputs of this commercial software program.

Background

Some accrediting and regulatory bodies are requiring CT facilities to manage patient radiation dose. This work helps to validate a significant time-saving tool for such a QA initiative. A commercially available CT dose calculation and data aggregation software program (Radimetrics) used by a medium-sized community hospital in Connecticut has the capability of reporting SSDE, calculated using a patient's effective diameter obtained at a single level at the mid slice of the z-axis of the scan range. This work compares the effective diameter results of the software program with those calculated via manually measured AP and lateral dimensions, and determines whether or not the software's reported patient effective diameter, and in turn its reported SSDE, are valid for use in a patient dose management QA initiative.

Evaluation

The mid z-axis slice from 52 consecutive patients undergoing CT abdomen pelvis was identified. AP and lateral measurements were performed manually within PACS. Effective diameter from manual measurement was compared with that of the software using a Bland Altman analysis.

Discussion

Software reported a mean effective diameter 3.2% higher than the manual method, with 95%CI of +/-5.3%. Resulting SSDE from software is 3.4% lower than the manual method, with a 95%CI of +/-5.5%.

LL-PHS-WE2A • Improving Best-Phase Image Quality in Cardiac CT by Motion Correction with MAM Optimization

PURPOSE

We propose a novel technique for motion estimation and compensation, which for the first time allows for a significant improvement of the clinical relevant best-phase image quality and does not need on a multiple phase (4D) data acquisition.

METHOD AND MATERIALS

The novel motion estimation algorithm is composed of three major components which will be detailed in the following. First, different motion artifact metrics (MAM) are defined which allow the relative quantification of local motion artifacts. Meaningful MAMs are the image entropy and/or image positivity. Locality of the motion artifacts requires the identification of corrupted volume areas (volume of interest) which we denote motion maps. As last component, an optimization algorithm for the MAMs is required which actually estimates the unknown parameters of the motion model. Motion estimation corresponds to finding a set of motion parameters s that minimizes one or more of the selected MAMs. For minimization a simple gradient descent algorithm with adaptive step size is utilized.

RESULTS

It can be observed that the image quality drastically improves single source acquisition datasets, i.e. the motion artifacts are clearly reduced by the novel algorithm. Also, in case of Dual Source in high pitch mode, where the maximum heart rate is currently limited to medium values, the heart rate limit can be released. We evaluated 10 patient data sets with heart rate above 70bpm and show that the image quality of coronary segments improved in any case. In Fig. 1 it can be seen how the proposed algorithm can significantly improve the best phase image quality at higher heart rates even in datasets with a very good temporal resolution of 75ms. Further the algorithm is capable to improve image quality reconstructed in non-ideal phases and in datasets with a low temporal resolution.

CONCLUSION

This demonstrates the generality of the proposed approach and that it can fully automatically optimize image quality. However, we are convinced that the software-based approaches cannot make hardware developments like dual source CT mandatory, but rather extend their applicability to a wider range of patients.

CLINICAL RELEVANCE/APPLICATION

Due to the encouraging results we think that image quality of the coronary arteries can be drastically increased without exposing the patient to more dose and without requiring the latest hardware.

LL-PHS-WE3A • Iterative Image Reconstruction for Low-dose Dedicated Breast CT

Junguo Bian PhD (Presenter) ; **Kai Yang** PhD ; **Xiao Han** MSc ; **Emil Y Sidky** PhD ; **John M Boone** PhD * ; **Xiaochuan Pan** PhD *

PURPOSE

A large number of projections are needed for FBP-based image reconstruction in breast CT while the total imaging dose is limited to that of a typical two-view mammography. This can result in low signal-to-noise ratio (SNR) in projection data and high noise in reconstruction images. Breasts are of small contrast and have fine tissue structures. Low SNR, small contrast, and fine structures thus make reconstruction improvement from low-dose dedicated breast-CT data very challenging. In the work, we carried out a study on image reconstruction from low-SNR patient data acquired with a dedicated breast CT by tailoring an iterative algorithm we developed. We demonstrate that iterative algorithms can improve on image quality over the currently used FBP-based algorithms when applied to low-SNR breast-CT data.

METHOD AND MATERIALS

We formulated image reconstruction in breast CT as a constrained-TV-minimization problem, and developed an ASD-POCS algorithm to obtain image reconstruction through solving the problem. Patient data were collected during an ongoing clinical trial performed at UC-Davis. From the collected low-SNR data, we reconstructed images by using ASD-POCS algorithms and compared to the images currently reconstructed by using FBP algorithms. Special attention in parameter selections was paid to minimize the blocky appearances that are typically observed in images reconstructed by use of TV-minimization-based algorithms from noisy data set. We performed image reconstruction of the whole breast volumes from more than 10 patient cases. The reconstruction programs were accelerated with CUDA programming.

RESULTS

Results of our study suggest that the ASD-POCS algorithm can yield images with improved spatial/contrast resolution over images currently reconstructed with FBP algorithms.

CONCLUSION

Our study indicates that the proposed iterative algorithm can improve image quality or be used for potential dose reduction in breast CT.

CLINICAL RELEVANCE/APPLICATION

The image quality improvement for the dedicated, cone-beam breast CT scanner may have impacts for breast cancer screening or diagnosis.

LL-PHS-WE4A • Ultra-high-Resolution CT of the Lung: Image Quality of a Prototype Scanner

Ryutaro Kakinuma MD, PhD (Presenter) ; **Noriyuki Moriyama** MD, PhD ; **Yukio Muramatsu** MD ; **Masahiko Kusumoto** MD ; **Akiko Maeshima** ; **Hisao Asamura**

PURPOSE

To evaluate the image noise and diagnostic performance of a prototype ultra-high-resolution CT (U-HRCT), compared with that of a conventional high-resolution CT (C-HRCT).

METHOD AND MATERIALS

A prototype U-HRCT scanner with 0.25 mm X 4 rows and 120 mAs was used. C-HRCT images were obtained using a 0.5 mm X 64 detector-row CT scanner operating at 150 mAs. Images were reconstructed at 0.1-mm intervals using both scanners; the slice thickness was 0.25 mm for the U-HRCT scanner and 0.5 mm for the C-HRCT scanner. For both modalities, the field of view was 8 cm, and all the images were displayed using lung field settings (WW1600, WL-600). Ten board-certified thoracic radiologists graded the U-HRCT and C-HRCT images of 53 slices derived from 36 lung nodules (21 resected adenocarcinomas and 15 miscellaneous nodules) using a five-point scale. The U-HRCT and C-HRCT images were presented to the observers randomly and in a blinded manner. The image noise of each scanner was evaluated using a phantom.

RESULTS

CONCLUSION

Despite a larger image noise, the diagnostic performance of the U-HRCT prototype scanner was significantly better than that of C-HRCT.

CLINICAL RELEVANCE/APPLICATION

U-HRCT might improve the diagnostic accuracy of indeterminate nodules detected using low-dose CT lung cancer screening.

LL-PHS-WE5A • Objective Evaluation of Low-contrast Detectability and High-contrast Resolution for Different Breast Imaging Modalities by Means of Breast Simulating Phantoms with Arbitrary Positionable Inserts

Ann-Christin Roessler MSc (Presenter) ; **Christian Steiding** MSc * ; **Daniel Kolditz** PhD * ; **Evelyn Wenkel** MD ; **Ruediger Schultz-Wendtland** ; **Willi A Kalender** PhD *

PURPOSE

Objective evaluation of image quality based on known phantom structures fixed in known positions is hard to do. We designed phantoms which allow arranging tumor-like masses, microcalcifications (\diamond Ca) and fibers freely with and without superpositioned structures to enable observer studies with the observer blinded to the ground truth.

METHOD AND MATERIALS

Phantoms were made of breast-equivalent material as a 40 mm slab and as a 14 cm diameter cylinder simulating the compressed breast for digital mammography (DM) and breast tomosynthesis (BT) and the pendant breast for breast CT (bCT), respectively. Both phantoms provide cavities (45×40^2 mm³) to insert structures such as cubes (10^3 mm³) and plates with different thicknesses simulating normal breast tissue or containing spherical soft-tissue masses (2-8 mm), \diamond Ca (0.1-0.4 mm) or connective tissue (fibers, 1 mm) which can be placed in different locations and superimpose each other. Measurements were done on clinical DM and BT systems and on a prototype high-resolution bCT system with and without superimposed structures. Exposure parameters for all systems were kept consistent with the standard clinical settings; i.e., spatial resolution was better than 100 \diamond m and dose was kept below 5 mGy. Images were acquired using random structure arrangements; ROC curves were generated based on 5 observers.

RESULTS

For DM and BT, low-contrast masses down to 4 mm were recognized without and down to 6 mm with added superimposing structures. All \diamond Ca objects were detected down to 200 \diamond m with and without superpositioned structures. Fibers were not seen in either arrangement. For bCT, low-contrast masses down to a size of 2 mm diameter, all \diamond Ca objects and all fibers were recognized by the observers. Standard ROC analysis revealed higher sensitivity and specificity for bCT in low-contrast detectability than for DM and BT.

CONCLUSION

Objective evaluation of low-contrast detectability with the reader blinded to structure type and position is feasible. In this test, high-resolution bCT showed performance superior to DM and DT, especially when confounding structures were superimposed.

CLINICAL RELEVANCE/APPLICATION

The proposed phantom setup allows conducting receiver operating characteristic (ROC) studies for the objective evaluation of scanners and scan protocols with ground truth clearly defined.

LL-PHS-WE6A • Detecting Osteoporosis Using Photoacoustic Spectroscopy

Behnoosh Tavakoli (Presenter) ; **Xiaoyu Guo** ; **Shadpour Demehri** MD ; **Abdullah Muhit** PhD ; **John A Carrino** MD, MPH * ; **Emad Boctor** PhD, MSc *

CONCLUSION

Photoacoustic spectroscopy is technically for detecting the osteoporosis at no radiation cost. This method may be sensitive to the micro structural changes in the bone. In addition with multi spectral imaging, it is possible to analyze different components of the bone tissue such as calcium by decomposing the photoacoustic spectrum to the standard tissue absorbers optical spectrums.

Background

Osteoporosis, is the most common metabolic bone disorder. Monitoring the micro architectural deterioration of the bone tissue and the decrease of the bone mineral density are necessary for early detection of the osteoporosis. Broadband attenuation of ultrasound signal is correlated with bone mineral density and its microstructure. In addition, the optical absorption spectrum of the bone tissue analyzes its mineral, water, lipid and oxy-deoxy hemoglobin content. Therefore photoacoustic spectroscopy as a hybrid functional method that combines both optical and ultrasound information is a promising technique for determination of osteoporosis in early stages.

Evaluation

In this study, the quantitative ultrasound calcaneal phantoms of normal and osteoporotic bone were imaged in the transmission mode and the corresponding photoacoustic spectrums were obtained. Our photoacoustic imaging system includes a tunable Q-switch Nd:YAG laser followed by an OPO system generating pulses at the wavelength range of 690 nm-950 nm. The photoacoustic signal is detected with the FDA approved Sonix RP ultrasound system including a data acquisition device for recording the raw data. Multiple points of each phantom were evaluated using a linear US probe with 128 elements. Finally the maximum raw data was extracted from the elements and the value was normalized to the illuminating laser energy.

Discussion

The result revealed a general decrease in the spectrum of the osteoporotic phantom compared to the normal one. The trend matches the optical spectrum of the calcaneus bone tissue. In this test, there was about two times contrast between the normal and osteoporotic case. These phantoms were modeling the bone microstructure and more contrast is expected in the real bone tissue including other tissue absorbers.

LL-PHS-WE7A • Automatic Coronary Calcium Scoring in ECG-triggered Cardiac CT

Jelmer M Wolterink MSc (Presenter) * ; **Tim Leiner** MD, PhD * ; **Pim A De Jong** MD, PhD ; **Max A Viergever** * ; **Ivana Isgum** PhD *

PURPOSE

Presence of coronary artery calcium (CAC) is a strong and independent predictor of cardiovascular events. Given the rapid increase in cardiac CT imaging, fully automated quantification of CAC is desired. We have developed an algorithm for quantification of CAC in routinely acquired cardiac CT employing a coronary calcium atlas and features previously proposed for automatic CAC scoring in non-ECG synchronized chest scans.

METHOD AND MATERIALS

The study included 161 consecutive cardiac patients who underwent CT for determination of CAC (256-detector row CT, 120 kV, 55 mAs, 3 mm section thickness). In all scans CAC was manually scored by experts. These annotations served as the reference standard and were used for training the algorithm.

To automatically detect calcifications, scans were thresholded at 130 HU and all connected components were considered CAC candidates. These were described by size, intensity and spatial features. Spatial features were computed using a CAC atlas previously created with non ECG-gated chest CT scans. Subsequently, true positives were identified by classification using a forest of extremely randomized trees. Ten-fold cross validation was performed. Using the detected calcifications, Agatston and volume CAC scores were computed for each patient. Agreement between reference and automatic scores was established with Spearman's ρ . Patients were assigned to a cardiovascular risk category based on their Agatston score (0, 1-10, 11-100, 101-400, >400) and linearly weighted ρ was calculated to evaluate the agreement in category assignment.

RESULTS

24 cases with stents and beam hardening artifacts due to metal implants were excluded. In the remaining 137 patients median reference Agatston score was 8.8 (range: 0-4067) and automatic median score was 11.2 (range: 0-2793). Spearman's ρ between automatic and reference scores was 0.93 for Agatston and 0.92 for volume. The correct risk category was assigned to 81% of patients, and 15% and 4% were one and two categories off, respectively ($\rho=0.85$).

CONCLUSION

The presented algorithm performs fully automatic CAC scoring. Based on the derived CAC scores, the vast majority of patients were assigned to the correct cardiovascular risk category.

CLINICAL RELEVANCE/APPLICATION

Automatic CAC scoring in cardiac CT can be performed using the features and CAC atlas described for scoring in chest CT. This eliminates the necessity for constructing a population specific CAC atlas.

LL-PHS-WE8A • Pregnant Female Anthropomorphic Phantom Dosimetry in Computed Tomography

Matthew R Hoerner MS (Presenter) ; **David E Hintenlang PhD**

PURPOSE

A study was performed to evaluate the conceptus doses from clinical radiation exposures in Computed Tomography (CT) using a series of pregnant female physical phantoms. The results of this evaluation will be used to validate Monte Carlo simulations performed on the phantom's computational equivalent.

METHOD AND MATERIALS

Four female abdomen/pelvis phantoms were constructed to represent the 2 week, 15 week, 25 week, and 35 week post conception gestation stages of the UF reference pregnant female library. The phantoms were re-constructed from the computational phantoms using various 3D engraving machines to create the molds for the soft tissue-equivalent and bone-equivalent substitutes. Each phantom was designed to accommodate specific measurement locations by building the phantom into smaller components that have segmented organ/fetal dose points. A fiber-optic dosimetry system was employed to quantify absorbed dose. The dosimeter was fabricated to include a secondary detector of a different material to evaluate the beam spectra incident to the detector. By evaluating the incident energy spectra, the energy dependence of the dosimeter was greatly minimized and provided necessary information to calculate absorbed dose to various tissues types.

RESULTS

The dosimeter was characterized for CT irradiations and displayed an energy dependence of less than 3% when benchmarked against the ion chamber, minimal angular dependence, and excellent sensitivity and reproducibility. The phantom materials were characterized to be within the range of their accepted HU values, and a measured HVL at 120 kVp within 0.5 mm of the Monte Carlo simulated value. The measured conceptus doses for common chest-abdomen-pelvis exams were found to be consistent with other studies using physical phantoms and less than 50 mGy.

CONCLUSION

The tools and methods employed by this study accurately quantify conceptus doses associated with the low levels of ionizing radiation used in CT and offer a great resource for benchmarking computational data associated with the UF hybrid pregnant female phantoms.

CLINICAL RELEVANCE/APPLICATION

This study addresses the risk associated with clinical CT examinations to unborn children, by correlating measured radiation exposure to relevant radiobiological data.

Physicists - Wednesday Posters and Exhibits (12:45pm - 1:15PM) Wednesday, 12:45 PM - 01:15 PM • Lakeside Learning Center [Back to Top](#) LL-PHS-WEB • AMA PRA Category 1 Credit™:0.5

LL-PHE-WE10B • MRI Pulse Sequence Survival Guide: Step-by-Step Explanations of Commonly Used Pulse Sequences and Their Clinical Relevance

David R Veal MD (Presenter) ; **Sachin Jambawalikar PhD** ; **Martin R Prince MD, PhD** *

PURPOSE/AIM

Navigating the literature of magnetic resonance imaging physics and understanding how different pulse sequences are performed can be challenging because the subject is intricate and resources on the topic frequently become technically overwhelming in scope or detail. In addition, the myriad of acronyms across different vendors only add to the confusion. This exhibit provides residents and radiologists an intuitive, step-by-step, and focused understanding of the different types of sequences and how commonly used sequences generate MR images. Key differences between the sequences as related to their clinical application will be reviewed.

CONTENT ORGANIZATION

1. Review of MR Physics Principles
2. Introduction to the Pulse Sequence Diagram
3. Two Households: Spin Echo versus Gradient Echo
4. Spin Echo Variations
5. Gradient Echo Variations
6. Review and Comparisons
7. Quiz Questions

SUMMARY

Understanding how MRI physics and pulse sequences generate images can become technically overwhelming, and sorting through the various acronyms of pulse sequences can be confusing. This exhibit will provide a more intuitive, step-by-step explanation of commonly used pulse sequences, and review how each of these different sequences are applied clinically.

LL-PHS-WE1B • Size Specific Dose Estimates in Chest, Abdominal and Pelvis CT: Impact of Z-axis Variations in Patient Size

Shuai Leng PhD (Presenter) ; **Maria Shiung** ; **Xinhui Duan PhD** ; **Lifeng Yu PhD** ; **Yi Zhang** ; **Cynthia H McCollough PhD** *

PURPOSE

To develop software for automatic size specific dose estimates (SSDE) and use it to investigate the impact of z-axis variations in patient size on SSDE in CT exams of the chest, abdomen and pelvis.

METHOD AND MATERIALS

Images from 102 consecutive chest, abdomen and pelvis CT exams were evaluated with a Matlab program developed to calculate SSDE. The program automatically removed the patient table and calculated water equivalent diameter (Dw) at every image position, from which conversion factors were calculated using AAPM Report 204. SSDE was calculated in two ways and compared: Method 1: SSDE at each position was calculated based on Dw and CTDIvol at the corresponding image position, and mean SSDE over the scan range calculated. Method 2: Mean CTDIvol over the scan range was used with the conversion factor corresponding to Dw at the middle of the scan range. Five types of exams were investigated, with scan ranges determined by the following anatomic landmarks: top of lung to bottom of lung (chest), top of liver to top of crest (abdomen), and top of crest to pubic symphysis (pelvis), top of liver to pubic symphysis (abdomen and pelvis, AP), and top of chest to pubic symphysis (chest, abdomen and pelvis, CAP).

RESULTS

A range of body sizes were included, with weight ranging from 36.9 to 183.1 kg and BMI from 14.7 to 56.6. The average difference between maximal Dw and minimal Dw was 5.2, 4.9, 2.5, 5.6 and 6.5 cm within a chest, abdomen, pelvis, AP, or CAP exam, respectively (maximum difference in any scan was 10.8 cm). The standard deviation of Dw values within each patients' scan range was, on average, 1.4, 1.3, 0.8, 1.4 and 2.0 cm. The root mean square difference between the two groups of SSDE values was 0.9,

0.5, 0.5, 1.0, and 1.1 mGy for the 5 types of exams.

CONCLUSION

For chest, abdomen and pelvis CT exams, the difference was very small between the mean SSDE values calculated using 1) the mean CTDIvol over the scan range and Dw at the middle of the scan range and 2) the CTDIvol and Dw at each position in the scan range. Although patient size varies in the longitudinal direction, Dw at the middle of scan range was adequately representative of the overall patient attenuation in the scan range.

CLINICAL RELEVANCE/APPLICATION

SSDE can be calculated based on mean CTDIvol and Dw at the middle of the scan range, which is easier to implement compared to calculating SSDE for each individual image.

LL-PHS-WE2B • A Photon-counting Silicon Strip Detector for Spectral-resolved Computed Tomography

Ben Huber (Presenter) ; **Hans Bornefalk** MS ; **Han Chen** ; **Mats Danielsson** PhD * ; **Staffan Karlsson** ; **Xuejin Liu** ; **Mats Persson** * ; **Cheng Xu**

PURPOSE

Spectral-resolved computed tomography (spectral CT) aims to complement conventional morphological CT imaging by additionally accessing spectral attenuation properties of the scanned object. One of the important benefits of a clinical application of spectral CT could be the quantification of different material compositions in the object, e.g. tissue and contrast-filled vessels.

METHOD AND MATERIALS

We have constructed a photon-counting silicon strip detector for spectral CT that enables energy-discrimination of incident X-ray photons with up to eight programmable energy thresholds.

The edge-on geometry of the detector provides sub-millimeter pixel sizes and is optimized in order to obtain a high detection efficiency for typical CT X-ray spectra.

The X-ray-induced pulses are read out with a dedicated ultra-fast application specific integrated circuit (ASIC) designed to cope with very high count rates, as they are expected in CT applications.

Making use of a first prototype detector, we evaluate the detector performance with respect to energy resolution, gain, charge collection efficiency and homogeneity of energy thresholds among the individual pixels.

In spectral CT, a homogenous distribution of energy thresholds across the different detector elements is crucial in order to avoid images that suffer from ring artefacts.

RESULTS

We will present the current status of our silicon strip detector for spectral CT and will discuss its performance in clinical CT environments. With the aid of synchrotron sources we have measured the energy resolution and gain, and we have characterized the dispersion of energy thresholds among different detector elements. Furthermore, we have evaluated the detector's count rate performance and the its charge collection efficiency.

CONCLUSION

We have developed a silicon strip detector for spectral CT applications, ready to be used in more advanced studies pointing towards clinical applications. The detector modules described here will be utilized in a full state-of-art CT gantry.

CLINICAL RELEVANCE/APPLICATION

One of the important benefits of a clinical application of spectral CT could be the quantification of different material compositions in the object, e.g. tissue and contrast-filled vessels.

LL-PHS-WE3B • The T₂ of Water in the Human Liver Changes with Age and Adiposity

Ronald Ouwerkerk PhD (Presenter) ; **Ahmed M Gharib** MBChB ; **Roderic I Pettigrew** MD, PhD

PURPOSE

To investigate changes in the liver with adiposity and age in normal and obese subjects.

METHOD AND MATERIALS

In 22 normal and 28 obese subjects (age 39±15, 19-64y., 16 male, BMI 34±9, 20-55 kg.m⁻² obese is BMI > 30) without known liver disease, the T₂ corrected fat fraction (ff) was determined with single volume MR spectroscopy. A set of six breath-hold PRESS acquisitions were obtained from a 2x2x2cm volume in the liver, each averaging two signals at 3s repetition time after one dummy scan. The TE of the sequences was varied from 24 to 144 ms and the T₂ corrected fat content was calculated from a back extrapolation of a linear fit of the logarithms of the water and lipid CH₂ and CH₃ resonances against TE. The relation of the T₂ for water with fat fraction and with subject age was tested with linear regression analysis (p < 0.05 deemed significant). Additionally the T₂ for water was tested for linear correlation with age in subjects with ff < 5%.

RESULTS

The T₂ of liver water decreases with fat fraction and also with age. The decrease of T₂ with age also correlated significantly in a subgroup of thirty six subjects with fat fractions < 5% (water T₂ = 35.5 - 0.063 * age, r²=0.19, p= 0.03), whereas no correlation was found between fat fraction and age.

CONCLUSION

The changes in T₂ indicate that the molecular environment of water changes in the ageing liver. The T₂ decrease observed in the liver is likely related to an increase in iron content in the liver accumulating over the years. The decrease in the T₂ of liver water with increasing fat fraction could also be due to diminishing liver function, or just to a decrease in aqueous space as a result of increases in lipid space.

CLINICAL RELEVANCE/APPLICATION

Age related changes in the hepatic cellular environment are likely related to iron accumulation over the years

LL-PHS-WE4B • Development of a New Device with an X-ray Phase Contrast Imaging Technology: Preliminary Study on Knee Joints

Junji Tanaka MD (Presenter) ; **Mamoru Niitsu** MD ; **Takashi Ushimi** MD, PhD ; **Kaiji Inoue** MD ; **Iichiro Osawa** MD ; **Hiroshi Oda** MD, PhD ; **Toshihide Mimura** MD, PhD ; **Sumiya Nagatsuka** MS ; **Kazuhiro Kido** MS ; **Yoshihide Hoshino** MS ; **Atsushi Momose** PhD

PURPOSE

The x-ray Talbot-Lau interferometry is one of the phase-contrast imaging methods, which works with a conventional x-ray tube. With the interferometry we obtain three different images, which are named as the attenuation-contrast(ATT) image, the differential phase-contrast(DPC) image, and the x-ray small angle scattering contrast(SAS) image, which correspond to images due to the absorption by an object, the refraction on the edges between different materials, and the small angle x-ray scattering by microscopic structures, respectively.

The purpose of this study is to investigate the possibility of depicting soft tissues in knee joints by use of the new imaging device.

METHOD AND MATERIALS

We designed the imaging system which includes an x-ray tube, an X-ray detector, and three gratings arranged in an x-ray beam. The pitches of the gratings were 22.8µm, 4.3µm and 5.3µm, respectively. The distance between the x-ray tube and the detector

was 1.4m. The system was also designed for imaging human limbs by considering the positioning of patients. With this system, patients with osteoarthritis and healthy volunteers as control were examined. This research is approved by the institutional review board.

RESULTS

The ATT images were comparable to conventional attenuation images. The SAS images did not depict detailed skeletal structures. With the DPC images, the surface of the cartilages and the meniscus in knee joints were depicted for both patients with osteoarthritis deformans and healthy volunteers. We confirmed the difference in the images of these tissues between the patients and healthy volunteers.

CONCLUSION

The new x-ray imaging device based on Talbot-Lau interferometry can demonstrate subtle changes in knee joints for patients with osteoarthritis.

CLINICAL RELEVANCE/APPLICATION

According to the result of depicting the soft tissues in knees, the x-ray Talbot-Lau interferometry has the possibility of diagnosing the patients suffering from the osteoarthritis.

LL-PHS-WE5B • Dose Reduction in Soft Tissue Imaging-The Use of a New Needle-based Detector System in Digital Mammography

Claus-Peter Wallner MD (Presenter) ; Markus Hittinger ; Fabian Mueck ; Stefan Wirth MD * ; Markus Koerner MD ; Maximilian F Reiser MD

PURPOSE

To evaluate diagnostic image quality of digital mammography with a new needle-based detector system with respect to a 30% dose reduction.

METHOD AND MATERIALS

We compared 358 consecutive mammographies with 30% dose reduction, performed on a GE Senographe DMR running the Agfa DX-M needle-based imaging plate system (NIP) to their corresponding preliminary examinations (mean interval 1.67 y) which were acquired at standard dose with the same GE mammography device and an Agfa CR85-X powdered storage phosphor imaging plate system (PIP). For dose reduction the automatic exposure control (AEC) settings were modified, dosimetry proved a dose reduction of 29.87% (50 mm PMMA-phantom). According to the ACR Breast Imaging Reporting and Data System (BI-RADS) the mammograms were category 1-3, breast tissue density was ACR level 1-4. Exclusion criteria were changes in ACR level and appearance of the scored lesions as well as non optimally positioned and exposed mammograms. The mammograms in cranio-caudal and oblique projection were blinded and read twice by 2 mammography experts according to a 3-point score (inferior-equal-better) on diagnostic image quality and the visualization of parenchyma, benign lesions (cysts, fibroadenomas, lymph nodes), scars as well as micro- and macrocalcifications.

RESULTS

Compared to PIP at standard dose NIP with 30% dose reduction showed a better visualization of parenchyma at ACR 1-3, high significantly better at ACR 2 and ACR 3 ($p < 0.001$). Breast tissue at ACR 4 was scored similar on NIP and PIP. With NIP at 70% dose microcalcifications were scored significantly better ($p = 0.023$) for all ACR levels while macrocalcifications showed an insignificantly better score ($p = 0.086$). For benign lesions and scars diagnostic image quality was equally scored on PIP with 100% dose and NIP with 70% dose. The reading showed a excellent intra- and interobserver agreement ($r = 0.967/0.956$).

CONCLUSION

With the needle-based imaging plate (NIP) technology in digital mammography, a dose reduction of 30% is possible without loss of diagnostic image quality. For the visualization of parenchyma and microcalcifications we even could demonstrate a significant improvement of image quality with the dose reduced NIP system.

CLINICAL RELEVANCE/APPLICATION

With digital mammography using the needle-based detector system a significant dose reduction is possible without loss of diagnostic image quality.

LL-PHS-WE6B • Uses for a Preclinical Electron Paramagnetic Resonance Oxygen Imager

Howard J Halpern MD, PhD (Presenter) * ; Boris Epel PhD ; Gage Redler ; Arthur Heiss

PURPOSE

This presentation will highlight results in animal models of the ability of pO_2 imaging with electron paramagnetic resonance (EPR) O_2 imaging to predict therapy outcome.

METHOD AND MATERIALS

Examples will be drawn from cancer biology and sleep apnea models. 1) EPR O_2 images were obtained from two different syngeneic tumor types in C3H mice, FSa fibrosarcomas grown intramuscularly and MCa4 breast carcinomas grown subcutaneously. Mice were then given single radiation doses at or near their 50% control dose (TCD50) and followed for 90 and 120 days respectively. 2) BNIP3 promotes mitochondrial autophagy and maintenance of tissue/tumor oxygenation. Tumor BNIP3 knock outs (KO) were imaged in C3H mice and compared with WT tumors. 3) C57 black mice were subjected to alternating atmospheres of 21% and 12% fraction of inhaled oxygen (FI_{O_2}). During each cycle phase, whole animal pO_2 images were obtained. We anticipate similar experiments will be obtained from HIF1a and HIF2a partial knock out mice. (Single gene copy knock out).

RESULTS

1) Both bivariate analysis of dose and fraction of tumor voxels less than 10 torr (HF10) and Kaplan-Meier analysis of control of tumors by radiation showed significant differences between hypoxic and well oxygenated tumors. 2) BNIP3 KO tumors show remarkable hypoxia, with mean pO_2 of ~ 3 torr. 3) Normal tissue pO_2 shows change of normal tissue oxygenation by a factor of ~ 2 . We anticipate data from partial KO to show blunted response.

CONCLUSION

Combination of O_2 image accuracy, non-invasiveness, rapid image acquisition, whole tumor/animal survey make this technology uniquely important for therapy assessment. This work is supported by NIH, grants number P41 EB002034 and R01 CA98575 (Chicago).

CLINICAL RELEVANCE/APPLICATION

Local pO_2 determines the effects of disease/therapy in a large fraction of diseases. pO_2 imaging determines early effects of pharmaceutical/therapeutic intervention on disease amelioration.

LL-PHS-WE7B • Comparison of Organ Dose for Patients with Varied Sizes undergoing Abdomen Pelvis CT Exam Using Patient-Specific Monte Carlo Simulation Coupled with Computational Human Phantoms

Jenifer W Siegelman MD, MPH (Presenter) ; Choonsik Lee PhD ; Mark P Supanich PhD *

PURPOSE

To compare organ doses specific to real patients with a range of body sizes undergoing abdomen pelvis (AP) computed tomography (CT) examinations by using computational human phantom-based Monte Carlo simulation.

METHOD AND MATERIALS

48 adult patients, meeting defined size and gender criteria, undergoing AP exam using automatic exposure control on any of four units in a community hospital, were randomly selected retrospectively using a commercial dose audit tool, eXposure (Radimetrics Inc., Toronto, ON). Technical parameters (e.g., CTDIvol, kVp, scan range) were abstracted from the CT images and utilized for organ dose calculation. We used an organ library which was pre-calculated by using Monte Carlo transport simulation coupled with a series of hybrid computational human phantoms with different sizes. We compared the organ doses from different sized patients and observed the degree of organ dose difference

RESULTS

Absorbed dose to a total of 14 organs were calculated for each patient using the abstracted parameters from the CT images. The patient of the highest BMI received up to 6.6 (active marrow), 5.6 (kidney), 5.6 (urinary bladder) times greater dose than the patient with the lowest BMI. Liver dose was least sensitive to the body size where the highest BMI patient received 2.6 times greater dose than the lowest BMI.

CONCLUSION

The study revealed that the high BMI adult patient may receive up to 5-6 times greater organ dose than the low BMI patient in AP CT exams.

CLINICAL RELEVANCE/APPLICATION

Larger patients undergoing AP CT using AEC may receive higher organ doses than smaller patients according to this method of calculation.

LL-PHS-WE8B • Automated Measurement of Mandibular Cortical Width on Dental Panoramic Radiographs for Early Detection of Osteoporosis: Improvement on Measurement Location

Kazuki Horiba ; Chisako Muramatsu PhD ; Akitoshi Katsumata DDS, PhD (Presenter) ; Tatsumasa Fukui ; Takeshi Hara PhD ; Hiroshi Fujita PhD

PURPOSE

It has been suggested that mandibular cortical width (MCW) on a dental panoramic radiograph (DPR) is significantly correlated with bone mineral density. Automated measurement of MCW on DPRs, which are obtained for dental purposes, may be useful for identifying asymptomatic patients with osteoporosis so that dentists can suggest further examination. In our previous study, one of the reasons for incorrect measurement was due to suboptimal measurement locations. The purpose of this study is to improve our scheme by adjusting measurement locations by variance analysis.

METHOD AND MATERIALS

Our database consists of 100 DPRs obtained from 27 osteoporotic and 73 control patients. First, potential lower mandible edges are detected by modified Canny edge detector. On the basis of the edge information, a most similar contour model is selected from reference data and is fitted to the test case by using an active contour model. In our previous study, the reference mental foramina positions of the model were employed as the right and left MCW measurement locations. By the profile analysis, 21 measurements were made around each location along the contour. However, even when the model is well fitted, the measurement locations on test cases may be shifted from mental foramina. In addition, measurements can sometimes be affected by noise. In this study, measurements are made in a wider range, and most reliable locations are selected on the basis of the variance.

RESULTS

By our previous method, the sensitivity and the specificity were 89% (24/27) and 95% (69/73), respectively. By the proposed method, the sensitivity and the specificity were both improved to 96% (26/27) and 96% (70/73), respectively.

CONCLUSION

The proposed method can be effective in improving MCW measurement by selecting reliable measurement locations. High sensitivity and specificity indicate a potential usefulness of our automated quantification scheme for early detection of osteoporosis.

CLINICAL RELEVANCE/APPLICATION

Detecting a possible risk for osteoporosis on dental panoramic radiograph can be a supplemental screening for osteoporosis with no cost.

LL-PHS-WE9B • Methodology For Robust MRI Simulations with a Dedicated MRI Scanner In Radiation Oncology

Eric Paulson (Presenter)

ABSTRACT

Purpose/Objective(s): The use of MRI in radiation oncology is expanding rapidly, and more clinics are considering whether to add a dedicated MRI scanner within their department. However, several issues specific to radiation oncology, if not properly addressed, can compromise the utility of MRI for radiation treatment planning. The goal of this work is to report our approach for robust MRI simulations.

Materials/Methods: A dedicated large bore (70cm) Siemens 3T MRI scanner was installed in our department in 2008. Since then, roughly 750 patients with brain, head and neck, breast, lung, pancreas, liver, prostate, cervix, or sarcoma cancers have undergone MRI simulations for radiation treatment planning. MRI simulation immediately followed CT simulation. Patients were setup in treatment position, by radiation therapists, on an MR-optimal G9 fiberglass flat table insert interfaced to the spine array coil. Flexible phased array receive coils were wrapped around the patients circumferentially to improve image intensity uniformity. High-order shimming and adiabatic RF pulses were employed to maximize field uniformity and fat suppression. Full field-of-view images were acquired using pulse sequences optimized for 3mm contiguous slices. For abdomen and pelvis imaging, bowel motion was suppressed using 0.5 mg IV injections of glucagon before and midway through the MRI simulation exam. Conventional and dynamic contrast abdominal images were acquired using respiratory gating and breath holds, respectively, both performed at end-expiration. Gradient nonlinearity-induced geometric distortion was minimized by positioning the imaging volume isocentrically within the magnet and by applying vendor-provided 3D distortion correction following image reconstruction. A lookup table relating site-specific applications for each MR image contrast (sequence) was created to guide Radiation Oncologists during contouring.

Results: The combination of a large bore, high field strength, and circumferentially wrapped, flexible phased array receive coils permitted acquisition of thin slice images with high signal-to-noise ratio and image intensity uniformity, while simultaneously accommodating patient setup and immobilization devices. Residual geometric distortion following 3D distortion correction was found to exist for large field of view and/or slice prescriptions. However, the magnitude of the residual distortion was estimated to be less than 2mm.

Conclusions: We have developed and successfully implemented a robust MRI simulation program using a dedicated MRI scanner. The methodology described herein is critical for the acquisition of high fidelity MR images suitable for radiation treatment planning. Our 5-years of experience has indicated that MRI simulation plays a critical role in improving target and critical structure definition for most tumor sites.

Physics (Quantitative Imaging III) Wednesday, 03:00 PM - 04:00 PM • N228 [Back to Top](#) [PH](#) [BQ](#) **SSM19 • AMA PRA Category 1 Credit™: 1 • ARRT Category A+ Credit: 1** **Moderator Bram Van Ginneken, PhD**

Moderator Seungrong Cho, PhD

SSM19-01 • Automated Pulmonary Nodule Elastometry as a Potential Diagnostic Tool

Mohammadreza Negahdar (Presenter) ; Billy W Loo MD, PhD * ; Maximilian Diehn MD, PhD * ; Dominik Fleischmann MD * ; Lu Tian ; Peter G Maxim PhD

SSM19-02 • Multisite Quantitative Evaluation of the Accuracy and Precision of a Novel Test Bolus-based CT Angiography Contrast-enhancement Prediction Algorithm

PURPOSE

To quantify the accuracy and precision of a novel test bolus-based CT angiography (CTA) contrast-enhancement prediction (CEP) algorithm by comparing the amplitude, timing and curve shape of the predicted and true enhancement in the descending aorta (DAo).

METHOD AND MATERIALS

After routine clinical scanning according to local scan and injection protocols, from three hospitals a total of 72 (3x24) anonymized cardiac CTA exams were collected for retrospective analysis. Patients (30f/42m) had a median age and body weight of respectively 74y (range 31-81) and 79kg (range 61-125).

Since existing data were retrospectively analyzed, injection protocols, image acquisitions and reconstructions differed substantially between hospitals.

Test bolus (TB) scans were performed at the level of the pulmonary artery, after which the TB signal in the DAo was processed by the CEP-algorithm. This novel algorithm takes the injection protocols and kV settings of the TB and CTA scan into account, and uses population-averaged information to predict the CTA enhancement. The true enhancement was extracted from the CTA scan with a 6mm ROI along the DAo-centerline.

For each patient, the relative errors in the accuracy and precision were calculated. Deviations in the amplitude were quantified with Bland-Altman analysis and shape differences with the mean absolute error (MAE) of the normalized curves. The predicted curve was shifted along the true enhancement to find the timing error, which is the time shift for which the MAE is minimal.

RESULTS

Although differences in injection and acquisition protocols existed, no significant differences in the precision and accuracy were found between the hospitals. For the entire patient group, the predicted enhancement has an average deviation of $1.0 \pm 15.4\%$ in the amplitude, $0.1 \pm 1.8s$ in the timing, and $5.5 \pm 2.4\%$ in the curve shape.

CONCLUSION

No clinically relevant offsets in the timing and amplitude of the predicted enhancement exist, and the curve shape corresponds well with the true enhancement. With its excellent accuracy and good precision, this algorithm has high potential for CTA scan timing and injection protocol optimization.

CLINICAL RELEVANCE/APPLICATION

Most efficient usage of contrast agent, and thus maximum CNR in CTA images, can potentially be achieved by using this algorithm for scan timing and injection protocol optimization.

SSM19-03 • Detecting Enhancing Lesions in Multiple Sclerosis Patients Using Visual Texture Analysis on Brain T2-weighted MR Images: A Feasibility Study

Nicolas Michoux (Presenter) ; Alain Guillet ; Denis J Rommel MD ; Thierry P Duprez MD

CONCLUSION

On-going research aims at assessing the performance of a texture-based decision system from T2 images acquired before Gd injection which, if effective, may offer an alternative to detect Gd-enhancing lesions in MS patients when Gd injection is contra-indicated or impossible. **References**

1. NMR Biomed 2010;23:865-72.
2. Am J Neuroradiol 2010;31:809 -16.
3. IEEE Trans Syst Man Cybern 1973;SMC-3:610-621.
4. IEEE Trans Image Process 1998;7:1602-9.

Background

MRI is the most sensitive technique for detecting multiple sclerosis (MS) lesions. While DCE-MRI is routinely used for evaluating the inflammatory activity, diffusion MRI is controversial (1). Texture analysis has been used with success to investigate pathological brain tissues (2). This study assesses the feasibility of **texture analysis on T2-weighted MRI** to detect changes within white matter in MS patients.

Evaluation

Patients

This retrospective study was approved by our institutional ethical committee. From post-Gd T1-weighted imaging, 44 enhancing lesions (EL), 37 non-enhancing lesions (non-EL) and contra-lateral regions in normal appearing white matter (NAWM) were identified in 21 patients diagnosed with MS.

MRI

Examinations were performed using a 3.0T whole body imaging system and a SENSE head 32 receiving coil. FSE T2, FSE FLAIR, EPI diffusion and 3D post-Gd GRE T1 sequences were acquired.

Computing

A 21-components vector (20 Textons + ADC) was derived for each region from grey level co-occurrence and run length matrices (3, 4).

Results

Differences between EL/non-EL and NAWM were statistically significant ($p < 0.05$) except for one Texton. Differences between EL and non-EL were significant except for one Texton and ADC. ROC analysis showed a performance of Textons and ADC ranging from moderate (AUC ADC = 0.58) to good (AUC Texton = 0.84). A good predictive model of EL (Se = 88 %, Sp = 81 %) was achieved based on a partial least squares classifier and a set of 6 Textons.

Discussion

Textons values result from the structural characteristics of the tissues and thus are affected by pathologic changes. Applying texture analysis to T2-weighted MRI is feasible and may help differentiating EL from non-EL in MS.

SSM19-04 • Comparison Study of Spectral Imaging Associated with Iso-Osmolar Contrast Media on Vascular Evaluation in Rabbits

Pan Liang (Presenter) ; Jianbo Gao MD

PURPOSE

To compare the vascular enhancement between spectral imaging associated with iso-osmolar contrast media and traditional 120kVp scans with high-osmolar contrast media on vessel.

METHOD AND MATERIALS

6 adult New Zealand rabbits of similar age and size were enrolled in this study. Each rabbit underwent two epigastric CT protocols and interval time among every protocol is 24 hours. Protocol A: traditional CT gastric angiography (CTGA) with Iopromide 350 (2ml/kg, 1.5ml/s). Protocol B: spectral CT enhanced sequence with Iodixanol 270 (2ml/kg, 0.5ml/s). Images of spectral CT series will be reconstructed at 55 keV. Signal intensity, image noise, signal-to-noise ratio (SNR) and contrast-to-noise ratio (CNR) measured within the parallel groups in aortaventralis and left gastric artery were calculated and compared. Overall diagnostic quality of images were evaluated using a five-point scale. Comparison of percentages of diagnostic images (score=3) were performed.

RESULTS

Compared with the traditional CTGA scans, 55 keV images demonstrated significantly higher signal intensity ($p=0.000$) in aortaventralis and left gastric artery, and inferior noise ($p=0.029$) only in left gastric arteries. The SNR and CNR of the 55 keV

images had no significant differences from that of the traditional CTGA images (23.33+5.54 vs. 24.45+1.65, P=0.646; 18.19+4.28 vs. 17.74+1.03, P=0.806). Also, spectral CT images provide better overall image quality scores ($p>0.05$), the proportion of diagnostic images was higher (p

CONCLUSION

Spectral imaging associated with iso-osmolar contrast media of Iodixanol 270 can provide excellent gastric vascular images at 55 keV at equivalent radiation of traditional CTGA scans. In the meanwhile, contrast media dose can be greatly reduced.

CLINICAL RELEVANCE/APPLICATION

The association of iso-osmolar contrast media with spectral imaging can greatly reduce the amount of iodine while maintaining high quality of vascular images.

SSM19-05 • Assessment of a New Image-based Method of Monoenergetic Imaging

Katharine Grant PhD (Presenter) * ; **Bernhard Krauss** PhD * ; **Martin U Sedlmair** MS * ; **Thomas G Flohr** PhD * ; **Christian Eusemann** PhD * ; **Bernhard Schmidt** PhD *

PURPOSE

Following the trend of low dose imaging, concerns regarding the detectability of low contrast lesions have been growing. The goal of this research is to evaluate if a new image-based algorithm (mono+) for monoenergetic imaging can improve the contrast-to-noise ratio and conspicuity of these low contrast objects.

METHOD AND MATERIALS

Three different anthropomorphic dual energy phantoms of different size representing a small medium and large phantoms containing 3 different iodine inserts (known values of 20, 50 and 100HU @120kV) were scanned at 3 different dose levels (full, half and quarter dose). Images were reconstructed at both 40keV and 70keV using both a standard image-based monoenergetic algorithm and mono+ at all three dose levels, resulting in 12 different images sets per phantom size. Hounsfield units and standard deviation (noise) measurements were recorded from ROIs placed within the three inserts and one background for each image set. To calculate monoenergetic images, similar to raw data approaches a two material decomposition into base materials is performed. Based on tabulated data, from the two material images, monoenergetic (keV) images can be calculated. Since by theory, any decomposition leads to an increase in noise, keV images of very low or high energy (e.g. 40 keV or 190 keV) show a substantial noise increase. Our newly developed method to calculate keV images suppresses this increase by applying a regional analysis-dependent frequency-based recombination of the high signal at lower energies and the superior noise properties at medium energies.

RESULTS

The mono+ algorithm resulted in a greatly improved image quality for both the 40 keV (Fig 1.) and 70 keV. Both keV level displayed lower image artifacts and a significant reduction in image noise. CNR improved for all inserts using mono+ compared to the standard algorithm. For example for the small phantom CNR could be improved for the 40 keV by about 50%.

CONCLUSION

Mono+ improves CNR and low contrast lesion conspicuity in particular for low dose imaging, independent of phantom size.

CLINICAL RELEVANCE/APPLICATION

Mono+ provides significantly increased CNR, resulting in increased lesion conspicuity. These improvements should allow for added diagnostic confidence, higher throughput and reduced reader fatigue.

SSM19-06 • Automated and Optimized Imaging Simulation Platform for Virtual Clinical Trials of Breast Cancer Screening

Predrag R Bakic PhD (Presenter) * ; **Andrew D Maidment** PhD * ; **Joseph H Chui** MSc * ; **Ali N Avanaki** PhD * ; **Cedric Marchessoux** * ; **David D Pokrajac** PhD ; **Kathryn S Espig** MSc * ; **Tom Kimpe** PhD * ; **Albert Xthona** * ; **Miguel A Lago** ; **Varsha Shankla**

PURPOSE

We have developed an automated pipeline for the simulation and analysis of x-ray breast images. The simulation has been used to conduct Virtual Clinical Trials (VCTs) of digital mammography and digital breast tomosynthesis imaging.

METHOD AND MATERIALS

An automated pipeline has been developed (in C++ and OpenCL) that includes simulation of the normal breast anatomy and lesions (e.g., microcalcification clusters), breast deformation, image acquisition, image processing, display modeling, and image analysis using model observers. The breast anatomy is simulated using an octree-based recursive partitioning method, which allows for fast simulation of a large number of phantoms with very small voxel size. Clusters of microcalcifications (derived from stereomammographic clinical images) are added after identifying potential locations of cluster insertion based upon the convolution of simulated dense tissue regions with the minimal bounding box surrounding the cluster. The phantom deformation resulting from mammographic compression is simulated using a finite element model. Images of the deformed breast are then synthesized using a fast ray tracing method. Image processing is applied to create DICOM images and display modeling takes into account medical monitors effects including temporal effects and an accurate browsing speed simulation. Detection of microcalcifications is estimated using 2D, 2D+time, and 3D channelized Hotelling observers equipped with the spatio-temporal contrast sensitivity function of the human visual system in response to the simulated display of images.

RESULTS

The developed pipeline supports the simulation of 2D and 3D breast imaging. The GPU implementation has resulting in significant acceleration, with the simulation duration at each pipeline stage now being on the order of seconds. For example, compressed versions of 450ml breasts with voxel size of 200 microns are generated at a rate of more than 30 per minute. Extensive pipeline testing has demonstrated that detection results follow the same trends as human observers in terms of contrast and browsing speed.

CONCLUSION

We have developed an automated and accelerated pipeline for performing VCTs of breast imaging.

CLINICAL RELEVANCE/APPLICATION

VCTs have role as a preclinical optimization and validation tool prior to clinical trials of new imaging equipment.

Physics (CT-Imaging Evaluation) Wednesday, 03:00 PM - 04:00 PM • S404AB [Back to Top](#) [PH](#) [CT](#) **SSM20 • AMA PRA Category 1 Credit™:1 • ARRT Category A+ Credit:1** **Moderator Kevin M Brown**, MS *

Moderator Josh Star-Lack, PhD

SSM20-01 • Quantitative Image Quality in CT: Detectability = f (Dose, Reconstruction, Contrast, Size)

Brendan Eck (Presenter) ; **Rachid Fahmi** PhD ; **Kevin M Brown** MS * ; **Nilgoun Raihani** ; **David L Wilson** PhD *

CONCLUSION

Detectability studies suggest that image quality can be preserved at reduced dose with IMR as compared to higher doses with FBP. The success of CHO over a range of independent variables encourages us to perform automated assessments of reconstruction parameters, greatly reducing the need for human detection studies.

Background

In CT, an important goal is to reduce dose but maintain image quality using advanced reconstruction techniques. There are

numerous image reconstruction approaches, each with parameters to optimize. One good way to evaluate methods is with quantitative detectability studies. However, human observer trials are labor intensive and costly. In this study, we performed observer studies as a function of dose, reconstruction, contrast, and target size, and tested computational observers over this wide range of applicability.

Evaluation

4-alternative forced choice experiments were used for human experiments. Images of 69x69 pixels were obtained from a simulated phantom of same size as a Catphan, with added low contrast pins. 200 images contained a low contrast target and 600 images contained no target. Over 200 4-AFC trials, a probability correct, PC, was computed. Channelized Hotelling with different internal noise models (CHO) was the model observer. Observers were students blind to hypotheses. The experiment was conducted in a dark room on a perceptually linear display. We compared a knowledge-based iterative reconstruction algorithm (IMR) and filtered back projection (FBP) over dose, contrast, and target size. Results are shown in Figure 1. Humans gave increased PC with increasing signal size, contrast, and dose. The CHO with internal noise gave similar trends across this wide range of variables.

Discussion

Compared to FBP, IMR substantially improved detection over all average data in the figure as well as for each subject. The improvement in detectability index was at least a factor of 2.7 in all cases. At 20% dose, IMR even gave better results than FBP at the highest dose. CHO with a single set of internal noise parameters reasonably fit experiments, even though image noise characteristics of FBP and IMR were quite different.

SSM20-02 • Measuring the Contrast-dependent Spatial Resolution of CT Iterative Reconstruction Methods at Very Low Contrast Values

Lifeng Yu PhD (Presenter) ; **Thomas J Vrieze** RT ; **Shuai Leng** PhD ; **Joel G Fletcher** MD * ; **Cynthia H McCollough** PhD *

PURPOSE

To measure the spatial resolution of iterative reconstruction (IR) methods at very low contrast values (

METHOD AND MATERIALS

The spatial resolution of IR is contrast- and noise-dependent because of the non-linear regularization term in IR. Studies exist that measure the spatial resolution at medium-contrast levels using the polyethylene (-90 HU) and acrylic (120 HU) test objects in the ACR CT phantom. However, because of the severe noise contamination of low-contrast edges, it is extremely challenging to perform precise spatial-resolution measurements at very low-contrast levels (

RESULTS

The spatial resolution of IR images was highly dependent on contrast level. At high contrast, IR_1 and IR_2 had an almost identical MTF as FBP. The degradation of the MTF by IR relative to FBP became more severe as the contrast level decreased. The differences in spatial frequencies at the 50%, 10%, 2% MTF values between IR_1 and FBP were (21 HU: -0.02, 0.02, 0.02 cm⁻¹; 14 HU: -0.04, -0.04, -0.02 cm⁻¹; 7 HU: -0.02, -0.06, -0.08 cm⁻¹). IR_2 degraded the MTF even more than IR_1 due to a stronger regularization setting.

CONCLUSION

A novel methodology was used to measure the spatial resolution of IR at very low contrast levels (

CLINICAL RELEVANCE/APPLICATION

Quantifying contrast-dependent resolution is important for clinical use of IR. This is the first experimental study to demonstrate the degradation of resolution for IR at very low contrast (

SSM20-03 • Evaluation of Geometric Irradiation Efficiency for CT System Architecture

Hewei Gao PhD (Presenter) * ; **Paul Fitzgerald** * ; **Yannan Jin** * ; **Jiao Wang** * ; **Peter Edic** * ; **Bruno De Man** PhD *

PURPOSE

Geometric iRradiation Efficiency (GiRE) of a CT system, a function of the percentage of applied X-ray radiation useful for reconstructing a volume of interest (VOI) and the uniformity of the radiation within the VOI, is an important factor when considering noise uniformity and dose optimization. In this study, we propose a fast evaluation approach for relative comparison of different CT system architectures.

METHOD AND MATERIALS

First, a pseudo-sinogram whose values equal unity is back-projected according to the scan geometry. Voxel values within the irradiation volume represent the number of times the voxel is irradiated by X-ray flux, normalized by the number of views. If the voxel is irradiated at each view for once and only once, then its normalized value is unity. Then, the percentage of the useful radiation administered to the VOI relative to the entire irradiation volume is computed, denoted as a useful-irradiation rate. Next, an irradiation uniformity index is calculated by computing the mean absolute difference between the values within an ideal, uniformly-irradiated VOI and those of the actually irradiation distribution within the VOI, and then subtracting this value from unity. Finally, we obtain the GiRE as the product of the two above. In order to better reveal the irradiation uniformity relative to the X-ray tube power capability, we further introduce a few new metrics: sufficient-irradiation and always-irradiation rates (percentages of irradiation to VOI voxels that have at least 180-degree of data or equal the maximum) versus their corresponding mean integrated X-ray tube power.

RESULTS

We evaluate the GiRE of 4 CT system architectures for cardiovascular imaging including single source CT (half scan), dual (transaxial) source CT (half scan), triple (transaxial) source CT (full scan), and dual twin-Z source CT (half scan). Using the proposed evaluation criteria, their GiREs are 0.88 for the first three architectures, and 0.64 for the last one. Triple source CT is identified as the best based on irradiation uniformity versus X-ray tube power.

CONCLUSION

An approach for evaluation of GiRE is proposed and applied to the architecture analysis of the cardiac CT-specific scanner of the future.

CLINICAL RELEVANCE/APPLICATION

Our method is beneficial in identifying CT system with the best noise uniformity and dose utilization. It provides an easy way to better understand and illustrate the relative irradiation efficiency.

SSM20-04 • Effect of Scan and Reconstruction Parameters on Grand Glass Opacity Visibility in Low-dose Lung Computed Tomography

Katsuhiko Ichikawa PhD (Presenter) ; **Takeshi Kobayashi** ; **Motoyasu Sagawa** MD

PURPOSE

This phantom-based multicenter study aimed to investigate the effect of scan and reconstruction parameters on grand glass opacity (GGO) visibility in low-dose lung computed tomography (LDLCT).

METHOD AND MATERIALS

Eighteen screening centers participated. Phantoms for physical measurements and an anthropomorphic chest phantom that included simulated GGOs with CT numbers of -630 Hounsfield units (HU) (LGGOs) and -800 HU (HGGOs) were employed. The phantoms were scanned using parameters used for screening in each center. In the total of 21 image sets, the slice thickness and CT dose index (CTDI_{vol}) ranged from 1.0 to 5.0 mm and 0.85 to 3.50 mGy, respectively, and a wide variety of reconstruction kernels was used. One thoracic surgeon and five radiologists evaluated nodule visibility in each chest phantom image set using a five-point

scoring system. For quantitative analysis, we used the nodule detectability index based on a signal-to-noise ratio (SNR) theorem, which could be calculated from resolution, noise property, and the spatial frequency property of the simulated nodule image.

RESULTS

Strong correlations between $CTDI_{vol}$ and the visual score were observed for 10-mm LGGOs ($R^2 = 0.843$, $p_2 = 0.725$, $p_2 = 0.761$, $p_2 = 0.709$, p 80%) for 6-mm HGGOs and 10-mm LGGOs were 2.0 and 3.0 mGy, respectively.

CONCLUSION

It has been experimentally known that the low contrast visibility in CT primarily depends on the dose, while the slice thickness and reconstruction kernels affect image sharpness. This fact was demonstrated through our results of visual and SNR evaluations corresponding to LDLCT. The dose level of 2.0 and 3.0 mGy were thought to be appropriate for HGGOs and LGGOs (subtle GGOs) respectively.

CLINICAL RELEVANCE/APPLICATION

The primary dependency on the radiation dose for GGO visibility, demonstrated in this study, would be contributed to easy settings of optimal scan condition for lung CT screening.

SSM20-05 • Patient Size Dependent Low Contrast Detectability in Abdominal CT

Yifang Zhou PhD (Presenter) ; **Alexander W Scott** PhD

PURPOSE

We chose to use the statistically defined minimum detectable contrast (MDC) as a gauge for image quality. We attempted to study MDC's relationship to patient size, dose and lesion size in typical abdomen CT scans.

METHOD AND MATERIALS

Seven abdomen phantoms (CIRS TE series) simulating patients from an infant to a large adult were used. Helical scans were conducted using a Siemens Sensation 64 (mCT) with 120 kVp and mAs ranged 35- 595 (kernel B30s, pitch 1.4 and width 5 mm). For each phantom, the uniform sections of the contiguous slices were subtracted and the resulted regions were divided by grids of cells sized from 1.37 mm- 6.84 mm. Standard deviations (sd) were computed from the means of all cells and scaled down by square root of 2. The MDC, quantified by the signal to background difference equal to 3.29sd, was fitted to dose D (phantom specific $CTDI_{vol}$) and cell sizes (d). MDC versus patient size relationship was established by extracting the fitting parameter's dependency

RESULTS

MDC versus D and d was fitted to a power law (R square larger than 0.94), with power indices close to -0.5 and -1, respectively. The proportional constant versus patient size follows an exponential relationship with the an index of 0.18 1/cm, close to the linear attenuation coefficient of the phantom.

CONCLUSION

The relationships of MDC versus patient size, dose and lesion size, were established. They can be used for task specific dose optimization.

CLINICAL RELEVANCE/APPLICATION

CT Dose optimization for different patient sizes

SSM20-06 • CT Evaluation of Coronary Artery Stents: Impact of an Integrated Circuit Detector with Iterative Reconstruction

Lucas L Geyer MD (Presenter) * ; **George R Glenn** BS ; **Christian Canstein** * ; **Justin R Silverman** ; **Mark Van Horn** PhD ; **U. Joseph Schoepf** MD * ; **Aleksander Krazinski** ; **Stefan Wirth** MD * ; **Fabian Bamberg** MD, MPH * ; **Maximilian F Reiser** MD ; **Philip Costello** MD

PURPOSE

To assess the influence of higher out-of-plane resolution and iterative reconstruction algorithms on the visualization of coronary artery stents using an integrated circuit CT detector.

METHOD AND MATERIALS

Vessel phantoms bearing coronary artery stents with different diameters (2.0, 2.5, 3.0 mm) were investigated on a second-generation dual-source CT system equipped with an integrated circuit detector allowing for 0.5 mm beam collimation. Data acquisition was performed at two different heart rates (0 bpm, 60 bpm) using an anthropomorphic moving heart phantom. Images were reconstructed with filtered back projection (FBP) at a section thickness of 0.75 mm (FBP75), and with sinogram-affirmed iterative reconstruction at both 0.75 mm (IR75) and 0.5 mm (IR50) section thickness. Multi-row HU intensity profiles were modeled by using a sum-of-Gaussian-fits to analyze in-plane image characteristics: xy-upslope (indicator of sharpness), standard deviation (SD, indicator of blurring), signal- (SNR) and contrast-to-noise ratio (CNR), and noise (general image quality parameters). Out-of-plane image characteristics were analyzed with z-upslope for multi-column HU intensity profiles.

RESULTS

Independent of stent diameter and heart rate, IR75 resulted in significantly increased xy-sharpness, SNR, and CNR as well as decreased blurring and noise compared with FBP75 (e.g., 2.0 mm-stent, 0 bpm: xy-upslope, 308.7 vs. 278.5; SNR, 46.6 vs. 33.5; CNR, 26.0 vs. 16.8; SD, 1.4 vs. 1.5; noise, 15.4 vs. 21.2, all p

CONCLUSION

The implementation of an integrated circuit CT detector with thinner beam collimation provides substantially sharper out-of-plane resolution of coronary artery stents in an ex-vivo analysis. In addition, the use of iterative image reconstruction contributes mostly to an improved in-plane stent visualization independent from stent diameter and heart rate.

CLINICAL RELEVANCE/APPLICATION

Implementation of an integrated circuit CT detector combined with iterative image reconstruction improves 3D visualization of coronary stents of clinically-relevant diameters.

Physics (X-ray Imaging Techniques) Wednesday, 03:00 PM - 04:00 PM • S406B [Back to Top](#)   **SSM21 • AMA PRA Category 1 Credit™:1 • ARRT Category A+ Credit:1** **Moderator Andrew Karellas**, PhD *

Moderator Wei Zhao, PhD *

SSM21-01 • Introduction and Benefits of an Anti-scatter Grid in Digital Breast Tomosynthesis

Colin Auclair Dipl Eng, MSc (Presenter) * ; **Jeffrey Shaw** PhD, MS * ; **Mathias Cisaruk** DIPLENG * ; **Remy Klausz** DiplEng * ; **Henri Souchay** PhD *

PURPOSE

Conventional grids for mammography (MG) with septa perpendicular to the chest wall are not suitable for digital breast tomosynthesis (DBT) because the trajectory of the x-ray tube relative to the grid moves the source out of the grid focus line. The performance of a new 3D-grid, compatible with DBT and MG, was evaluated and its benefits compared with a conventional grid for MG, and with no grid at equal dose for DBT.

METHOD AND MATERIALS

The septa of the 3D-grid are designed to be parallel to the tube sweep trajectory. To eliminate grid line visibility, the septa interspace is matched to the detector pixel pitch. During image acquisition, the 3D-grid moves with sub-mm amplitude, preserving

tissue visibility at chestwall side. Grid performance was determined using methods derived from IEC 60627 standards, which allows to estimate the theoretical image quality improvement at same dose for average breasts. Evaluation of the image quality performance in 2D used a CDMAM phantom sandwiched between 2cm PMMA plates. For DBT, image quality performance was compared from the detectability of inserts in an ACR phantom imaged directly and on top of 2.5cm PMMA. All images were acquired on a Senographe Essential (GE Healthcare) using the same technique factors for each comparison.

RESULTS

For 5cm PMMA and at 28kV MoMo, primary transmission of the 3D-grid was $70.1\% \pm 0.5\%$, indicating that the grid contribution to $SDNR^2$ for average breast patient was 0.99 ± 0.03 .

For MG, automatic CDMAM scoring (CDMAM Analyser, Artinis) provided similar IQF scores for the 3D-grid (122) and conventional grid (127) when using the same acquisition parameters.

For DBT, at the central plane of the inserts, ACR phantom scores were similar with (13.3 ± 0.5) and without (13.2 ± 0.5) grid. When adding 2.5 cm PMMA, ACR phantom scores were higher with (10.3 ± 0.5) than without (8.3 ± 0.5) grid. In addition, the 3D-grid significantly improved signal uniformity throughout the phantom.

CONCLUSION

The 3D-grid demonstrated a potential of improving detectability of features for breasts above the average thickness, while preserving the dose in DBT.

CLINICAL RELEVANCE/APPLICATION

For breasts above the average thickness, most difficult to image in mammography, the 3D-grid offers scatter rejection benefits comparable to MG grids, yet capable of operating both in MG and in DBT.

SSM21-02 • X-ray Differential Phase Contrast Tomosynthesis Imaging based on a Clinical Digital Breast Tomosynthesis System

Ke Li MS (Presenter) ; John W Garrett MS * ; Yongshuai Ge ; Guang-Hong Chen PhD *

PURPOSE

To systematically investigate the feasibility and clinical relevance of grating-based x-ray differential phase contrast (DPC) tomosynthesis imaging constructed based on the hardware setup of a clinical digital breast tomosynthesis (DBT) system.

METHOD AND MATERIALS

The feasibility of DPC tomosynthesis imaging was first demonstrated using a benchtop system (40 kVp, 80 micron pixel size), from which tomosynthetic images of three different contrasts (refraction angle, phase shift, and absorption) of physical phantoms were acquired. Next, the feasibility of DPC tomosynthesis imaging using the hardware setup of a clinical digital breast tomosynthesis system with a rotary x-ray source and static detector (Hologic Selenia Dimensions) was studied using a framework that quantitatively relates the detection performance of DPC tomosynthesis with the associated absorption DBT. X-ray spectrum, noise power spectrum, and MTF of the absorption DBT involved in the framework was physically measured and the imaging task was created based on the materials' phase and absorption properties provided by NIST.

RESULTS

Reconstructions of physical phantoms show improved signal difference to noise ratio ($SDNR$) compared with absorption images acquired under the same exposure ($SDNR_{PMMA} = 5.9$ and 0.6 for DPC and absorption, respectively). Equivalent spatial resolution for the two contrast mechanisms was observed. Design parameters of the DPC tomosynthesis system are compatible with the current clinical DBT system. The accuracy of the framework that predicts detectability in DPC-DBT was validated experimentally, and it suggests that the DPC mechanism will result in improved detectability of both small objects (e.g. calcification) and irregular-shaped objects (e.g. spiculated lesions).

CONCLUSION

It is feasible to build a DPC tomosynthesis system using the hardware setup of an existing clinical DBT system. The system shows promise in improving lesion and calcification detectability, and therefore merits further investigation.

CLINICAL RELEVANCE/APPLICATION

This study demonstrates potential improvement in lesion/calcification detection performance by combining the DPC mechanism with the tomosynthesis imaging method.

SSM21-03 • Dynamic Four-dimensional Contrast-enhanced Tomosynthesis

Brian C Lee (Presenter) ; Susan Ng * ; Johnny Kuo PhD * ; Peter A Ringer BS * ; Andrew D Maidment PhD *

PURPOSE

To explore the feasibility of performing four-dimensional dynamic contrast-enhanced tomosynthesis (4D DCE-DT).

METHOD AND MATERIALS

A custom bench-top tomosynthesis system was designed and built to perform 4D DCE-DT. The system consists of a stationary x-ray source and selenium x-ray detector, and a computer-controlled filter wheel with a variety of filter materials and thicknesses; phantoms are mounted on a rotary stage set atop of an x-y linear translation stage. A computer system coordinates all components, including a contrast injector. Images are acquired using a slow-scanning method in which each projection image is acquired after a fixed delay. Between each acquisition the phantom orientation is changed; it is also possible to change the x-ray energy and filter type, as well as perform injections. Both temporal and dual-energy subtraction are supported. Real-time reconstructions are performed by backprojection filtering using a customized commercial software package. A dynamic flow phantom was constructed and imaged to test the feasibility of 4D DCE-DT. One projection was acquired per energy per angle per timepoint and reconstructions were performed on subsets of these images; e.g., if projections 1 through N are used in the reconstruction for one timepoint, projections 2 through N+1 are used for the next timepoint.

RESULTS

Real-time reconstruction is possible to allow viewing of arbitrary tomographic planes and timepoints. Measured data from reconstructed waveforms of iodine concentration over time observed in the dynamic flow phantom matched the expected iodine concentration over time after convolution with a square wave with width equal to the number of projections per reconstruction. Experiments involving binary pulses of iodine (simulating the movement of a bolus of iodine through a vessel) confirmed the linearity and shift-invariance of the system. It can be observed that as the number of projections per timepoint/reconstruction decreases an increase in temporal resolution is achieved at the cost of a decrease in tomographic ability.

CONCLUSION

4D dynamic contrast-enhanced tomosynthesis can be performed in a dose-efficient fashion.

CLINICAL RELEVANCE/APPLICATION

4D dynamic contrast-enhanced tomosynthesis should allow for measurement of both spatial and temporal characteristics of blood flow and lesion perfusion.

SSM21-04 • Characterization of the Dependence of the Modulation Transfer Function in Tomosynthesis on Acquisition Geometry and Reconstruction Parameters

Brian C Lee (Presenter) ; Raymond Acciavatti ; Andrew D Maidment PhD *

PURPOSE

To characterize the spatial dependence of the in-plane modulation transfer function (MTF) in tomosynthesis and investigate the influence of the acquisition geometry.

METHOD AND MATERIALS

The in-plane MTF was calculated from measured edge spread functions using a custom test tool consisting of a 0.250 mm thick lead sheet affixed to a 5.88 mm acrylic sheet. Images were obtained using a non-clinical benchtop tomosynthesis system; reconstructions were performed using customized commercial software (Briona, RTT Inc., Villanova PA). The dependence of the MTF was measured with respect to the following factors: 1) the offset of the reconstruction plane from the plane containing the edge; 2) the obliquity of the reconstruction plane with respect to the detector; 3) the number of projections per reconstruction; and 4) the acquisition's angular range. Findings were validated by developing an analytical model of the MTF (accounting for blurring due to focal spot size, magnification, detector element size, out-of-focus plane, and reconstruction filter) and by replicating the experiment on a clinical tomosynthesis system.

RESULTS

The MTF is degraded when the edge is located between two reconstruction planes. The degree of degradation of the MTF increases as the distance between the edge and the reconstruction plane increases and as the angular range of acquisition increases. Degradation increases very slightly as the obliquity of the reconstruction plane with respect to the detector increases over the range 0° to 32° . The number of projections per reconstruction does not affect the degradation. The simulated MTFs generated by the analytical model were concordant with findings on the MTF degradation factors, and the validation experiment on the clinical tomosynthesis system provided independent confirmation that the MTF degrades with increasing distance between the edge and the reconstruction plane.

CONCLUSION

The MTF of tomosynthesis systems is anisotropic and varies with sub-slice spacing. Reconstruction of oblique planes results in minimal degradation of the MTF and thus may be clinically acceptable.

CLINICAL RELEVANCE/APPLICATION

Sub-slice misalignment of objects with the reconstructed DBT slices may adversely affect the conspicuity of small clinical features such as calcifications.

SSM21-05 • Comparative Performance Evaluation of Contrast-detail in Full Field Digital Mammography Systems Using Hotelling Observer Signal to Noise Ratio versus Automated CDMAM Image Analysis

Ioannis Delakis PhD, MSc (Presenter) ; **Robert Wise** ; **Eugenia Kulama** MSc ; **Donald Mcrobbie**

CONCLUSION

We compared the Hotelling observer SNR against the CDMAM technique. to evaluate the performance of FFDM detectors. Results showed that the Hotelling observer SNR methodology is more consistent and can be more representative of the system's performance characteristics.

Background

Image quality evaluation plays an important role in ensuring and enhancing the diagnostic value of mammography studies. According to EUREF (www.euref.org), image quality in mammography is assessed using images acquired with the Contrast Detail mammography (CDMAM) phantom (Artinis medical systems, Netherlands). However, CDMAM analysis can suffer from intra-observer variations, limited statistics and structural differences between CDMAM phantoms. The purpose of this work was to evaluate detector performance for a range of full field digital mammography systems using Hotelling observer SNR analysis and ascertain whether it can be an alternative to CDMAM evaluation.

Evaluation

FFDM units used in West of London Breast Screening were evaluated. Detector performance was first analysed using CDMAM phantom methodology. As part of Hotelling observer SNR analysis, the generalised normalised noise power spectrum (GNNPS) was measured by collecting flat field images of a 5cm PMMA phantom. The generalised modulation transfer function (GMTF) was measured by placing a 0.2mm Tungsten edge in the middle of the PMMA phantom. This setup allowed for scatter and focal spot unsharpness to be incorporated in the measurements. The Hotelling observer SNR was calculated for input signal originating from gold discs of varying thicknesses and diameters.

Discussion

The Hotelling SNR values were used to estimate the threshold gold thicknesses for each diameter as per CDMAM analysis. The Hotelling SNR technique was more consistent than CDMAM results. There were small differences between the two techniques, especially in small diameter details, which can be attributed to structural characteristics of the CDMAM, as confirmed by previous comparative work from our group. Overall, the Hotelling SNR technique showed variations in the performance of FFDM detectors, demonstrating the use of this metric as a differentiator.

SSM21-06 • Improving Image Quality for Digital Breast Tomosynthesis: Automatic Detection and Inpainting Method for Metal Artifact Reduction

Yao Lu PhD (Presenter) ; **Heang-Ping Chan** PhD ; **Jun Wei** PhD ; **Lubomir M Hadjiiski** PhD ; **Ravi K Samala** PhD

PURPOSE

Image quality is an important factor that will affect breast cancer detection in digital breast tomosynthesis (DBT). The high-attenuation metal clips embedded in the breast marking a previous biopsy site cause errors in the estimation of attenuation along the ray paths intersecting the clips during reconstruction, which result in interplane and inplane metal artifacts (MAs). Because of the small number of projection views (PVs) acquired in a limited angular range, the voxel value errors in the artifact region cannot be compensated for. This causes stronger MAs for DBT than those for CT reconstruction. We developed a new MA reduction (MAR) method to improve image quality.

METHOD AND MATERIALS

Our MAR method uses iterative detection and segmentation to automatically generate a clip location map for each PV. Correlation among different PVs is used to reduce false positive detections. Iterative diffusion-based inpainting is designed to replace the labeled clip pixels with estimated tissue intensity from the neighboring regions in each PV. The inpainted PVs are then used for DBT reconstruction. A voting technique is used to determine the location and shape of the clips and label them in the reconstructed volume. The MAR method does not depend on specific reconstruction techniques. With IRB approval and informed consent, DBT of human subjects was acquired with a GE prototype system (60° arc, 21 PVs, 3° increments). 20 DBT views from 10 breasts of various densities with clips were reconstructed with and without MAR. Five breasts had multiple large clips from lumpectomy, two of which and five other breasts had microclips from core biopsy. The improvement in MAs was visually assessed.

RESULTS

The clip detection rate in the PVs was 100% with no false positives. The interplane and inplane MAs were reduced to a level that was not visually apparent in the reconstructed slices regardless of the size and number of clips in the breast. The visibility of microcalcifications and breast tissues along the ray paths of the clips was improved.

CONCLUSION

The inpainting-based MAR method reduced the MAs while preserving the structured background and microcalcifications. The visibility of breast lesions obscured by the MAs was improved.

CLINICAL RELEVANCE/APPLICATION

DBT has strong potential to improve breast cancer detection. Reducing the MAs in DBT can improve detection and assessment of

Medical Physics 2.0: Ultrasonography Thursday, 08:30 AM - 10:00 AM • S102C [Back to Top](#)   **RC621** • AMA PRA Category 1 Credit™:1.5 • ARRT Category A+ Credit:1.5 **Co-Director Ehsan Samei**, PhD *
Co-Director Douglas E Pfeiffer, MS *
RC621A • Ultrasonography Perspective

Paul L Carson PhD (Presenter) *

LEARNING OBJECTIVES

1) Understand the roles of medical physicists and other providers of ultrasound system QC, performance evaluation and user education. 2) Gain an understanding of the longer term potential of medical ultrasound to aid in medical physics planning and training.

ABSTRACT

A very brief overview is given of the innovations that have led to current medical ultrasound systems and QC thereof. A clear connection to clinical performance/cost effectiveness has not been established, but the ratio is improving. To aid in medical physics planning and training, more distant (beyond 10 years) and less robust predictions are ventured than in Dr. Hangiandreous' talk. The reduction in artifacts and improvement in resolution will be surprisingly large. It is posed that ultrasound will be headed toward almost ubiquitous use in personal hands as well as those of medical personnel, for monitoring and control of chronic conditions, for direct treatment and for precisely localized drug delivery and enhancement of radiation therapy. Medical physicists who can help keep the computer controls integrated, the systems properly calibrated and the users properly trained will find a substantial role in society.

RC621B • Ultrasonography 1.0

Zheng Feng Lu PhD (Presenter)

LEARNING OBJECTIVES

1) Describe the current role of ultrasound medical physics in clinical practice. 2) Explain the ultrasound image quality metrics utilized in current ultrasound QA/QC testing. 3) Outline the methods and tools available for ultrasound system QA/QC in current clinical practices. 4) Survey the available standards and voluntary accreditation guidelines for medical ultrasound imaging systems. 5) Understand the need for QC at different levels of time and financial investment.

ABSTRACT

This talk will focus on the present role of ultrasound medical physics in clinical practices. It will review the ultrasound image quality metrics currently utilized in ultrasound QA/QC testing. It will describe testing procedures required and/or recommended by accreditation programs and advisory organizations. General guidelines and available standards will be discussed regarding tolerances for acceptance testing and commissioning of these devices, as well as periodic quality control tests, as applicable to diagnostic B-mode imagers. A brief review of ultrasound phantoms used in these testing procedures will be presented.

RC621C • Ultrasonography 2.0

Nicholas J Hangiandreou PhD (Presenter)

LEARNING OBJECTIVES

1) Identify the roles expected for medical physics to play in future clinical ultrasound practices. 2) Demonstrate understanding of emerging ultrasound imaging performance metrics that are expected to be in routine practice in the future. 3) Demonstrate understanding of emerging ultrasound imaging technologies that are expected to be in routine practice in the future. 4) Identify approaches for implementing comprehensive medical physics services in future clinical ultrasound practices.

ABSTRACT

Ultrasound imaging is evolving at a rapid pace, adding new imaging functions and modes that continue to enhance its clinical utility and benefits to patients. This talk will look ahead 10-15 years and consider how medical physicists can bring maximal value to the clinical ultrasound practices of the future. The roles of physics in accreditation and regulatory compliance, image quality and exam optimization, clinical innovation, and education of staff and trainees will all be considered. A detailed examination of expected technology evolution and impact on image quality metrics will be presented. Clinical implementation of comprehensive physics services will also be discussed.

Uncertainties in Imaging for Radiation Oncology: Sources and Mitigation Techniques-Imaging Moving Targets Thursday, 08:30 AM - 10:00 AM • S102D [Back to Top](#)   **RC622** • AMA PRA Category 1 Credit™:1.5 • ARRT Category A+ Credit:1.5

Co-Director, Moderator Kristy K Brock, PhD *
LEARNING OBJECTIVES 1) Describe techniques for imaging moving targets. 2) Propose methods to account for uncertainties. 3) Highlight clinical integration.

RC622A • Uncertainties in Moving Targets

Jasper Nijkamp PhD (Presenter)

LEARNING OBJECTIVES

View learning objectives under main course title.

RC622B • Clinical Practice

Laura A Dawson MD (Presenter) *

LEARNING OBJECTIVES

View learning objectives under main course title.

Minicourse: Recording and Reporting Radiation Dose: Interventional/Angiography/Fluoroscopy Thursday, 08:30 AM - 10:00 AM • N229 [Back to Top](#)    **RC623** • AMA PRA Category 1 Credit™:1.5 • ARRT Category A+ Credit:1.5 **Director J. Anthony Seibert**, PhD

RC623A • Issues in Interventional Fluoroscopy Procedures

Stephen Balter PhD (Presenter)

LEARNING OBJECTIVES

1) Be able to describe effects on patient's skin, hair, eyes, and other tissues resulting from fluoroscopically-guided interventional procedures. 2) Be able to adequately communicate FGI radiation risk as part of the informed consent process. 3) Understand the use of real-time displays of radiation quantities and their relation to radiation risks.

ABSTRACT

Some fluoroscopically-guided interventional procedures (FGI) require the use of a substantial amount of radiation for their completion. Radiation can be regarded as a toxic agent in the same sense that contrast-media and drugs can be toxic if inappropriately used. The interventional radiologist should have reasonable knowledge of the toxic effects of radiation on patients at

dose levels that may occur during IR procedures. These include short-term tissue reactions on the skin, hair loss, and radiogenic cataracts. Longer term effects such as cancer induction are of importance for some patients. Because radiation is potentially toxic, its risks should be appropriately discussed during the informed consent process. The display of reference air kerma and kerma area product provide risk information to the radiologist while performing a procedure. This is intended to provide ongoing inputs into a continuous evaluation of benefit-risk.

RC623B • Measurements and Dose Calculations

Beth A Schueler PhD (Presenter)

LEARNING OBJECTIVES

1) Review methods of measuring patient radiation dose during fluoroscopically-guided interventional procedures. 2) Compare the advantages and limitations of dose measurement methods. 3) Understand parameters that are used to describe patient entrance dose. 4) Learn about new methods for skin dose calculation and recording.

ABSTRACT

The measurement of patient dose during fluoroscopically-guided interventional procedures is an important tool for assessment of individual patient radiation risk. Moreover, the display of patient dose is valuable as feedback to the operator to aid in optimization of radiation exposure. Many different methods of measuring fluoroscopy dose have been developed, including direct methods (dosimeters and film) and indirect methods (fluoroscopy time, dose-area-product meters and reference point air kerma estimation). This presentation will review the advantages and limitations of each of these methods, along with common dose metrics that fluoroscopy operators, medical physicists and technologists should be familiar with. In addition, we will discuss skin dose mapping methods that are currently being developed.

RC623C • Establishing an Interventional Radiology Patient Radiation Safety Program

Aaron K Jones PhD (Presenter)

LEARNING OBJECTIVES

1) List the radiation dose descriptors that should be recorded at the conclusion of a fluoroscopy-guided procedure. 2) Describe the actions that may be taken during the three phases of a fluoroscopy-guided procedure to enhance patient safety. 3) Discuss how to recognize cases that are outside the normal control limits of an interventional radiology practice.

ABSTRACT

An interventional radiology patient safety program is essential to better educate patients who are scheduled to undergo fluoroscopically guided interventional radiology procedures; monitor radiation doses delivered during procedures and reduce the risk of tissue effects; ensure appropriate medical management of patients experiencing significant peak skin doses; and for practice quality improvement through analysis of procedural data and exceptional cases. The program combines preprocedure evaluation and counseling, intraprocedure monitoring, and postprocedure documentation and counseling consistent with guidelines from the National Cancer Institute and the Society of Interventional Radiology. Implementation of a patient safety program is straightforward, requires little infrastructure and few resources, and can be applied in most interventional radiology practices.

Quantitative Imaging: Volumetric CT as a Biomarker for Disease Thursday, 08:30 AM - 10:00 AM • N226 [Back to Top](#) PH CT
BO **RC625 • AMA PRA Category 1 Credit™:1.5 • ARRT Category A+ Credit:1.5 Director Michael F McNitt-Gray, PhD ***
RC625A • Why is Quantitative Imaging (Tumor Volumes) Needed in Oncologic Imaging

Lawrence H Schwartz MD (Presenter)

LEARNING OBJECTIVES

1) To understand the role and value of quantitative volumes in oncology. 2) To understand the challenges associated with quantitative volume calculations in oncology.

RC625B • Understanding Measurement Variation: Lessons Learned from Phantom Studies

Nicholas Petrick PhD (Presenter)

LEARNING OBJECTIVES

1) To review how changes in CT acquisition parameters and nodule characteristics affect measurement error. 2) To review how phantom studies can be used to systematically probe, identify and potentially minimize measurement error and improve our ability to perform quantitative CT imaging. 3) To understand which CT and analysis parameters should be held constant across multiple CT scans, if at all possible, to optimize the evaluation of a patient's response to therapy.

ABSTRACT

In this refresher course, we will update the audience on the methods and results obtained from various phantom studies developed to assess both absolute lesion size measurements and change over time measurements involving both automated and semi-automated lesion sizing tools.

RC625C • Variability in CT Measurement of Tumor Volumes and Its Impact on Response Assessment

Binsheng Zhao DSc (Presenter)

LEARNING OBJECTIVES

1) Demonstrate the feasibility of computer-aided (tumor) volume measurement and explain its potential to improve conventional response assessment in oncology. 2) Familiarize the audience with sources of variation in measuring tumor volume and tumor volume change. 3) Discuss the need for standardizing both imaging and measurement techniques in the interpretation of tumor measurement and thus in response assessment.

ABSTRACT

Volumetric CT (VolCT) shows potential as a better method to assess tumor response, especially early response, to therapy than the conventional diameter methods. This refresher course will first show how the volumes of solid tumors can be accurately and practically obtained with the help of computer software, then discuss the factors that can affect measurement reproducibility of in vivo tumors during image acquisition and tumor measurement. By becoming acquainted with a well-designed series of (clinical) variability studies, the audience will learn the magnitudes of variability that can occur in the measurement of tumor volumes, as well as in tumor diameter(s).

ASRT@RSNA 2013: Mastering Digital Radiography: CR and DR Exposures, Techniques and Doses Thursday, 09:20 AM - 10:20 AM • N230 [Back to Top](#) PH **MSRT52 • AMA PRA Category 1 Credit™:1 • ARRT Category A+ Credit:1 Dennis Bowman ***

LEARNING OBJECTIVES 1) Understand that hand images taken with both CR and DR equipment from 50-100 kV are all passable. 2) Describe the differences between film/screen and digital radiography. 3) Demonstrate understanding of the Exposure Index (EI) numbers and ranges of these numbers. 4) Identify what factors are needed to corrupt; an Exposure Index (EI) number. 5) Describe 3 different ways to critique a digital image. 6) Understand how Automatic Rescaling allows up to 100 times too much mAs to be used. 7) Explain the legal implications of changing algorithms and post processing collimation. 8) Recognize how much radiation dose can be saved using higher kV and lower mAs. 9) Analyze the new CR and DR Universal Technique Charts. **ABSTRACT** One of the main focuses of this talk will be to prove without a doubt that the Dose Index (DI) numbers that come up with both CR and DR are extremely reliable almost all the time. In fact they can barely be corrupted more than 75% regardless of the centering and collimation.

I will also cover the new high kV/low mAs techniques that should be used with all digital equipment. This means doing a minimum of the 15% Rule over what was used with f/s systems. Since dropping the radiation dose is one of the major topics, I will prove by increasing kV and dropping the mAs you can always decrease the radiation dose. We will also discuss my Universal Digital Technique Charts for both CR and DR systems as well as finding out if your facility is using the proper DI ranges according to your radiologists. Additionally, there will be a section on the three ways to properly critique a digital image. Following that I will show how different brands of CR and DR react when too much mAs is used in an exposure. Also discussed will be the legal issues that concern radiographers, including reprocessing images with different algorithms and shuttering (post process collimation). My goal is for you to be able to take this information back to your facility and immediately make changes in the way you expose and critique your images.

Physics (MRI Techniques III) Thursday, 10:30 AM - 12:00 PM • S403B [Back to Top](#)   **SSQ19** •AMA PRA Category 1 Credit™:1.5 •ARRT Category A+ Credit:1.5 **Moderator Savannah C Partridge**, PhD *

Moderator Yi Wang, PhD

SSQ19-01 • Accurate Temperature Measurements in the Presence of Field Inhomogeneities for MR Guided Thermal Therapies

Chang-Sheng Mei PhD (Presenter) ; **Renxin Chu** PhD ; **W. Scott Hoge** PhD ; **Lawrence P Panych** PhD ; **Bruno Madore** PhD *

PURPOSE

The present study aimed at developing an MRI-based temperature monitoring strategy capable of providing accurate temperature measurements even in the presence of field inhomogeneities. Such inhomogeneities commonly occur near air-tissue transitions, for example, around the sphenoid sinuses, and can significantly degrade the accuracy of temperature measurements.

METHOD AND MATERIALS

The use of a multi-pathway steady-state sequence is proposed here to help detect and correct for susceptibility-induced temperature measurement errors. The two different signal pathways sampled by the sequence lead to temperature errors of different polarity, ΔT and $-\Delta T$, making it possible to detect and correct for such errors. These two pathways correspond to the so-called \diamond fast imaging with steady-state precession \diamond (FISP) signal and the inverse-FISP (PSIF) signal. The heating curve from both signal pathways can be measured, on a pixel-by-pixel basis, and a single-variable equation can be solved to evaluate the temperature errors, allowing them to be corrected for. The method was tested in gel phantoms and in a rabbit model.

RESULTS

Measurement errors of several \diamond C were observed and corrected for in controlled phantom experiments where known field inhomogeneities were intentionally introduced by de-adjusting high-order shim settings. Temperature errors were also observed and corrected for in a rabbit model, where field inhomogeneities were unavoidably present despite shimming, due to nearby air-tissue interfaces. After the proposed correction scheme was applied on a pixel-by-pixel basis, agreement was obtained between both FISP and PSIF measurements. Errors by up to about 20% in temperature elevation (overestimation by 5 \diamond C on a 25 \diamond C peak temperature elevation) have been observed and avoided.

CONCLUSION

We have demonstrated a method for detecting and correcting for susceptibility-induced temperature measurement errors. The method allows accurate temperature measurements to be performed even near air-tissue interfaces, with potential benefits in prostate, uterus, and brain MR-guidance applications.

CLINICAL RELEVANCE/APPLICATION

The proposed thermometry method allows susceptibility-induced temperature errors to be detected and corrected for. As a result, improved MR guidance may be achieved, during thermal therapies.

SSQ19-02 • Improving Reconstruction Speed for Dynamic MRI Using Parallel Imaging with Combined Coil Compression and Direct Virtual Coil

Kang Wang PhD (Presenter) * ; **Scott K Nagle** MD, PhD * ; **Harald Kramer** MD ; **Tao Zhang** ; **Philip Beatty** ; **Mahdi Rahimi** ; **Courtney K Morrison** ; **Frank R Korosec** PhD * ; **Scott B Reeder** MD, PhD ; **Dan W Rettmann** BS * ; **Ersin Bayram** PhD * ; **James H Holmes** PhD *

PURPOSE

Coil-by-coil (CBC) data-driven auto-calibrating parallel imaging has become more widely used for dynamic MR applications, such as dynamic contrast-enhanced (DCE) MR angiography (MRA). However, for high spatial resolution, high parallel imaging factors and high channel count coil array protocols, the image reconstruction time can be clinically unacceptably long. This work demonstrates an initial comparison of combining Coil Compression and Direct Virtual Coil (CCDVC) to significantly reduce reconstruction times vs. the currently used conventional method of CBC in the setting of dynamic contrast enhanced peripheral runoff MR angiography.

METHOD AND MATERIALS

Twenty-four volunteers (7 healthy, 17 with pathology) were imaged and informed consent was obtained prior to all scanning. All scans were conducted on a clinical scanner (3.0T MR750, GE Healthcare), with 48cm FOV, 1.0mm isotropic resolution, 32-channel coil array and parallel imaging factor of 3 (phase) \times 2 (slice) = 6. Temporal view-sharing was used to generate raw data for each time frame. The same raw data sets were then reconstructed twice: once with CBC and once with CCDVC. Time-resolved images reconstructed using CBC and CCDVC were randomized and blindly scored by two radiologists using a 5-point scale: image 1 much better (clinically significant); image 1 slightly better (not clinically significant); equivalent; image 2 slightly better (not clinically significant); image 2 much better (clinically significant).

RESULTS

The reconstruction times for CCDVC were about 18 \times faster than the conventional CBC method (17 sec vs. 311 sec per phase on an offline computer) in the parallel imaging synthesis/FFT/coil combination module. One radiologist scored 18 cases as \diamond equivalent \diamond , 3 cases as CCDVC \diamond slightly better \diamond , and 3 cases as CBC \diamond slightly better \diamond ; the second radiologist scored 17 cases as \diamond equivalent \diamond , and 7 cases as CCDVC \diamond slightly better \diamond .

CONCLUSION

The combined CCDVC technique was shown to significantly reduce the reconstruction time for high spatial and temporal resolution peripheral MRA, with no significant loss in image quality.

CLINICAL RELEVANCE/APPLICATION

The reconstruction speed for a DCE peripheral MRA scan can be significantly improved by using CCDVC to enable more aggressive clinical protocols or improve clinical workflow.

SSQ19-03 • Exercise System for Using 31-phosphorus MR Spectroscopy to Monitor Phosphocreatine Recovery from Exercise as Index for Mitochondrial Metabolism

Floyd Settles (Presenter) ; **Geoffrey D Clarke** PhD

PURPOSE

Measurement of mitochondrial function is relevant to aging, diabetes and sports medicine. Phosphorus-31 magnetic resonance spectroscopy (31P-MRS) can be used to evaluate the rate of phosphocreatine (PCr) recovery following exercise as a noninvasive index of the rate of ATP synthesis. The project's aim is to develop a reproducible measurement technique using an exercise apparatus to quantify PCr recovery in the vastus lateralis muscle (VL).

METHOD AND MATERIALS

The apparatus was designed to exercise the VL with subjects in supine position with a dual-tuned 1H-31P TX/RX surface coil strapped to the thigh. PCr depletion levels and recovery times were measured for 8 minutes following a 5 min period of exercise. Slice-selective 31P-MRS was performed on 5 subjects (4 male, 15-56 y.o.) with TR=3000 ms, NSA=2, BW=2200 Hz. The time for return of PCr values to their half-maximum (T-half) was used as an index for the rate of ATP synthesis. PCr recovery data were fit to the function $PCr(t) = PCr(0) + D[1 - \exp(-bt)]$ using the Marquardt-Levenberg algorithm (nlsLM function) in the R statistical package, where D and b were the fitted variables.

RESULTS

The prototyped apparatus is a compact, single-piece PVC assembly with little mass (

CONCLUSION

The exercise apparatus works, supporting and immobilizing the thigh and surface coil during baseline, dynamic flexion exercise and recovery phases of the protocol. Spectral data acquired consistently demonstrated PCr depletion and recovery in VL across all subjects. Predictable extension of the lower leg is obtained with a constant resistance without the use of large weights.

CLINICAL RELEVANCE/APPLICATION

Noninvasive, reproducible measures of mitochondrial function by a well-characterized in-vivo biomarker can provide insights for the characterization and treatment of metabolic diseases.

SSQ19-04 • Transcranial Magnetic Stimulation-Induced Heating of Deep Brain Stimulation Implants: An Empirical Specific Absorption Rate Evaluation Using a Tissue Equivalent Phantom

Goldie R Boone MS (Presenter) ; Geoffrey D Clarke PhD

PURPOSE

Transcranial magnetic stimulation (TMS) uses electromagnetic induction to generate weak electric currents by application of rapidly changing magnetic fields to depolarize or hyperpolarize neurons in the brain. The potential for induced heating of brain tissues located near bilaterally implanted deep brain stimulation (DBS) electrodes during application of single pulse and repetitively pulsed TMS was investigated. This study provides empirical evidence for the reasonable assurance of safety in the FDA classification of TMS as a Class II (special controls) device.

METHOD AND MATERIALS

TMS was conducted using the MagPro R30 system (MagVenture, Denmark) with a liquid cooled butterfly coil (model Cool-B65). TMS-induced heating was measured using a proprietary phantom and a clinical/research stimulation protocol. Fiber optic thermometry probes acquired real-time temperature measurements of the induced heating at the surface of the metallic DBS electrodes during TMS. The three specific aims of this study were to evaluate the 1) spatially localized temperature increase, 2) spatially localized specific absorption rate (SAR), and 3) the average head SAR in the phantom in the absence and presence of the DBS implant over a 6 minute averaging period in saline and gelled-saline solutions at stimulation frequencies of 1 and 5 Hz. The differences in the average temperatures in the presence and absence of bilateral DBS implants were analyzed by ANOVA ($p = 0.05$, power = 0.80) with Bonferroni correction.

RESULTS

In the clinical/research stimulation orientation, no evidence of induced heating effects was observed above the thermal noise. However, stimulation of the lead loops at 5 Hz in gelled saline at a distance of 0.5 cm from the coil surface and peak intensity region resulted in temperatures that tripled the spatially localized temperature limit and SAR values that doubled the spatially localized SAR limit. TMS-induced heating effects of this nature may result in localized tissue damage.

CONCLUSION

The observations in this research study support the use of repetitive TMS of patients with a bilateral DBS device implant provided prior knowledge is used to guide surgical lead configuration and careful coil placement during stimulation.

CLINICAL RELEVANCE/APPLICATION

The data support the use of repetitive TMS as a safe adjuvant therapy to surgery and pharmaceuticals in the treatment of neurological movement and major depressive disorders.

SSQ19-05 • How to Improve the Quality and Speed of 3T MR Imaging in Cervical and Lumbar Spine by Multiple RF Transmission?

Chuan Shuai Tian (Presenter) ; Bing Zhang PhD ; Fei Chen MS ; Bin Zhu ; Haiping Yu ; Ming Li ; Danyan Li ; Huiting Wang MS ; Weibo Chen MSc ; Queenie Chan PhD

PURPOSE

We aimed to study how to improve the quality and speed of cervical and lumbar imaging by TX technology compared with single transmission (without TX).

METHOD AND MATERIALS

Thirty-seven healthy volunteers (seventeen (5 male and 12 female), aged 21-55yr (mean 38.47±13.02yr) for cervical; twenty (8 male and 12 female), aged 20-64yr (mean 29.25±8.48yr) for lumbar) were scanned at 3.0T scanner (Achieva TX, Best, the Netherlands), acquiring the T2WI and T1WI images of the cervical and lumbar with and without TX. We compared the parameters, as well as the average signal intensity in different region of interest (ROIs) between the cervical and lumbar MRI with and without TX (Fig.a.b). P values less than 0.05 were considered statistically significant by Paired t-test.

RESULTS

TR was shortened by 1224ms(26.67%) on T2WI, and 97ms (17.64%) on T1WI in lumbar MRI. Packages reduced by 1.5±1 (37.5%), scanning time is shortened by 97.2±31.15s (44.02%). On T2WI of the cervical, the average signal intensity of ROIs 3/4/9 for vertebrae, ROIs 10/11 for fat were increased, ROIs 6/7 for the spinal cord, ROI 12 for the pons were decreased (P 0.05 have no statistical significance). On T1WI, the average signal intensity of ROIs 1/2 for vertebrae, ROIs 5-8 as the spinal cord, ROI 12 for the pons, ROI 13 for the cerebellum were reduced, ROIs 10/11 for fat were increased (P0.05 have no statistical significance). On T2WI of the Lumbar, the average signal intensity of ROIs 1-6/10 for vertebrae, ROI 9(on the same level of lumbar 5) for fat were reduced; ROI 8(on the same level of lumbar 1) for fat was increased (P 0.05, no statistical significance). On T1WI, the average signal intensity of ROIs 2-6/10 for vertebral, ROI 7 for the spinal cord were reduced; ROI 8 for fat was increased (P 0.05 have no statistical significance).

CONCLUSION

In the cervical and lumbar MRI, multiple-transmit parallel RF transmission can improve B1 homogeneity, shorten TR, reduce local SAR value and scanning packages, thereby improve the image quality and reduce scanning time.

CLINICAL RELEVANCE/APPLICATION

Multiple-transmit parallel RF transmission can improve the image quality and reduce scanning time.

SSQ19-06 • High B-value Diffusion Weighted Imaging in Defining the Infiltration Zone of Cerebral Glioma

Chunhui Jiang BMedSc, MMedSc ; Jian Wang (Presenter)

CONCLUSION

It is demonstrated in this study that DWI may be useful in defining the infiltration zone of glioma, especially with high B-values.

Larger studies are needed to prospectively validate the utility of ADC from high B-values DWI scan as a noninvasive imaging biomarker for quantitatively measuring the infiltration zone of glioma.

Background

To evaluate the role of the ADC value in patients with glioma (WHO II-IV) using high B-value diffusion weighted imaging (DWI), as a potential noninvasive quantitative index in defining the boundary of glioma.

Evaluation

18 cases of surgical pathologically confirmed glioma underwent the DWI scan with $b=1000$ and 3000s/mm^2 respectively in a 3T MR scanner. The ADC values of the glioma substantial zone, cerebral parenchyma within 0-10/10-20mm radius and the cerebral parenchyma of the opposite sphere are statistically analyzed by SPSS17.

SSQ19-07 • Comparison of Signal as a Function of Position for a 1H/31P Surface Coil Used in Exercise Studies

Erika Ripley (Presenter) ; **Geoffrey D Clarke** PhD

PURPOSE

MRI-compatible exercise studies are reported in the literature for measuring phosphorus-31 (31P) metabolites in the vastus lateralis muscle (VL). For these studies the thigh is positioned at an angle with respect to the main magnetic field to allow leg movement, which is a non-optimal orientation for the MRS coil. This study determines the performance degradation in the RF coil due to orientation.

METHOD AND MATERIALS

A dual-tuned rigid TX/RX surface coil (Rapid Biomedical, Rimpac, Germany) was used on a 3T MRI system (TIM Trio, Siemens, Malvern, PA) to collect 31P spectra from a leg phantom (15 cm diameter, 4 L plastic cylindrical jug with 10 mM H_3PO_4) and a small standard (6 mL plastic vial with a 850 mM concentration of methylenediphosphonic acid (MDP)). The standard was positioned on the surface coil and a 1-pulse 31P sequence was performed (TR 8000 ms, 4 NSA, 4 prep scans, BW=3000 Hz). Spectra were taken with the MDP vial at the center of the coil, 5 cm, 8 cm and 10 cm away from the center in the R/L and H/F directions. Measurements were repeated with the leg phantom flat on the table parallel to B_0 (0°) and secured to the exercise device at an angle of 38.9° with respect to B_0 . Spectra were analyzed using jMRUI software to determine the area under each peak. Paired t-tests were used to evaluate the statistical significance (p

RESULTS

The areas of the MDP peaks were plotted with respect to position. For both orientations, the signal from right to left was symmetric about the center of the coil with the highest signal at ± 8 cm. The signals across the coil R/L were reduced by 30% ($p=0.015$) at 38.9° compared to 0°. Along the z axis, with the phantom flat on the table, the signal was almost symmetric, but spectra obtained at an angle were skewed with the maximum signal at +8 cm and no signal below -5 cm, an overall -56% average difference.

CONCLUSION

Signal intensity changes from the acquired phantom data suggest that over 60% of the total signal is lost at the 38.9° angle compared to acquisitions with the coil parallel to B_0 . Also, most of the signal will come from the portion of the VL muscle that is near the knee-end of the coil.

CLINICAL RELEVANCE/APPLICATION

Signal sensitivity profiles that take into account position and coil orientation must be considered for 31P metabolite quantification in exercise studies.

SSQ19-08 • Cerebrospinal Fluid Fluctuation in the Ventricular System in Idiopathic Normal Pressure Hydrocephalus

Naoki Ohno MS (Presenter) ; **Tosiaki Miyati** PhD ; **Mitsuhiro Mase** MD ; **Noam Alperin** PhD * ; **Harumasa Kasai** MSc ; **Shinnosuke Hiratsuka** ; **Makoto Kawano** ; **Yuta Shibamoto** MD, PhD ; **Toshifumi Gabata** MD ; **Osamu Matsui** MD

PURPOSE

We have reported that temporal changes in the brain parenchyma's apparent diffusion coefficient (ADC) during the cardiac cycle (?ADC) reveal the degree of fluctuation of water molecules likely resulting from arterial inflow (volume loading) during systole, and this information potentially facilitates the diagnosis of idiopathic normal pressure hydrocephalus (iNPH). However, we assessed the ADC change only in white matter. Moreover, several studies have shown that analysis of intraventricular CSF flow can provide the intracranial condition in iNPH. We therefore determined the temporal change in ADC over the cardiac cycle in the ventricular system of iNPH.

METHOD AND MATERIALS

On a 1.5-T MRI, ECG-triggered single-shot diffusion echo planar imaging ($b = 0$ and 1000 s/mm^2) was used with sensitivity encoding and half-scan techniques to minimize the bulk motion. Then ADC image of each cardiac phase were made. Next, a normalized-?ADC image was calculated from all cardiac phase ADC images (20 phases) on a pixel-by-pixel basis using the following equation: $\text{Normalized-?ADC} = (\text{ADC}_{\text{max}} - \text{ADC}_{\text{min}}) / (\text{ADC}_{\text{max}} + \text{ADC}_{\text{min}})$, where ADC_{max} and ADC_{min} represent the maximum and minimum ADC during the cardiac cycle, respectively. We assessed normalized-?ADC and ADC values in the three ventricular regions, i.e. the anterior and posterior horns of the lateral ventricles and the third ventricle, and compared those values among the iNPH ($n=14$), atrophic ventricular dilatation (atrophic VD group; $n=9$), and healthy volunteers (control group; $n=8$).

RESULTS

Normalized-?ADC of the third ventricle was significantly higher in iNPH compared with the control and atrophic VD groups, whereas there were no significant differences for normalized-?ADC in the other regions among the groups. This result can be explained by the fact that large compression on the ventricular system increases the fluctuation of the water molecules. However, there were no significant differences in ADC of all ventricular regions among the groups.

CONCLUSION

Normalized-?ADC analysis as a fluctuation MRI in the ventricular system makes it possible to noninvasively obtain more detailed information on the intracranial condition in iNPH and thereby possibly assist in the diagnosis.

CLINICAL RELEVANCE/APPLICATION

Fluctuation analysis of the intraventricular CSF makes it possible to noninvasively obtain more detailed information on the intracranial condition in iNPH and thereby possibly assist in the diagnosis.

SSQ19-09 • Accurate T1 Relaxivities (r_1) of Gadolinium-based Magnetic Resonance Contrast Agents (GBCAs) in Human Whole Blood at 1.5T and 3T

Yaqi Shen PhD, MD ; **Christopher G Snyder** BS ; **Frank L Goerner** PhD (Presenter) * ; **Regina Moritz** ; **Val M Runge** MD *

PURPOSE

The current available values for T_1 relaxivity (r_1) of Gadolinium based MR contrast agents (GBCAs) at 1.5T and 3T are either provided for non-clinically relevant scenarios or in only a portion of the available GBCAs. This is likely due to the complex nature of obtaining these values. This study determines and compares the r_1 values of eight commercially available GBCAs in human whole blood at 1.5T and 3T.

METHOD AND MATERIALS

RESULTS

CONCLUSION

CLINICAL RELEVANCE/APPLICATION

The results of this experiment are the most relevant r_1 measurements to a clinical scenario. This will give clinicians a more accurate idea of the enhancement of each GBCA in MR imaging.

Physics (CT Reconstruction) Thursday, 10:30 AM - 12:00 PM • S404AB [Back to Top](#) PH CT **SSQ20** • AMA PRA Category 1 Credit™: 1.5 • ARRT Category A+ Credit: 1.5 **Moderator Xiaochuan Pan, PhD ***
Moderator Bruno De Man, PhD *
SSQ20-01 • Proper Weighting of Redundant Data in Cardiac Reconstruction Enables Repeatable Quantitative Imaging at Large Cone Angles

Brian E Nett PhD (Presenter) * ; Zhye Yin * ; Jed Pack *

PURPOSE

To assess the performance of a new image reconstruction algorithm, which properly weights redundant data, for the case of a half-scan type temporal weighting function.

METHOD AND MATERIALS

The most common method to achieve half-scan type temporal weighting for cone-beam tomography is to extend the standard Parker type weighting function which accounts for redundancies in sinogram space (P-FDK). This weighting is exact in the central slice but leads to data mishandling away from the central slice. More recent methods have been developed which properly account for redundant data (e.g. application of Katsevich framework for exact reconstruction to a single arc source trajectory). In this work a method which properly weights redundant frequency data is evaluated for repeated quantitative imaging. The effect of the reconstruction algorithm is studied in isolation from other physical effects by using a monoenergetic simulation of an anthropomorphic phantom (ie. the XCAT phantom). The central view angle of the image reconstruction was sampled in 15 deg intervals over 360 deg.

RESULTS

The standard deviation of reconstruction values as a function of central view angle was computed in order to visually demonstrate the strong angular dependence of standard methods. Automated regions of interest (ROIs) were defined for myocardium and fat tissue types in the phantom and measured as a function of cone-angle. For cone angles greater than +/-2 deg the percentage of voxels which had a std. w.r.t. central view angle of greater than 10 HU was [P-FDK] (96.9%,96.4%) , [improved recon] (0.14%,1.4%) for myocardium and fat ROIs respectively.

CONCLUSION

New image reconstruction methods indicate that repeatable quantitative imaging is possible for CT acquisitions with a large cone angle.

CLINICAL RELEVANCE/APPLICATION

Advanced image reconstruction techniques can improve repeatable quantitative reconstruction for half-scan reconstruction.

SSQ20-02 • Image-based Partial Scan Artifact Reduction for Dynamic Contrast Enhanced CT

Adam M Alessio PhD (Presenter) * ; Aaron So PhD ; Ting-Yim Lee MSc, PhD *

PURPOSE

Partial scan (PS) CT acquisitions lead to artifacts due to inconsistencies from scatter contributions and inexact cone-beam reconstruction. Dynamic cardiac studies, which benefit from PS acquisitions and require high CT number fidelity, require corrections for these view-angle dependent shading artifacts. PS artifact reduction methods have been proposed based on raw projections, images, or combinations of projection and temporal information. We propose a PS artifact reduction (PSAR) method requiring only access to images to reduce the influence of cone-beam and scatter induced artifacts.

METHOD AND MATERIALS

The cone-beam issues are mitigated with an error term derived from the error-reduction-based algorithm (ERB, Zeng et al, 2004). In addition, the scatter contribution is estimated based on the convolution of pencil-beam scatter distribution and a forward scatter model. These two components are iteratively estimated through successive cone-beam forward projections and Feldkamp reconstructions of the original artifact-present images. The proposed PSAR algorithm was tested with simulations of a 64-slice CT acquisition of a thoracic phantom. The view-angle dependent error was evaluated in simulations and verified with measured images from DCE-CT porcine studies.

RESULTS

Simulation studies revealed that for a realistic thoracic morphology, CT numbers in slices at the edge of the axial field of view (from large cone-angles) vary by 30 HU as a function of the center view angle of the PS acquisition. Scatter alone causes variations of ~6 HU at different view angles. PS's from porcine studies confirmed HU variations in soft-tissue regions of 29 HU as view angle varied. In simulations, the application of the PSAR algorithm reduced the RMSE in the myocardial region from 14.5 HU to 6.3 HU across all slices and view angles.

CONCLUSION

PSAR reduced view-angle dependent artifacts in PS acquisitions. This method benefits from not requiring access to raw projection data or full-scan information, offering a practical method for artifact reduction in DCE-CT studies.

CLINICAL RELEVANCE/APPLICATION

The proposed PSAR method reduces scatter and cone-beam artifacts in partial scan acquisitions to improve the quantitative information from these fast, lower-dose dynamic cardiac CT acquisitions.

SSQ20-03 • Performance Evaluation of a CT Iterative Reconstruction Algorithm in Detection and Discrimination Tasks Using Model Observer

Yi Zhang (Presenter) ; Shuai Leng PhD ; Lifeng Yu PhD ; Cynthia H McCollough PhD *

PURPOSE

The performance correlation between human observers and a channelized Hotelling observer (CHO) has been previously demonstrated in low contrast lesion detection and lesion shape discrimination tasks using CT images. The purpose of this study was to use CHO to quantitatively assess the performance of an iterative reconstruction (IR) method and a traditional filtered backprojection (FBP) method in these two tasks.

METHOD AND MATERIALS

11 lesion-mimicking rods were placed in a 35 x 26 cm torso-shaped water phantom and scanned on a 128-slice CT scanner (Definition Flash, Siemens) with 120 kV at 4 different mAs settings: 120, 240, 360 and 480 quality reference mAs (CAREdose4D), each repeated 100 times. CT images were reconstructed using FBP and IR (SAFIRE) methods available from the scanner. 3 rods had -15 HU contrast to mimic low contrast lesions. The other 8 rods had a relative higher contrast (2 shapes x 2 contrasts x 2 sizes), which were used to construct shape discrimination tasks, in which hexagon and circle rods were displayed side-by-side in a randomized order. A total of 5600 2-alternative forced-choice trials were analyzed using CHO with Gabor filters (6 passbands, 5 orientations and 2 phases) and percent correct (PC) was calculated for each task. Internal noise was added to test variables to estimate the variation of PC.

RESULTS

For the low-contrast lesion detection task, CHO didn't predict improved performance with SAFIRE for most dose and size settings. The only improvements were observed for 3 mm lesion at 360 mAs, from $96\pm 2\%$ to $98\pm 1\%$ (p

CONCLUSION

Image quality and performance improvement of IR depends on diagnostic tasks. A previously validated CHO predicted that there is a significant improvement of performance with IR for lesion shape discrimination task but not for low-contrast lesion detection task.

CLINICAL RELEVANCE/APPLICATION

IR can be used to improve performance or reduce dose, with the amount of dose reduction dependent on lesion size and contrast, as well as the diagnostic task.

SSQ20-04 • Prior-based Artifact Correction in Computed Tomography

Thorsten Heuser (Presenter) ; **Marcus Brehm** ; **Ludwig Ritschl** ; **Stefan Sawall** DIPL ENG ; **Marc Kachelriess** PhD

PURPOSE

To improve image quality in x-ray computed tomography (CT) in cases of missing or corrupt data.

METHOD AND MATERIALS

CT image quality often suffers from artifacts due to missing or corrupt data. Numerous approaches to reduce these artifacts have been published. These approaches typically use inter- or extrapolation techniques specific for the kind of artifact investigated and in many cases tend to introduce new artifacts. Often, however, prior data are available which can, potentially, be used to better compensate for the missing or corrupt data and thereby to help reduce artifacts without introducing new artifacts. These prior data may be images from a different scan of the same patient, e.g. a planning CT, or images of a similar patient taken from a patient data base. We propose a prior-based artifact correction (PBAC) algorithm, a generalized correction method for prominent artifacts in CT resulting from missing or corrupt data. To compensate for differences in patient shape and position PBAC performs a non-rigid registration to match the prior with the patient, and it accounts for differences in the CT values by histogram matching. The registered prior is forward projected and its projections are used to smoothly inpaint the missing or corrupt data regions into the patient projections. Image reconstruction of the obtained projection data results in the corrected image. PBAC is evaluated using several data sets measured with a clinical spiral cone-beam CT device (Somatom Definition Flash, Siemens Healthcare, Forchheim, Germany).

RESULTS

Compared to the uncorrected CT images PBAC reduces the artifacts by 79% in case of metal pedicle screws in a thorax scan, by 99% for a hip patient with 12.2 cm truncation, and by 67% in case of a head scan with a limited scan angle of 150° . In all cases PBAC significantly outperforms the conventional correction methods which achieve artifact reduction values of only 42%, 90%, and 5%, respectively.

CONCLUSION

PBAC is a highly effective method to correct for CT artifacts resulting from missing or corrupt data by making use of prior knowledge. It significantly increases the image quality and preserves the patient-specific anatomy to allow for reliable medical diagnosis.

CLINICAL RELEVANCE/APPLICATION

PBAC is relevant for clinical CT which often suffers from metal artifacts, and it is relevant for flat detector CT which additionally suffers from truncation or limited angle artifacts.

SSQ20-05 • Clinical Evaluation of Coronary Artery Image Quality with Second Generation Iterative Model Reconstruction

Ethan J Halpern MD (Presenter) ; **Eric L Gingold** PhD ; **Hugh White** MD ; **Katrina M Read** MS *

PURPOSE

Iterative Model Reconstruction (IMR), as implemented in the second generation Philips software for multislice CT, is a knowledge-based reconstruction with marked reduction in image noise. The purpose of this study was to evaluate image quality with the application of IMR to coronary CT angiography (cCTA).

METHOD AND MATERIALS

We evaluated 20 consecutive cCTA cases acquired with a 256-slice iCT scanner, following reconstruction with traditional filtered back projection (FBP), first generation iterative reconstruction (iDose) and second generation IMR (Philips Medical Systems; Cleveland, OH). Each case was reconstructed in a diastolic phase (75% of the R-R interval) and evaluated by two independent reviewers. The mean and standard deviation (sd) of pixel values were computed in a standardized region of interest in the left ventricle and left main coronary artery. Subjective rating scores were obtained from each reviewer (1-5 scale for poor-excellent) for definition of 1) contours of small coronary arteries (

RESULTS

There was no significant difference in mean pixel intensity among FBP, iDose and IMR ($p > 0.8$). However, image noise within a contrast-enhanced region of interest in the left ventricle was reduced by a factor of 1.5 from FBP to iDose ($sd=123$ vs $80, p_{3.2} > 2.1$ ($p_{3.3} > 2.2$ ($p_{2.8} > 1.7$ ($p_{3.8} > 2.6$ (p

CONCLUSION

Second generation IMR reduces intravascular noise on cCTA by 86% compared with FBP, allowing better definition of smaller coronary arteries, better discrimination of coronary calcification, better definition of non-calcified plaque, and improved overall diagnostic confidence in the presence or absence of coronary stenosis.

CLINICAL RELEVANCE/APPLICATION

IMR provides images with decreased noise and improved definition of fine anatomical details in the coronary circulation without requiring additional radiation exposure.

SSQ20-06 • Iterative Metal Artifact Reduction in Computed Tomography

Andreas Krauss PhD (Presenter) * ; **Rainer Raupach** PhD * ; **Bernhard Schmidt** PhD * ; **Thomas G Flohr** PhD *

PURPOSE

To quantitatively evaluate the performance of a novel algorithm for metal artifact reduction in computed tomography (CT).

METHOD AND MATERIALS

The proposed iterative metal artifact reduction algorithm starts with standard CT reconstruction. Metal pixels are then identified through HU thresholding and a metal sinogram is generated by forward projection. A prior image is calculated from the initial image by assigning soft tissue pixels (identified by upper and lower HU thresholds) to 0 HU. Then normalized sinogram interpolation is performed: The prior image is forward projected and the original rawdata is normalized pixelwise with the prior sinogram. In the normalized sinogram, pixels within the metal trace are replaced by linear interpolation from the edges of the metal trace. The interpolated sinogram is de-normalized and standard reconstruction of the corrected sinogram is performed. The procedure is repeated iteratively with the output of the previous iteration used as input for prior image calculation. Finally, a frequency split is performed to preserve valid edge information of the non-corrected images: The high frequency part of non-corrected images is merged with the low frequency part of MAR-corrected images. The algorithm was applied to 10 hip replacement cases.

RESULTS

Streak artifacts from hip prostheses as well as the typical dark band between bilateral hip prostheses were almost completely eliminated. Pelvic soft tissue and organ structure was restored. Typical drawbacks of previous MAR algorithms such as introduction of new artifacts or compromised bone structure close to the prostheses were minimal due to iterative normalized interpolation and frequency split, respectively. Between bilateral hip prostheses, mean HU values within regions of interest located inside the bladder (expected to be water, i.e. 0 HU) were improved from -440 HU to -7 HU on average; the maximum improvement was from (-732 ± 252) HU to (-7 ± 38) HU.

CONCLUSION

The proposed algorithm substantially reduces artifacts from hip prostheses.

CLINICAL RELEVANCE/APPLICATION

The proposed algorithm strongly facilitates the visualization of pelvic anatomy. Due to the recovery of HU values, improvements for radiotherapy treatment planning are expected.

SSQ20-07 • Optimization-based Image Reconstruction with Variable Resolution in Diagnostic CT

Zheng Zhang MA, BS (Presenter) ; **Junguo Bian** PhD ; **Xiao Han** MSc ; **Daxin Shi** PhD * ; **Alexander Zamyatin** PhD * ; **Emil Y Sidky** PhD ; **Xiaochuan Pan** PhD *

PURPOSE

In diagnostic computed tomography (CT) imaging, it is often of interest to obtain detailed information within a region of interest (ROI), while rough knowledge outside the ROI may be sufficient. This novel imaging approach leads to an image reconstruction problem that requires voxels of different sizes within and outside the ROI. In this work, we develop and investigate an optimization-based algorithm to reconstruct images with variable spatial resolution, that is, images with non-uniform voxel sizes.

METHOD AND MATERIALS

We used a Toshiba 320-slice diagnostic CT scanner to collect data from a patient and a swine using a circular geometry. Both data sets were acquired at 1200 views over 2?. We performed image reconstruction by using a modified adaptive-steepest-descent-projection-onto-convex-sets (ASD-POCS) algorithm, which is specifically adapted to accommodate image arrays with variable resolution. Using this modified algorithm, we performed reconstruction on a variable-resolution array, which consists of voxels of size 0.06 cm within a selected ROI, and voxels of size 0.12 cm outside the ROI. We then carried out additional reconstructions by further increasing the voxel size outside the ROI to 0.24 and 0.48 cm. As references, we also applied ASD-POCS algorithm to reconstructing images on uniform-resolution arrays, consisting of voxels of sizes ranging from 0.06 cm to 0.48 cm.

RESULTS

By visual comparison, we observed that in the variable-resolution images, as the ratio of voxel size outside the ROI to that within the ROI increased from 1 to 8, although the region outside the ROI becomes progressively coarser, the image quality within the ROI remains virtually identical to that of the reference image reconstructed with uniform voxels of size 0.06 cm.

CONCLUSION

The results demonstrate that by employing an optimization-based algorithm tailored to variable-resolution images, we are able to reconstruct images within ROI of quality comparable to that obtained with uniform, high-resolution arrays.

CLINICAL RELEVANCE/APPLICATION

Variable-resolution optimization-based reconstruction can reduce computation time and memory consumption. It may also have potential impact on ROI images reconstructed from data containing truncation.

SSQ20-08 • Mitigation of Windmill Artifacts at Large Cone Angles

Hye Sun Na (Presenter) * ; **Akira Hagiwara** * ; **Brian E Nett** PhD *

PURPOSE

To assess windmill artifact mitigation performance for a new reconstruction algorithm at large cone angles

METHOD AND MATERIALS

Windmill artifacts are caused by insufficient sampling in the z-direction and objects with high z-gradient. In this work, a new reconstruction algorithm is evaluated for correction of windmill artifacts which occur at large cone angles in axial scans. A phantom was simulated with wires at a slope of 4:1, axial to transaxial, to assess the severity of windmill artifacts and to measure z-axis spatial resolution before and after the correction is applied. The images were reconstructed with a pixel size of 0.375mm.

RESULTS

A windmill artifact metric was developed, which is the sum of the image after applying a mask and a Sobel edge filter. The mask was created by applying two dilations from the ground truth image. A 20x20 pixel matrix was used as the structuring element for the first dilation to mask out the wire and a 140x140 pixel matrix was used for the second dilation to mask out regions beyond where the artifacts are generated around the wire. In this manner, images with severe windmill artifacts will receive a higher value for this metric. In the FDK images the level of artifact increases as the cone angle increases; the ratio of the mean artifact metric values for central ($\pm 1.5^\circ$) to outer cone angles ($\pm 3.1-6^\circ$) is 0.23. In the improved recon the artifact level in the outer cone angles is lower than the artifact level in the central cone angles of the FDK images. The ratio of the mean artifact metric for outer cone angles [improved/FDK] is 0.18. Additionally, the improved recon reduces artifacts in the central cone angle case. The ratio of the mean artifact metric [improved/FDK] is 0.15. The z-resolution was measured at the same locations. With the new recon the mean MTF50% and MTF10% is 100% and 99% of the FDK recon and varies from 96.2%-105.0% and 97.9%-102.7%, respectively.

CONCLUSION

At large cone angles, a new reconstruction algorithm reduces windmill artifacts without significantly degrading z-resolution.

CLINICAL RELEVANCE/APPLICATION

A new reconstruction algorithm, which reduces windmill artifacts in clinical head CT scans at large cone angles, is an enabling technology for single axial scans which cover all neuro anatomy.

SSQ20-09 • Performance Evaluation of a New Analytic Reconstruction Algorithm for Axial CT with Large Cone-angle Coverage

Zhuhua Qi PhD (Presenter) ; **Brian E Nett** PhD *

PURPOSE

There are a number of emerging clinical applications for computed tomography from systems which collect axial scan data with a large cone angle. The clinical use of these systems, faces challenges from cone beam artifacts caused by: data insufficiency, data mishandling and data truncation associated with an axial cone beam CT scan. This study aims to evaluate the performance of a newly developed analytical algorithm, referred to here as the improved algorithm, with a focus on cone beam artifact evaluation, for axial cone beam CT in cardiac imaging.

METHOD AND MATERIALS

Numerical simulations of an anthropomorphic phantom (i.e XCAT) were performed with a total coverage of 14.6 deg. Images were reconstructed by both the traditional FDK algorithm and the improved algorithm for both full-scan and cardiac modes. Then three types of tissue: cardiac muscle, soft tissue, and lung, were segmented and separately analyzed for the effect of cone beam artifacts. The severity of cone beam artifacts for a certain type of tissue in different slices is evaluated using the metric of mean CT# deviation from the ground truth.

RESULTS

For both full-scan and cardiac acquisitions, the mean CT# deviation in the images reconstructed with the improved algorithm remains significantly lower than the FDK type algorithm for all slices and all tissues. For a full-scan acquisition the images reconstructed with the improved algorithm, compared with the FDK reconstruction, show a reduction of the mean CT# deviation of $52\% \pm 16\%$, $39\% \pm 21\%$, and $53\% \pm 19\%$, for cardiac muscles, soft tissues, and lungs, respectively, over the studied cone angle coverage. For a cardiac acquisition, the reductions of the mean CT# deviation from FDK to WC reconstructed images for the three tissue types are $79\% \pm 24\%$, $77\% \pm 20\%$, and $79\% \pm 17\%$, respectively.

CONCLUSION

Compared to the traditional FDK-type algorithm, the newly developed Wide-Cone algorithm substantially reduces the cone-beam artifacts without degrading the other image quality aspects.

CLINICAL RELEVANCE/APPLICATION

A new analytic reconstruction algorithm for large cone-angles can enable quantitative imaging of whole organs such as the heart.

Physics - Thursday Posters and Exhibits (12:15pm - 12:45pm) Thursday, 12:15 PM - 12:45 PM • Lakeside Learning Center

[Back to Top](#) [PH] **LL-PHS-THA** • AMA PRA Category 1 Credit™: 0.5 Host **Alexander Zamyatin**, PhD *

LL-PHE-TH10A • Initial Experience with SilentMR - Feasibility Study

Sedat Alibek MD (Presenter) *; **Siegfried A Schwab MD**; **Michael Burke PhD ***; **Birgit Anders ***; **Hubertus Gloger MD**

Background

High noise/sound levels of gradients during MRI scans are the worst feature of this technique of which patients complain most. A new scanning technique called SilentMR reduces noise levels at the gradient level without reducing the power of gradients used during scan.

Evaluation

SilentMR (GE Healthcare, Milwaukee/WI) was performed in 32 patients referred to brain MRI with 12 channel head coil on a 3T system (Discovery 750w, GE Healthcare). Ethical committee waiver as well as written informed consent from each patient was obtained. Patients completed written survey regarding previous experience with subjective level of sound during MRI on a 6-point scale (0=no noise, 5=extreme sound/not bearable) before the exam. SilentMR (T1w, T2w or PDw 3D-Sequence) was performed in sagittal plane, 1 mm slice thickness, 256x256 matrix, field of view 25,6x25,6 cm. Patients completed another survey regarding subjective experience of SilentMR noise level after exam and were asked to report acceptance for this new sequence. Statistical analysis of differences in subjective noise level scores was performed with a two paired t-test to calculate significance level. Scan time was recorded as well as technical difficulties occurring during scanning process to measure technical success. Diagnostic image quality was evaluated by a radiologist with experience >10 years qualitatively on a 2-point scale (0=not diagnostic, 1=diagnostic with some constrictions, 2=diagnostic without constrictions). In 9% of scans online reconstruction of images was delayed due to technical reasons. Image quality of 6% of scans was rated as diagnostic with some constrictions (e.g. increased background noise, limited SNR), 94% as diagnostic without limitations. Patients' feedback of mean noise level score was 1,15 for SilentMR vs. 3,25 for conventional scans (P

Discussion

SilentMR was technically successful, delivering diagnostic image quality, significantly reduced subjective sound levels leading to 100% patient acceptance.

CONCLUSION

SilentMR could lead to a more comfortable scan environment for patients

LL-PHS-TH1A • Optimization of Contrast-enhanced Spectral Mammography (CESM) Depending on Clinical Indications

Clarisse Dromain MD (Presenter); **Sylvie Saab-Puong ***; **Ann-Katherine Carton ***; **Serge L Muller PhD ***; **Corinne Balleyguier MD**; **Eva M Fallenberg MD ***

PURPOSE

To optimize low (LE) and high-energy (HE) exposure parameters of CESM examinations in 4 different clinical applications: staging of extent of disease, problem solving, screening and CESM-guided biopsy for which different levels of average glandular dose and different ratios between LE and total doses are required

METHOD AND MATERIALS

The optimization was performed on a Senographe DS with CESM SenoBright (GE Healthcare). Simulations were performed for each of the 4 clinical indications to find the optima for the acquisition parameters by maximizing the signal-difference to noise ratio (SDNR) on the recombined CESM image using different targeted doses and LE image quality. The linearity between iodine concentration and SDNR as well as minimal detectable iodine concentration were assessed for each set of optimized parameters and compared with SenoBright. The image quality of the LE was assessed on the CDMAM contrast-detail phantom and compared with EUREF guideline limits.

RESULTS

CONCLUSION

Optimization of low and high energy exposure parameters according to different clinical indications allows increased contrast uptake detectability compared to parameters currently used in clinical routine CESM examinations, without significant loss in low energy image quality.

CLINICAL RELEVANCE/APPLICATION

Optimization of CESM exposure parameters depending on the clinical indication has the potential to improve the diagnostic performance of CESM examination in clinical routine

LL-PHS-TH2A • Improved K-edge Imaging in Spectral Mammography with a Photon Counting Detector for Dose Reduction

Yu-Na Choi (Presenter); **Seungwan Lee**; **Hee-Joung Kim PhD**

PURPOSE

Conventional K-edge imaging with a specific energy window can improve the contrast-to-noise ratio (CNR) compared to the charge integrating mode with a full energy range. However, the detected X-ray photons with low energy below the K-edge absorption energy of the material are not used in K-edge imaging. X-ray photons at low energies contribute to the absorbed radiation dose for the target object. To resolve the above limitation, this study proposed an improved K-edge imaging method for spectral mammography.

METHOD AND MATERIALS

Improved K-edge imaging method uses various additional filters with different thicknesses for reducing the number of X-ray photons at low energy range. To perform the improved K-edge imaging for gadolinium, copper (Cu) filters with thicknesses of 0.25, 0.5, 0.75, 1.0, 1.25, 1.5, and 1.75 mm were used. In cases of improved K-edge imaging for iodine, Al filters with thicknesses of 4.0, 6.0, 8.0, 10.0, and 12.0 mm were used. To prevent an increase of statistical noise as the thickness of the additional filter increases, we adjusted the number of X-ray photons passed through each filter. We used PCXD (model: PID-350, Ajat Oy Ltd., Finland), which had an active area of 44.8 mm * 44.8 mm with a pixel pitch of 0.35 mm * 0.35 mm for small animal imaging. To evaluate the improvements in K-edge imaging, CNR, absorbed radiation dose, and the figure of merit (FOM) were used.

RESULTS

We achieved up to 75.60 and 31.88% reductions of the absorbed radiation dose for gadolinium and iodine, respectively, while maintaining image quality. The FOM values from improved K-edge imaging are increased by factors of 2.34-3.39 compared to the charge integrating method.

CONCLUSION

We have shown that the absorbed radiation dose of our improved K-edge imaging method was substantially reduced compared to the charge integrating mode and conventional K-edge imaging, while maintaining the image quality of conventional K-edge imaging.

CLINICAL RELEVANCE/APPLICATION

Our results can be used for spectral mammography. We designed breast phantoms with four different thicknesses of 10, 20, 30, and 40 mm, which included two contrast media: gadolinium and iodine.

LL-PHS-TH3A • Dynamic Digital Subtraction Angiography-An Innovative Method for Overcoming Patient Movement Artifacts

Reuven Shreiber MD (Presenter) * ; Guy Engelhard PhD * ; Roni Shreter MD

CONCLUSION

A novel method that can reduce motion artifact during DSA studies is presented. Initial results appear to improve DSA reading in cases of patient motion.

Background

Digital Subtraction Angiography (DSA) is a two-step technique, whereby an acquisition of a 'mask' image is followed by the production of a series of images using rapid injections of contrast material. Each of the contrast images are then post-processed by subtracting the mask image from the contrast image, yielding images that ideally display the contrast material only.

However, during the time elapsed between mask image acquisition and native image production patient movement may occur due to a number of reasons such as the injection of iodine. To compensate for the undesired motion, registration algorithms and other post-processing methods are used.

A novel Dynamic DSA (DDSA) method is described, with initial results suggesting automatic compensation for patient movements, thus eliminating the need for a mask image.

Evaluation

In the DDSA procedure, images are created by obtaining the difference between each image and its successive one. A threshold operation may be utilized or the absolute value instead.

A new series of images is reconstructed by creating a Time MIP (TMIP) study that extracts the maximum value from several (2 or more) difference images for each pixel and creates a new series of TMIP images.

Several TMIP series can be created with varying numbers of difference images.

The TMIP series can be displayed in a cine mode or viewed individually.

Discussion

An innovative DDSA method is presented that allows an almost 'on-line' view of DSA studies even when a patient has moved during the study. Several studies were tried with good results, where the bones were canceled compared with the original DSA images. The subtraction algorithm is currently being improved; however the overall outcome is promising, indicating that the study can be used for diagnosis even in cases of massive motion.

An additional benefit is the reduction in radiation exposure to the patients as a mask image is not needed.

LL-PHS-TH4A • Classification of HiSS-Imaged Breast Lesions Using DISPersion vs. Absorption (DISPA) Plots to Quantify Water Resonance Distortions

William Weiss BS (Presenter) ; Milica Medved PhD ; Gregory S Karczmar PhD * ; Maryellen L Giger PhD *

PURPOSE

Water resonance lineshape characteristics acquired using high spectral and spatial resolution (HiSS) MRI have been shown to discriminate between benign and malignant breast lesions. Here, we present a novel approach to the analysis of water resonance lineshape by comparing dispersion vs. absorption components (DISPA) plots of spectra obtained from HiSS datasets to those of an ideal Lorentzian lineshape, in an attempt to characterize overall spectral shape differences between malignant and benign breast lesions.

METHOD AND MATERIALS

HiSS MR images were collected under an IRB-approved protocol. Following image and spectral reconstruction, water resonance spectra are obtained in each small voxel and normalized to their peak amplitude. A phase correction is applied by maximizing the integral of the real part of each complex water resonance. A 2D DISPA plot is created by plotting the real vs. the imaginary spectrum. These plots are compared to that of a perfectly phased Lorentzian peak - a circle with diameter 1, intersecting the origin and symmetric about the x-axis. The difference between the DISPA plots and the ideal Lorentzian is defined as the square-root of the sum of squared distances from each spectral point to the Lorentzian circle. This difference metric is calculated for every voxel in each lesion. We examine the voxels exhibiting the top 10% of differences in each lesion, but including no less than 10 and no more than 50 voxels.

Using ROC analysis, the DISPA differences in each voxel, as well as the mean and variance of those in each lesion, were evaluated using the clinical biopsied diagnosis (15 malignant; 8 benign lesions) as truth, and the performances of these features were assessed using the area under the ROC curve (AUC) as the figure of merit.

RESULTS

In the task of distinguishing between malignant and benign lesions, ROC analysis of DISPA differences on all voxels, as well as on their mean and variance over entire lesions, yielded AUC values of 0.82 ± 0.02 , 0.77 ± 0.09 , and 0.86 ± 0.08 , respectively.

CONCLUSION

We present a new spectral-analysis technique to quantify distortions in the shape of the water resonance of voxels in breast lesions, yielding a predictor of malignancy.

CLINICAL RELEVANCE/APPLICATION

A novel HiSS MRI spectral-analysis approach reveals more general spectral distortions than Fourier component analysis and may improve the performance of CADx systems when classifying breast lesions.

LL-PHS-TH5A • Tumor Tracking Using Consecutive Deformable Registration in 4D Chest CT Images

Helen Hong PhD (Presenter) ; Hyun Hee Jo ; Young-Nam Kang

PURPOSE

To predict varying tumor location during free-breathing in radiotherapy treatment planning, we propose a tumor tracking method using consecutive deformable registration for all respiratory phase images in 4DCT.

METHOD AND MATERIALS

Chest 4DCT images acquired at respiratory interval of 25% and were composed of ten different phases. Each phase image has spatial resolution of 512×512 pixels \times 90~200 slices with voxel dimension of $0.98 \times 0.98 \times 3$ mm³. In first step, we estimate global and local motions of the lung. The global motion is estimated by calculating a respiration rate of each phase through the affine registration between end-inspiration(EI) and end-expiration(EE). The local motion is estimated by using Demon-based deformable

registration between neighbor phases from EI to EE. In second step, tumors between EE and EI are tracked by applying the estimated global and local motion vectors.

RESULTS

To evaluate the accuracy of proposed tumor tracking method, locations of tumor tracking in the different phase images were qualitatively assessed with a color-coded mapping. The result show that proposed tumor tracking method well predicts tumor locations between EI and EE regardless of respiration rate. To evaluate the efficiency of proposed registration procedure, normalized cross correlation(NCC) was measured between A(typical registration procedure) and B(proposed registration procedure). The NCC of right(or left) lung of B was $0.95 \pm 0.02(0.97 \pm 0.01)$ and it was similar to the NCC of A. The total processing time of B was decreased by 32%(36%) for right(or left) lung than that of A. These results show that the proposed method efficiently calculates global and local lung motions and reduces the processing time of whole respiratory phases.

CONCLUSION

Our tumor tracking using consecutive deformable registration can predict varying tumor location during free-breathing and reduce the processing time by simplifying the procedure of affine and deformable registrations for all respiratory images in chest 4DCT.

CLINICAL RELEVANCE/APPLICATION

Our tumor tracking method is useful to quantify tumor trajectory and irradiate the tumor while avoiding surrounding normal tissues in radiotherapy planning and irradiation delivery.

LL-PHS-TH6A • Development of a Method \diamond Double Total Variation (DTV) \diamond Intended to Improve the Reduction of Radiation Exposure and Quality of CT Images

Katsumi Tsujioka PhD (Presenter) ; **Hironori Otsubo** RT ; **Yasukata Takahashi** RT ; **Ayako Gonaka** ; **Rina Terauchi**

CONCLUSION

Using the DTV method we have successfully demonstrated that image noise can be reduced while maintaining the edge enhancement of the image compared to the TV method and IR of the DT device. The DTV method is effective in reducing image noise and controlling the edge enhancement. Furthermore a large reduction in radiation exposure is possible while maintaining diagnostic quality images. Since the DTV method is an independent image based image processing apparatus it can be used in a variety of clinical practice areas.

Background

The Total Variation (TV) method of successive approximation image processing performs well reducing image noise and with the reduction of radiation exposure. Furthermore we have developed a Double Total Variation (DTV) method, which performs an image subtraction of images before and after of the TV method. This we have found further reduces the image noise as well as improves the spatial resolution.

Evaluation

This experiment was performed using the image \diamond s digital data. The experiments herein were performed using a cylindrical water phantom and a low-contrast phantom ladder. Additionally, experiments were conducted using CT clinical images. The comparison of the TV method and the DTV method and the effects on exposure reduction while utilizing a changing tube current (mA) are shown herein. The effects of the TV method and the DTV method with respect to spatial resolution are also included herein.

Discussion

(1)Both the TV and DTV method demonstrated a reduction in image noise. (2)Using the TV method the edge enhancement of the image is reduced. (3)Using the DTV method did not affect the edge enhancement and maintained the visually high spatial resolution. (4)The DTV method was able to maintain the high spatial resolution because of the variations used to the signal and noise component separation factor and by controlling the number of approximations performed. (5)Image registration is unaffected by the DTV method.

LL-PHS-TH7A • Evaluation of Improved Cone-beam CT Image Quality by Optimization-based Reconstruction Algorithms

Xiao Han MSc (Presenter) ; **Erik A Pearson** BS, BEng ; **Junguo Bian** PhD ; **Emil Y Sidky** PhD ; **Charles A Pelizzari** PhD * ; **Xiaochuan Pan** PhD *

PURPOSE

Cone-beam CT (CBCT) has become an important tool for a wide range of clinical applications. Currently, considerable effort has been made toward improving CBCT image quality through enhancing performance of hardware components and optimizing data-acquisition conditions. However, the full potential of CBCT image-quality remains to be explored by advanced image-reconstruction techniques. In the work, we employed an optimization-based algorithm to experimentally characterize the reconstructed CBCT images of a quality-assurance phantom. We quantitatively evaluated technical-efficacy metrics such as spatial resolution and contrast resolution, and explored the image-quality potential by varying the algorithm parameter.

METHOD AND MATERIALS

We used the on-board imaging system to collect cone-beam data from a Catphan 504 phantom under the high-quality head protocol. The adaptive-steepest-descent-POCS (ASD-POCS) algorithm was tailored and applied to reconstructing images from acquired data, where an algorithm parameter accounting for data-model inconsistency was varied over a range. We then quantitatively characterized the spatial resolution and contrast resolution from the reconstructed images as functions of the parameter, and identified the range of parameter values that yielded the optimal image quality.

RESULTS

In ASD-POCS reconstructions, some inserts of 0.5% and 0.3% contrast can be discerned, and bar phantoms of up to 12 line pair per cm can be resolved. In comparison, inserts of contrast below 1.0% and bar phantoms above 9 line pair per cm are difficult to discern/resolve in reference FDK reconstructions.

CONCLUSION

The ASD-POCS reconstructions with appropriately chosen parameter appeared to yield images of higher spatial resolution and higher contrast resolution than the reference FDK reconstructions.

CLINICAL RELEVANCE/APPLICATION

The work has the implication of improved CBCT image quality, which may benefit a number of clinical applications requiring high spatial and/or contrast resolution.

LL-PHS-TH8A • To Explore the 6 Degree Registration Marker and Method for Patients with Esophageal Cancer after CBCT Scan

Jiancheng Li (Presenter)

LL-PHE-TH9A • T1 and T2 Relaxation and Relaxivity: What They Mean and How to Measure Them

Yaqi Shen PhD, MD ; **Frank L Goerner** PhD (Presenter) * ; **Christopher G Snyder** BS ; **Regina Moritz** ; **Val M Runge** MD *

PURPOSE/AIM

The most important metrics related to Gadolinium based MR contrast agents (GBCAs) and tissue enhancement are T1 and T2 relaxivities. This exhibit reviews the concepts and importance of T1 and T2 relaxation and relaxivities. This is followed by a demonstration and explanation of how to accurately measure them, providing as well a current comparison of the agents that are approved worldwide for clinical use.

CONTENT ORGANIZATION

- Review concepts of T1 and T2 relaxation and relaxivity.
- Demonstrate how to calculate T1 and T2 relaxation and relaxivity.
- Outline optimal MR protocols for T1 and T2 measurements at 1.5T and 3T
- Explain a practical method for obtaining clinically relevant T1 and T2 relaxation and relaxivity measurements.

SUMMARY

The objective of this exhibit is to improve the Radiologist's and Medical Physicist's understanding of the most important metrics related to GBCAs and how to accurately obtain those metrics.

Physics - Thursday Posters and Exhibits (12:45pm - 1:15pm) Thursday, 12:45 PM - 01:15 PM • Lakeside Learning Center

[Back to Top](#) **LL-PHS-THB** • AMA PRA Category 1 Credit™:0.5

LL-PHE-TH9B • A Multi-vendor, Multi-kV Evaluation of Material CT Numbers Using the ACR Phantom

Robert Cropp PhD (Presenter) ; **Yogesh Thakur** PhD ; **Petar Seslija** MSc, BEng

PURPOSE

An effective Quality Control program focuses on ensuring imaging equipment provides stable image quality over a wide range of clinical use. When monitored metrics fall outside an acceptable range, imaging equipment may be removed from clinical use for investigation. Tight tolerances may lead to unnecessary equipment downtime, while wide tolerances may lead to poor image quality and thus affect clinical decisions. Our regional QC program uses the ACR CT accreditation phantom to monitor the CT linearity for all scanners in our region. Most clinical scans are performed at 120 kV, which is the potential used in the ACR manual for defining acceptable material HU ranges. With efforts in dose reduction shifting from mA optimization to kV selection, patient size-based kV selection is gaining traction clinically. Therefore, our QC program expanded CT number monitoring to all available tube potentials. Our group noticed systematic differences in the solid water, air and bone values between GE and Siemens scanners, which had to be taken into account when defining new tolerance ranges. This presentation provides manufacturer and kV specific HU ranges for all 5 materials in module 1 of the ACR phantom.

METHODS

Module 1 of the ACR phantom contains solid water, acrylic, bone-equivalent, air and polyethylene material inserts. The phantom was scanned on 25 GE and 7 Siemens CT scanners at 80, 100, 120 and 140 kV, using an axial head protocol with 300 mAs, 22 cm DFOV and the largest available collimation. Measurements for each material were made using a 2 cm² circular ROI at the centre of each insert.

RESULTS

One complete round of test results on all 32 scanners was analyzed. For solid water, all Siemens values were between -5 and 5 HU, while for GE values over 5 HU were common. However, when re-scanning using the GE-supplied water phantom, only one of those scanners was found to be out of calibration (it was subsequently recalibrated). For air, GE scanners also tended to give higher values than Siemens ones: often over -970 HU. Values for acrylic and polyethylene were similar on Siemens and GE scanners, and increased with kV as expected. Values for bone decreased strongly with kV as expected, but were higher on GE than on Siemens scanners.

Based on these results, we then defined tolerance ranges for each material, to use in our QC program. For acrylic, polyethylene and bone, a separate range is defined for each kV. For solid water, air and bone, separate ranges are defined for GE and Siemens scanners, due to the systematic differences observed. On five scanners, values for either bone, air or both lay outside the defined ranges and were considered outliers. These scanners were investigated and recalibrated, but this did not change the results, suggesting these values are normal behavior on these units.

Since the new ranges were defined, 17 of the GE scanners and 6 of the Siemens scanners have undergone the next round of tests. The new measured CT numbers fall within the defined ranges, with some exceptions: firstly, 8 GE scanners have solid water values over 7 HU for at least one kV, but when re-scanning with the water phantom, only two of these were found to be out of calibration, and only at 80 kV. Secondly, the 5 scanners with outlier air and bone values continue to give those values consistently. An additional comparison has been made between CT numbers measured in the above scans, and those measured in a separate QC scan using a 120 kV helical abdomen protocol. With the abdomen protocol, bone values on GE scanners are significantly lower. Therefore care should be taken if using these tolerance ranges with body protocols.

CONCLUSION

CT number measurements using the ACR phantom have been compared over multiple scanners using a standardized scan protocol. Using these results, we have defined tolerance ranges for the five insert materials, taking into account the kV dependence of acrylic, polyethylene and bone, and some systematic differences between GE and Siemens scanners. These ranges are now used in our QC program to verify that each scanner's CT number calibration is acceptable over a wide range of HU values.

LL-PHS-TH1B • Development of Cascaded Systems Analyses for the Evaluation of Energy-resolving Photon-counting X-ray Detectors

Jesse Tanguay (Presenter) ; **Seungman Yun** ; **Ian A Cunningham** PhD *

PURPOSE

Advances in x-ray detector technology are leading to the development of energy-resolving photon-counting (EPC) detectors with the potential to determine the energy spectrum of interacting photons. These devices carry the promise of advanced spectroscopic procedures such as energy-resolved angiography to generate iodine-specific images from a single exposure without the need for a pre-injection mask image and thereby reduced motion artifacts. However, there are a number of challenges that must be overcome before the full benefits of EPC detectors can be achieved. The purpose of this study is to describe the extension of cascaded systems analysis (CSA), widely used for the description of image noise and detective quantum efficiency of conventional systems, to describe signal and noise in energy-resolving detectors.

METHOD AND MATERIALS

The CSA approach is used to describe mechanisms of energy deposition in the detector with the objective of predicting detector performance. It is shown this can be achieved by propagating the probability density function (PDF) of the number of secondary image quanta through each stage of a cascade of image-forming processes. This results in the PDF of the number of detected image quanta and incorporates the statistical properties of each process on the absorbed energy spectrum. This approach is used to include emission and reabsorption of characteristic and Compton scatter, conversion to secondary quanta, incomplete collection of secondary quanta, and additive electronic noise. The mean and variance in the number of detected photons in energy-bin data is calculated. Comparisons are made with Monte Carlo (MC) calculations.

RESULTS

The CSA approach agrees very well with MC calculations. In general, our analysis suggests that detectors with poor collection efficiencies and high additive noise will result in loss of photon counts from low-energy bins and escape of Compton scatter x rays will result in loss of photon counts from high-energy bins.

CONCLUSION

The CSA approach allows for an accurate understanding of the distribution of detected photon energies obtained with EPC detectors, critical for an evaluation of detector performance and the development of new detector designs.

CLINICAL RELEVANCE/APPLICATION

Models of signal and noise in energy-resolving photon-counting detectors are required for the development and evaluation of new

LL-PHS-TH2B • Assessing Needle Accuracy of Stereotactic Breast Biopsy Equipment

Zheng Shi PhD (Presenter)

CONCLUSION

A new phantom is proposed to replace the gelatin phantom for the needle accuracy test on stereotactic breast biopsy equipments. It gives a quantitative result that is a measurable distance between the needle tip and target instead of a visual estimation. The ACR 1 mm accuracy criterion can be assessed.

Background

The ACR stereotactic breast biopsy accreditation program requires a needle accuracy test by using a gelatin phantom. The sampling aperture must be within 1 mm of the simulated lesion. The large target is always 'grabbed' by a large size needle. The method is essentially a visual check that does not yield a quantitative result. The intrinsic system accuracy is virtually impossible to assess.

Evaluation

The new phantom is inelastic and made of styrofoam. An aluminum foil and a thin plastic film are sandwiched between two styrofoam blocks. To simulate a microcalcification target, a small hole of about 1 mm diameter is poked on the aluminum foil. A real needle without a vacuum system is used. The small hole on images is calculated for the position. After the needle aims at the target, the needle is pushed manually until the needle tip just touches the aluminum foil. The needle tip mark on the foil is simply compared with the pre-made hole location. The off target distance is measured using a loupe with a scale. In the past 5 years, author has using this method at multiple. In contrary to the gelatin phantom that resulted 'almost all pass'. The styrofoam phantom yields a 75% overall pass rate. For a single unit, some show consistent high pass rate. Other show consistent high fail rate. The needle tip off the target more than 1 mm usually indicates poor calibration, loose needle holder and guide.

Discussion

A successful result will require the needle tip just marking the foil without piercing a large hole. It can be achieved by control the push force, using a thicker plastic film so the tip will not go deeper, using a multimeter and displayed depth data to control the needle stop. Before the test, one must make sure that there is no excessive movement of the needle holder and guide.

LL-PHS-TH3B • An X-ray Phase Contrast Method Suitable for Clinical Translation

Alessandro Olivo (Presenter) ; **Marco Endrizzi** PhD ; **Spyros Gkoumas** PhD ; **Charlotte Hagen** ; **Magdalena Szafraniec** MSc ; **Paul C Diemoz** PhD ; **Peter Robert Thomas Munro** PhD ; **Julie Horrocks** PhD ; **Massimo Marenzana** PhD ; **Sarah J Vinnicombe** MRCP, FRCR ; **Louise Jones** MBBCh, PhD ; **Robert Speller** PhD *

CONCLUSION

Our system, built with commercially available components, provides significantly enhanced image quality and feature detection over conventional methods, at doses, exposure times and alignment requirements compatible with a clinical environment. We thus believe it can be translated into clinical practice quickly and with minimal engineering investment.

Background

Much effort has been devoted to the translation of X-ray Phase Contrast Imaging (XPCI) into clinical practice. Thus far, this has not been successful, as all proposed implementations (e.g. grating interferometry) require excessive delivered dose, excessive exposure times, alignment requirements on the nanometer scale, incompatible with a clinical setting.

Evaluation

We previously adapted the edge-illumination XPCI technique for use with conventional sources, through two x-ray masks placed either side of the sample. We have now modified the system to reduce the delivered dose without affecting phase sensitivity, by employing a narrower aperture in the pre-sample mask and a smaller displacement between masks. The pre-sample mask protects the sample from unwanted dose, whilst the smaller aperture size preserves phase sensitivity. We used the system to image breast tissue and cartilage specimens in vitro, showing significant enhancements over conventional absorption methods.

LL-PHS-TH4B • Performance Assessment of a New CT Detector with Minimal Electronic Noise for Low Dose Abdominal Perfusion Imaging

Ernst Klotz DiplPhys (Presenter) * ; **Ulrike Haberland** * ; **Bernhard Schmidt** PhD *

PURPOSE

80 kV are not routinely used for abdominal CT perfusion imaging with conventional detectors because non-linear effects occur when the electronic noise of the detector dominates the measured signal. We evaluated a new detector design (Stellar, Siemens Healthcare) with minimal electronic noise for this special application.

METHOD AND MATERIALS

Inserts with iodine concentrations of 0.5, 1.0 and 15 mg/ml were placed in a 30 and a 40 cm water phantom. Both phantoms were examined with 100 kV and 80 kV on two otherwise identical scanners equipped with a conventional and a Stellar detector (SOMATOM Definition Flash). Scans were performed using dynamic modes (scan duration 30 s). We varied mAs per time point from 15 to 300 (CTDIvol 0.3 to 12 mGy) and measured image noise and iodine contrast. As $\text{noise} \cdot \sqrt{\text{CTDI}}$ is constant for Poisson distributed photon noise at the same kV, we determined when this product started to increase as an indicator of the onset of relevant electronic noise. We also compared iodine contrast-to-noise ratios (CNR) between 100 kV and 80 kV in order to determine mAs settings of equal performance.

RESULTS

Noise was at least 14% lower for the Stellar detector at all kV and mAs settings. For the conventional detector at 80 kV electronic noise became dominant below 1.2 mGy for the 30 cm phantom and below 6 mGy for the 40 cm phantom with increasingly prominent visual artifacts if dose was further reduced. For the Stellar detector at 80 kV dose could be reduced to 0.3 mGy for 30 cm and to 2 mGy for 40 cm without electronic noise contamination and without any visual artifacts. Using 80 kV the same CNR and image quality of the clinical default setting of 100 kV were obtained at 60% (30 cm phantom) and at 65% (40 cm phantom) of the dose.

CONCLUSION

The Stellar detector allows the routine use of 80 kV for abdominal perfusion imaging. Depending on patient size this reduces the dose by 35% to 40% compared to the current standard of 100 kV at identical CNR and image quality.

CLINICAL RELEVANCE/APPLICATION

With the Stellar detector 80 kV can be safely used for routine abdominal perfusion imaging without any reduction in CNR or image quality at up to 40% lower dose values.

LL-PHS-TH5B • A Dynamic-programming Projection-domain Extrapolation Method for CT Wide-Cone Reconstruction

Paulo R Mendonca PhD (Presenter) * ; **Zhye Yin** * ; **Bruno De Man** PhD *

PURPOSE

In a circular cone-beam scan, voxels in regions at the edge of a volume (typically corresponding to the initial and final z positions) are not always in the path of the x-ray beams during the rotation of the x-ray source, and these gaps in projection data result in z-truncation artifacts during reconstruction. Such artifacts are often mitigated through projection-based extrapolation methods, a

critical step in reconstruction algorithms for wide-cone CT geometries. The most common of these extrapolation methods is the copying of the initial and final rows of projection data, or extrapolation by duplication.

METHOD AND MATERIALS

The limitations of extrapolation by duplication motivate the search for a method that considers the local smoothness of projection data. In the dynamic-programming extrapolation method, a set of transformations that maps sequences of nearby rows at either edge of the projection data is estimated through the minimization of spatial and intensity distortion between a transformed input row and a target row. This optimization problem is solved through dynamic programming, guaranteeing global optimality. Once the optimal mappings are estimated, extrapolation is carried out by applying the transformations to the edge rows of the data, thereby creating virtual rows that follow the trend of the data on immediately adjacent areas.

RESULTS

We applied the dynamic-programming extrapolation approach to simulated dynamic nCAT chest phantom data with wide-cone geometry and a cone angle of 14.6 degrees. Both pre-filtered and filtered views were processed to generate additional 6 rows at top and bottom edges of the projection data, for a total of 12 extrapolated rows. The augmented data were reconstructed using Advanced Wide-Cone Filtered Backprojection to improve the image quality of the edge slices.

CONCLUSION

We developed a projection-domain method for row-extrapolation technique based on estimating optimal extrapolation functions via dynamic programming. The method is effective to mitigate the truncation artifacts of CT reconstructions, particularly for wide-cone geometries, resulting in weaker truncation artifacts from highly attenuating anatomical features while maintaining CT values elsewhere.

CLINICAL RELEVANCE/APPLICATION

In CT geometry with cone angle as large as 14.6 degree, z-truncation artifacts become one of limiting factors to achieve full diagnostic image quality at edge slices.

LL-PHS-TH6B • Non-ECG-assisted High-pitch Dual Source MDCT Angiography of the Thoracoabdominal Aorta: How Does the Radiation Dose and Noise Compare to Standard-pitch MDCT in Different Size Patients?

Achille Mileto MD (Presenter) ; Rendon C Nelson MD * ; Lynne M Hurwitz MD * ; Juan Carlos Ramirez Giraldo PhD ; Kingshuk Roychoudhury ; Danielle Seaman MD ; Jared D Christensen MD ; Daniele Marin MD

PURPOSE

To investigate within the same patient the relationship between radiation dose and noise to patient body size in thoracoabdominal aortic CT angiography (CTA), using non-ECG-assisted high-pitch dual-source and standard-pitch acquisitions.

METHOD AND MATERIALS

This HIPAA-compliant retrospective study received IRB approval with a waiver of informed consent. Fifty consecutive patients (29 men, 21 women; mean age, 68 years \pm 13 standard deviation [SD]; mean body mass index [BMI], 29.9 kg/m² \pm 7) underwent clinically-indicated CTA of the thoracoabdominal aorta using a second-generation dual-source scanner. Standard-pitch (pitch=0.8) unenhanced acquisition was followed by a non-ECG-assisted high-pitch (pitch=1.6-3.0; mean, 2.8 \pm 0.2) dual-source contrast-enhanced acquisition. Radiation dose was calculated for each patient as CTDIvol and size-specific dose estimate (SSDE). Noise was measured as voxel SD from a region-of-interest in the subcutaneous fat of the thoracic and abdominal wall. The relationship between CTDIvol, SSDE, and noise as a function of BMI was assessed using linear regression models.

RESULTS

Mean CTDIvol and SSDE (\pm SD) were significantly lower with high-pitch compared to standard-pitch acquisition (8.2 \pm 1.0 vs 10.6 \pm 3.0 mGy and 9.0 \pm 1.5 vs 11.2 \pm 2.1 mGy, respectively [P

CONCLUSION

Non-ECG-assisted high-pitch dual-source acquisition for aortic CTA yields lower radiation dose, at the cost of higher noise in large patients.

CLINICAL RELEVANCE/APPLICATION

Radiologists should be aware of the higher noise using high-pitch settings in large patients, likely reflecting limitation of the scanner output.

LL-PHS-TH7B • A MR-compatible Laparoscope and Pneumatic Bone-drill for Real-time MR-guided Interventions and Orthopaedic Surgery

Felix V Guettler (Presenter) ; Kim Winterwerber ; Christian Seebauer ; Jens Rump ; Andreas Heinrich ; Ulf K Teichgraber MD

CONCLUSION

Real-time MR-image-guidance using an MR-compatible laparoscope or bone-drill is feasible. Professional manufacturing methods might allow better handling and performance of the introduced devices.

Background

The background of this proof-of-concept study is to demonstrate the feasibility of complex RT-MR-guided interventions and orthopedic surgery developing prototype MR-compatible surgical equipment applying to pre-clinical MR-guided methods i.e. bone biopsies or retrograde drilling of the talus.

Evaluation

Laparoscope: Ex-vivo phantoms (n=5) with lumbar vertebral segments were treated using interactive PDw TSE with a custom-made surgical coil (Philips Research, HH, Germany). MR- and corresponding endoscopic images were displayed on two in-room monitors. For the laparoscope and endoscopic subsystem an artifact size of 7mm/22mm (TSE/GE) respectively 4mm/12mm were measured from the device boundary to the fringe of the artefact. All probands (n=5) were able to completely extract marked disc tissue from the phantom. Bone drill: MR-compatibility and -artifacts were determined. X-ray images were acquired to examine radio-density. Torque, power, speed, weight, air consumption, operating pressure and noise level were measured and compared to a non-MR-compatible (Synthes Corp. Compact Air II) and a MR-compatible (Invivio/Daum Pi-Lectric) system. An ex-vivo experiment (n=10) was performed drilling the substantia compacta and placing a Kirschner wire. Furthermore autoclavability was tested. The bone-drill prototype is fully MR-compatible according to ASTM F2503 and is almost transparent to x-ray. The drill has a weight 0.8kg and a variable speed of 0-825rpm. The torque amounted a max. of 0.4Nm resulting in a power of 18W. The operating pressure is 6-7bar with an air consumption of ca. 250l/min. The noise level in operator position is 50dB(A). Autoclave of the drill at 134°C and 2bar proceeded without any impairment of the function.

Discussion

The development of a MR-compatible laparoscope and bone-drill might allow MR-guided methods using an additional intraoperative view of the inner organ with high soft-tissue contrast. Also an X-Ray transparent bone-drill might allow intraoperative CT-imaging.

LL-PHS-TH8B • Advanced Glycation End-Products: A Novel Therapeutic Target for Radiation Toxicity

Colin E Champ MD (Presenter)

Thursday Plenary Session Thursday, 01:30 PM • Arie Crown Theater [Back to top](#) [PH](#) [RO](#) [OI](#) [BQ](#) **PS50** • AMA PRA Category 1 Credit™: 1.25 • ARRT Category A+ Credit: 1.5 To receive credit, relinquish attendance voucher at end of session.

RSNA/AAPM Symposium

Moderator
Jeffrey H Siewerdsen, PhD *, Baltimore, MD
AAPM Liaison to the RSNA Scientific Program Committee

LEARNING OBJECTIVES

1) Learn how multi-modality imaging methods are being used in combination with high-precision radiation therapy delivery techniques to understand fundamental mechanisms of cancer pathogenesis, progression, and treatment response. 2) Learn the challenges and advances associated with quantitative imaging, and understand how more accurate and quantitative imaging is central to advancing the understanding of major questions in 21st century medicine. 3) Learn how imaging in partnership with medical physics and other technical and clinical disciplines provides a vital tool and multidisciplinary expertise for such advances.

Imaging in Partnership: With Radiation Therapy

David A Jaffray, PhD *, Toronto, ON, CANADA

LEARNING OBJECTIVES

View learning objectives under main course title.

Imaging in Partnership: With Physics and Quantitative Medicine

James A Deye, PhD, Bethesda, MD

LEARNING OBJECTIVES

View learning objectives under main course title.

Medical Physics 2.0: Information Management and Display Thursday, 04:30 PM - 06:00 PM • N229 [Back to Top](#) [PH](#) [IN](#)

RC721 • AMA PRA Category 1 Credit™:1.5 • ARRT Category A+ Credit:1.5 **Co-Director Ehsan Samei**, PhD *

Co-Director Douglas E Pfeiffer, MS *

RC721A • Information Management and Display Perspective

Ehsan Samei PhD (Presenter) *

LEARNING OBJECTIVES

1) To gain an appreciation for interaction between medical physics and information technology in modern medicine. 2) To understand how physics can add value to patient care in the area of information and image management and technology.

RC721B • Information Management and Display 1.0

Donald Peck PhD (Presenter)

LEARNING OBJECTIVES

1) Review the different areas of imaging informatics. 2) Understand the methodology for developing informatics standards and the role of physicists and radiologists in the process. 3) Review the current status of informatics standards 4) Review current technology for validating the function of these systems.

ABSTRACT

Imaging informatics is part of every radiology practice today. Imaging informatics covers everything from the ordering of a study, through the data acquisition and processing, display and archiving, reporting of findings and the billing for the services performed. The standardization of the processes used to manage the information and methodologies to integrate these standards is being developed and advanced continuously. These developments are done in an open forum and imaging organizations and professionals all have a part in the process. In this presentation the flow of information and the integration of the standards used in the processes will be reviewed. The role of radiologists and physicists in the process will be discussed. Current methods for validation of informatics systems function will also be discussed.

RC721C • Information Management and Display 2.0

Michael J Flynn PhD (Presenter)

LEARNING OBJECTIVES

1) Information management; a. Decision support for Radiology examination orders. b. Dose monitoring for radiographic, interventional, CT and Nuclear Medicine procedures. 2) Data storage and distribution; a. Enhanced DICOM objects. b. Vendor neutral archives for enterprise image storage. c. Web distribution protocols. 3) Study viewing and report generation; a. Color calibration and presentation management. b. Structured reports.

Uncertainties in Imaging for Radiation Oncology: Sources and Mitigation Techniques-Image Registration Thursday, 04:30 PM - 06:00 PM • S502AB [Back to Top](#) [PH](#) [RO](#) **RC722** • AMA PRA Category 1 Credit™:1.5 • ARRT Category A+ Credit:1.5

Co-Director, Moderator Kristy K Brock, PhD *

LEARNING OBJECTIVES 1) Describe methods to perform QA/QC of deformable registration. 2) Propose methods to account for uncertainties. 3) Highlight clinical integration.

RC722A • Uncertainties in Deformable Registration

Kristy K Brock PhD (Presenter) *

LEARNING OBJECTIVES

View learning objectives under main course title.

RC722B • Clinical Practice

Patrick Kupelian MD (Presenter) *

LEARNING OBJECTIVES

View learning objectives under main course title.

Minicourse: Recording and Reporting Radiation Dose: CT Thursday, 04:30 PM - 06:00 PM • E351 [Back to Top](#) [QA](#) [PH](#) [CT](#)

RC723 • AMA PRA Category 1 Credit™:1.5 • ARRT Category A+ Credit:1.5 **Director J. Anthony Seibert**, PhD

RC723A • Measurements and Indices in CT Dose

John M Boone PhD (Presenter) *

LEARNING OBJECTIVES

1) The audience will be able to identify and discuss the standard parameters used for reporting dose in computed tomography, including the volume CTDI, DLP, and effective dose using the k-coefficients. 2) The audience will be able to identify and discuss parameters which influence the radiation dose to the patient, including patient size, dose modulation protocols, and scan length. 3) Participants will be able to identify the limitations of using effective dose in describing radiation dose levels to individual patients.

ABSTRACT

Computed tomography has experienced rapid growth in utilization over the past 10 years, due in part to the dramatic increase in image quality and decrease in scan time that helical and multi-slice CT scanners have allowed. This increased utilization has raised legitimate concerns about the radiation dose levels in CT. Traditional dose metrics such as the volume computed tomography index (CTDI_{vol}) and the dose length product (DLP) will be discussed. The limitations of these metrics in the context of individual patient dosimetry will also be explained. In recent years, a number of new CT dose concepts have been introduced in the peer-reviewed literature, in task group reports, and in other documents. A number of these new dose metrics will be discussed, including the rise-to-equilibrium-dose, H(L), and the site-specific dose estimate (SSDE). CT dosimetry has historically been performed using integrating ion chambers. In light of the dynamic scanning capabilities of modern CT scanners, the utility of a real-time radiation meter will be discussed. Real-time dose meters can substantially reduce the time required by the physicist in the CT scanner suite, while increasing the quantity and quality of the dose information that is measured. Niche applications include the rapid assessment of beam quality (half value layer) and the characterization of the beam shaping filters used in CT. In summary, this presentation will discuss existing CT dose parameters, and will then review a number of proposed new CT dose parameters which will likely be useful for CT dose assessment in the future. The recent growth of CT technology has outgrown the simple dose metrics of the past, and there is a need for the CT community to embrace new and more accurate CT dose metrics.

RC723B • Estimating Patient Dose

Dianna D Cody PhD (Presenter) *

LEARNING OBJECTIVES

1) Recognize the limitations of current approaches to estimate CT patient dose. 2) Understand several methods available for estimating CT patient dose. 3) Understand potential future options for patient CT dose estimations.

RC723C • Initial Experience with California Law on Reporting Dose from CT

J. Anthony Seibert PhD (Presenter)

LEARNING OBJECTIVES

1) Describe the provisions of the California State law on dose reporting for computed tomography (CT) scanners. 2) Demonstrate ways in which the required elements volume Computed Tomography Dose Index (CTDI_{vol}) and Dose Length Product (DLP) can be placed into the radiology report. 3) Discuss discrepancies regarding the relationship between CTDI_{vol} and patient dose, and issues in accumulating dose indices for CT scans in a multi-series exam and for individual exams over time. 4) Report on the status of compliance with the statutes of the law.

ABSTRACT

Radiation over-exposure for computed tomography (CT) perfusion studies occurring in the 2008-2009 timeframe resulted in California Senate Bill 1237, legislation that was authored by Senator Padilla in response to these incidents. The legislation was signed by the Governor in September 2010. The law contains three parts: (1) Recording CT dose indices for each patient, placing these values in the radiology report, and verifying accuracy of the volume Computed Tomography Dose Index (CTDI_{vol}); (2) Requiring accreditation for all CT scanners performing diagnostic exams that are under the authority of the California Department of Public Health; (3) Reporting of radiation exposures that exceed specified limits to organs, cause unanticipated erythema or hair loss, or inappropriate irradiation to body parts not ordered by a physician. Part 1 of the law commenced on July 1, 2012, and the other two parts are to commence on July 1, 2013. This presentation describes the steps taken to comply specifically with Part 1 of the law. To ensure compliance, an automated extraction and delivery of the CTDI_{vol} and DLP indices to the radiology report were implemented. However, the legislation does not provide guidance on how to: (1) adjust CTDI_{vol} for patient size; (2) deal with CT exams having multiple different series, each with individual dose indices; (3) sum CTDI_{vol} and DLP for the same or different body areas scanned (if appropriate). The consequence is variable reporting at the initial implementation of the law, which requires standardized reporting metrics. Recommendations by the University of California Dose Optimization and Standardization Endeavor (UC DOSE) is discussed in this context, with relevant solutions described and specific examples demonstrated. To conclude, an update from the users perspective of compliance, as well as reporting of the status from the State of California Department of Public Health office is provided.

Quantitative Imaging: Informatics Thursday, 04:30 PM - 06:00 PM • E352 [Back to Top](#) [PH](#) [IN](#) [BQ](#) **RC725** • AMA PRA Category 1 Credit™: 1.5 • ARRT Category A+ Credit: 1.5 **Director Michael F McNitt-Gray**, PhD *

RC725A • The Role of Informatics in Quantitative Imaging

Katherine P Andriole PhD (Presenter)

LEARNING OBJECTIVES

1) Understand the role of informatics in quantitative imaging. 2) Be able to identify existing limitations in information technologies with respect to quantitative imaging, and conversely see how informatics may assist in filling some of the current gaps in quantitative imaging methods. 3) Become familiar with on-going efforts to address current challenges facing research into and clinical implementation of quantitative imaging applications.

ABSTRACT

Quantitative imaging is increasingly becoming an essential part of biomedical research as well as being incorporated into clinical diagnostic activities. Referring clinicians are asking for more objective information to be gleaned from the imaging tests that they order so that they may make the best clinical management decisions for their patients. Medical Physicists, Researchers, Imaging Scientists, and others may be called upon to identify existing issues as well as develop, validate and implement new approaches and technologies to help move the field further toward quantitative imaging methods. Biomedical imaging informatics tools and techniques such as standards, integration, data mining, cloud computing and new systems architectures, ontologies and lexicons, data visualization and navigation tools, and business analytics applications can be used to overcome some of the existing limitations. The RSNA's Quantitative Imaging Biomarkers Alliance (QIBA) is an initiative with international participation from medical physicists, clinicians, researchers, industry scientists, and government officials all interested in optimizing the potential of quantitative imaging. A major QIBA informatics activity, the imaging data warehouse is in progress. Current status and future plans will be described.

RC725B • Standards for Quantitative Imaging

David A Clunie MBBS (Presenter) *

LEARNING OBJECTIVES

1) Identify the importance of quantitative imaging principles in the setting of clinical trials. 2) Identify the role of standards, including DICOM and others, in the successful application of quantitative imaging principles. 3) Analyze quantitative imaging techniques and apply this knowledge to protocol development in the setting of clinical trials.

RC725C • Clinical and Research Needs for Quantitative Imaging Informatics Tools

Bradley J Erickson MD, PhD (Presenter) *

LEARNING OBJECTIVES

1) Become familiar with the quantitative imaging tools that are available for clinical and research uses. 2) Become familiar with the clinical and research problems that are being addressed by quantitative imaging. 3) Become familiar with the clinical and research problems that might be addressed by quantitative imaging in the near future and how to prepare one's practice for these uses.

ABSTRACT

Quantitative imaging is more than just the measurement of structures in images. It is a new way of approaching diagnosis and therapy assessment. While simple linear measurements might qualify as quantitative imaging, it is important to think of QI in a much broader context. In addition to measuring spatial quantities like length, area, and volume, one can measure image values on functional imaging, which might represent a physiologic value. One can measure textures and edge properties, potentially replacing the *it just looks like it* answer to why an expert can diagnose a certain disease. Measuring change can also be more than just spatial. Spatial change detection is important, of course, and doing it well is a critical component of QI. Measuring change in non-spatial properties is likely to become more important in the future. Finally, while some might believe that genomics will largely replace imaging, there is currently much interest in the use of imaging to provide pervasive and non-destructive prediction of genomic, proteomic, and metabolomic properties that are likely to be of great value to patient care.

Medical Physics 2.0: Magnetic Resonance Imaging Friday, 08:30 AM - 10:00 AM • S405AB [Back to Top](#) [PH](#) [MR](#) **RC821** • AMA PRA Category 1 Credit™:1.5 • ARRT Category A+ Credit:1.5 **Co-Director Ehsan Samei, PhD ***

Co-Director Douglas E Pfeiffer, MS *
RC821A • Magnetic Resonance Imaging Perspective

Douglas E Pfeiffer MS (Presenter) *

LEARNING OBJECTIVES

1) Understand the history and development of magnetic resonance imaging equipment. 2) Understand the impact of equipment development on testing protocols. 3) Understand the requirements for medical physics support in image quality and safety.

ABSTRACT

Magnetic resonance imaging equipment has developed significantly since its inception. Field strength increases and technology development increase the complexity of the equipment and the need for medical physics and MRI scientist support. This talk will briefly introduce the developments that have taken place and discuss the impact that this development has had on testing and support.

RC821B • Magnetic Resonance Imaging 1.0

Ronald R Price PhD (Presenter)

LEARNING OBJECTIVES

1) Review the image quality metrics that are currently used as part of an MRI system performance report. 2) Discuss how the medical physicist can assist in the development and evaluation of imaging sequences used as part of clinical protocols. 3) To review items that should be included as part of an MRI safety survey. 4) Discuss the steps necessary for establishing and maintaining a routine quality assurance program. 5) Review aspects of AAPM Report No. 100 regarding acceptance testing of new MRI systems. 6) Review modality and system specific requirements for MRI accreditation.

ABSTRACT

MRI 1.0: Magnetic Resonance Imaging Ronald R. Price The purpose of this presentation is to review the current role of the medical physicist in clinical Magnetic Resonance Imaging (MRI). The discussion will first discuss MRI acceptance testing with reference to the recommendations of AAPM Report No. 100 and will specifically include items that should be part of both the initial and annual MRI safety survey. This discussion will be followed by a review or the image quality metrics that are currently used as part of an MRI system performance report as well as how the medical physicist may go about assisting in the development and evaluation of imaging sequences used as part of clinical protocols. The presentation will also discuss the steps necessary for establishing and maintaining a routine quality assurance program with emphasis on the necessity of establishing a strong working relationship with the MRI quality assurance technologist. There will also be a review of the system specific requirements for MRI accreditation.

RC821C • Magnetic Resonance Imaging 2.0

David R Pickens PhD (Presenter) *

LEARNING OBJECTIVES

1) Identify requirements for ongoing quality assurance of ultra-high field MRI systems and hybrid MR/PET systems. 2) Identify the need for new quality assurance tools and testing procedures for advanced systems with many parallel imaging channels. 3) Identify site safety issues for ultra-high field and hybrid MR systems and expanded concerns for patient and staff safety. 4) Understand increased requirements from oversight and accreditation organizations. 5) Identify the need for improved continuing education for medical physicists/MRI scientists.

ABSTRACT

This talk will look into the future of clinical MR imaging and the role of the physicist as the technology of MR imaging evolves. Many of the quality assurance techniques used today will need to be extended to address the advent of higher field imaging systems and dedicated imagers for specialty applications. Included will be the need to address quality assurance and testing for hybrid devices such as MR/PET systems. Many new coil systems will be routinely provided in systems with large numbers of parallel receive channels along with parallel transmit channels. New pulse sequences and acquisition methods, increasing use of MR spectroscopy, and real-time guidance procedures will place the burden on the medical physicist to develop and use new phantoms and test procedures to evaluate clinical imagers. Many of these systems will have different potential side effects including potential problems associated with patient and staff safety. New software tools will be available for testing, but these must be understood by the physicist in order that they be used correctly for quality assurance purposes. Finally, new rules, requirements, and regulations undoubtedly will mean that the medical physicist must work closely with staff technologists to keep her/his sites compliant with the latest requirements and must actively keep abreast of these developments.

Minicourse: Recording and Reporting Radiation Dose: Nuclear Medicine Friday, 08:30 AM - 10:00 AM • S403B [Back to Top](#)

[QA](#) [PH](#) [NM](#) **RC823** • AMA PRA Category 1 Credit™:1.5 • ARRT Category A+ Credit:1.5 **Director J. Anthony Seibert, PhD**
RC823A • Nuclear Medicine Dose Indices

Wesley E Bolch PhD (Presenter)

LEARNING OBJECTIVES

1) Identify the more common radiopharmaceuticals used in functional imaging of normal and diseased tissues. 2) Demonstrate understanding of the parameters needed to estimate tissue dose during nuclear medicine imaging and therapy. 3) Identify fundamental data sources for organ and effective dose per unit administered activity. 4) Demonstrate understanding of the physiological and anatomic sources of individual variability in organ and effective dose per unit administered activity. 5) Identify key features of new generation anatomical models that can reduce dose uncertainties through improved matching of patient body morphometry.

ABSTRACT

A main clinical application of nuclear medicine is that of functional imaging of normal and diseased tissue, and the localization of malignant tissue and its potential metastatic spread. In these applications, the amount of administered activity is such that the absorbed dose to both imaged and non-imaged tissues are typically very low and thus stochastic risks of cancer induction are greatly outweighed by the diagnostic benefit of the imaging procedure. Nevertheless, these tissues doses and their stochastic risks should be quantified for each patient, and placed in context of both their cumulative values received over multiple imaging sessions,

and of doses and risks received by other diagnostic imaging procedures they may have (fluoroscopy and computed tomography, for example). The role of internal dosimetry in diagnostic nuclear medicine is thus to provide the basis for stochastic risk quantification. Once this risk is quantified, it may be used to optimize the amount of administered activity in order to maximize image quality while minimizing patient risk. This optimization process is of particular importance for pediatric patients owing to their enhanced organ radiosensitivities and years over which any stochastic effects may become manifest. This optimization should consider, as much as possible, patient age, gender, and body morphometry, and pharmacokinetics, along with all available image acquisition and processing techniques. Unlike other forms of diagnostic imaging, for which dose indices are readily measured, only the administered radioactivity is typically available for dose tracking. In this course, we will review data sources for organ and effective dose per unit administered activity for the more common molecular imaging radiopharmaceuticals. Particular attention will be given to sources of individual variability in both organ and effective dose attributed to both physiological and anatomical variations among patients. Advances in computat

RC823B • Tracking Doses in the Pediatric Population

Frederic H Fahey DSc (Presenter)

LEARNING OBJECTIVES

1) List three considerations in estimating the radiation dose from pediatric nuclear medicine. 2) Discuss three factors that affect the radiation dose from the CT component of hybrid imaging. 3) Describe three factors that can affect the appropriate choice of administered activity for a nuclear medicine study. 4) List 2 advances that may lead to further reduction in the administered activity in pediatric nuclear medicine.

Quantitative Imaging: Quantitative Imaging in Ultrasound Friday, 08:30 AM - 10:00 AM • E263 [Back to Top](#) [PH](#) [US](#) [BQ](#)

RC825 • AMA PRA Category 1 Credit™: 1.5 • ARRT Category A+ Credit: 1.5 Director Michael F McNitt-Gray, PhD *

RC825A • Elasticity and Backscatter Related Measures

Timothy J Hall PhD (Presenter) *

LEARNING OBJECTIVES

1) Describe the various approaches and history of Quantitative Ultrasound. 2) Understand the difference in system-dependent and system-independent backscatter parameters. 3) Understand the benefits of system-independent backscatter parameters. 4) Describe the state of the art in elasticity imaging and quantitative ultrasound from backscattered echoes.

ABSTRACT

There is a long history of attempts to use the backscattered echo signals from medical ultrasound to describe disease conditions of various tissue types. For example, from the initial application of ultrasound in breasts, the investigators attempted to differentiate benign from malignant disease based on characteristics of the echo signals. Along the way, there have been substantial successes. For example, it was only 30yrs ago that we debated how to estimate blood flow based on ultrasound echo signals and how to interpret that data. Just over 20yrs ago we began to display flow dynamics with color flow imaging. More recently, elasticity imaging methods, which also began in the tissue characterization or quantitative ultrasound community, have become commercially viable products with clear diagnostic potential. These were tissue characterization methods in their early days. Now they are recognized as specific procedures with quantifiable diagnostic merit. Numerous other quantitative ultrasound (QUS) methods have been proposed, developed, tested and have demonstrated varying degrees of success. Many of these methods are still under development.

This presentation will discuss quantitative ultrasound methods based on backscattered echo signals focusing on the most recent techniques that are either commercially available or that show the greatest potential as diagnostic tools.

RC825B • Volume Flow and Measures From Contrast Agents

Oliver D Kripfgans (Presenter) *

LEARNING OBJECTIVES

1) Understand the pitfalls of ultrasound based blood flow acquisition, analysis, and interpretation. 2) Become familiar with current approaches of quantitative estimation of blood flow and learn how to minimize associated errors. 3) Obtain an overview of current commercial ultrasound contrast agents as well as their availability in the US. 4) Learn about contrast agent enhanced measurements in a clinical setting.

ABSTRACT

Clinical ultrasound scanners typically offer three methods of blood flow acquisition, namely pulse wave, color flow and power Doppler. While real-time blood flow visualization is one of the perks of ultrasound, standardized quantitative methods are still unavailable to the radiologist. Pulse wave offers volumetric flow computation based on assumptions that are often violated. Color flow has never been directly quantitative as no angle correction can be dialed-in. The advent of 2D ultrasound arrays (electronic or mechanically swept) has enabled color flow and power Doppler acquisition in the coronal plane thus yielding Doppler angle as well as geometry independent flow information for direct quantification of in situ real-time volumetric flow. Ultrasound contrast agents have been approved for many clinical applications in Europe, Asia and Canada. The FDA has limited the use of ultrasound contrast agents in the US and essentially only cleared ultrasound contrast agents for cardiac applications. However, off-label application is practiced in the US. Its extend and benefits will be discussed in this course along with current approaches for ultrasound contrast agents based clinical measurements.

URL's

www.ultrasound.med.umich.edu/ODK/RSNA2012

RC825C • Ultrasound Measurements and FDA Criteria for Display of New Quantitative Measures




Brian S Garra MD (Presenter)

LEARNING OBJECTIVES

1) Review the main types of quantification of Ultrasound images. 2) Review some recent examples exploring sources of error in ultrasound morphometric quantification. 3) Summarize new ultrasound based parameters that might be displayed. 4) Discuss the formation of the Ultrasound QIBA Technical Committee and its objectives. 5) Review recent changes in FDA policy regarding display of quantitative features on ultrasound images.

ABSTRACT

Ultrasound images are probably the most frequently measured images and extensive literature on a wide variety of ultrasound image measurements exists going back to the 1960's. Most morphometric and Doppler measurements are well documented and are at a mature stage. Automated measurements of volume and structures such as arterial intimal medial thickness are also finding increasing clinical application but each method of image segmentation and quantification has its own characteristic problems and sources of error. Some newer measurements including measurement of tissue strain (elastography) and strain rate and one of the newest, shear wave speed, are the subject of considerable research activity and the sources of error and bias are just now being identified and quantified. The RSNA Quantitative Imaging Biomarker Alliance (QIBA) has recently undertaken the task of developing standardized protocols for measurement of ultrasound related parameters. The first project of the US QIBA technical committee is to develop a profile for measurement of shear wave speed in tissue using ultrasound. The FDA has long allowed many types of measurements to be displayed as part of the ultrasound image. A demonstration of reasonable accuracy and precision important for obtaining clearance to display a new measurement. Display of measurement accuracy may also be required and users should be informed of situations where the measurement may be inaccurate. The efforts of the QIBA may provide data that in the future will help to speed up FDA clearance for display of new types of measurements.

Physics (CT-Dose Optimization) Friday, 10:30 AM - 12:00 PM • S403B [Back to Top](#)    **SST14** • AMA PRA Category 1
Credit™: 1.5 • ARRT Category A+ Credit: 1.5 **Moderator Cynthia H McCollough**, PhD *
Moderator Robert G Gould, DSc
SST14-01 • ACRIN PA 4006: Effect of Device Technical Factors on Patient Dose in a Prospective Digital Breast Tomosynthesis Screening Trial

Mathew Thomas BS (Presenter) ; **Yohei Matsutani** ; **Emily F Conant** MD * ; **Andrew D Maidment** PhD *

PURPOSE

To characterize the effect of kVp, mAs, and filter-anode combinations on mean glandular dose (MGD) in digital mammography (DM) and digital breast tomosynthesis (DBT).

METHOD AND MATERIALS

A prospective multi-site trial was conducted to compare the recall rates of DM and DBT. The DBT image set consisted of 2D and 3D images obtained at approximately a 15% reduced dose effected by using a phototimer setting of $\diamond-1\diamond$; the DM images were acquired without modification of dose. All image data were stored in a centralized DICOM server and the image metadata were automatically extracted from the DICOM headers. These data included breast laterality, image orientation, kilovoltage (kV), exposure (mAs), target and filter materials, entrance surface dose and mean glandular dose (MGD). Regression analysis was performed to ascertain the influence of the various acquisition parameters on MGD.

RESULTS

The 2D component of the combined-DM/DBT acquisition was on average 18.5% less than (p

CONCLUSION

For both DM and DMT, the key determining factor of MGD is mAs. The kVp of DM and 2D DBT images is significantly lower than the kVp of 3D DBT images for breast thicknesses in the range of 70-100mm due to filter change in DM.

CLINICAL RELEVANCE/APPLICATION

This paper characterizes the key technical parameters that determine the cumulative dose exposure for patients during digital breast tomosynthesis screening.

SST14-02 • Assessment of Patient Dose from CT Localizer Radiographs

Natalia Saltybaeva (Presenter) ; **Bernhard Schmidt** PhD * ; **Daniel Kolditz** PhD * ; **Willi A Kalender** PhD *

PURPOSE

CT localizer radiographs (LR), also known e.g. as topogram or scout view, in the past were not perceived as contributing significantly to the effective dose of a CT examination. In modern low-dose CT, however, this contribution has to be taken into account. The purpose of our study was to assess typical LR dose values based on simulations and measurements.

METHOD AND MATERIALS

Four anthropomorphic phantoms representing 2 adults (male and female, Rando-Alderson Research Laboratories, New York, USA) and 2 children (5 and 1 y.o., CIRS, Norfolk, VA, USA), equipped with 30-60 TLD chips, underwent LR scans (SOMATOM Definition Flash, Siemens AG, Forchheim, Germany). Three different body regions (head, thorax, and abdomen-pelvis) and three positions of the X-ray tube (AP, PA and lateral) were considered. We simulated 3D dose distribution for each setup using a validated Monte Carlo tool (ImpactMC, CT Imaging GmbH, Erlangen, Germany) and compared simulated and measured dose values point by point. Organ and effective doses for the different LRs were calculated and compared to typical dose values in CT examinations.

RESULTS

The differences between measured and simulated dose values for all projections (AP, PA and lateral) were below 15% on average. Organ doses varied significantly depending on the tube position; the largest differences were observed for breast dose in female chest LR (AP: 2.4 mSv vs. PA: 0.5 mSv). Overall effective dose values per LR ranged from 0.04 mSv for adult head to 0.7 mSv for 1 y.o. child abdomen. This adds from 5% to 42% to effective dose of typical low-dose CT exams.

CONCLUSION

MC simulations provide accurate estimates of LR dose distributions. Localizer radiographs may contribute substantially to organ and effective dose of the total CT examination. Organ doses from LRs can be significantly reduced by choosing the appropriate projection angle.

CLINICAL RELEVANCE/APPLICATION

Dose from localizer radiographs should be taken into account. LR parameter optimizations should be performed in order to decrease total dose of CT examinations.

SST14-03 • CT Radiation Dose Optimization of Coronary Calcium Scanning: Comparing Different Image Reconstruction Methods at 100kVp and 120kVp

Joerg Blobel PhD (Presenter) * ; **Jurgen Mews** * ; **Joanne Schuijf** * ; **Willem Overlaet** *

PURPOSE

The effects of tube voltage reduction and different reconstruction methods on coronary calcium scoring remain largely unknown. We performed a quantitative phantom study to determine the lowest applicable volume CTDI thresholds ($CTDI_{vol}$) at 100kVp versus 120kVp while controlling Agatston and volume score accuracy.

METHOD AND MATERIALS

ECG-gated volume scans of an anthropomorphic thoracic phantom with calcium calibration inserts, containing 200, 400 and 800mg HA/cm³ calcium mass spheres of 1, 3 and 5mm diameter (QRM GmbH, Germany), were performed on 320-row CT (Aquilion ONE, Toshiba Medical Systems, Japan). Using 100kVp and 120kVp with 10-580mA variations in 32 steps, each acquisition was reconstructed with Filtered Back-Projection (FBP), Quantum Denoising Software (QDS) and Adaptive Iterative Dose Reduction (AIDR 3D). To determine the minimum $CTDI_{vol}$ thresholds for the six groups a statistical 2S-outlier test (WinStat 2007.1 software) was performed on the semi-automatically detected Agatston and volume scores. The Kruskal-Wallis-Test was used to evaluate statistical differences between the three reconstructions and both kVp scan series.

RESULTS

At equal kVp settings, there were no significant differences in average scores between the three reconstruction methods (p>0.21). The use of 100kVp, as compared to 120kVp, resulted in a 3% lower Agatston score average (672 vs. 694, p3, pvol thresholds were reduced from 5.98mGy to 2.37mGy (120kVp, QDS), 1.86mGy (120kVp, AIDR 3D), 4.13mGy (100kVp, FBP), 1.94mGy (100kVp, QDS) and 1.12mGy (100kVp, AIDR 3D) (Fig.). The averages of 10 repeated scans at low dose level (1.12 mGy, AIDR3D, 100kVp) showed no significant difference with the reference group (12 dose steps, FBP, 120kVp) for both Agatston (p=1.00) and volume (p=0.75) score.

CONCLUSION

Mean dose reductions of 37% using 100kVp instead of 120kVp and 71% using the novel iterative reconstruction AIDR 3D instead of FBP can be achieved for coronary calcium scanning. Combining 100kVp with AIDR 3D resulted in an 81% lower $CTDI_{vol}$ threshold compared to a standard scan protocol (120kVp, FBP).

CLINICAL RELEVANCE/APPLICATION

Considerable radiation dose reduction can be achieved for coronary calcium scanning using AIDR 3D at 100kVp. Low dose coronary calcium scanning is possible with good accuracy and reproducibility.

SST14-04 • Synthetic Cone-beam CT for Determining Patient- and Task-specific Minimum-dose Techniques in Repeat Scans

Adam S Wang PhD (Presenter) * ; **Joseph W Stayman** PhD * ; **Yoshito Otake** * ; **Jeffrey H Siewerdsen** PhD *

PURPOSE

To evaluate a newly developed method (Synthetic Cone-Beam CT) for accurately determining the impact of lower-dose techniques in C-arm CBCT, allowing identification of minimum-dose protocols suitable to a given imaging task in scenarios that require repeat scans.

METHOD AND MATERIALS

An initial CBCT acquired at nominal scan protocol at the beginning of a procedure provides a patient-specific basis for synthetic CBCT. To accurately simulate lower-dose techniques, noise of the proper magnitude and correlation is added to the projections, accounting for object-dependent noise levels and correlations introduced by the detector. The resulting noisy projections are then reconstructed to yield synthetic CBCT images accurately portraying the image quality in lower-dose scans. Validation studies were conducted on a mobile C-arm using a 16 cm acrylic phantom to first assess the detector signal-variance relationship and correlations. Synthetic CBCT was then applied to a head phantom (100 kVp, 320 mAs initial scan), synthesizing projections across a range of lower-dose techniques (160, 80, 40, and 20 mAs). Real CBCT scans were also obtained at each technique for image quality comparison.

RESULTS

Comparison of synthetic and real CBCT images across the full range of techniques demonstrated accurate noise magnitude (within ~3%) and correlation (matching noise-power spectrum, NPS). Other image quality characteristics (e.g., spatial resolution, contrast, beam hardening, and scatter) remain intact and are realistically presented in synthetic CBCT. Generating synthetic CBCT for a broad range of protocols gives a useful method to select minimum-dose techniques that accounts for complex factors of imaging task, patient-specific anatomy, artifacts, and physician preference.

CONCLUSION

Synthetic CBCT accurately portrays the increased noise in lower-dose protocols while preserving other image quality characteristics, providing a method to define minimum-dose, task-specific protocols in repeat CBCT. Ongoing work includes translation to clinical studies and application to iterative reconstruction, where potential dose reduction is even greater and synthetic CBCT accurately portrays low-dose limits that are difficult to predict.

CLINICAL RELEVANCE/APPLICATION

Selection of minimum-dose, task-specific techniques for intraoperative C-arm cone-beam CT is enabled by synthesizing patient-specific images that accurately reflect image quality at lower dose.

SST14-05 • Preliminary Clinical Evaluation of an Online Intrascan Motion-correction Algorithm for Interventional C-arm Flat-detector CT

Julia Wicklein * ; **Oliver Beuing** * ; **Martin Skalej** MD, PhD * ; **Steffen Serowy** * ; **Willi A Kalender** PhD * ; **Yiannis Kyriakou** PhD (Presenter) * ; **Holger Kunze** MS *

PURPOSE

Intrascan Motion-artifact-correction in C-arm-based flat-detector CT (FD-CT) is an important issue in interventional imaging because of longer scan times as compared to Multi-Slice CT. Our aim was the development and evaluation of an online image-content-based motion-correction technique without using any kind of markers or external motion knowledge.

METHOD AND MATERIALS

The correction method is based on a gradient descent method, minimizing a gray-value entropy criterion optimizing the underlying acquisition trajectory parameters. It is formed as a multistep approach, including a global, local and projection wise optimization. We are using a locally rigid variation of the systems trajectory parameters like detector- or source-translation or a detector rotation to compensate patient motion. The retrospective evaluation of 30 arbitrary (with weak and strong motion, without motion artifacts) patient head scans included 5s 3D angiography and 20s soft-tissue protocols. All scans were performed on an Artis Q System (Siemens AG). For each dataset three volumes were computed: 1) original reconstruction using the system's geometry calibration (OR), 2) motion corrected reconstruction without any system information (MCR) and 3) motion corrected reconstruction using the system's geometry calibration as initialization (MCR+). Two neuroradiology experts performed a visual evaluation according to a 5-point grading scale with respect to general image quality, motion-artifact-content and spatial resolution of the structures of interest, e.g. 3D vessels.

RESULTS

The average scores for OR, MCR and MCR+ were 2.75, 3.0 and 3.15, respectively. The combined compensation of unknown trajectories and unknown patient motion (MCR) can lead to comparable results to OR. Both experts confirmed a distinct reduction of artifacts by the motion correction algorithm (MCR+), e.g. blurring and streaks. Especially for 3D angiography even small distal vessels were depicted clearly. MCR+ application on soft-tissue protocols illustrated a constantly better delineation of bone and soft-tissue in the border zones.

CONCLUSION

Image-based motion correction is possible without a-priori knowledge of the motion pattern and can improve interventional FD-CT imaging.

CLINICAL RELEVANCE/APPLICATION

Using the proposed algorithm enables good image quality even for unsteady patients and can be helpful for longer FD-CT acquisitions in cases where anaesthesia is contraindicated.

SST14-06 • Supervised Conversion of Ultra-low-Dose to Higher-dose CT Images by Using Pixel-based Machine Learning: Phantom and Initial Patient Studies

Kenji Suzuki PhD (Presenter) * ; **Yipeng Liu** MS ; **Toru Higaki** PhD ; **Yoshinori Funama** PhD ; **Kazuo Awai** MD *

PURPOSE

Reduction of radiation dose in CT is highly demanded. Our purpose was to develop a supervised pixel-based machine-learning technique for converting ultra-low-dose (ULD) CT to virtual higher-dose (HD) CT images with less noise or artifact.

METHOD AND MATERIALS

We developed a pixel-based machine-learning technique based on a massive-training artificial neural network (MTANN) filter that is trained with input ULDCT images and corresponding teaching HDCT images. Through training, the MTANN learns the relationship between the input and teaching images to convert ULDCT into HDCT images. Once trained, the MTANN no longer requires HDCT images; and it produces HDCT-like images from non-training ULDCT images. To train our MTANN filter and make a reference, we acquired 6 sets of CT scans of an anthropomorphic chest phantom (Kyoto Kagaku, Kyoto, Japan) with a tube voltage of 120kVp, tube currents of 10, 25, 50, 100, 150, and 300 mA, and a collimation of 5 mm. A 10 mA ULDCT image and the corresponding 300 mA HDCT image were used for training our MTANN filter. To evaluate the performance of our MTANN, we acquired ULDCT scans of 3 patients with a tube voltage of 120kVp and a tube current of 10 mA. The effective radiation dose of an ULDCT study was 0.1 mSv. We evaluated the image quality of CT images by using signal-to-noise ratio (SNR) in each image.

RESULTS

With our trained MTANN filter, noise and artifacts (e.g., streaks) in ULDCCT images (0.1 mSv) were reduced substantially, while details of soft tissue such as pulmonary vessels and bones were maintained. The average SNR of 0.1 mSv ULDCCT images for patients was improved from 2.3 (± 1.8) to 13.0 (± 2.5) dB (two-tailed t-test; P

CONCLUSION

With our supervised MTANN dose-reduction technique, the image quality of 0.1 mSv ULDCCT was improved substantially to the quality comparable to 1.5 mSv HDCT; thus, radiation dose can potentially be reduced by 93%.

CLINICAL RELEVANCE/APPLICATION

Advantage of our technique over iterative reconstruction is substantial reduction of radiation dose in CT with a very short processing time, which would be beneficial to patients and radiologists.

SST14-07 • The Influence of kV and Patient Positioning on CT Image Quality and Dose: Why Low kV CT Scans Have a Higher Sensitivity to Patient Positioning

Timothy P Szczykutowicz PhD (Presenter) * ; **Frank N Ranallo** PhD ; **Kara Gill** MD ; **Myron A Pozniak** MD *

PURPOSE

Higher levels of noise non-uniformity were noticed in our pediatric scans. Investigation into the problem lead to the conclusion that due to the low kV used for pediatric scans, errors in patient positioning caused larger increases in noise non-uniformity for pediatric patients relative to similar adult protocols using higher kV settings. The purpose of this work is to explore the physical reason behind this effect and provide guidelines to avoid this problem in the clinic.

METHOD AND MATERIALS

Several clinical cases flagged by our pediatric radiologists were analyzed and motivated an anthropomorphic phantom study. A pediatric protocol was applied using 80 and 140 kV. The phantom was purposely mis-centered low by 0 and 6 cm. The noise uniformity was reported as the ratio of the standard deviation in uniform region located in the anterior and posterior regions of the phantom. In addition, a numerical simulation was performed in which a bowtie filter was forward projected using an 80 and 140 kV polychromatic spectra and the transmitted fluence examined. This numerical study was meant to provide insight onto why changing the kV can influence noise uniformity when a patient is mis-centered.

RESULTS

It was found that the noise non-uniformity of the 80 and 140 kV scans was 1.33 and 1.27 at 0 cm offset and 1.86 and 1.58 at 6 cm offset respectively. The numerical simulation showed the 140 kV spectra provided a 23% wider fluence profile than 80 kV when both spectra were normalized to have equal fluence through the center of the bowtie.

CONCLUSION

Novel to this study, it was shown that the degree of non-uniformity depends on kV and the physical reason for this effect was shown via phantom measurements and numerical simulation. This study identifies a new reason to stress the importance of patient positioning, especially for low kV exams (i.e. pediatrics).

CLINICAL RELEVANCE/APPLICATION

Low kV settings, commonly used in pediatric protocols, can increase the chance for an un-diagnosable scan due to the higher dependence of noise non-uniformity on patient mis-centering at lower kVs.

SST14-08 • Radiation Dose in Dual-energy Computed Tomography: Axial Dose Distributions in Specific Thoracic and Abdominal Regions

Kosuke Matsubara PhD (Presenter) ; **Haruka Koshida** ; **Keita Sakuta** RT ; **Tadanori Takata** ; **Kichiro Koshida** PhD ; **Yukihiro Matsuura** RT ; **Toshifumi Gabata** MD

PURPOSE

Polyenergetic x-rays with low (100 or 80 kVp) and high tube voltage [140 kVp with or without a tin (Sn) filter] are used in dual-energy computed tomography (DECT). We aimed to evaluate the radiation doses administered during thoracic and abdominal DECT and compare them with those administered during single-energy CT (SECT) of the same regions.

METHOD AND MATERIALS

A 128-section dual-source CT device (SOMATOM Definition Flash; Siemens Healthcare, Erlangen, Germany), an anthropomorphic female phantom (RAN-110; Phantom Laboratory, Salem, NY, USA), and calibrated radiophotoluminescent glass dosimeters (RPLDs) (GD-302M; Chiyoda Technol, Tokyo, Japan) were used to acquire axial absorbed dose distributions in specific regions of the thorax and abdomen that were imaged using CT with one SE (120 kVp) and three DE (100 and Sn/140 kVp, 80 and Sn/140 kVp, and 140 and 80 kVp) modes. The energy modes were in accordance with the standard clinical protocols for thoracic and abdominal CT, and the tube current was adjusted so that the displayed volumetric CT dose indices (CTDIvol) were equivalent among the four energy modes. Axial absorbed dose distributions in the thoracic and abdominal regions were acquired by placing RPLDs within all holes of one thoracic or abdominal section and pasting them around the section.

RESULTS

The absorbed doses in the thoracic region were 12.8 ± 2.3 , 12.5 ± 2.2 , 11.7 ± 1.9 , and 12.2 ± 1.6 mGy ($p < 0.01$, Friedman's test) when the 120 kVp, 100 and Sn/140 kVp, 80 and Sn/140 kVp, and 140 and 80 kVp modes, respectively, were used. The corresponding values for the abdominal region were 24.8 ± 2.2 , 24.3 ± 2.0 , 22.9 ± 1.7 , and 23.3 ± 1.6 mGy ($p < 0.01$), respectively. The doses absorbed at the surface and center of the abdomen were higher and lower, respectively, when the 140 and 80 kVp mode was used than when the other three modes were used for abdominal CT.

CONCLUSION

DECT can be performed with a radiation dose that is equivalent to or lower than that required during SECT when the displayed CTDIvol is equivalent. The additional Sn filter used in abdominal DECT can approximate the axial absorbed dose distribution of DECT to that of SECT.

CLINICAL RELEVANCE/APPLICATION

DECT has advantages over SECT. Evaluation of the radiation dose administered during DECT is necessary to determine its indications for application and the energy modes required.

SST14-09 • CT Image Quality Improvement and Dose Reduction Potential with Model-based Iterative Reconstruction Using Autopsy Imaging in the Abdomen: Evaluation of Image Noise and DOSE Estimation with Different Noise Index

Tomokatsu Tsukamoto (Presenter) ; **Takashi Takahata** RT ; **Yue Dong** ; **Keisuke Nishihara** MD ; **Kazunari Mesaki** MD ; **Hiroki Mori** MD ; **Ye Ju** ; **Katsuhide Ito** MD

PURPOSE

To assess the dose reduction potential and image quality improvement with model-based iterative reconstruction algorithm (Veo) using autopsy imaging by comparing image noise and DOSE (DLP mGy-cm) with the adaptive statistical iterative reconstruction (ASiR) and the filtered back projection (FBP) reconstructions.

METHOD AND MATERIALS

With institutional review board approval, 8 autopsy imaging (AI) underwent abdomen CT with different noise index (NI: 8.5, 10.5, 14.5, 20.5, 30.5) on Discovery CT750HD was included. In addition to the 3 sets of 0.625mm slice thickness CT images were

reconstructed with FBP, 50% ASiR and Veo. The image noise (SD) was measured with the same size of regions of interest at the same slice in 3 locations for liver and pelvis. The image noise reduction ratio was defined by SD (at NI30.5)/SD (at NI8.5). Using a 5-point score (1: poor; 3: diagnosis, 5 excellent), 3 radiologists independently and graded overall noise and delineation of the abdomen image.

RESULTS

For the Liver, the image noise reduction with Veo compared with FBP and 50%ASiR for the NI: 8.5, 10.5, 14.5, 20.5, 30.5 and the average were (47.3%, 52.2%, 61.0%, 70.6%, 79.0% and 62.0±13.0%) and (37.7%, 32.2%, 44.4%, 58.1%, 70.1% and 48.5±15.5%), respectively; for Pelvis, (49.2%, 54.3%, 66.3%, 74.1%, 79.8% and 64.7±12.9%) and (28.5%, 34.9%, 52.4%, 63.3%, 71.8% and 50.2±18.4%), respectively. The reduction ratio (NI30.5/NI8.5) of image noise about (Liver and Pelvis) for the Veo, 50%ASiR and FBP were (1.5 and 1.5), (3.2 and 3.9) and (3.9 and 3.9), respectively. All the differences were statistically significant between Veo and FBP (p

CONCLUSION

The model-based iterative reconstruction algorithm (Veo) advanced reconstruction algorithms greatly reduced image noise to compare FBP and ASiR .

CLINICAL RELEVANCE/APPLICATION

Veo reconstruction technique has the ability to reduce radiation dose through their improvement in image quality compared with the current algorithms such as FBP and ASiR.

Physics (Image-guided Radiation Therapy II) Friday, 10:30 AM - 12:00 PM • S403A [Back to Top](#)    **SST15 • AMA PRA Category 1 Credit™:1.5 • ARRT Category A+ Credit:1.5** **Moderator Peter Balter** , PhD *

Moderator Lei Xing , PhD *

SST15-01 • Artifact-resistant Motion Estimation for Motion-compensated CT

Marcus Brehm ; **Thorsten Heuser** (Presenter) ; **Pascal Paysan** PhD * ; **Markus Oelhafen** DPhil, DSc * ; **Marc Kachelriess** PhD

PURPOSE

Image quality of respiratory-correlated 4D volumes from flat detector cone-beam CT scans (4D CBCT) is deteriorated by severe sparse projection artifacts. These artifacts complicate motion estimation and therefore motion compensation. The aim is to robustly estimate motion in presence of dominating image artifacts and to allow for a subsequent motion-compensated image reconstruction that guarantees full dose usage.

METHOD AND MATERIALS

To estimate respiratory motion in artifact-dominated images we developed a patient-specific artifact model: A 3D reconstruction of the 4D data is segmented into air, soft tissue, and bone by simple but robust hard thresholding (at -800 HU, +300 HU). The resulting three-valued image is forward projected and the thus-obtained rawdata undergo a 4D reconstruction (phase binning and independent reconstruction of each respiratory phase) yielding 4D CBCT images free of patient motion but full of sparse projection artifacts. The artifacts change from respiratory phase to respiratory phase. Deformable registration of those artifact volumes yields an approximation of the motion induced by the artifacts. This information is used to correct motion vector fields that were estimated on the conventional 4D CBCT volumes. The method is verified using simulated rawdata obtained by deforming a clinical patient dataset by realistic deformation fields, and by processing patient data acquired with the TrueBeam 4D CBCT system (Varian Medical Systems).

RESULTS

The motion-compensated reconstructions, from simulated and patient data, do not contain any streak artifacts, they are free from motion blurring, and their image noise is similar to the standard 3D reconstruction. The high temporal resolution is maintained. Pulmonary blood vessels that have been hidden by motion blurring or streak artifacts before now become clearly visible.

CONCLUSION

The proposed patient-specific artifact model allows for a robust registration between images that are severely degraded by artifacts. Combined with motion compensation one is able to remove streak and motion artifacts while maintaining a good spatial and good temporal resolution. Full dose usage is guaranteed because now all data contribute to each time frame.

CLINICAL RELEVANCE/APPLICATION

High quality 4D images are a prerequisite for precise adaptive radiation treatment.

SST15-02 • The Effect of CT Image Quality on Deformable Image Registration in Radiotherapy

Vern P Hart PhD (Presenter) ; **Guang-Pei Chen** PhD ; **Allen Li** PhD

PURPOSE

Various CT modalities of different image quality are used to plan and guide radiation therapy (RT). This work is to assess the effect of CT image quality on deformable image registration (DIR) and its impact on auto-segmentation and dose accumulation in adaptive RT (ART).

METHOD AND MATERIALS

A variety of CT data sets with different soft-tissue contrasts were acquired for prostate cancer patients in different treatment fractions. Conventional diagnostic CT with standard protocols (SCT) and high soft-tissue contrast protocols (increased dose) (HCT), kilovoltage cone beam CT (CBCT), and megavoltage tomotherapy CT (MVCT) were registered using an in-house DIR tool based on the symmetric force Demons algorithm. Targets and critical organs were contoured on the SCTs and populated to other CT images with DIR. Of particular interest was the impact of soft-tissue contrast on intensity-based algorithms. DIR results were assessed with the Dice similarity coefficient (DSC) and were correlated with differences in image quality observed between CT image types.

RESULTS

Differences in soft-tissue contrast had a significant impact on DIR accuracy, as demonstrated in the registration of SCT-SCT, SCT-HCT, SCT-CBCT, and SCT-MVCT between different fractions. The inclusion of binary masking partly compensated for this effect and yielded excellent results. In the case of SCT-CBCT registration, binary masking provided DSC values exceeding 96, 97, and 98% for rectum, prostate, and bladder, respectively. Initial results have also shown that contour smoothing using morphological warping can improve accuracy in the absence of binary masks on daily images, which is of interest for ART.

CONCLUSION

Decreased soft-tissue image contrast generally leads to decreased DIR accuracy during ART. A number of techniques can be implemented to improve the accuracy of contouring and dose mapping. Binary masking provides excellent results and research is currently underway to increase the clinical robustness of this approach, such as auto-segmentation for mask generation and morphological smoothing of image contours. These approaches would allow ART based on commonly used CT modalities.

CLINICAL RELEVANCE/APPLICATION

DIR is essential in ART for accounting for interfraction variations and thereby improving RT delivery accuracy. As such, compensating for decreased CT quality in DIR is of great interest to ART.

SST15-03 • Deformable Registration Guided Correlation of Post-radiotherapy Recurrent Disease to Pre-radiotherapy PET Positive Volume in Patients with Head and Neck Cancer

Michalis Aristophanous (Presenter) ; **Abdallah S Mohamed** MD, MSc ; **Adam S Garden** MD ; **David I Rosenthal** * ; **Clifton**

PURPOSE

Investigate the predictive role of pre-radiotherapy (pre-RT) FDG-PET/CT scans for head and neck cancer local and/or regional recurrence (LRR).

METHOD AND MATERIALS

Thirty-five patients that developed LRR following radiotherapy (RT) for primary SCC of the head and neck between May 2003 and July 2010 were identified under an IRB approved protocol. Each patient had an FDG-PET/CT scan on average 2 months prior to RT. The PET-based gross tumor volume (GTV) was defined utilizing an automated segmentation algorithm developed in-house to obtain a pre-RT GTV-PET. The recurrent disease was identified and contoured on follow up post-radiotherapy (post-RT) CT imaging to obtain the GTV-REC. The post-RT CT scan was fused to the pre-RT PET/CT using an in-house developed deformable registration algorithm. The deformation map was applied to the contours to obtain GTV-REC_def that was registered to the pre-RT PET/CT. A uniform 1cm margin was added to the GTVs to account for the various uncertainties in the segmentation and registration process. Several SUV statistics inside the recurrent and PET defined GTVs were obtained and analyzed, along with the overlap of the GTV-REC_def with the GTV-PET.

RESULTS

Primary sites were oral cavity (8.6%), oropharynx (68.5%), and hypopharynx (22.9%). The mean (range) GTV-PET and GTV-REC_def were 29.2ml (3.1-145.6ml) and 10.9ml (0.9-92.9ml) respectively with the Pearson correlation coefficient between the two volumes being 0.82. The SUV maximum in the GTV-PET and GTV-REC_def+1cm was found to have no statistically significant difference. Finally, an overlap of 1 between GTV-REC_def and GTV-PET+1cm indicating complete inclusion of the recurrence in the pre-RT defined GTV-PET was obtained for 68.6% of the cases, and increased to 82.9% for an overlap greater than 0.5.

CONCLUSION

The results suggest that the volume of the PET positive GTV on a pre-RT FDG-PET scan can be predictive of the size of disease in cases of recurrence. In addition, utilizing deformable registration to relate the recurrent GTV to the pre-RT SUVs on the FDG-PET scan confirmed that greater than 80% of recurrence occurs within or at the PET positive volume boundary.

CLINICAL RELEVANCE/APPLICATION

Predictions of post-radiotherapy recurrent disease patterns based on pre-radiotherapy PET characteristics can result in treatment plan strategy modifications that improve loco-regional control.

SST15-04 • Monte Carlo Based Estimation of Pediatric Dose from CBCT Imaging Head Protocols for Patient Positioning and Target Localization in Radiotherapy

Kyle McMillan (Presenter) * ; **Maria Zankl** PhD ; **Michael F McNitt-Gray** PhD * ; **Dan Ruan** PhD *

PURPOSE

The purpose of this investigation is to estimate the organ doses to a pediatric patient undergoing repeat CBCT imaging as part of an image-guided radiation therapy (IGRT) procedure.

METHOD AND MATERIALS

A Monte Carlo model was developed with application to kV-CBCT dose quantification on the Varian On-Board Imager platform. This model was validated against experimental measurements with an average agreement within 4%. Using this validated model, dose to a pediatric patient was simulated for the GSF "Child" model. This whole-body voxelized phantom was derived from CT imaging data of a 7-year-old female and contains 144 slices of 8 mm thickness with each slice consisting of a 256 x 256 matrix of 1.54 mm x 1.54 mm pixels. Simulations were performed using a standard-dose, low-dose and high-quality head CBCT protocol. For each protocol, the clinical default x-ray field size of 27.2 x 18.4 cm² at 100 cm source-to-surface distance was simulated. The reference center of the scan was set in the infratentorial region of the brain, and dose was tallied in all relevant organs near the collimated x-ray beam. Results for each simulated protocol were reported for both an individual scan as well as the accumulated dose expected from 30 repeated scans throughout the course of an IGRT treatment regimen consisting of 5 treatment fractions a week for 6 weeks.

RESULTS

For a standard-dose protocol, dose per scan to the brain, skull, lens of the eye, head skin and cervical spine was 2.9, 10.6, 0.47, 3.3 and 14.9 mGy, respectively. These doses were decreased by a factor of 2 when the low-dose protocol was used and increased by a factor of 5 when the high-quality protocol was used. Accumulated dose as high as 2240 mGy was observed for the cervical spine when the high-quality protocol was used for all 30 repeated scans.

CONCLUSION

Dose to bony structures such as the skull and cervical spine is significantly higher than dose to soft tissue. In pediatric patients whose bones are in a proliferative state, this CBCT imaging dose increases the risk of retardation of growth and induction of bone cancer. Therefore, it is important that the dose from CBCT imaging of pediatric patients be carefully considered and monitored.

CLINICAL RELEVANCE/APPLICATION

Organ-specific dose quantification from this study provides distributional knowledge about CBCT imaging dose and facilitates designing protocols to reduce risk of late effects in pediatric patients.

SST15-05 • 4D Cone Beam CT in Image Guided Radiation Therapy without Data Truncation Artifacts

Kai Niu MS (Presenter) ; **Ke Li** MS ; **Guang-Hong Chen** PhD *

PURPOSE

To evaluate the capability of solving the data truncation and detector shift problem common in clinical applications of 4D cone beam CT (CBCT) using an adapted Prior Image Constrained Compressed Sensing (PICCS) reconstruction method and to quantify the robustness of the adapted PICCS-4DCBCT algorithm under different data truncation conditions.

METHOD AND MATERIALS

RESULTS

For PICCS-4DCBCT, the rRMSEs are 0%, 4%, 6%, 7% for each case from no data truncation to most aggressive data truncation. In contrast, for TV-CS, the corresponding rMSEs are 4%, 6%, 8%, 9%, and for FDK, the rRMSEs are 17%, 18%, 19% and 20%. The UQIs for PICCS-4DCBCT images are 1, 0.996, 0.991 and 0.986 (score=1 means perfect); for TVCS, the UQIs are 0.970, 0.957, 0.951 and 0.947, and for FDK images, the UQIs are 0.630, 0.630, 0.630 and 0.629.

CONCLUSION

(1) PICCS-4DCBCT offers much better image quality and reconstruction accuracy compared with TV-CS and E-FDK at all data truncation levels. (2) No meaningful variations in performance were observed when the amount of truncation was changed.

CLINICAL RELEVANCE/APPLICATION

PICCS-4DCBCT can be performed accurately and stably with almost arbitrary data truncation scanning conditions in 4DCBCT to guided radiation therapy for lung cancers.

SST15-06 • Optimization of the Design of Portal Imaging Systems Incorporating Thick, Segmented Scintillating Detectors Employed for Megavoltage Cone-beam CT through a Novel Hybrid Modeling Technique

Langechuan Liu (Presenter) ; **Larry E Antonuk** PhD ; **Hao Jiang** ; **Youcef El-Mohri** PhD ; **Qihua Zhao** PhD

PURPOSE

Active matrix flat-panel imagers (AMFPIs) incorporating thick, segmented scintillators have demonstrated order-of-magnitude improvements in DQE at radiotherapy energies compared to systems based on conventional phosphor screens. Such improved DQE values facilitate megavoltage cone-beam CT (MV CBCT) at clinically practical doses providing distinct advantages over kV CBCT performed using additional on-board imaging equipment. However, the MV CBCT performance of such AMFPIs is highly dependent on the design parameters of the scintillators. In this presentation, a theoretical examination of imaging performance as a function of these parameters is reported.

METHOD AND MATERIALS

The imaging performance of various scintillator designs was examined through a hybrid approach involving Monte Carlo simulation of radiation transport and determination of optical point spread functions. For each design, a full tomographic scan of a contrast phantom incorporating various soft-tissue inserts was simulated at a total dose of 3 cGy. This novel technique was validated through comparisons of theoretical predictions of contrast, noise and contrast-to-noise ratio (CNR) with measurement results obtained from a 1.13 cm thick, 1016 μm pitch BGO prototype.

RESULTS

Theoretical values for contrast, noise and CNR were found to be in close agreement with measurements for the BGO prototype, strongly supporting the validity of the modeling technique. For various other scintillator designs, results for CNR demonstrate improvement by a factor of ~ 2.2 when the scintillator thickness is increased from 1.13 to 6 cm, and an improvement by a factor of ~ 2.6 when the pitch is increased from 508 to 1016 μm . Finally, optimization of design based on a trade-off between thickness and pitch, along with evaluation of the corresponding spatial resolution performance, is discussed.

CONCLUSION

A new technique to model both radiation and optical effects was validated and employed to accurately evaluate the MV CBCT performance of MV-AMFPIs incorporating various segmented scintillator designs. It appears that significant improvement in the imaging performance of such AMFPIs can be achieved through optimization of scintillator design parameters.

CLINICAL RELEVANCE/APPLICATION

Enhanced performance of MV-AMFPIs with segmented scintillators should greatly facilitate soft tissue visualization in external beam radiotherapy through MV CBCT imaging at clinically practical doses.

SST15-07 • 2D kV Orthogonal Pair vs. 3D Cone Beam CT Localization for Breathhold Breast Radiation Therapy Treatment

Michelle Howard BS (Presenter) ; **Sean S Park** MD, PhD ; **Robert W Mutter** MD ; **Elizabeth S Yan** MD ; **Deanna H Pafundi** PhD ; **Debra Brinkmann** PhD

PURPOSE

To assess the accuracy of breast and heart localization between 3D cone beam CT (3D-CBCT) registration to soft tissue and 2D kV orthogonal pair (2D-OP) registration to bony anatomy for assessment of matching criteria and imaging modality for accurate localization of breast and heart for left-sided breast patients treated with breath-hold (BH) technique. Previous research has shown a linear correlation between major coronary events and increased radiation dose to heart [1]. 1. Darby SC, et al. Risk of ischemic heart disease in women after radiotherapy for breast cancer. *NEJM* 2013; 368(11):987-98.

METHOD AND MATERIALS

3D-CBCT and 2D-OP from 9 left-sided breast cancer patients treated with BH were retrospectively reviewed. Weekly 3D-CBCTs were acquired after manual 2D-OP registration to chest wall (anterioposterior) and sternum (lateral) was applied. 3D-CBCT images were then compared offline to planning CT with automatch applied to breast tissue, heart, or spine using translations only. The role of 2D vs 3D imaging for daily patient positioning was also evaluated.

RESULTS

CONCLUSION

Shift differences between 3D breast tissue automatch and 2D bony manual match were = 5mm in 7 patients and = 1cm in 4 patients. Accurate patient positioning is sensitive to the breast tissue placement and the degree of body roll which are difficult to ascertain with 2D imaging. 3D-CBCT registration allows for improved assessment and accurate localization of breast tissue, heart, and body roll. Further analysis will evaluate the dosimetric impact to heart based on localization to 2D-OP manual registration and 3D-CBCT automatch to breast, heart, and spine.

CLINICAL RELEVANCE/APPLICATION

This investigation will directly impact clinical practice decisions on which imaging modality and matching criteria are used daily to localize left-sided BH breast radiation therapy patients.

SST15-08 • CT Number Changes Observed during Radiotherapy for Head and Neck Cancer

Ion Moraru (Presenter)

ABSTRACT

Purpose/Objective(s): Radiation induced anatomic changes, such as tumor regression, are common during the delivery of radiotherapy (RT) for head and neck cancer. In an effort to measure treatment response and identify indicators for adaptive RT, we investigate changes of CT number in target and organs at risk (OAR) from the CT data acquired during RT delivery and study correlations with anatomic variations.

Materials/Methods: Daily diagnostic-quality CT data acquired using an in-room CT (CT-on-Rails) for image-guided IMRT of 9 patients with stage III and IV squamous cell carcinoma of the oropharynx were analyzed. The patients were treated with 70 Gy in 35 fractions concurrently with chemotherapy. The gross tumor volume (GTV) and OARs were contoured on each daily CT set. All selected patients exhibited GTV reduction over the course of the treatment. We examined the distribution of CT numbers in Hounsfield units (HU) of various volumes of interest (VOI), including GTV and spinal cord, on daily CT sets. Statistical analysis of CT number distributions was performed for each patient for different fractions and trends were examined across the entire cohort. Various parameters including the mean, width, CT number of peak and asymmetry of each histogram were used to measure differences in the CT number distributions.

Results: Patient-specific changes in the CT number histograms as a function of fraction number for the GTV and spinal cord were observed. For the GTV, the mean CT number was observed to vary as much as +28% (+13 HU) and -27% (-12.5 HU) over 30 fractions, corresponding to +40% (+17.5 HU) and -38% (-18 HU) shifts in the CT number of the histogram peaks, respectively. These were associated with large differences in the histogram widths, namely 24% and 48%, and strong changes in symmetry, which may indicate that only part of the GTV experiences a shift CT numbers over the course of treatment for these patients. By contrast, a much more limited range of changes in the mean CT numbers was observed for the spinal cord, namely between +7.5% (+2.5 HU) and -11% (-4 HU), with less modifications in histogram width and symmetry. These maxima in the mean were not correlated with the data from those patients exhibiting the largest shifts in the GTV. This supports the idea that the observed differences in CT distributions of the GTV are largely radiation induced, as the spinal cord typically receives limited radiation dose. **Conclusions:** Radiation induced non-negligible, patient-specific CT number changes were observed in volumes of interest during the delivery of RT for head and neck cancer. The pattern of variation is complex and no strong trend and/or correlation with tumor regression is identified for the small group of patients studied. More work is required to understand the mechanisms involved in these changes and how these will be used for adaptive RT to account for radiation response.

SST15-09 • Offline CBCT Quantification of Translational and Rotational Displacements Using Automated Image Matching in Head and Neck Radiotherapy: A Feasibility Study
Jillian Hayes (Presenter) ; **Maeve L McGarry** BSc ; **Gregory Perkins** BSc ; **Rabih W Hammoud** MSc, BSc ; **Saju Divakar** ; **Mohamed P Riyas** MBBS, MD ; **Noora Al Hammadi**

Disclosure Index A

Able, C. M. - Supported, Varian Medical Systems, Inc
Abujudeh, H. H. - Research Grant, Bracco Group Consultant, RCG HealthCare Consulting
Alessio, A. M. - Research Grant, General Electric Company Consultant, Lantheus Medical Imaging, Inc
Alibek, S. - Consultant, General Electric Company Speakers Bureau, General Electric Company Speakers Bureau, Siemens AG
Allmendinger, T. - Employee, Siemens AG
Alperin, N. - Stockholder, Alperin Noninvasive Diagnostics, Inc
Anders, B. - Employee, General Electric Company
Andre, M. P. - Research Consultant, Almen Laboratories, Inc
Angel, E. - Employee, Toshiba Corporation
Aoyagi, K. - Employee, Toshiba Corporation
Arbique, G. - Research Grant, Toshiba Corporation
Auclair, C. - Employee, General Electric Company
Avanaki, A. N. - Employee, Barco nv
Awai, K. - Research Grant, Toshiba Medical Sysmtes Research Grant, Hitachi Medical Corporation Research Grant, Bayer AG Research Consultant, DAIICHI SANKYO Group Research Grant, Eisai Ltd

B

Bae, K. T. - Patent agreement, Covidien AG Patent agreement, Bayer AG
Bakic, P. R. - Research collaboration, Barco nv Research collaboration, Hologic, Inc
Balter, P. - Research, Koninklijke Philips Electronics NV
Bamberg, F. - Speakers Bureau, Bayer AG Speakers Bureau, Siemens AG Research Grant, Bayer AG Research Grant, Siemens AG
Bauman, G. S. - Research Grant, sanofi-aventis Group
Baydush, A. - Research Grant, Varian Medical Systems, Inc
Bayram, E. - Employee, General Electric Company
Beister, M. - Employee, CT Imaging GmbH
Beuing, O. - Consultant, Siemens AG
Blake, M. A. - Editor with royalties, Springer Science+Business Media Deutschland GmbH
Blobel, J. - Employee, Toshiba Corporation
Boctor, E. - Co-founder, Clear Guide Medical LLC
Boedeker, K. L. - Employee, Toshiba Corporation
Boone, J. M. - Research Grant, Siemens AG Research Grant, Hologic, Inc Consultant, Varian Medical Systems, Inc
Boonn, W. W. - Founder, Montage Healthcare Solutions, Inc Shareholder, Montage Healthcare Solutions, Inc
Bosmans, H. - Co-founder, Qaelum NV Research Grant, Siemens AG
Bowman, D. - Speaker, Medical Technology Management Institute Speaker, Digital Radiography Solutions
Bracco, C. - Speaker, Bracco Group Speaker, ABC Medical Imaging Consultant, Bayer AG
Branch, K. - Speakers Bureau, Pfizer Inc
Brock, K. K. - License agreement, RaySearch Laboratories AB Research Grant, Varian Medical Systems
Brown, K. M. - Employee, Koninklijke Philips Electronics NV
Brown, M. S. - Director, MedQIA Imaging Core Laboratory
Bruder, H. - Employee, Siemens AG
Budde, A. - Employee, General Electric Company
Burke, M. - Employee, General Electric Company
Bye, J. - Employee, General Electric Company

C

Canstein, C. - Employee, Siemens AG
Carrino, J. A. - Research Grant, Siemens AG Research Grant, Carestream Health, Inc Research Consultant, General Electric Company
Carson, P. L. - Research collaboration, General Electric Company Research collaboration, Sonetics Ultrasound, Inc Research collaboration, ZONARE Medical Systems, Inc Research collaboration, Light Age, Inc
Carton, A. - Principal investigator of clinical study sponsored by GE Healthcare
Chalek, C. - Employee, General Electric Company
Chen, G. - Research funded, General Electric Company Research funded, Siemens AG Research funded, Varian Medical Systems, Inc Research funded, Hologic, Inc
Cheng, D. W. - Consultant, Bayer AG Consultant, Navidea Biopharmaceuticals, Inc
Choyke, P. L. - Researcher, Koninklijke Philips Electronics NV Researcher, General Electric Company Researcher, Siemens AG Researcher, F. Hoffmann-La Roche Ltd Researcher, iCAD, Inc
Chu, J. C. - Research Grant, Varian Medical Systems, Inc
Chui, J. H. - Research collaboration, Barco nv Research collaboration, Hologic, Inc
Chung, M. - Patent agreement, General Electric Company Patent agreement, Samsung Electronics Co Ltd
Cisaruk, M. - Employee, General Electric Company
Clunie, D. A. - Employee, Bioclinica, Inc Owner, PixelMed Publishing LLC Research support, Siemens AG
Cody, D. D. - In-kind support, General Electric Company
Cohan, R. H. - Consultant, General Electric Company
Cohen-Bacrie, C. - Executive Vice President, SuperSonic Imagine Officer, SuperSonic Imagine
Conant, E. F. - Consultant, Hologic, Inc
Cool, D. W. - Patent agreement, Eigen
Craig, T. - Research Grant, Raysearch Laboratories AB
Crotty, D. - Employee, General Electric Company
Cunningham, I. A. - Founder, DQE Instruments Inc

D

Danielsson, M. - Stockholder, Koninklijke Philips Electronics NV Stockholder, Sectra AB Stockholder, Prismatic Sensors AB Stockholder, Innovicum AB Stockholder, Biovica International AB
Das, M. - Research Consultant, Bayer AG Research Grant, Siemens AG Speakers Bureau, Siemens AG
Davis, B. - Research Grant, Siemens AG
Dawson, L. A. - Research Grant, Bayer AG License agreement, RaySearch Laboratories AB
De Las Heras, H. - Research Consultant, QUART GmbH
De Man, B. - Employee, General Electric Company
Desponds, L. - Employee, General Electric Company
DeWerd, L. A. - Stockholder, Standard Imaging, Inc
Deyoe, E. A. - Stockholder, Prism Clinical Imaging, Inc Board of Directors, Prism Clinical Imaging, Inc
Diehn, M. - Research Consultant, Varian Medical Systems, Inc Research Grant, Varian Medical Systems, Inc
Dixon, R. L. - Research Consultant, Koninklijke Philips Electronics NV
Dobbins, J. T. III - Research Grant, General Electric Company Research Grant, Carestream Health, Inc Patent agreement, General Electric Company
Dong, L. - License agreement, Varian Medical Systems, Inc

E

Ebbini, E. S. - Consultant for International Cardio Corporation, LLC Royalties, International Cardio Corporation, LLC
Eckstein, F. - Co-owner, Chondrometrics GmbH Co-founder, Chondrometrics GmbH CEO, Chondrometrics GmbH Consultant, Novartis AG Consultant, Merck KGaA Consultant, sanofi-aventis Group
Edelstein, W. A. - Grant, Gamma Medica, Inc
Edic, P. - Employee, General Electric Company
Ehtiyati, T. - Employee, Siemens AG
Engelhard, G. - Employee, Algotec Limited
Erickson, B. J. - Stockholder, Evidentia Health
Escott, E. J. - Royalties, Thieme Medical Publishers, Inc Researcher, Athersys, Inc Grant, Athersys, Inc

Espig, K. S. - Employee, Barco nv
Eusemann, C. - Employee, Siemens AG
Evangelista, P. T. - Consultant, BioMimetic Therapeutics, Inc
Evelhoch, J. L. - Employee, Merck & Co, Inc Stockholder, Merck & Co, Inc
F
Fahrig, R. - Research Grant, Siemens AG Research Consultant, Siemens AG
Fallenberg, E. M. - Research Grant, Bayer AG Research Grant, Siemens AG Research Grant, General Electric Company Speaker, Siemens AG Speaker, General Electric Company Speaker, Bayer AG Speaker, Guerbet SA Travel support, Bayer AG
Feig, S. A. - Medical Advisory Board, Hologic, Inc
Fenster, A. - License agreement, Eigen
Fichs, D. - Employee, FUJIFILM Holdings Corporation
Filipiak, I. - Support, Siemens AG
Fishman, E. K. - Research support, Siemens AG Advisory Board, Siemens AG Research support, General Electric Company Advisory Board, General Electric Company Co-founder, HipGraphics, Inc
Fitzgerald, P. - Employee, General Electric Company
Fleischmann, D. - Research support, Siemens AG Research support, General Electric Company
Fletcher, J. G. - Grant, Siemens AG
Flohr, T. G. - Employee, Siemens AG
Foos, D. - Employee, Carestream Health, Inc
Forsberg, F. - Equipment support, Toshiba Corporation Equipment support, Siemens AG Research collaboration, General Electric Company Research collaboration, Ultrasonix Medical Corporation Research collaboration, Toshiba Corporation Advisory Board, Siemens AG Advisory Board, Toshiba Corporation
Fredenberg, E. - Employee, Koninklijke Philips Electronics NV
Fromme, S. - Employee, MeVis Medical Solutions AG
Fuld, M. K. - Researcher, Siemens AG
Fuller, C. D. - Research Consultant, General Electric Company
Fung, G. S. - Research support, Siemens AG
G
Gandhi, D. - Research funded, General Electric Company
Gao, H. - Employee, General Electrical Company
Garrett, J. W. - Research Grant, Hologic, Inc
Geeraert, N. - Employee, General Electric Company
Geyer, L. L. - Speaker, General Electric Company
Giger, M. L. - Stockholder, Hologic, Inc Shareholder, Quantitative Insights, Inc Royalties, Hologic, Inc Royalties, General Electric Company Royalties, MEDIAN Technologies Royalties, Riverain Technologies, LLC Royalties, Mitsubishi Corporation Royalties, Toshiba Corporation Researcher, Koninklijke Philips Electronics NV Researcher, U-Systems, Inc
Goerner, F. L. - Research Grant, Siemens AG Research Grant, Bayer AG Research Grant, Bracco Group
Goodsitt, M. M. - Research collaboration, General Electric Company
Grant, K. - Employee, Siemens AG
Green, O. - Research Consultant, ViewRay, Inc
Greenspan, B. S. - Consultant, CareCore National
H
Haberland, U. - Employee, Siemens Healthcare
Hagiwara, A. - Employee, General Electric Company
Hall, T. J. - Equipment support, Siemens AG
Halpern, H. J. - Consultant, Bruker Corporation
Heath, M. D. - Employee, Carestream Health, Inc
Helvie, M. A. - Institutional Grant, General Electric Company
Hendrych, R. - Employee, CT Imaging GmbH
Holmes, J. H. - Employee, General Electric Company
Hsieh, J. - Employee, General Electric Company
Huisman, H. - Stockholder, QView Medical, Inc
Hupfer, M. - Employee, CT Imaging GmbH
Hurwitz, L. M. - Research Grant, Siemens AG Research Grant, General Electric Company
I
Inokawa, H. - Employee, Toshiba Corporation
Isgum, I. - Research Grant, Pie Medical Imaging BV Research Grant, 3mensio Medical Imaging BV
Izhaky, D. - Employee, Real Imaging Ltd
J
Jacobs, C. - Research Grant, MeVis Medical Solutions AG
Jaffray, D. A. - Research Grant, Koninklijke Philips Electronics NV Research Grant, Elekta AB Research Grant, Raysearch Laboratories AB Research Grant, IMRIS Inc Research Grant, Varian Medical Systems, Inc Research Grant, Modus Medical Devices Inc Royalties, Raysearch Laboratories AB Royalties, Modus Medical Devices Inc Royalties, Elekta AB Royalties, IMRIS Inc
Jara, H. - Patent holder, Synthetic-MR algorithms Patent holder, Q-MRI algorithms
Jin, Y. - Employee, General Electric Company
Johnson, P. T. - Research funded, Becton, Dickinson and Company
Joshi, M. - Employee, Koninklijke Philips Electronics NV
K
Kalender, W. A. - Consultant, Siemens AG Consultant, Bayer AG Founder, CT Imaging GmbH Scientific Advisor, CT Imaging GmbH CEO, CT Imaging GmbH
Kalra, M. K. - Faculty, General Electric Company
Kamel, I. R. - Research support, Bracco Group Research support, Bayer AG
Karczmar, G. S. - Research Consultant, Perceptive Informatics, Inc Research Consultant, BioClinica, Inc
Karellas, A. - Institutional research collaboration, Koninklijke Philips Electronics NV Institutional research collaboration, Hologic, Inc
Karssemeyer, N. - Shareholder, Matakina International Limited Scientific Board, Matakina International Limited Shareholder, QView Medical, Inc Research Grant, Riverain Medical
Kassai, Y. - Employee, Toshiba Corporation
Kawamoto, S. - Research support, Siemens AG
Khatonabadi, M. - Research Support, Siemens AG
Kimpe, T. - Employee, Barco nv
Kimura, F. - Stockholder, JMS Co, Ltd Reseach Grant, DAIICHI SANKYO Group Reseach Grant, Bayer AG Reseach Grant, Eisai Co, Ltd Research Grant, Covidien AG Speakers Bureau, Bayer AG Speakers Bureau, Terumo Corporation
Kinahan, P. E. - Research Grant, General Electric Company Co-founder, PET/X LLC
Kirov, A. S. - Research Grant, Biospace Lab SA
Klausz, R. - Employee, General Electric Company
Klotz, E. - Employee, Siemens AG
Koestler, H. - Research support, Siemens AG
Kolditz, D. - Employee, CT Imaging GmbH
Korosec, F. R. - Research Support, General Electric Company
Korporaal, J. G. - Employee, Siemens AG
Kowarschik, M. - Employee, Siemens AG
Krauss, A. - Employee, Siemens AG
Krauss, B. - Employee, Siemens AG
Kripfgans, O. D. - Research support, General Electric Company Equipment support, General Electric Company
Kruskal, J. B. - Author, UpToDate, Inc
Kuhl, C. K. - Advisory Board Member, Bayer AG
Kundra, V. - License agreement, Introgen Therapeutics Inc
Kunimatsu, A. - Speakers Bureau, Eisai Co, Ltd Speakers Bureau, General Electric Company
Kunze, H. - Employee, Siemens AG
Kuo, J. - Employee, Real Time Tomography, LLC

Kupelian, P. - Consultant, ViewRay, Inc Consultant, Accuray Incorporated Speakers Bureau, Siemens AG Research Grant, Varian Medical Systems, Inc License agreement, VisionTree Software, Inc
Kurziel, K. A. - Researcher, General Electric Company Researcher, Siemens AG Researcher, Koninklijke Philips Electronics NV
Kyriakou, Y. - Employee, Siemens AG

L
Laghi, A. - Speaker, Bracco Group Speaker, im3d SpA Speaker, Bayer AG Research Consultant, General Electric Company
Larson, D. B. - Royalties, Bayer AG

Lassau, N. B. - Speaker, Toshiba Corporation Speaker, Bracco Group Speaker, Novartis AG Speaker, Pfizer Inc Speaker, F. Hoffmann-La Roche Ltd
Lauritsch, G. - Employee, Siemens AG

Lee, K. S. - Research Consultant, SuperSonic Imagine Speakers Bureau, Medical Technology Management Institute
Lee, T. - Grant, General Electric Company Royalties, General Electric Company

Lee, Y. Z. - Research Grant, Carestream Health, Inc
Leiner, T. - Speakers Bureau, Koninklijke Philips Electronics NV Consultant, Bayer AG Research Grant, Bracco Group

Lell, M. M. - Research Grant, Siemens AG Speakers Bureau, Siemens AG Research Grant, Bayer AG Speakers Bureau, Bayer AG Research Consultant, Bracco Group
Lenkinski, R. E. - Research Grant, Koninklijke Philips Electronics NV Research Consultant, Aposense Ltd Research Consultant, Aspect Imaging

Li, Q. - Patent agreement, General Electric Company Patent agreement, Hologic, Inc Patent agreement, Riverain Technologies, LLC Patent agreement, MEDIAN Technologies Patent agreement, Mitsubishi Corporation
Lin, C. - Research Grant, Siemens AG

Lin, Y. - Former intern, Carestream Health, Inc
Lindfors, K. K. - Research Grant, Hologic, Inc

Link, T. M. - Research Grant, General Electric Company Research Grant, InSightec Ltd
Litt, H. I. - Research Grant, Siemens AG

Liu, J. - Research Grant, GluMetrics, Inc
Loo, B. W. JR - Speaker, Varian Medical Systems, Inc Speaker, General Electric Company

Lu, J. - Research Grant, Carestream Health, Inc
Lueck, F. - Employee, CT Imaging GmbH

Lundqvist, M. - Employee, Koninklijke Philips Electronics NV
Lynch, D. A. - Research support, Siemens AG Scientific Advisor, Perceptive Informatics, Inc Consultant, Actelion Ltd Consultant, InterMune, Inc Consultant, Gilead Sciences, Inc Consultant, F. Hoffmann-La Roche Ltd

M
Mackie, T. R. - Consultant, Accuray Incorporated
Madabhushi, A. - Research partner, Siemens AG Research partner, General Electric Company Research partner, F. Hoffman-La Roche Ltd Founder and President, IbRIS, Inc

Madore, B. - Research Consultant, Millikelvin Technology LLC
Mahesh, M. - Royalties, Lippincott Williams & Wilkins
Mahnken, A. H. - Speaker, Bayer AG

Maidment, A. D. - Research support, Hologic, Inc Research support, Barco nv Spouse, Employee, Real-Time Radiography, Inc Spouse, Stockholder, Real-Time Radiography, Inc
Majumdar, S. - Research Grant, Merck & Co, Inc

Manak, J. - Employee, General Electric Company
Marchessoux, C. - Employee, Barco nv

Margolis, D. J. - Research Grant, Siemens AG
Mason, R. P. - Stockholder, AstraZeneca PLC Stockholder, GlaxoSmithKline plc Stockholder, Smith and Nephew plc Stockholder, Unilever

Matsumoto, S. - Research Grant, Toshiba Corporation
Mattrey, R. F. - Investigator, Bracco Group

Mayer, A. - Research Consultant, Real Imaging Ltd
McAleavey, S. - Research collaboration, General Electric Company

McCollough, C. H. - Research Grant, Siemens AG
McKenney, S. E. - Intern, General Electric Company

McMillan, K. - Institutional research agreement, Siemens AG Research support, Siemens AG
McNitt-Gray, M. F. - Institutional research agreement, Siemens AG Research support, Siemens AG

Mendonca, P. R. - Employee, General Electric Company
Metz, S. - Employee, Koninklijke Philips Electronics NV

Mews, J. - Employee, Toshiba Corporation
Michalski, D. - Research Grant, Varian Medical Systems, Inc Research Grant, General Electric Company

Milkowski, A. - Employee, Siemens AG
Mistretta, C. A. - Grant, General Electric Company Founder, Mistretta Medical Intellectual Property Licensing Activities Research, Siemens AG

Mitsumori, L. M. - Research Grant, Bayer AG Research Grant, General Electric Company Speaker, Bayer AG
Moa, E. - Employee, Koninklijke Philips Electronics NV

Molloi, S. Y. - Research Consultant, Koninklijke Philips Electronics NV
Muller, S. L. - Employee, General Electric Company

Munley, M. T. - Research Grant, Varian Medical Systems, Inc
N

Na, H. - Employee, General Electric Company
Nagle, S. K. - Stockholder, General Electric Company

Napel, S. - Medical Advisory Board, Fovia, Inc Consultant, Carestream Health, Inc Scientific Advisor, Echopixel, Inc
Natsuaki, Y. - Researcher, Siemens AG

Neal, C. H. - Consultant, Medken LLC
Nelson, R. C. - Consultant, General Electric Company Research support, Nemoto Kyorindo Co, Ltd Research support, Bracco Group Research support, Becton, Dickinson and Company Speakers Bureau, Siemens AG Royalties, Lippincott, Williams & Wilkins

Nett, B. E. - Employee, General Electric Company
Newstead, G. M. - Medical Advisory Board, Bayer AG Consultant, Three Palm Software LLC

Ng, S. - CEO, Real Time Tomography, LLC
Nichols, K. - Royalties, Syntermed, Inc Consultant, Gilead Sciences, Inc

Nightingale, K. - Research support, Siemens AG
Nikolaou, K. - Speakers Bureau, Siemens AG Speakers Bureau, Bracco Group Speakers Bureau, Bayer AG

Nishikawa, R. M. - Royalties, Hologic, Inc Royalties, Mitsubishi Corporation Royalties, MEDIAN Technologies Royalties, Toshiba Corporation Royalties, Riverain Technologies, LLC Consultant, iCAD, Inc
Nwoke, F. - Founder, Innovent Health LLC Consultant, Med Observerships, LLC

O
Oberstar, E. - Research Grant, Siemens AG
O'Connell, T. - President, Resolve Radiologic Ltd

O'Donnell, K. - Employee, Toshiba Corporation
Oelhafen, M. - Employee, Varian Medical Systems, Inc

Ohno, Y. - Research Grant, Toshiba Corporation Research Grant, Koninklijke Philips Electronics NV Research Grant, Bayer AG Research Grant, DAIICHI SANKYO Group Research Grant, Eisai Co, Ltd Research Grant, Terumo Corporation Research Grant, Covidien AG Research Grant, FUJIFILM Holdings Corporation
Ohtomo, K. - Research Grant, Bayer AG Research Grant, DAIICHI SANKYO Group

Oishi, S. - Employee, Toshiba Corporation
O'Kane, P. L. - Research Consultant, NPS Pharmaceuticals Research Consultant, Johnson & Johnson

Otake, Y. - Research support, Siemens AG
Oto, A. - Honorarium, Koninklijke Philips Electronics NV Research Grant, Koninklijke Philips Electronics NV Research Grant, Bayer AG Research Grant, Visualase Inc Research Grant, General Electric Company

Overlaet, W. - Employee, Toshiba Corporation
P

Pack, J. - Employee, General Electric Company
Padhani, A. R. - Consultant, IXICO Limited Advisory Board, Acuitus Medical Ltd Advisory board, Siemens AG

Pack, J. - Employee, General Electric Company
Padhani, A. R. - Consultant, IXICO Limited Advisory Board, Acuitus Medical Ltd Advisory board, Siemens AG

Pack, J. - Employee, General Electric Company
Padhani, A. R. - Consultant, IXICO Limited Advisory Board, Acuitus Medical Ltd Advisory board, Siemens AG

Pack, J. - Employee, General Electric Company
Padhani, A. R. - Consultant, IXICO Limited Advisory Board, Acuitus Medical Ltd Advisory board, Siemens AG

Pack, J. - Employee, General Electric Company
Padhani, A. R. - Consultant, IXICO Limited Advisory Board, Acuitus Medical Ltd Advisory board, Siemens AG

Pack, J. - Employee, General Electric Company
Padhani, A. R. - Consultant, IXICO Limited Advisory Board, Acuitus Medical Ltd Advisory board, Siemens AG

Pack, J. - Employee, General Electric Company
Padhani, A. R. - Consultant, IXICO Limited Advisory Board, Acuitus Medical Ltd Advisory board, Siemens AG

Pack, J. - Employee, General Electric Company
Padhani, A. R. - Consultant, IXICO Limited Advisory Board, Acuitus Medical Ltd Advisory board, Siemens AG

Pan, X. - Research Grant, Koninklijke Philips Electronics NV Research Grant, Toshiba Corporation Consultant, UtopiaCompression Corporation
Parker, D. L. - Research funded, Siemens AG
Partridge, S. C. - Research Grant, Koninklijke Philips Electronics NV
Paysan, P. - Employee, Varian Medical Systems, Inc
Pelc, N. J. - Research Grant, General Electric Company Board of Directors, Real-Time Radiography, Inc Stockholder, General Electric Company Scientific Advisory Board, Samplify Systems, Inc Scientific Advisory Board, Radguard Medical, Inc Scientific Advisory Board, Albatross Medical Imaging
Pelizzari, C. A. - Research Grant, Varian Medical Systems, Inc Scientific Advisory Board, RefleXion Medical Inc
Penzkofer, T. - Travel support, Koninklijke Philips Electronics NV
Persson, M. - Stockholder, Prismatic Sensors AB
Pfeiffer, D. E. - Consultant, Radcal Corporation
Pickens, D. R. III - Stockholder, Johnson & Johnson
Pickhardt, P. J. - Research Consultant, Bracco Group Research Consultant, Check-Cap Ltd Co-founder, VirtuoCTC, LLC
Pillai, J. J. - Medical Advisory Board, Primm Clinical Imaging, Inc Research Grant, Siemens AG
Podberesky, D. J. - Author, Amirsys, Inc Speakers Bureau, Toshiba Corporation Travel support, General Electric Company Travel support, Koninklijke Philips Electronics NV
Pozniak, M. A. - Stockholder, Novelos Therapeutics, Inc
Prince, M. R. - Patent agreement, General Electric Company Patent agreement, Hitachi, Ltd Patent agreement, Siemens AG Patent agreement, Toshiba Corporation Patent agreement, Koninklijke Philips Electronics NV Patent agreement, Nemoto Kyorindo Co, Ltd Patent agreement, Bayer AG Speaker Honorarium, Bayer AG Patent agreement, Lantheus Medical Imaging, Inc Patent agreement, Bracco Group Speaker Honorarium, Bracco Group Patent agreement, Covidien AG Patent agreement, Topspins, Inc Stockholder, Topspins, Inc
Prokop, M. - Speakers Bureau, Bayer AG Speakers Bureau, Bracco Group Speakers Bureau, Toshiba Corporation Speakers Bureau, Koninklijke Philips Electronics NV Research Grant, Toshiba Corporation
R
Radvany, M. G. - Research Consultant, ArtVentive Medical Group, Inc Stockholder, ArtVentive Medical Group, Inc Research Grant, Siemens AG
Raupach, R. - Employee, Siemens AG
Read, K. M. - Employee, Koninklijke Philips Electronics NV
Rettmann, D. W. - Employee, General Electric Company
Ringer, P. A. - Employee, Real Time Tomography, LLC Shareholder, Real Time Tomography, LLC
Rohkohl, C. - Employee, Siemens AG
Romman, Z. - Employee, Koninklijke Philips Electronics NV
Rosenthal, D. I. - Speakers Bureau, ImClone Systems Incorporated Speakers Bureau, Bristol-Myers Squibb Company Speakers Bureau, sanofi-aventis Group Research support, Amgen Inc Research support, MedImmune, Inc
Rowley, H. A. - Research Consultant, Eli Lilly and Company Research Consultant, W.L. Gore & Associates, Inc Research Consultant, H. Lundbeck A/S Research Consultant, General Electric Company Speaker, Bracco Group Researcher, Guerbet SA
Royalty, K. - Employee, Siemens AG
Ruan, D. - License agreement, VisionTree Software, Inc
Rudin, S. - Research Grant, Toshiba Corporation
Runge, V. M. - Research Grant, Bayer AG Research Grant, Bracco Group
Rybicki, F. J. III - Research Grant, Toshiba Corporation Research Grant, Bracco Group
S
Saab-Puong, S. - Investigator, General Electric Company
Saam, T. - Research Grant, Diamed Medizintechnik GmbH Research Grant, Bayer AG
Sabol, J. M. - Employee, General Electric Company
Sakai, O. - Royalties, The McGraw-Hill Companies
Sakuma, H. - Departmental Research Grant, Siemens AG Departmental Research Grant, Koninklijke Philips Electronics NV Departmental Research Grant, General Electric Company Departmental Research Grant, Bayer AG Departmental Research Grant, Eisai Co, Ltd Departmental Research Grant, Guerbet SA
Samei, E. - Research Grant, Siemens AG Research Grant, General Electric Company Research Grant, Carestream Health, Inc
Sammet, S. - Research Grant, Koninklijke Philips Electronics NV
Sandrin, L. - Director, Echosens Employee, Echosens
Schaefer-Prokop, C. M. - Advisory Board, Riverain Technologies, LLC
Schafer, S. - Consultant, Siemens AG
Schalekamp, S. - Research Grant, Riverain Technologies, LLC
Schmidt, B. - Employee, Siemens AG
Schmitgen, A. - Employee, Localite GmbH
Schmitz, A. - Employee, General Electric Company
Schoenberg, S. O. - Institutional research agreement, Siemens AG
Schoepf, U. - Research Grant, Bracco Group Research Grant, General Electric Company Research Consultant, Siemens AG Research Grant, Siemens AG
Schofer, F. - Officer, QUART GmbH
Scholz, B. G. - Employee, Siemens AG
Schuijff, J. - Employee, Toshiba Corporation
Sedlmair, M. U. - Employee, Siemens AG
Serowy, S. - Consultant, Siemens AG
Shaw, C. C. - Investigator, Stellarray, Inc Editor, Taylor & Francis Group, LLC
Shaw, J. - Employee, General Electric Company
Shen, Y. - Employee, General Electric Company Researcher, General Electric Company
Shepard, J. O. - Consultant, Agfa-Gevaert Group
Shi, D. - Employee, Toshiba Corporation
Shiraishi, J. - Research Grant, Konica Minolta Group
Shreiber, R. - Employee, Algotec Limited
Shuman, W. P. - Research Grant, General Electric Company
Siebers, J. V. - Research Grant, Varian Medical Systems, Inc Research Grant, Koninklijke Philips Electronics NV
Siewerdsen, J. H. - Research Grant, Siemens AG Consultant, Siemens AG Research Grant, Carestream Health, Inc Royalties, Elekta AB
Silver, M. D. - Employee, Toshiba Corporation
Skalej, M. - Institutional research collaboration, Siemens AG
Sklair-Levy, M. - Shareholder, Real Imaging Ltd
Sosna, J. - Consultant, ActiViews Ltd Research Grant, Koninklijke Philips Electronics NV
Soto, J. A. - Researcher, General Electric Company
Souchay, H. - Employee, General Electric Company
Speller, R. - Research Grant, Nikon Group
Spraws, P. - Author, Koninklijke Philips Electronics NV
Stayman, J. W. - Research Grant, Varian Medical Systems, Inc
Steiding, C. - Employee, CT Imaging GmbH
Stevens, G. M. - Employee, General Electric Company
Stierstorfer, K. - Employee, Siemens AG
Strother, C. M. - Research Consultant, Siemens AG Research support, Siemens AG License agreement, Siemens AG
Sugimura, K. - Research Grant, Toshiba Corporation Research Grant, Koninklijke Philips Electronics NV Research Grant, Bayer AG Research Grant, Eisai Co, Ltd Research Grant, DAIICHI SANKYO Group
Summers, R. M. - Royalties, iCAD, Inc Grant, iCAD, Inc Stockholder, Johnson & Johnson Grant, Viatronix, Inc
Sun, M. R. - Investigator, Bracco Group
Sunde, P. B. - Shareholder, Radcal Corp Employee, Radcal Corp
Supanich, M. P. - Research Grant, Siemens AG
Suzuki, K. - Royalties, General Electric Company Royalties, Hologic, Inc Royalties, AlgoMedica Royalties, MEDIAN Technologies Royalties, Riverain Technologies, LLC Royalties, Toshiba Corporation Royalties, Mitsubishi Corporation
Suzuki, Y. - Employee, Koninklijke Philips Electronics NV
Szczykutowicz, T. P. - Grant, General Electric Company Grant, Siemens AG
T
Taguchi, K. - Research Grant, Siemens AG
Tang, X. - Research Grant, Ningbo Xingaoyi Magnetism Co Ltd

Taniguchi, A. - Employee, Toshiba Corporation
Tanter, M. - Co-founder, SuperSonic Imagine
Thibault, J. - Employee, General Electric Company
Thomas, J. A. - Stockholder, General Electric Company Stockholder, Hologic, Inc Stockholder, Stryker Corporation Speaker, Medical Technology Management Institute Speaker, Cassling Speaker, Landauer Medical Physics
Thomenius, K. E. - Employee, General Electric Company
Thorner, G. - Employee, Siemens AG
Togashi, K. - Research Grant, Bayer AG Research Grant, DAIICHI SANKYO Group Research Grant, Eisai Co, Ltd Research Grant, FUJIFILM Holdings Corporation Research Grant, Nihon Medi-Physics Co, Ltd Research Grant, Shimadzu Corporation Research Grant, Toshiba Corporation Research Grant, Covidien AG
Toth, T. L. - Former Employee, General Electric Company Co-owner, Plexar Associates, Inc
Tsui, B. - Research Consultant, Hybridyne Imaging Technologies, Inc Research Grant, Gamma Medica Ideas, Inc Research Grant, Siemens AG License agreement, General Electric Company License agreement, Gamma Medica Ideas, Inc
Turski, P. A. - Research support, General Electric Company
V
Van Der Putten, W. J. - Director, Bio-PHYSICA Ltd Shareholder, Bio-PHYSICA Ltd Co-founder, Bio-PHYSICA Ltd Research Consultant, QUART GmbH
Van Tosh, A. - Consultant, Pfizer Inc Consultant, Bracco Group Consultant, Cardinal Health, Inc Consultant, Ion Beam Applications, SA
Viergever, M. A. - Research Grant, Koninklijke Philips Electronics NV Research Grant, Pie Medical Imaging BV
W
Wallace, K. - Employee, General Electric Company
Wang, A. S. - Research support, Siemens AG
Wang, J. - Employee, General Electric Company
Wang, K. - Employee, General Electric Company
Wang, S. - Grant, Koninklijke Philips Electronics NV
Wang, X. - Employee, Carestream Health, Inc
Wicklein, J. - Research collaboration, Siemens AG
Willmann, J. K. - Research Consultant, Bracco Group Research Grant, Siemens AG Research Grant, Bracco Group
Wilson, D. L. - Owner, BioInVision Inc Research Grant, Koninklijke Philips Electronics NV
Winkel, A. - Employee, Koninklijke Philips Electronics NV
Wirth, S. - Speaker, General Electric Company
Wolterink, J. M. - Research Grant, Pie Medical Imaging BV
X
Xing, L. - Research Grant, Varian Medical Systems, Inc
Xthona, A. - Employee, Barco nv
Y
Yaffe, M. J. - Research collaboration, General Electric Company Founder, Matakina Technology Ltd Shareholder, Matakina Technology Ltd Co-Founder, Mammographic Physics Inc
Yamagata, H. - Employee, Toshiba Corporation
Yamashita, Y. - Consultant, DAIICHI SANKYO Group
Yao, J. - Royalties, iCAD, Inc
Yin, Z. - Employee, General Electric Company
Yorkston, J. - Employee, Carestream Health, Inc
Yoshida, H. - Patent holder, Hologic, Inc Patent holder, MEDIAN Technologies
Z
Zabic, S. - Employee, Koninklijke Philips Electronics NV
Zamyatin, A. - Employee, Toshiba Corporation
Zbijewski, W. - Research Grant, Carestream Health, Inc
Zelakiewicz, S. - Employee, General Electric Company
Zhao, W. - Research Grant, Siemens AG
Zhou, O. - Board of Directors, XinRay Systems Inc Research Grant, Carestream Health, Inc